

TIME EVOLUTION OF THE FLOW CHARACTERISTICS AROUND BRIDGE  
ABUTMENTS DURING SCOURING PROCESS

A THESIS SUBMITTED TO  
THE GRADUATE SCHOOL OF NATURAL AND APPLIED SCIENCES  
OF  
MIDDLE EAST TECHNICAL UNIVERSITY

BY

BURHAN YILDIZ

IN PARTIAL FULFILLMENT OF THE REQUIREMENTS  
FOR  
THE DEGREE OF DOCTOR OF PHILOSOPHY  
IN  
CIVIL ENGINEERING

FEBRUARY 2014



Approval of the Thesis:

**TIME EVOLUTION OF THE FLOW CHARACTERISTICS AROUND BRIDGE  
ABUTMENTS DURING SCOURING PROCESS**

submitted by **BURHAN YILDIZ** in partial fulfillment of the requirements for the degree of **Doctor of Philosophy in Civil Engineering Department, Middle East Technical University** by,

Prof. Dr. Canan Özgen  
Dean, Graduate School of **Natural and Applied Sciences**

\_\_\_\_\_

Prof. Dr. Ahmet Cevdet Yalçiner  
Head of Department, **Civil Engineering**

\_\_\_\_\_

Assoc. Prof. Dr. Mete Köken  
Supervisor, **Civil Engineering Dept., METU**

\_\_\_\_\_

Prof. Dr. Mustafa Göğüş  
Co-supervisor, **Civil Engineering Dept., METU**

\_\_\_\_\_

**Examining Committee Members:**

Prof. Dr. Melih Yanmaz  
Civil Engineering Dept., METU

\_\_\_\_\_

Assoc. Prof. Dr. Mete Köken  
Civil Engineering Dept., METU

\_\_\_\_\_

Prof. Dr. A. Burcu Altan-Sakarya  
Civil Engineering Dept., METU

\_\_\_\_\_

Assoc. Prof. Dr. Şahnaz Tiğrek  
Civil Engineering Dept., METU

\_\_\_\_\_

Assist. Prof. Dr. Önder Koçyiğit  
Civil Engineering Dept., Gazi University

\_\_\_\_\_

Date: 07/02/2014

**I hereby declare that all information in this document has been obtained and presented in accordance with academic rules and ethical conduct. I also declare that, as required by these rules and conduct, I have fully cited and referenced all material and results that are not original to this work.**

Name, Last Name: Burhan Yıldız

Signature:

## **ABSTRACT**

### **TIME EVOLUTION OF THE FLOW CHARACTERISTICS AROUND BRIDGE ABUTMENTS DURING SCOURING PROCESS**

Yıldız, Burhan  
Ph.D., Department of Civil Engineering  
Supervisor : Assoc. Prof. Dr. Mete Köken  
Co-Supervisor: Prof. Dr. Mustafa Göğüş

February 2014, 218 Pages

This study involves numerical and experimental investigation of the velocity field and the time evolution of the scour pattern forming around bridge abutments. The experimental part of the study includes velocity field recordings by using an ADV device and eroded bed bathymetry measurements by an ultrasonic ranging system. Using the ADV measurements; the velocity components, the upstream part of the primary vortex and the change of downstream recirculation region dimensions by the change in abutment length, type and closeness to the channel bed was investigated. Scour recording part of the experimental study included scour pattern recordings for various abutment lengths, types and experiment durations; and continuous measurements of scour at some predefined sections around abutments for eight hours. Maximum scour depth, scour hole dimensions and scour volume are related to scour time and abutment length. It was observed that, the contraction scour occurs together with the local scour at contraction ratios larger than 15-20% depending on the abutment type. The second part of the study includes a numerical analysis of the problem by using a commercially available CFD software. The numerical analysis consisted of simulations both for non-erodible and erodible channel bed conditions. The capability of the scour model of the software was tested.

Keywords: Abutment Scour, Local Scour, Contraction Scour, Bridge Hydraulics

## ÖZ

### ÖYULMA ESNASINDA KÖPRÜ YAN AYAKLARI ETRAFINDA ZAMANA BAĞLI OLARAK AKIM KARAKTERİSTİKLERİNDE OLUŞAN DEĞİŞİMLERİN İNCELENMESİ

Yıldız, Burhan  
Doktora, İnşaat Mühendisliği Bölümü  
Tez Yöneticisi : Doç. Dr. Mete Köken  
Ortak Tez Yöneticisi: Prof. Dr. Mustafa Göğüş

Şubat 2014, 218 Sayfa

Bu çalışma köprü kenar ayakları etrafında oluşan hız alanının ve oyulma şemasının zamanla gelişmesini deneysel ve sayısal metodlarla incelenmesini içerir. Çalışmanın deneysel kısmı ADV cihazı ile yapılan hız alanı ölçümleri ve sesötesi tarama cihazı yardımı ile alınmış olan oyulmuş zemin değişim ölçümlerini içermektedir. ADV ölçümleri kullanılarak; hız bileşenleri, memba bölgesinde ana girdap oluşumları ve mansap resirkülasyon bölgesi boyutlarının ayak boyu ile değişimi incelenmiştir. Deneysel çalışmanın oyulma ölçümü bölümü ise, değişik kenar ayak boyları, şekilleri ve deney süreleri için oyulma şemalarının ölçülmesi ve 8 saatlik süreler boyunca devamlı ölçümler yardımı ile oyulmanın zamanla değişimini incelemeyi içermektedir. Maksimum oyulma derinliği, oyulma çukurunun boyutları ve oyulma hacmi oyulma zamanı ve ayak boyu ile ilişkilidir. Daralma oyulmasının yerel oyulmaya katılımı ayak tipine bağlı olarak daralma oranları yüzde 15 ila 20'nin üzerindeyken gerçekleşmiştir. Çalışmanın ikinci bölümü problemin, piyasada bulunan bir CFD yazılımı kullanılarak yürütülen, sayısal bir analizini içerir. Sayısal analiz simülasyonları düz ve aşınabilir zemin koşulları için değerlendirilmiştir. Yazılımın oyulma modelinin kapasitesi test edilmiştir.

Anahtar Kelimeler: Köprü kenar ayak oyulması, Yerel oyulma, Daralma oyulması,  
Köprü Hidroliđi

*To my mother,*

## ACKNOWLEDGMENTS

The author wishes to express his deepest gratitude to his supervisor Assoc. Prof. Dr. Mete Köken and co-supervisor Prof. Dr. Mustafa Göğüş for their guidance, advice, criticism, encouragements and insight throughout the research.

I would like thank to the thesis monitoring committee members, Prof. Dr. Melih Yanmaz, emeritus Prof. Dr. Ali Günyaktı and Assist. Prof. Dr. Önder Koçyiğit for their support and guidance during the study. Prof. Dr. A. Burcu Altan-Sakarya and Assoc. Prof. Dr. Şahnaz Tiğrek have contributed a lot to give the final shape of the thesis as thesis committee members. Their effort is appreciated.

The technical assistance of METU Hydraulics Laboratory staff is gratefully acknowledged.

Some parts of this study were supported by the Scientific and Technological Research Council of Turkey (TUBITAK) under Project No: 111M377, which is gratefully acknowledged here.

And last but not the least, I am grateful to my family for their invaluable support, patience and love.

## TABLE OF CONTENTS

ABSTRACT.....	v
ÖZ.....	vii
ACKNOWLEDGMENTS.....	x
TABLE OF CONTENTS.....	xi
LIST OF TABLES.....	xiv
LIST OF FIGURES.....	xv
CHAPTERS	
1. INTRODUCTION.....	1
1.1 Background.....	1
1.2 Dimensional Analysis.....	5
1.3 Objectives of the Present Study.....	8
1.4 Outline of the Thesis.....	9
2. LITERATURE REVIEW.....	11
2.1 Experimental Studies.....	12
2.1.1 Scour Mechanisms.....	12
2.1.2 Equilibrium Scour Depth.....	14
2.1.3 Contraction Scour.....	16
2.1.4 Temporal Variation of Scour Pattern.....	17
2.2 Numerical Studies.....	21
2.2.1 Studies for Non-Erodible Bed.....	21
2.2.2 Studies for Erodible Bed.....	25
3. MORPHOLOGICAL CHANGES ON RIVER BED AROUND AN ISOLATED BRIDGE ABUTMENT.....	27
3.1 General Experimental Conditions.....	27
3.2 Bathymetry Measurements.....	32
3.2.1 Experimental Equipment and Procedure.....	33
3.2.2 Results.....	34

3.2.2.1 Discussion of Results.....	54
3.2.2.2 Comp. of Res. w/ Res. of Si. Stu. in Lit.....	61
3.3 Temporal Scour Measurements.....	64
3.3.1 Experimental Equipment and Procedure.....	65
3.3.2 Results.....	66
3.3.2.1 Discussion of Results.....	77
3.3.2.2 Comp. of Res. w/ Res. of Si. Stu. in Lit .....	80
4. MORPHOLOGICAL CHANGES ON RIVER BED AROUND A PAIR OF BRIDGE ABUTMENTS AT CONTRACTED SECTIONS.....	87
4.1 Bathymetry Measurements.....	87
4.1.1 Experimental Equipment and Procedure.....	88
4.1.2 Results.....	91
4.1.2.1 Discussion of Results.....	111
4.1.2.2 Comp. of Res. w/ Res. of Si. Stu. in Lit .....	129
4.2 Temporal Scour Measurements.....	130
4.2.1 Experimental Equipment and Procedure.....	130
4.2.2 Results.....	132
4.2.2.1 Discussion of Results.....	143
4.2.2.2 Comp. of Res. w/ Res. of Si. Stu. in Lit .....	146
5. MEASUREMENT OF VELOCITY FIELD AROUND BRIDGE ABUTMENTS.....	155
5.1 Experimental Equipment and Procedure.....	155
5.2 Results.....	157
5.2.1 Discussion of Results.....	167
5.2.2 Comp. of Res. w/ Res. of Si. Stu. in Lit .....	170
6. NUMERICAL ANALYSES ON FLOW AND SCOURING AROUND BRIDGE ABUTMENTS.....	173
6.1 Overview.....	173
6.1.1 Turbulence Solver Models.....	173
6.1.2 Sediment Scour Model.....	174
6.1.3 Preliminary Runs.....	177

6.2 Flat Bed Simulations.....	181
6.2.1 Simulations Using RNG Model.....	181
6.2.2 Simulations Using LES Model.....	183
6.3 Erodible Bed Simulations.....	184
6.3.1 Erodible Bed Simulations using RNG Model.....	187
6.3.2 Erodible Bed Simulations using LES Model.....	188
6.3.2.1 Calibration of the Model.....	188
6.3.2.2 Comp. of the Simul. Res. with the Exp. Res.....	199
7. CONCLUSION.....	203
7.1 Summary of the Conclusions.....	203
7.2 Recommendations for the Future Researches.....	206
REFERENCES.....	207
APPENDICES	
A. SIEVE ANALYSIS.....	215
B. CALCULATION OF CRITICAL SHEAR VELOCITY FROM EXPERIMENTS AND FROM SHIELDS DIAGRAM.....	216
VITA.....	217

## LIST OF TABLES

### TABLES

Table 3.1 Test Conditions.....	34
Table 3.2 Parameters obtained from the experiments.....	53
Table 3.3 Parameters used in modeling the problem with Coleman et al. (2003).....	81
Table 4.1 Test Conditions.....	89
Table 4.2 Parameters obtained from the experiments.....	111
Table 4.3 Parameters used in modeling the problem with Coleman et al. (2003).....	148
Table 5.1 Parameters related to the downstream recirculation region.....	169
Table 6.1 Maximum scour depths obtained in testing $\theta_{cr}$ effect.....	193
Table 6.2 Maximum scour depths obtained in testing Entrainment Coefficient effect..	197
Table 6.3 Maximum scour depths obtained in testing Bed Load Coefficient effect.....	198
Table 6.4 Comparison of simulation results with the experimental results.....	202

## LIST OF FIGURES

### FIGURES

Figure 1.1 Visualization of flow structures around a bridge abutment.....	2
Figure 1.2 Scour types that can occur at a bridge cross. (Melville and Coleman, 2000)...	3
Figure 1.3 Temp. development of scour depth (after Chabert and Engeldinger, 1956)....	4
Figure 3.1 A schematic representation of the flume .....	28
Figure 3.2 Seatek Ultrasonic Ranging System.....	29
Figure 3.3 Laboratory flume view from upstream with no abutment models installed...	30
Figure 3.4 Dimensions of the SCE Abutment .....	31
Figure 3.5 The transducers while data recording.....	32
Figure 3.6 Scour and deposition pattern after a 2 hours test duration for the abutment length, $L=15$ cm: a) top view; b) 3-D view; c) 1-D section view which is tangent to the tip of the abutment.....	35
Figure 3.7 Scour and deposition pattern after a 4 hours test duration for the abutment length, $L=15$ cm: a) top view; b) 3-D view; c) 1-D section view which is tangent to the tip of the abutment.....	36
Figure 3.8 Scour and deposition pattern after an 8 hours test duration for the abutment length, $L=15$ cm: a) top view; b) 3-D view; c) 1-D section view which is tangent to the tip of the abutment.....	37

Figure 3.9 Scour and deposition pattern after a 2 hours test duration for the abutment length,  $L=20$  cm: a) top view; b) 3-D view; c) 1-D section view which is tangent to the tip of the abutment.....38

Figure 3.10 Scour and deposition pattern after a 4 hours test duration for the abutment length,  $L=20$  cm: a) top view; b) 3-D view; c) 1-D section view which is tangent to the tip of the abutment.....39

Figure 3.11 Scour and deposition pattern after an 8 hours test duration for the abutment length,  $L=20$  cm: a) top view; b) 3-D view; c) 1-D section view which is tangent to the tip of the abutment.....40

Figure 3.12 Scour and deposition pattern after a 2 hours test duration for the abutment length,  $L=25$  cm: a) top view; b) 3-D view; c) 1-D section view which is tangent to the tip of the abutment.....41

Figure 3.13 Scour and deposition pattern after a 4 hours test duration for the abutment length,  $L=25$  cm: a) top view; b) 3-D view; c) 1-D section view which is tangent to the tip of the abutment.....42

Figure 3.14 Scour and deposition pattern after an 8 hours test duration for the abutment length,  $L=25$  cm: a) top view; b) 3-D view; c) 1-D section view which is tangent to the tip of the abutment.....43

Figure 3.15 Scour and deposition pattern after a 2 hours test duration for the abutment length,  $L=30$  cm: a) top view; b) 3-D view; c) 1-D section view which is tangent to the tip of the abutment.....44

Figure 3.16 Scour and deposition pattern after a 4 hours test duration for the abutment length,  $L=30$  cm: a) top view; b) 3-D view; c) 1-D section view which is tangent to the tip of the abutment.....45

Figure 3.17 Scour and deposition pattern after an 8 hours test duration for the abutment length,  $L=30$  cm: a) top view; b) 3-D view; c) 1-D section view which is tangent to the tip of the abutment.....46

Figure 3.18 Scour and deposition pattern after a 2 hours test duration for the abutment length, $L=35$ cm: a) top view; b) 3-D view; c) 1-D section view which is tangent to the tip of the abutment.....	47
Figure 3.19 Scour and deposition pattern after a 4 hours test duration for the abutment length, $L=35$ cm: a) top view; b) 3-D view; c) 1-D section view which is tangent to the tip of the abutment.....	48
Figure 3.20 Scour and deposition pattern after an 8 hours test duration for the abutment length, $L=35$ cm: a) top view; b) 3-D view; c) 1-D section view which is tangent to the tip of the abutment.....	49
Figure 3.21 Scour and deposition pattern after a 2 hours test duration for the abutment length, $L=40$ cm: a) top view; b) 3-D view; c) 1-D section view which is tangent to the tip of the abutment.....	50
Figure 3.22 Scour and deposition pattern after a 4 hours test duration for the abutment length, $L=40$ cm: a) top view; b) 3-D view; c) 1-D section view which is tangent to the tip of the abutment.....	51
Figure 3.23 Position of the maximum scour depth in terms of $r$ and $\alpha$ .....	53
Figure 3.24 Var. of $d_s/D$ with $L/D$ for 2, 4 and 8 hours.....	54
Figure 3.25 Var. of $X_s/D$ with $L/D$ for 2, 4 and 8 hours.....	55
Figure 3.26 Var. of $X_i/D$ with $L/D$ for 2, 4 and 8 hours.....	56
Figure 3.27 Var. of $X_r/D$ with $L/D$ for 2, 4 and 8 hours.....	57
Figure 3.28 Comparison of the values of $X_i/D$ and $X_r/D$ for the entire data.....	57
Figure 3.29 Var. of $r/D$ with $L/D$ for 2, 4 and 8 hours.....	58
Figure 3.30 Var. of $\alpha$ with $L/D$ for 2, 4 and 8 hours.....	59
Figure 3.31 Var. of $V_s/D^3$ with $L/D$ for 2, 4 and 8 hours.....	60

Figure 3.32 Var. of $V_s/D^3$ with the dimensionless maximum scour depth.....	61
Figure 3.33 Comparison of the experimental data with Garde's (1961).....	63
Figure 3.34 Comparison of the experimental data with Kayatürk's (2005).....	64
Figure 3.35 Positions of the measurement sections for the abutments of (a) $L= 15$ cm (b) $L= 35$ cm (dimensions are in cm, red drawings stand for the transducers).....	66
Figure 3.36 Temp. chan. of Bed Profiles at Section #1 for the abutment of $L= 15$ cm....	67
Figure 3.37 Temp. chan. of Bed Profiles at Section #2 for the abutment of $L= 15$ cm...68	
Figure 3.38 Temp. chan. of Bed Profiles at Section #3 for the abutment of $L= 15$ cm....69	
Figure 3.39 Temp. chan. of Bed Profiles at Section #4 for the abutment of $L= 15$ cm....70	
Figure 3.40 Temp. chan. of Bed Profiles at Section #5 for the abutment of $L= 15$ cm....71	
Figure 3.41 Temp. chan. of Bed Profiles at Section #1 for the abutment of $L= 35$ cm...72	
Figure 3.42 Temp. chan. of Bed Profiles at Section #2 for the abutment of $L= 35$ cm...73	
Figure 3.43 Temp. chan. of Bed Profiles at Section #3 for the abutment of $L= 35$ cm...74	
Figure 3.44 Temp. chan. of Bed Profiles at Section #4 for the abutment of $L= 35$ cm...75	
Figure 3.45 Temp. chan. of Bed Profiles at Section #5 for the abutment of $L= 35$ cm...76	
Figure 3.46 Temporal development of scour depth for $L= 15$ cm.....	78
Figure 3.47 Temporal development of scour depth for $L= 35$ cm.....	79
Figure 3.48 Comp. of experimental findings with Coleman et al. (2003) for $\beta= 0.10$ ....	82
Figure 3.49 Comp. of experimental findings with Coleman et al. (2003) for $\beta= 0.23$ ....	83
Figure 3.50 Comp. of Bathymetry Data with Coleman et al. (2003) for $t= 2$ hours.....	85
Figure 3.51 Comp. of Bathymetry Data with Coleman et al. (2003) for $t= 4$ hours.....	85
Figure 3.52 Comp. of Bathymetry Data with Coleman et al. (2003) for $t= 8$ hours.....	86

Figure 4.1 Dimensions of the shortest abutment model (in cm).....89

Figure 4.2 A view of the flume and scour pattern when  $\beta= 0.452$  and  $t= 2$  hrs.....90

Figure 4.3 Top view of the illustration of scour hole.....91

Figure 4.4 Scour pattern after a 2 hrs period experiment for the contraction ratio  $\beta= 0.119$ : a) top view; b) 3-D view; c) longitudinal section view which is taken tangent to the toe of the abutment.....93

Figure 4.5 Scour pattern after a 4 hrs period experiment for the contraction ratio  $\beta= 0.119$ : a) top view; b) 3-D view; c) longitudinal section view which is taken tangent to the toe of the abutment.....94

Figure 4.6 Scour pattern after a 8 hrs period experiment for the contraction ratio  $\beta= 0.119$ : a) top view; b) 3-D view; c) longitudinal section view which is taken tangent to the toe of the abutment.....95

Figure 4.7 Scour pattern after a 2 hrs period experiment for the contraction ratio  $\beta= 0.185$ : a) top view; b) 3-D view; c) longitudinal section view which is taken tangent to the toe of the abutment.....96

Figure 4.8 Scour pattern after a 4 hrs period experiment for the contraction ratio  $\beta= 0.185$ : a) top view; b) 3-D view; c) longitudinal section view which is taken tangent to the toe of the abutment.....97

Figure 4.9 Scour pattern after a 8 hrs period experiment for the contraction ratio  $\beta= 0.185$ : a) top view; b) 3-D view; c) longitudinal section view which is taken tangent to the toe of the abutment.....98

Figure 4.10 Scour pattern after a 2 hrs period experiment for the contraction ratio  $\beta= 0.252$ : a) top view; b) 3-D view; c) longitudinal section view which is taken tangent to the toe of the abutment.....99

Figure 4.11 Scour pattern after a 4 hrs period experiment for the contraction ratio  $\beta=0.252$ : a) top view; b) 3-D view; c) longitudinal section view which is taken tangent to the toe of the abutment.....100

Figure 4.12 Scour pattern after a 8 hrs period experiment for the contraction ratio  $\beta=0.252$ : a) top view; b) 3-D view; c) longitudinal section view which is taken tangent to the toe of the abutment.....101

Figure 4.13 Scour pattern after a 2 hrs period experiment for the contraction ratio  $\beta=0.319$ : a) top view; b) 3-D view; c) longitudinal section view which is taken tangent to the toe of the abutment.....102

Figure 4.14 Scour pattern after a 4 hrs period experiment for the contraction ratio  $\beta=0.319$ : a) top view; b) 3-D view; c) longitudinal section view which is taken tangent to the toe of the abutment.....103

Figure 4.15 Scour pattern after a 8 hrs period experiment for the contraction ratio  $\beta=0.319$ : a) top view; b) 3-D view; c) longitudinal section view which is taken tangent to the toe of the abutment.....104

Figure 4.16 Scour pattern after a 2 hrs period experiment for the contraction ratio  $\beta=0.385$ : a) top view; b) 3-D view; c) longitudinal section view which is taken tangent to the toe of the abutment.....105

Figure 4.17 Scour pattern after a 4 hrs period experiment for the contraction ratio  $\beta=0.385$ : a) top view; b) 3-D view; c) longitudinal section view which is taken tangent to the toe of the abutment.....106

Figure 4.18 Scour pattern after a 8 hrs period experiment for the contraction ratio  $\beta=0.385$ : a) top view; b) 3-D view; c) longitudinal section view which is taken tangent to the toe of the abutment.....107

Figure 4.19 Scour pattern after a 2 hrs period experiment for the contraction ratio  $\beta=0.452$ : a) top view; b) 3-D view; c) longitudinal section view which is taken tangent to the toe of the abutment.....108

Figure 4.20 Scour pattern after a 4 hrs period experiment for the contraction ratio  $\beta=0.452$ : a) top view; b) 3-D view; c) longitudinal section view which is taken tangent to the toe of the abutment.....109

Figure 4.21 Scour pattern after a 8 hrs period experiment for the contraction ratio  $\beta=0.452$ : a) top view; b) 3-D view; c) longitudinal section view which is taken tangent to the toe of the abutment.....110

Figure 4.22 Var. of  $d_s/D$  with the contraction ratio for various experiment times.....112

Figure 4.23 Var. of  $X_s/D$  with the cont. ratio for various exp. times.....112

Figure 4.24 Var. of  $X_l/D$  with the contraction ratio for 2, 4 and 8 hrs.....113

Figure 4.25 Var. of  $X_r/D$  with the contraction ratio for 2, 4 and 8 hours.....113

Figure 4.26 Comparison of the values of  $X_l/D$  and  $X_r/D$  for the entire data.....114

Figure 4.27 Variation of the dimensionless radius with the contraction ratio.....114

Figure 4.28 Variation of the  $\alpha$  with the contraction ratio.....115

Figure 4.29 Variation of the  $\theta/\alpha$  ratio for all experimental sets.....115

Figure 4.30 Var. of  $V_s/D^3$  with the contraction ratio for various exp. times.....116

Figure 4.31 Var. of  $V_s/D^3$  with the dimensionless maximum scour depth.....116

Figure 4.32 Var. of  $d_s/D$  with the contraction ratio for various abutment type.....121

Figure 4.33 Var. of  $X_s/D$  with the contraction ratio for various abutment types.....122

Figure 4.34 Var. of  $X_s/D$  with  $d_s/D$  for various abutment types.....122

Figure 4.35 Var. of  $r/D$  with the contraction ratio for various abutment types.....123

Figure 4.36 Variation of  $\alpha$  with the contraction ratio for various abutment types.....124

Figure 4.37 Var. of  $V_s/D^3$  with the contraction ratio for various abutment types.....125

Figure 4.38 Var. of  $V_s/D^3$  with  $d_s/D$  for various abutment types.....126

Figure 4.39 Comparison of Equations (4.3) and (4.4).....	128
Figure 4.40 $V_s$ vs $d_s^3$ relation by using every experimental data .....	129
Figure 4.41 Pos. of the measurement sections for (a) $\beta= 0.119$ (b) $\beta= 0.452$ .....	132
Figure 4.42 Temporal changes of Bed Profiles at Section #1 for $\beta= 0.119$ .....	133
Figure 4.43 Temporal changes of Bed Profiles at Section #2 for $\beta= 0.119$ .....	134
Figure 4.44 Temporal changes of Bed Profiles at Section #3 for $\beta= 0.119$ .....	135
Figure 4.45 Temporal changes of Bed Profiles at Section #4 for $\beta= 0.119$ .....	136
Figure 4.46 Temporal changes of Bed Profiles at Section #5 for $\beta= 0.119$ .....	137
Figure 4.47 Temporal changes of Bed Profiles at Section #1 for $\beta= 0.452$ .....	138
Figure 4.48 Temporal changes of Bed Profiles at Section #2 for $\beta= 0.452$ .....	139
Figure 4.49 Temporal changes of Bed Profiles at Section #3 for $\beta= 0.452$ .....	140
Figure 4.50 Temporal changes of Bed Profiles at Section #4 for $\beta= 0.452$ .....	141
Figure 4.51 Temporal changes of Bed Profiles at Section #5 for $\beta= 0.452$ .....	142
Figure 4.52 Temporal development of scour depth for $\beta= 0.119$ .....	145
Figure 4.53 Temporal development of scour depth for $\beta= 0.452$ .....	145
Figure 4.54 Comp. of Experimental Findings with the past studies for $\beta= 0.119$ .....	150
Figure 4.55 Comp. of Experimental Findings with the past studies for $\beta= 0.452$ .....	151
Figure 4.56 Comp. of Bathymetry Data with Coleman et al. (2003) for $t= 2$ hours.....	153
Figure 4.57 Comp. of Bathymetry Data with Coleman et al. (2003) for $t= 4$ hours.....	153
Figure 4.58 Comp. of Bathymetry Data with Coleman et al. (2003) for $t= 8$ hours.....	154
Figure 5.1 Horizontal velocity data measurement planes around abutment.....	156

Figure 5.2 SonTek Micro ADV Device.....	156
Figure 5.3 Picture of a SCE abutment model at the non-erodible part of the flume.....	156
Figure 5.4 SCE abutment with abutment length, $L=15$ cm, and at flow depth, $D_1= 0.1D$ : (a) Streamwise velocity contours (b) Lateral velocity contours (c) Velocity contours in gravity direction (d) Streamlines of the flow (e) <i>tke</i> contours with streamlines.....	159
Figure 5.5 SCE abutment with abutment length, $L=15$ cm, and at flow depth, $D_2= 0.5D$ : (a) Streamwise velocity contours (b) Lateral velocity contours (c) Velocity contours in gravity direction (d) Streamlines of the flow (e) <i>tke</i> contours with streamlines.....	160
Figure 5.6 SCE abutment with abutment length, $L=25$ cm, and at flow depth, $D_1= 0.1D$ : (a) Streamwise velocity contours (b) Lateral velocity contours (c) Velocity contours in gravity direction (d) Streamlines of the flow (e) <i>tke</i> contours with streamlines.....	161
Figure 5.7 SCE abutment with abutment length, $L=25$ cm, and at flow depth, $D_2= 0.5D$ : (a) Streamwise velocity contours (b) Lateral velocity contours (c) Velocity contours in gravity direction (d) Streamlines of the flow (e) <i>tke</i> contours with streamlines.....	162
Figure 5.8 SCE abutment with abutment length, $L=35$ cm, and at flow depth, $D_1= 0.1D$ : (a) Streamwise velocity contours (b) Lateral velocity contours (c) Velocity contours in gravity direction (d) Streamlines of the flow (e) <i>tke</i> contours with streamlines.....	163
Figure 5.9 SCE abutment with abutment length, $L=35$ cm, and at flow depth, $D_2= 0.5D$ : (a) Streamwise velocity contours (b) Lateral velocity contours (c) Velocity contours in gravity direction (d) Streamlines of the flow (e) <i>tke</i> contours with streamlines.....	164
Figure 5.10 Spill-through abutment with abutment length, $L=8.9$ cm, and at flow depth, $D_1 = 0.1D$ : (a) Streamwise velocity contours (b) Lateral velocity contours (c) Velocity contours in gravity direction (d) Streamlines of the flow (e) <i>tke</i> contours with streamlines.....	165
Figure 5.11 Spill-through abutment with abutment length, $L=8.9$ cm, and at flow depth, $D_2 = 0.5D$ : (a) Streamwise velocity contours (b) Lateral velocity contours (c) Velocity	

contours in gravity direction (d) Streamlines of the flow (e) <i>tke</i> contours with streamlines.....	166
Figure 5.12 Demons. of parameters reg. the downstream recirculation region.....	169
Figure 6.1 Boundary conditions defined for the preliminary simulation.....	178
Figure 6.2 A view of the mesh constructed for the preliminary simulation.....	178
Figure 6.3 GUI of the software showing the Physics Tab of the model.....	180
Figure 6.4 Comp. of the vel. dist. obtained from sim. output with the theo. eq.....	180
Figure 6.5 A view of the mesh constructed for the flat bed (RNG) simulation.....	182
Figure 6.6 X-velocity comp. of RNG sim. at depth $z= 0.0675$ m.....	182
Figure 6.7 A view of the mesh constructed for the flat bed (LES) simulation.....	183
Figure 6.8 X-velocity comparisons of LES Simulation at depth $z= 0.0675$ m.....	184
Figure 6.9 The GUI of the sediment scour model.....	185
Figure 6.10 A view of the mesh constructed for the erodible bed simulation.....	186
Figure 6.11 The eroded bed bathymetry obtained after RNG Model.....	187
Figure 6.12 The eroded bed bathymetry obtained for $\theta_{cr} = 0.03852$ after 2 hours.....	188
Figure 6.13 The eroded bed bathymetry obtained for (a) $\theta_{cr} = 0.018$ , (b) $\theta_{cr} = 0.020$ ...189	189
Figure 6.14 The eroded bed bathymetry obtained for (a) $\theta_{cr} = 0.022$ , (b) $\theta_{cr} = 0.024$ ...190	190
Figure 6.15 The eroded bed bathymetry obtained for (a) $\theta_{cr} = 0.026$ , (b) $\theta_{cr} = 0.028$ ...191	191
Figure 6.16 The eroded bed bathymetry obtained for $\theta_{cr} = 0.030$ .....	192
Figure 6.17 Effect of $\theta_{cr}$ change on maximum scour depth.....	193
Figure 6.18 The eroded bed bathymetry obtained for (a) $\varphi = 0.005$ (b) $\varphi = 0.009$ .....	194

Figure 6.19 The eroded bed bathymetry obtained for (a) $\varphi = 0.012$ (b) $\varphi = 0.027$ .....	195
Figure 6.20 The eroded bed bathymetry obtained for (a) $\varphi = 0.036$ (b) $\varphi = 0.060$ .....	196
Figure 6.21 Effect of Entrainment Coefficient change on maximum scour depth.....	197
Figure 6.22 Effect of Bed Load Coefficient change on maximum scour depth.....	198
Figure 6.23 Comp. of bed profiles of simulation output and experimental results.....	200
Figure 6.24 Comp. of bed profiles of sim. outputs with coarse mesh and fine mesh....	201
Figure 6.25 The eroded bed bathymetry obtained for $L= 35$ cm and $t= 2$ hours.....	202

## LIST OF SYMBOLS

$A_p$  : unit area in sediment pickup equation

$A_l$  : abutment alignment factor

$C_D$  : drag coefficient

$C_u$  : uniformity coefficient

$D$  : flow depth

$D_1$  : depth at 0.1D above the flume bed

$D_2$  : depth at 0.5D above the flume bed

$D_c$  : critical flow depth

$d$  : particle sediment diameter

$d_{50}$  : median grain size

$d_s$  : maximum scour depth

$d_{se}$  : equilibrium scour depth

$E$  : sediment pickup rate

$F_d$  : densimetric Froude number

$Fr$  : Froude number

$f_s$  : volume fraction of sediment

$g$  : gravitational acceleration

$k$  : turbulent kinetic energy

$K$  : drag coefficient

$K_{y1}$  : K-coefficient stands for the effect of flow depth and abutment length (Melville and Coleman, 2000)

$K_I$  : K-coefficient stands for the effect of flow intensity (Melville and Coleman, 2000)

$K_d$  : K-coefficient stands for the effect of sediment size (Melville and Coleman, 2000)

$K_s$  : K-coefficient stands for the effect of abutment shape (Melville and Coleman, 2000)

$K_\theta$  : K-coefficient stands for the effect of foundation alignment (Melville and Coleman, 2000)

$K_G$  : K-coefficient stands for the effect of approach channel alignment (Melville and Coleman, 2000)

$L$  : abutment length perpendicular to the flow direction

$L_a$  : spill-through abutment base length perpendicular to the flow direction

$L_b$  : abutment length parallel to the flow direction (abutment width)

$L_1$  : the length of the downstream recirculation region perpendicular to the flow direction

$L_2$  : the length of the downstream recirculation region parallel to the flow direction

$L_c$  : the distance of the core of the downstream recirculation region to the abutment axis

$L_R$  : Characteristic length

$N$  : shape factor

$n_s$  : normal vector pointing outwards

$P$  : pressure

$Q$  : discharge

$q_b$  : volumetric bed load transport rate per unit width

$Q_{si}$  : volumetric rate of sediment inflow to the scour hole

$Q_{so}$  : volumetric rate of sediment pickup from the scour hole

$r$  : length parameter defined to identify the position of the maximum scour point in polar coordinates

$Re$  : Reynolds number

$R_i^*$  : Rouse Reynolds number

$R^2$  : coefficient of determination

$s$  : irregular coordinate axis defined around the abutment

$S_0$  : channel bed slope

$Sh$  : abutment shape factor

$t$  : time

$T_s$  : dimensionless time parameter

$t_e$  : equilibrium time

$tke$  : turbulence kinetic energy

$u$  : x-component of the velocity

$U$  : mean approach flow velocity

$\bar{u}$  : mean bulk fluid velocity

$U_c$  : critical mean approach flow velocity

$u_{drift}$  : drift velocity

$u_f$  : fluid velocity

$u_{lift}$  : lift velocity

$u_r$  : relative velocity

$u_s$  : sediment velocity

$u_*$  : bed shear velocity

$v$  : y-component of the velocity

$V$  : volume of sediment

$V_s$  : scour hole volume

$w$  : z-component of the velocity

$W$  : channel width

$x$  : primary axis in cartesian coordinate system

$X/D$  : symbol stands for both  $X_l/D$  and  $X_t/D$

$X_s$  : scour hole length in the flow direction measured from the most upstream point of the scour hole to the most downstream point

$X_l$  : scour hole length in flow direction measured from the upstream face of the abutment to the most upstream point of the scour hole

$X_t$  : scour hole length in the direction perpendicular to the flow measured from the tip of the abutment

$y$  : secondary axis in cartesian coordinate system

$y^+$  : dimensionless wall distance

$z$  : tertiary axis in cartesian coordinate system

$\alpha$  : angle defined to identify the position of the maximum scour depth location in polar coordinates

$\beta$  : contraction ratio

$\Delta$  : relative density

$\varepsilon$  : turbulent dissipation rate

$\rho$  : water density

$\bar{\rho}$  : mean bulk density

$\rho_s$  : sediment density

$\theta$  : angle of repose of the sediment material

$\theta_a$  : angle between the diagonal line starting from the abutment axis through abutment upstream corner

$\theta_i$  : local Shields parameter at the interface

$\theta_{cr,i}$  : dimensionless critical Shields parameter

$\nu$  : kinematic viscosity of water

$\omega$  : bed load coefficient

$\sigma_g$  : geometric standard deviation of the sediment size distribution ratio

$\lambda$  : coefficient in sediment pickup equation

$\phi$  : entrainment coefficient

$\phi_1$  : angle between flow and the upslope direction

$\phi_2$  : angle between the computed normal vector of the packed sediment interface and the gravitational vector,  $g$

## CHAPTER 1

### INTRODUCTION

#### 1.1 Background

Flow passing through blunt bodies has been among the major research topics in Fluid Mechanics for centuries. Flow around bridge hydraulic structures is one of the main application areas for this topic. In particular, for flow around bridge abutments, due to the existence of an obstruction in the flow direction, the flow converges towards the main channel and downflow is observed at the abutment upstream side wall. The primary vortex, which is comparable to the horseshoe vortex of bridge piers, develops as a result of these flow features. It is the main agent for local scour around bridge abutments (Kwan and Melville, 1994). Passing the abutment, the flow separates at the tip of the abutment and wake vortices develop at the separated regions. At the downstream side of the abutment, the downstream recirculation region forms. Main flow structures observed around an isolated bridge abutment is visualized in Figure 1.1.

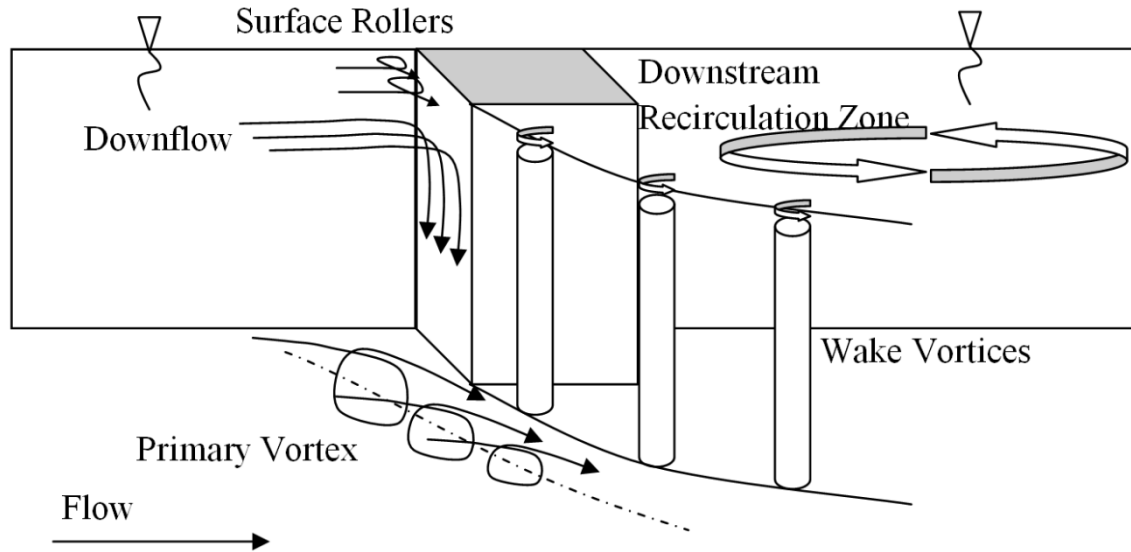


Figure 1.1 Visualization of flow structures around a bridge abutment

In practice, the most important outcome of the flow around bridge hydraulic structures is the scour developed around these structures. Scour is the river bed level decrease as a consequence of the erosion created by the flow. The excessive amount of it can threaten the bridge safety by leaving the footings exposed and vulnerable against the stream power. Yanmaz (2002) has briefly stated some of the bridge failures occurred in Turkey after 1990. Besides, Melville and Coleman (2000) analyzed some bridge failures occurred in New Zealand. The degree of scour is generally measured by the scour depth, which shows the amount of scour occurred compared to the natural bed level. The amount of scour can be controlled by some countermeasures, such as riprap layers and collars.

Melville and Coleman (2000) has categorized the scour occurred at bridge crossings in three groups as; (i) general scour, (ii) local scour and (iii) contraction scour. Figure 1.2 summarizes the scour types that can occur at a bridge crossing.

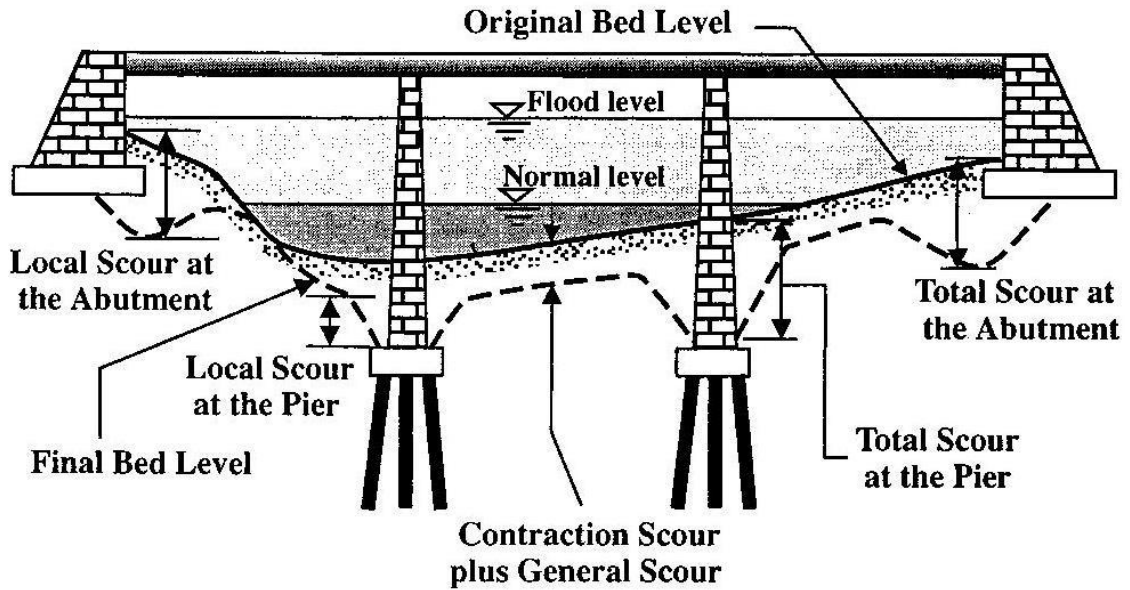


Figure 1.2 Scour types that can occur at a bridge crossing (Melville and Coleman, 2000)

General scour is defined as the scour that occurs on river bed independent of the existence of a bridge hydraulic structure. It occurs by the effect of human and natural causes, such as channel alterations, dam/reservoir construction, land-use changes, volcanic activities and climate change. The development of general scour may extend throughout several years. On the contrary, local scour and contraction scour occur due to the existence of a bridge or a river training structure like spur dike or groyne. These two are named as localized scour together. Local scour occurs only around the foundation of the hydraulic structures due to the erosive effect of the flow structures developed around the foundation. Due to the mean position of the primary vortex, which is the main source for the scour at bridge abutments, the scour initiates at the upstream side of the abutment tip which then extends through mostly downstream direction by time.

Temporal development of local scour around bridge piers and abutments is given in Figure 1.3. This figure was obtained after the early works of Chabert and Engeldinger

(1956) and shows that, the scour depth increases with time until the equilibrium scour depth value is reached. Compared to the live bed condition, equilibrium scour depth is slightly larger for clear water scour, which corresponds to the scour phase while there is not any sediment transport on the main channel bed. In the live bed scour case, which means that there is sediment transport at the main channel, sediment is transported into the scour hole from the main channel. In the clear water scour case, the stream power does not lessen by the bed load transport of sediment and this leads larger equilibrium scour depth values than the ones corresponding to the live bed scour case. It should be noted that, due to the sediment inflow to the scour hole, the equilibrium scour depth value oscillates around a time-averaged value in the live bed scour case.

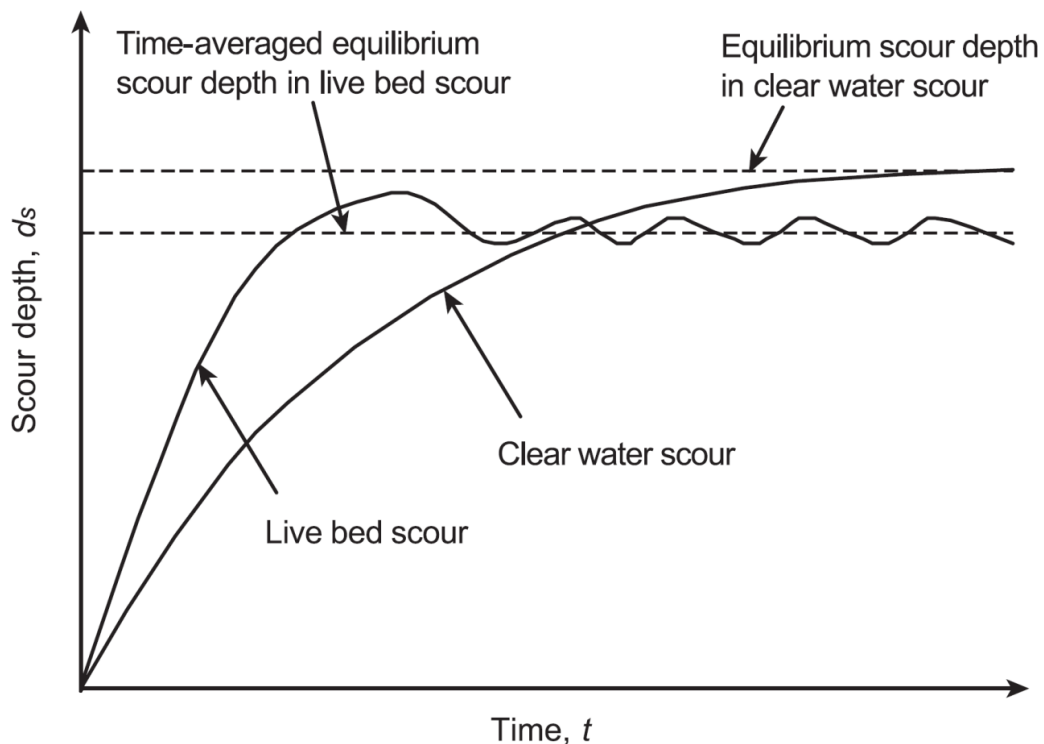


Figure 1.3 Temporal development of scour depth (after Chabert and Engeldinger, 1956)

In addition to the general and local scour, contraction scour occurs at bridge sites as a result of flow acceleration at the bridge crossings due to cross section constriction. Ballio and Orsi (2001) have stated that, the cross sectional area of the contracted section increases and the flow acceleration diminishes by the development of the scour hole in bridge crossings. It follows that, in calculating the total scour around a bridge hydraulic structure, the superposition of the obtained values of the local scour and contraction scour calculated by some methods available in literature is not an acceptable technique, which is applied mostly in design studies. Instead, the interaction of local scour and contraction scour should be analyzed carefully. Contraction scour is not observed on some small contraction degrees, however; the degree of it over which the contraction leads scour at contracted sections is not accurately determined in literature.

## 1.2 Dimensional Analysis

The scour at an unsubmerged bridge abutment depends on many parameters corresponding to the flow properties, fluid properties, bed material properties, abutment geometry and alignment, and time. The dependent parameter of the problem has been chosen as the scour depth in the most of the literature studies. Besides, there exists several dependent parameters of the study concerning the scour hole geometry. Equation (1.1) is written to define the parameters effecting scour around bridge abutments, considering homogeneous and alluvial bed material in straight rectangular channels. The right hand side of the equation consists of the dependent variables of the problem, whereas the right hand side includes the independent problem variables.

$$\left\{ \begin{array}{l} d_s \\ X_s \\ X_l \\ X_t \\ V_s \\ r \\ \alpha \end{array} \right\} = f(g, D, U, U_c, S_0, W, \rho, \vartheta, d_{50}, \sigma_g, \rho_s, L, \beta, Sh, Al, t) \quad (1.1)$$

where these parameters are as follows;  $d_s$  is the maximum scour depth,  $X_s$  is the scour hole length in the flow direction measured from the most upstream point of the scour hole to the most downstream point,  $X_l$  is the scour hole length in flow direction measured from the upstream face of the abutment to the most upstream point of the scour hole,  $X_t$  is the scour hole length in the direction perpendicular to the flow measured from the tip of the abutment,  $V_s$  is the scour hole volume,  $r$  is the length parameter defined to identify the position of the maximum scour depth location in polar coordinates,  $\alpha$  is the angle defined to identify the position of the maximum scour depth location in polar coordinates,  $g$  is the gravitational acceleration,  $D$  is the approach flow depth,  $U$  is the mean approach flow velocity,  $U_c$  is the critical mean approach flow velocity for entrainment of bed sediment,  $S_0$  is the channel bed slope,  $W$  is the channel width,  $\rho$  is the density of water,  $\nu$  is the kinematic viscosity of water,  $d_{50}$  is the median size of the bed material,  $\sigma_g$  is the geometric standard deviation of the sediment particle size distribution,  $\rho_s$  is the density of the sediment,  $L$  is the abutment length perpendicular to the flow direction,  $\beta$  is the channel contraction ratio and it has additional meaning besides abutment length if the contraction is achieved with more than one abutment,  $Sh$  and  $Al$  are the parameters describing the shape and alignment of the abutment, respectively and  $t$  is the time.

The dimensionless parameters were found using the Buckingham  $\pi$ -theorem by selecting  $\rho$ ,  $D$  and  $U$  as repeating variables. The dimensional analyses were applied and the following relation was obtained after arranging the terms;

$$\left\{ \begin{array}{c} d_s/D \\ X_s/D \\ X_l/D \\ X_t/D \\ V_s/D^3 \\ r/D \\ \alpha \end{array} \right\} = f \left( \frac{U}{\sqrt{gD}}, \frac{U}{U_c}, S_0, \frac{W}{D}, \frac{UD}{g}, \frac{d_{50}}{D}, \sigma_g, \frac{\rho_s}{\rho}, \frac{L}{D}, \beta, Sh, Al, \frac{Ut}{D} \right) \quad (1.2)$$

Here, it can be seen that, the term  $U/\sqrt{gD}$  is the Froude number of the approach flow,  $U/U_c$  is the flow intensity where critical flow occurs when it is equal to 1. Clear water flow conditions occur for values smaller than 1 and live bed flow conditions occur for values bigger than 1. The term  $UD/g$  is the Reynolds number of the flow. The effects of terms  $S_0$  and  $W/D$  were included in other terms, so, they can be excluded from the analysis. Besides, Breusers and Raudkivi (1991) showed that, for uniform bed material, the sediment coarseness does not have a significant effect on scour depth unless the sediment is relatively large with  $d_{50}/D > 0.02$ . Dongol (1994) has presented a similar conclusion with  $d_{50}/L > 0.02$ . Therefore,  $d_{50}/D$  was excluded from the analysis by keeping the analysis within the ranges presented above. In addition, the effects of the terms  $\rho_s/\rho$  and  $Al$  were eliminated by using constant relative density of sediment and placing the abutments vertically to the channel walls, respectively. In the present study, the approach flow conditions were remained constant which leads constant Froude number, Reynolds number and flow intensity. The bed material properties were remained as constant which makes  $\sigma_g$  constant. Then, the relation presented in Equation (1.2) was simplified into the relation given below;

$$\left\{ \begin{array}{c} d_s/D \\ X_s/D \\ X_l/D \\ X_t/D \\ V_s/D^3 \\ r/D \\ \alpha \end{array} \right\} = f(L/D, \beta, Sh, Ut/D) \quad (1.3)$$

In the framework of the study,  $L/D$  and  $\beta$  can be used interchangeably in the case of isolated abutment at bridge crossings. The use of only  $\beta$  is more reasonable for the case of contraction by using two abutments. In the present study abutment shape effect is taken into account by using two abutment types in the analyses. Besides, instead of using  $Ut/D$  as the time parameter the simple dimensional parameter,  $t$ , is used to denote the time in order to compare the results with the previous study results easily.

### 1.3 Objectives of the Present Study

The main objective of the study is to analyze flow passing an abutment and scour development around it by experimental and numerical approaches. The study aims to provide experimental material to the literature to help to analyze the problem in details and to make a study to test the competency of a numerical approach on the analysis of scouring around bridge abutments. The overall objectives of the study can be summarized as follows;

- Analyses on the time development of the scour pattern, which includes recording the temporal changes in the scour depth at several sections.
- Detailed analysis of the scour pattern at abutments after various experimental durations. This analysis includes obtaining several geometric variables of the scour pattern including various length parameters and the volume of the scour

hole. The analysis is extended by including the effect of varying abutment length on scour pattern.

- An analysis of the contribution of contraction scour on total localized scour around bridge abutments. This analysis includes the experiments conducted from low to very high contraction ratios.
- Measurement of flow field around abutments. The aim in these measurements is to identify major flow structures around the abutment and to make comparisons among various abutment lengths of two abutment types.
- A numerical analysis of the problem for erodible bed conditions. Although the three dimensional analysis of the sediment transport problem has not been solved accurately yet, the study aims to test the ability of a scour model available in the market. The analysis includes selecting the appropriate turbulence model solver for scour problems. The simulation results will be compared with the experimental findings of the study.

#### **1.4 Outline of the Thesis**

The presentation of the works done within this study is covered in 7 chapters including the present Introduction chapter. The outline of the thesis is given as follows. Chapter 2 includes the literature review with the reviews of the scholars studied abutment scour experimentally and numerically. Chapters 3, 4 and 5 include the presentation of the experimental works conducted within the present study. In particular, Chapter 3 provides the details of the scour experiments conducted using an isolated bridge abutment with giving the general laboratory conditions of the whole study. Chapter 4 gives details about the scour experiments conducted using two abutments to contract the bridge crossing. Chapter 5 provides the velocity field measurements and corresponding analysis using two abutment types. Chapter 6 presents the numerical analysis of the problem, which were conducted for flat bed and erodible bed cases separately. Chapter 7 is the Conclusion chapter which presents a summary of the study and the recommendations for the future researches.



## **CHAPTER 2**

### **LITERATURE REVIEW**

Bridge scour problem has attracted a numerous number of researchers in the history of science. These studies are mainly collected in two groups. The first group of studies is extended to more early dates and investigated the problem with experimental approaches. They searched for the empirical solutions of the problem. The second group of researches has started with the development in the numerical and computational techniques. They tried to obtain a reliable numerical model for the scour problem. By the increase in the computer processing capabilities, recently some progress has been achieved for this type of study. The two headlines of this chapter will cover these two groups and the review of the researches will be presented in detail within this chapter.

The problems of pier scour and abutment scour have treated to be similar by some early researchers. However, now it is acknowledged that boundary layers created by the presence of side walls near abutments affect the complexity of the flow around abutments, this fact differs these two problems. Therefore, the problems of pier scour and abutment scour should be treated separately. In this chapter, the studies dealing with pier scour are mainly disregarded with some exceptions which were reviewed to underline some notable issues which will help to analyze the present study. Besides, as the structures like, spur dikes and groins have similar boundaries like abutments; the studies for these structures are also reviewed in the present study.

The studies in the literature mainly focused on the clear water scour. As it is being the case in the present study, mainly the studies concerning clear-water scour are reviewed in this chapter.

## **2.1 Experimental Studies**

The earliest studies of the bridge scour problems were experimental studies. In a general manner, experimental studies can be classified in 4 groups in terms of the aim of the studies. The first group of the studies is the ones searching for the mechanisms creating the scour. This group of studies generally used the experimental findings conducted in flat bed channels. It includes the studies investigating velocity distribution, vortex developments and bed shear stresses around abutments. The second group of the studies tried to obtain relations among the parameters of the study and the equilibrium scour depth,  $d_{se}$ . The studies dealing with the effect of contraction differs from the other studies, as most of the studies in the literature analyzed the problem for only local scour effect. The studies examined the contraction scour are grouped separately in this review chapter. Another experimental study group can be classified as the studies searching for the temporal development of scour depth. In reality, in practice the equilibrium scour depth is never reached, so the importance of the latter group shines by giving more applicable results. The review of the experimental studies will be presented under the headings of these 4 groups of studies.

### **2.1.1 Scour Mechanisms**

Since the researchers showed interest on scour problems, several studies have investigated the mechanisms leading to the scour process. Among the early researches on this issue, Rajaratnam and Nwachukwu (1983) studied on the bed shear stresses around a groin in a planar bed and they showed that, an increase in the bed shear stress at the upstream corner of the groin occurs, which is around five times of the value observed at the approach channel. Ahmed and Rajaratnam (2000) studied on the flow

field around wing-wall abutment and they concluded that the bed shear stress ratio measured near the abutment nose and at the approach channel is 3.63.

Kwan (1988) investigated the velocity field around short wing-wall abutments. After analyzing the developed vortex regions around abutments, he addressed the primary vortex, which is similar to the pre-defined horseshoe vortex in bridge piers, as the main cause for the scour around abutments. Then, Kwan and Melville (1994) measured the flow field around a wing-wall bridge abutment with hydrogen bubble technique. They conducted recordings at the sections around abutment. They expressed the existence of a secondary vortex next to the primary vortex with counter rotational direction and having an inverse effect on scour development compared to the primary vortex. Also, in the same study it is stated that the maximum value of the downflow velocity was measured to be 75% of the approach flow velocity.

Molinas et al. (1998) conducted an experimental study to measure velocity field around vertical wall abutments for various contraction ratios. They have used contraction ratios,  $\beta = 0.1, 0.2$  and  $0.3$  in their experiments. They have recorded the velocity data by using two devices; a pitot tube and a 2D electromagnetic current meter. The velocity values were recorded in vertical sections with varying longitudinal coordinates. They have resulted the maximum amplification of velocity as 1.5 times the approach velocity and maximum amplification in shear stress up to 10 times the approach channel shear stress.

Dey and Barbhuiya investigated the turbulent flow field around abutments in different studies for vertical wall abutments, wing-wall abutments and semicircular abutments; for planar bed and scoured bed cases separately (Barbhuiya and Dey (2003), Barbhuiya and Dey (2004), Dey and Barbhuiya (2005a), Dey and Barbhuiya (2005b), Dey and Barbhuiya (2006a), Dey and Barbhuiya (2006b)). They measured the flow data with ADV and obtained Reynolds stresses besides the velocity gradients. They demonstrated the existence of the primary vortex at the upstream of the abutment for the plane bed

cases and within the scour hole for the scoured bed cases. Controversially, the flow field at the downstream is observed as chaotic mainly due to the vortex shedding for the flow past the abutment.

Chrisohoides and Sotiropoulos (2003) demonstrated the coherent structures at the upstream recirculation zone of a rectangular abutment by using digital photography technique. They made an analysis on coherent time scale for the formation of eddies within the upstream recirculation zone. Besides, Koken (2005) expressed that, Chen and Ikeda (1997) published their study on the investigation of downstream recirculation zone. They stated that, this zone extends up to 14 abutment lengths long downstream.

### **2.1.2 Equilibrium Scour Depth**

After Chabert and Engeldinger (1956) introduced the presently well-known equilibrium scour depth, the studies mainly concentrated on the estimation of it and tried to establish design methods for the problem. The researchers concentrated mostly on pier scour rather than abutment scour in the early research period. However, there exist some early works studied abutment scour such as, Garde et al. (1961), Laursen (1962) and Laursen (1963). In the manual prepared by Breusers and Raudkivi (1991), while giving a detailed design methodology for bridge piers, it is stated that the abutment scour design methodology was offered for some limited cases due to the lack of data in the literature.

Then, Melville (1992) offered a methodology for the local scour around abutments by using the experimental data of the studies done at the Auckland University of New Zealand. He presented the data of large number of experiments. In the study, abutments are categorized with respect to length as short abutments for  $L/D < 1$ , long abutments for  $L/D > 25$  and intermediate abutments for  $1 < L/D < 25$ , where L stands for abutment length and D stands for flow depth. Also it was suggested that, choosing L for short abutments and y for long abutments as the characteristic length is appropriate. He proposed the methodology by considering flow intensity, flow depth, sediment size, sediment

gradation, abutment length, abutment shape, abutment alignment and approach channel geometry as variables. According to Melville (1992)'s method; the variation of equilibrium scour depth is directly proportional to the flow intensity ( $U/U_c$ ) for clear water scour and constant for live bed scour case. The effect of flow depth and abutment length was summarized as follows; the equilibrium scour depth is in the order of  $2L$  for short abutments,  $10D$  for long abutments and  $2*(DL)^{0.5}$  for intermediate abutments. Abutment shape was taken into account by considering four types of abutments; vertical wall abutment, vertical wall abutment with semicircular end, wing wall abutment and spill-through abutment. Each type got a multiplier in the methodology, while vertical wall abutment giving the highest scour depth, spill-through abutment gave the least scour depth among all. Although the method has practical advantages, the author stated that, for his study, the effects of sediment size, gradation and river channel geometry took part conservatively in the method due to the shortage of data, and the method was open to development.

On the discussion of Melville (1992), Richardson and Richardson (1993) stated, by relying on their field experience that, the proposed method was conservative as the effect of river geometric characteristics were not included appropriately into the design method. Afterwards, the analysis for compound channels were done by Melville (1995) and Cardoso and Bettess (1999). Melville (1997) made some developments to the abutment scour prediction methodology proposed by Melville (1992). By the help of additional experiments, the method was developed mostly considering the sediment size effect. Melville and Coleman (2000) have improved this model more.

Melville and Coleman (2000) stated that, by the help of the experimental data of Dongol (1994), for uniform size sediment, the effect of sediment size on scour depth is negligible for the range of  $L/d_{50} > 50$ . A similar argument was stated by Breusers and Raudkivi (1991). They stated that, for  $D/d_{50} > 50$ , where  $D$  being the flow depth, the effect of sediment size on scour depth is small.

Lim (1997) proposed a semi empirical approach for the local scour around abutments for clear-water case. The analysis was based on continuity equation, scour geometry, the law of resistance on the alluvial channels and his experimental results together with the previous experimental results. An equation was developed including the effects of approach flow depth, sediment particle size, abutment length, approach flow velocity and viscosity. The effect of abutment shape was included into the equation by the method developed by Melville (1992). The ability of this methodology was limited with the range of the experiments.

Kohli and Hager (2001) and Kayatürk (2005) demonstrated that the change in width of the abutment, parallel to the flow direction, has no significant effect on scour development. Meanwhile, Kothyari and Raju (2001) introduced the term ‘analogous pier’, which is defined as the pier having the same equilibrium scour depth with the given abutment under similar hydraulic conditions.

### **2.1.3 Contraction Scour**

The studies in literature generally focused on the local scour part of the localized scour and disregarded the contraction scour occurring due to the decrease in flow area in the bridge crossings. Laursen (1960), Laursen (1963), Vanoni (1975), Gill (1981) and Webby (1984) investigated the constriction scour on erodible beds. However, they focused on the smooth constriction of the channel, which is unlike of the contraction scour part of the localized scour. In localized flow, while the mean velocity of the channel increases due to the decrease in flow area, the interaction of mean flow with the vortices occurred around abutments makes the problem more complicated. Therefore, the contraction scour differs from the constriction scour with smooth transition. As the effect of contraction cannot be analyzed by separating it from the local effect due to the placement of the abutment, the analyses were focused on the limiting cases where the effect of contraction is significant on the scour. From Ballio and Orsi (2001)’s literature

survey; it is observed that the contraction ratio has significant effect on scour for contraction ratios greater than 0.09 – 0.10 (Cunha (1973) and Franzetti et al. (1994)).

In their manual, Breusers and Raudkivi (1991) have demonstrated Liu et al. (1961)'s experimental data showing the effect of contraction ratio on scour depth. The experiments were carried out for thin vertical spurs and abutments, on live bed scour conditions, in two flumes with different width. They observed no trend on the variation of the scour depth with contraction ratio.

Ballio and Orsi (2001) investigated the effect of contraction on the maximum scour depth. They obtained channel contraction by not changing the abutment length but changing the flume width. They noted no significant increase in the scour depth with the increase in contraction ratio for contraction ratios up to 0.33. They only noted a considerable increase in scour depth for the largest contraction ratio they tried, which is 0.50. Also, it was noted that the models in the literature for contraction scour estimations makes overestimations up to 300%, as they don't count the effect of flow area increase in the contracted cross-section by the temporal development of scour hole. They stated that, the linear superposition of local scour depth and contraction scour depth values gathered from the models in the literature was not reasonable.

Ballio et al. (2009) investigated the constriction effects on clear-water scour. Also, they took temporal development of the scour depth into account. They conducted experiments for uniform sediment size and offered a scour enhancement function for the constriction effects, which was defined as valid within the range of experimental data measured in the study.

#### **2.1.4 Temporal Variation of Scour Pattern**

Generally the floods in the nature do not last so long to permit the development of equilibrium scour depth. Therefore, knowing the scour pattern at any time before it

reaches the equilibrium state has a significant importance on the precise design of the bridge structures. While, the studies concerning the temporal variation of pier scour has developed much earlier, similar studies for abutment scour has improved only in the last years. Cardoso and Bettess (1999) investigated the temporal evolution of scour at abutments for the channels with floodplains. Although they showed the asymptotic behavior of the scour depth increase with time, they concentrated mainly on the influence of floodplain on the main flow.

When Ballio and Orsi (2001) studied on the temporal variation of scour pattern around abutments, they could not find much study in the literature handled the similar topic. They conducted experiments for uniform sediment size in the clear-water case. The variation of the experiment set was obtained by changing contraction ratios. They measured the scour height at nine sections around abutment. By this purpose, they obtained geometric characteristics of the scour hole by interpolating the measured data. They have measured the bed levels with either depth gage or with a laser proximity sensor. There exists no information in the article on how they took the temporal depth measurements. Although Lim (1997) reported the equilibrium time for any abutment scour as 3-8 days, Ballio and Orsi (2001)'s data did not show any sign of reaching equilibrium phase after runs lasted even for 5 weeks.

Then Oliveto and Hager (2002) conducted experiments to search for the temporal development of pier and abutment scour. All experiments were conducted for vertical wall abutment with varying lengths. They concluded their study with an equation giving scour depth as a function of time. Oliveto and Hager (2005) have developed the methodology by conducting over 150 experiments. They added sloping abutments into account and also they concluded to add a limiting minimum abutment length which equals to 0.05 m in a channel with a width of 1 m because of the boundary layer development.

Coleman et al. (2003) introduced another model for the temporal development of abutment scour. The model is based on the design methodology offered by Melville and Coleman (2000). They have conducted experiments for uniform sediment size with clear-water conditions. Scour depths were measured by using an ultrasonic depth recorder at varying time intervals.

Dey and Barbhuiya (2005) introduced a semi empirical model for the solution of the temporal development of scour depth for short abutments. The experiments of the study were conducted under clear-water conditions for uniform and non-uniform sediment sizes by using vertical wall, wing wall and semicircular abutments. The model was constructed based on the mass balance on the scour hole and the sediment entrainment function developed by Dey and Debnath (2001). After constructing the model a first order differential equation was obtained for the solution of time development of scour depth and it was solved with fourth order Runge Kutta method. The model was developed further and calibrated with experiment data. Effect of sediment gradation was included in the model. While it was stated that, the model agreed well with the experiment data, it was added that, especially for nonuniform sediments, the model gave higher scour depths than the experimental data at the initial stages of the scouring process. The reason of it was explained as the lack of the ability to include armor effect into the model. The model was compared with the experimental data of Ballio and Orsi (2001) and Kohli and Hager (2001) for vertical wall abutment experiments. It was seen that, the model gave higher results at the initial stages, while gave smaller results at the final stages. However, the comparison of the model with the previous studies for 45° wing-wall abutments (Wong (1982) and Tey (1984)) showed that, the model gave more reasonable results for 45° wing-wall abutments. Although it was explained that, the durations of the tests were not sufficient, it was seen that the tests for the uniform sediment did not reach the equilibrium stage, while the tests for non-uniform sediment reached the equilibrium stage.

Kumcu et al. (2007) has carried out a research on the temporal development of scour around a bridge abutment while a collar was placed as a countermeasure.

Yanmaz and Kose (2007) have presented the results of their experimental study. They introduced their model for the temporal development of local scour depth around abutments. The experiments were carried out under clear water conditions, for vertical wall abutments and for uniform sediment. Within the study, 23 experiments were conducted lasting up to six hours. The equilibrium time could not be reached at the experiments, but it was stated that, the rate of increase in scour depth decelerated significantly in six hours. The offered model was compared with Oliveto and Hager (2002) and Coleman et al. (2003), and it showed an agreement with those models. Also, in the same study, an equation was tried to be obtained for the scour hole area and the volume. Measurements were taken at some sections around abutment, and the geometry of the scour hole was approximated to the inverted semi cone with a rectangular base.

Then, Yanmaz and Kose (2009) introduced their semi empirical model for the solution of temporal development of scour depth based on the sediment continuity equation and the sediment pickup function under clear water scour conditions. Use of sediment pickup function is given below;

$$Q_{so} = \lambda \frac{EA_p}{\Delta\rho_s} \quad (2.1)$$

where  $Q_{so}$  stands for the volumetric rate of sediment pickup from the scour hole,  $\lambda$  is the coefficient including the effects of scour hole geometry, flow and sediment properties,  $E$  is the sediment pickup rate proposed by Dey and Debnath (2001),  $A_p$  is the unit area from which the sediment is picked up and  $\Delta$  and  $\rho_s$  are sediment properties. The model was constructed based on the sediment continuity in the scour hole given below;

$$\frac{dV}{dt} = Q_{so} - Q_{si} \quad (2.2)$$

where the rate of change of volume was obtained by the development of the method offered by Yanmaz and Kose (2007), and  $Q_{si}$  indicated the sediment inflow to the scour hole which equals to zero for clear-water scour. The rate of change of scour hole volume was calculated in terms of abutment length and width, scour depth and angle of repose of the sediment. The side angles of the scour hole were accepted as equal to the angle of repose of the sediment and the shape of the scour hole was approximated to the inverted

semi cone with a rectangular base. The experiments for the study were conducted under clear-water conditions, for vertical wall abutments and uniform sediment size with two different  $d_{50}$  values of 1.8 mm and 0.9 mm. The conducted experiments were lasted up to six hours. The ability of the proposed model was tested for the experiment data and compared with the previous studies of Oliveto and Hager (2002) and Coleman et al. (2003). It was stated that the proposed model had a higher predictive ability and also it was stated that Coleman et al. (2003) model resulted smaller scour depths, while Oliveto and Hager (2002) model resulted higher scour depths than the experimental results.

## **2.2 Numerical Studies**

Researches dealing with the scour problem using numerical techniques have increased in number recently by the developments in computer processing capabilities. Numerical simulations have started with 2-D simulations due to the practical reasons. In these studies, the problem was modeled in terms of depth-averaged parameters and by this manner, the developed model required less number of grid points and reduced computer processor capabilities compared to the 3-D models. The aims of all studies including 2-D and 3-D models were to model the vortex flow field around abutments and to investigate the sediment behavior inside the scour hole. Mainly, the researches using numerical approaches were divided into two groups; (i) the researches simulating the problem for non-erodible bed and (ii) the researches simulating the problem for erodible bed. The first group of researchers conducted CFD simulations with non-erodible bed to analyze and model the vortex flow field around bridge abutments. Second group of researchers have simulated the flow with erodible bed to model the sediment motion within the scour hole making equilibrium and temporal scour depth analyses. In this numerical studies part of the literature review chapter, the two headings will cover the studies done for non-erodible and erodible beds.

### **2.2.1 Studies for Non-Erodible Bed**

Non-erodible bed simulations were done to model the flow field around bridge abutments. The early studies handled the problem with 2-D models, although it should be handled with 3-D models due to the high three dimensionality of the problem.

According to Morales and Ettema (2013); 2-D models give ideas about some limited parameters by using the depth averaged quantities and these models have practical advantages due to the reduced amount of cell size compared to 3-D models. Among the early studies; Zaghloul and McCorquodale (1973), Liu et al. (1994) and Biglari and Sturm (1998) modeled the problem by using 1400, 3000 and 8000 computation cells, respectively. They have observed the separation line and the velocity increase region due to the contraction. Morales and Ettema (2013) compared the 2-D simulation outputs with the experimental data at spill through abutment in a compound channel. They investigated the velocity and unit discharge values at the contracted section and observed strong correlation with the experimental data. They used the computer software FESWMS developed by Federal Highway Administration of US to model depth averaged simulations.

In spite of some of its advantages, 2-D models could not answer most of the questions arising for the abutment scour problems. The 3-D models require more processing resources than the 2-D models; however they gave valuable information related to complex flow physics around the abutments. The early 3-D CFD models of the open channel flow problems were done by Krishnappan and Lau (1986), Prinos (1990), Naot et al. (1993) and Pezzinga (1994) mainly concerning on the uniform open channel flow on the compound channels. Among the studies for bridges; Mayerle et al. (1995) have constructed a 3-D model for the flow around a spur dike. They constructed a finite element-finite differences mixture model solving time dependent nonlinear Navier-Stokes equations, where eddy viscosity term was computed with six alternative ways. The time derivative was solved explicitly with fourth order Runge-Kutta method and they assumed hydrostatic pressure distribution. They observed some worthy correlations after comparing the simulation results with experimental data, some inconsistencies are also observed with the experimental data which was based on the use of hydrostatic pressure distribution assumption.

Oullion and Dartus (1997) have constructed a 3-D model for the flow around groyne by using  $k-\varepsilon$  turbulence model. The constructed mesh has included around 9000 grid points. They also assumed hydrostatic pressure distribution except very close locations to

groyne. They compared the results with the experimental findings and they gave importance mainly on the prediction of the downstream recirculation area. The model underestimated the recirculation area slightly by 7%.

Chrisohoides et al. (2003) modeled the fluid flow around an abutment by using 3-D unsteady RANS simulations with  $k-\omega$  turbulence model. They used a grid with  $1.16 \times 10^6$  node points. By the help of the large grid size, they analyzed the flow features more consistently. As making the simulation for flat bed conditions, they observed the position of bed shear stress increase at the tip of the abutment, where local scour would take place.

Koken and Constantinescu (2008a) and (2008b) have analyzed the initiation and the final stages of the scouring process around spur dikes by using LES turbulence model with  $Re = 18000$ . The first study analyzed the coherent structures at the initiation of the scouring. The simulations were conducted for a flat bed channel to visualize the vortices at the initiation of the motion. Also, by dye visualization experiments the vortices were observed physically. An unstructured mesh was generated with around  $4 \times 10^6$  elements. The minimum grid spacing was 0.7 non-dimensional wall units ( $y^+$ ) near all solid boundaries and  $y^+ = 4$  to 10 at the zones inside the vortex flow field. The velocity and 2-D streamline comparisons with the experiments gave good correlations. The temporal and the spatial changes of the vertical flow structures within the flow field were investigated in the study. The primary vortex was found to undergo bimodal aperiodic oscillations which resulted in an increase on the pressure fluctuations and the Turbulence Kinetic Energy ( $tke$ ).

The second study (Koken and Constantinescu (2008b)) investigated the vortex flow field around bridge abutments at the final stages of the scouring process. By this manner, an equilibrium scour hole bathymetry obtained from an experiment was fitted to the bed of the channel and the simulations were performed for non-erodible bed. This study has showed that, while the flow past the abutment, some eddies of the detached shear layer were randomly entrained to the downstream recirculation area. This evolution was pointed out as the main reason for the motion of the deposition area through

downstream. The authors of this study have suggested using 3-D eddy-resolving CFD models to handle the scour problem.

Koken and Constantinescu (2009) have analyzed the problem by using DES turbulence model. They conducted simulations for two Reynolds numbers ( $Re= 5 \times 10^5$  and  $Re= 18000$ ) to account for the scale effects. It was stated that; with the increase in Reynolds Number, the eddy content of the Detached Shear Layer and the coherency of the eddies increased significantly. By comparing the verification results, it has stated that DES model shows higher competency for high Reynolds number flow.

Teruzzi et al. (2009) have constructed an LES model with  $1.57 \times 10^6$  nodes, for the flow past a trapezoidal abutment. They focused on the coherent structures at the upstream side of the abutment, as well as shear and normal stresses at the solid boundaries. They concluded that; the maximum mean bed shear stress values observed at a small area at the upstream of the abutment explains the initial period of the scouring process. However, the mean values would not be sufficient to analyze the whole scour phenomena; instead, fluctuation parts should be inserted into the analyses.

Koken and Constantinescu (2011) have used DES model to analyze the flow past a bridge abutment with a scour hole around it at a Reynolds number of 240000. This study was aimed to explain the coherent structures at the final stages of the scouring. The bathymetry was obtained from an experiment conducted till the equilibrium was reached. The simulations were conducted for flat bed and with scour hole cases and for high and low Reynolds number cases also. The meshes of the models were generated containing up to  $7.4 \times 10^6$  cells. As a consequence of the experiments, the shape of the equilibrium scour hole was observed to be changing with Reynolds number. Some conclusions of the simulations were related with this fact, such as; while there was a second necklace vortex observed for high Reynolds number flow which was not observed for low Reynolds number flow. Additionally, it was seen that, Reynolds number change affected the instabilities in the flow. On the contrary, the turbulence amplifications within the primary vortex zone were found to be independent of Reynolds number. Also, the developing scour hole had a stabilizing effect on the primary vortex.

Koken (2011) have performed detached eddy simulations for the flow around bridge abutments with approach flow angles; 60, 90 and 120 degree for flat bed conditions. It was observed that larger scour depths were expected for 60 degree case because of the increasing eddy producing capacity of the increased upstream recirculation area in that case. On the other hand, the largest scour hole area was expected for the 90 degree case at which the abutment was placed perpendicular to the channel wall.

### **2.2.2 Studies for Erodible Bed**

There exists very limited number of studies in the literature concerning the computational model of the flow around bridge abutments with erodible bed. This type of model should include a sediment scour model in order to achieve the observation of the transport of bed material through or outward to the scour hole. Modeling sediment motion has always been a challenge for researchers and a reliable model has not been offered yet. There exist some studies including scour mechanism in literature like, Duc and Rodi (2008), which has investigated the long contraction of a channel without any obstruction. Since the mechanism in this type of problems is totally different, they have been excluded in this literature review.

Olsen and Melaaen (1993) have modeled the sediment scour around circular piers with  $k-\varepsilon$  turbulence model. They have constructed their sediment scour model based on the convection-diffusion equation. They have neglected the transient terms in the model and modeled the sediment motion with bed load formulas. They calibrated their model with the scour depth value of the experimental study by iterations and after that process, scour hole geometry fitted well with the experimental one. Olsen and Kjellesvig (1998) have developed the previous analysis by including the transient terms. They solved for the scour around a circular pier. They used the same methodology to solve the sediment scour and compared the results of the maximum scour depth with the empirical equations. They obtained close results with some of the empirical methods. However,

they have not compared the shape of the resultant bathymetry with the empirical cases and they have applied the method to just one case.

Zhang et al. (2005) have modeled the scour around spur dikes. They simulated the flow past a number of spur dikes. For turbulence closure  $k-\varepsilon$  model was used. In handling the sediment scour, they used a semi-empirical equation based on the mass conservation of sediment. In this study, sediment motion within the scour hole was defined by modified bed load equations. They compared the results of scour profiles and flow fields with the experiment results and obtained a reasonable agreement.

Nagata et al. (2005) have studied the 3D modeling of flow field and scour mechanism around river hydraulic structures, including spur dikes. They have modeled turbulence with  $k-\varepsilon$  model. The sediment scour and deposition was modeled based on the sediment pick up and deposition equations. The main principle of the method was the sediment mass momentum equation written for the scour hole. Sediment pickup rate was used as introduced by Nakagawa (1986). After comparing the velocity profiles of non-erodible bed simulations with the previous experiment results, they obtained good agreement. Then, in another case, the simulations were run for the erodible bed. The results of the model were tested by comparing them with the results of the experimental study of Michuie and Hinokidani (1992). The correlation was searched in terms of maximum scour depth values and the results showed a reasonable agreement.

Kayser and Gabr (2013) have made analysis for pier scour using FLOW-3D. They used a mesh with 48000 cells with no refinement around the obstacle. They searched for the optimum values of the coefficients used in the model and they ended up with 0.018 and 5.7 for entrainment and bed load coefficients, respectively. They have compared the value of maximum scour depth with in situ measurements and empirical equations. They have observed good correlations with the values.

## **CHAPTER 3**

### **MORPHOLOGICAL CHANGES ON RIVER BED AROUND AN ISOLATED BRIDGE ABUTMENT**

The measurements of bed elevation changes were taken by two methods after placing a single vertical wall abutment with semicircular end (SCE Abutment) within the sediment storage part of the flume (Figure 3.1). In the first method, the experiment was conducted and after the experiment has been finished running, the bathymetry of the eroded bed was measured. In the second approach, the bed profiles around the abutment were simultaneously recorded while the experiments were running. In the first type of experiments, various abutment lengths were used for different test durations; whereas in the second type, the experiments were repeated several times for obtaining bed profiles at different cross-sections for the selected two abutment lengths. All the measurements were taken with an Ultrasonic Ranging System (Figure 3.2).

With the help of these experiments, the effect of abutment length variation on scour pattern for various test durations, and the temporal changes on bed elevations were obtained.

The three headings cover this chapter. First, the general experimental conditions in the laboratory are discussed which is also valid for all of the experimental work conducted within this thesis. The following two headings cover the presentation of the results with the two experimental approaches under: “Bathymetry Measurements” and “Temporal Scour Measurements” headings.

#### **3.1 General Experimental Conditions**

All experiments of this study were conducted at METU Hydraulics Laboratory. A laboratory flume was used in the experiments with 28.5 m length and 1.5 m width. The

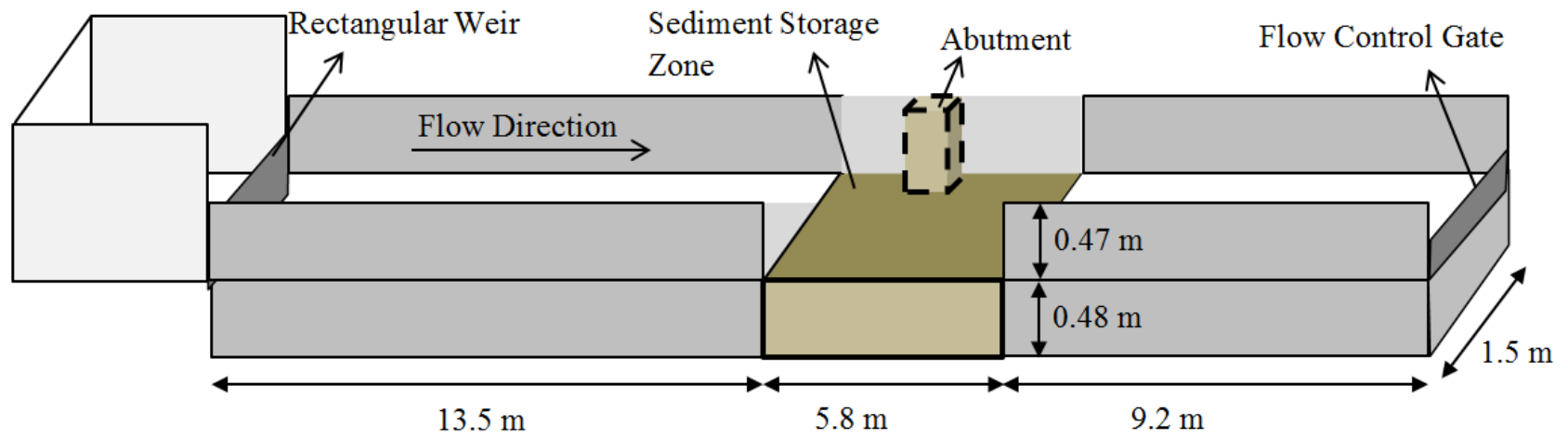


Figure 3.1 A schematic representation of the flume



Figure 3.2 Seatek Ultrasonic Ranging System

flume is rectangular in cross-section with bed slope,  $S_0 = 0.001$ . The flume includes a sediment storage region of 5.8 m length and 0.48 m depth, located 13.5 m downstream of the entrance of the flume. The inlet flow to the flume was controlled by a weir and flow regulators. There is a tail water gate at the outlet to control the flow depth in the flume. Figure 3.1 demonstrates a schematic representation of the flume including the dimensions and Figure 3.3 shows a picture taken at the upstream of the flume.

The sediment storage portion of the flume was filled with uniform and erodible sand material with the following properties; median grain size,  $d_{50} = 1.5$  mm, geometric standard deviation of the sediment size distribution ratio,  $\sigma_g = 1.29$ , angle of repose,  $\theta = 30^\circ$  and uniformity coefficient,  $C_u = 1.7$ . The same roughness height was obtained in the remaining parts of the flume by pasting sand particles of  $d_{50} = 1.5$  mm to the flume bed by means of a cement slurry. Sieve analysis graph of the sand material is given in Appendix A.

All the experiments were conducted under clear-water conditions. The flow intensity value,  $U/U_c = 0.90$ , was used for the flow in the flume. This value was selected as it gives scour depth values close to maximum while keeping the stable clear water conditions in the flume. Also, in the literature, most of the scour studies were conducted

at clear water conditions; therefore, the selection of clear-water flow gives the ease in comparing results with the previous works. The discharge and the velocity of the flow were determined in the following way; preliminary experiments were conducted in the flume with no abutment model installed, starting with a small value, the discharge was increased gradually and the threshold of bed motion was observed visually. The discharge, flow depth and average flow velocity were recorded at the threshold condition and then, while keeping the discharge constant, the flow depth was increased by the help of tail water gate to have mean velocity,  $U$ , to be 0.9 times the critical velocity,  $U_c$ , measured for the threshold conditions. By this manner, the discharge of the flow, the velocity at the main channel and the flow depth were obtained as  $Q= 67.8$  lt/s,  $U= 0.335$  m/s and  $D= 0.135$  m, respectively. The Froude number and the Reynolds number of the flow were calculated as 0.29 and 45000, respectively.



Figure 3.3 Laboratory flume view from upstream with no abutment models installed

Although, in this study, the critical velocity and the intensity of the flow were obtained from visual observations, the value of the critical shear velocity was also calculated with both the empirical formulas found in literature and the parameters obtained from the experiment to make a comparison. The obtained values agreed well with the theoretical ones. The calculations about this comparison are given in Appendix B.

The experiments were conducted by using two abutment types: SCE abutment and spill-through abutment. All abutment models were produced from plexiglass material in the laboratory. The experiments covered in this chapter were conducted by using SCE abutment. Figure 3.4 shows the model dimensions of the shortest SCE abutment model. The remaining abutment models were obtained by adding 5 cm long rectangular prisms to the wall-end of the shortest abutment model while keeping the abutment width constant as  $L_b = 10$  cm.

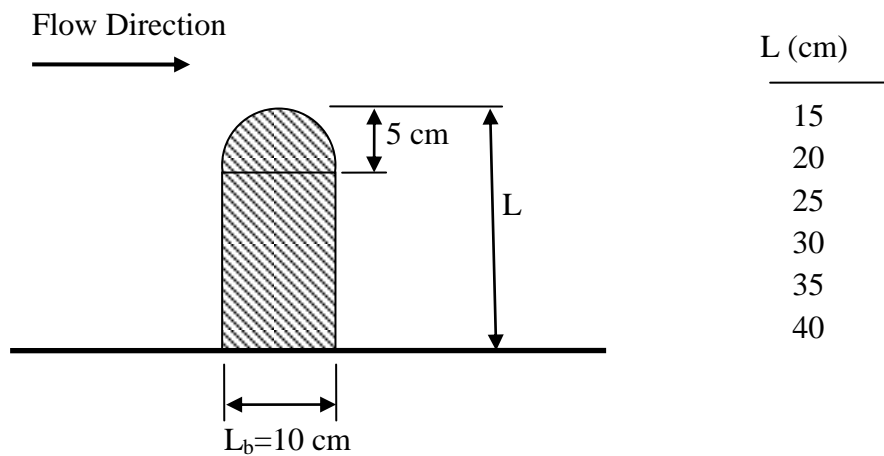


Figure 3.4 Dimensions of the SCE abutment

The measurements of the eroded bed were taken by the Seatek Ultrasonic Ranging System (Figure 3.2). The Ultrasonic Ranging System records the data by its transducers via transmitting sonic waves. For data recording, 34 transducers were available for use at METU Hydraulics laboratory, having 3 plates of transducers including 8 transducers in

each and 10 single transducers. Maximum 32 transducers could be installed for data recording at the same time due to the limitations of the device. While taking the measurements, the transducers of the device were placed on a mobile carrier installed above the flume (Figure 3.5). The transducers were kept exactly parallel to the flume base and checked with bubble level at the beginning of each recording. The transducers were also kept submerged during the recording as they can transmit and receive data only while they are inside water.



Figure 3.5 The transducers while data recording

### **3.2 Bathymetry Measurements**

17 sets of experiments were conducted to examine the effect of abutment length on the scour pattern for different test durations while a single SCE abutment was installed. The

eroded bathymetries were measured after the tests. By this manner the relations of the important parameters of the problem, with varying abutment lengths were obtained. Analyses of the scour pattern were made for each case after taking bathymetry measurements. The experiment durations were selected as two, four and eight hours.

This section includes the “Experimental Equipment and Procedure” and “Results” parts, which are given in detail below.

### **3.2.1 Experimental Equipment and Procedure**

A single SCE abutment was placed vertically to the flow direction in the sediment storage part of the flume. six abutments of various lengths were tested within this experimental set. Figure 3.3 shows the abutment dimensions and the tested abutment lengths. The tests were run for two, four and eight hours of durations. Table 3.1 shows the test conditions for the bathymetry measurements. For the longest abutment length,  $L= 40$  cm, the eight hour long experiment resulted with a scour hole which extended up to the opposite wall of the flume. As this situation changes the characteristics of flow and the structure of the scouring agents, this test was excluded from the experimental set.

While conducting the experiments, the inlet vane of the flume was opened gradually with small increments. This was done not to disturb the erodible flume bed with waves. The start of the test durations were counted after the desired flow depth and discharge were reached. When the test duration has been reached, the inlet vane and the tailwater gate were closed to fill the flume with water as the measurement device can only record the data within water. In doing this, any additional scouring around the abutments were not observed. The measurements were taken by the Ultrasonic Ranging System (Figures 3.2 and 3.5). Starting from the upstream of the abutment, the bathymetry measurements were taken by scanning the flume bed around the abutment with one cm intervals by the help of mobile carrier of the transducers. After the measurement recording finished, the water in the flume was discharged and the bed was flattened to make it ready for the next set. The experiments were started from the beginning for each set separately.

Table 3.1 Test Conditions

Set Nr.	$L$ (cm)	$t$ (hrs.)	$D$ (cm)	$d_{50}$ (mm)	$L/W$	$L/L_b$
1	15	2	13.5	1.50	0.100	1.5
2	15	4	13.5	1.50	0.100	1.5
3	15	8	13.5	1.50	0.100	1.5
4	20	2	13.5	1.50	0.133	2.0
5	20	4	13.5	1.50	0.133	2.0
6	20	8	13.5	1.50	0.133	2.0
7	25	2	13.5	1.50	0.167	2.5
8	25	4	13.5	1.50	0.167	2.5
9	25	8	13.5	1.50	0.167	2.5
10	30	2	13.5	1.50	0.200	3.0
11	30	4	13.5	1.50	0.200	3.0
12	30	8	13.5	1.50	0.200	3.0
13	35	2	13.5	1.50	0.233	3.5
14	35	4	13.5	1.50	0.233	3.5
15	35	8	13.5	1.50	0.233	3.5
16	40	2	13.5	1.50	0.267	4.0
17	40	4	13.5	1.50	0.267	4.0

### 3.2.2 Results

After the measurements have been taken, the obtained data have been digitalized. For each case, 3-D views of the scour pattern, top views of the scour pattern and the longitudinal sections taken tangent to the toe of the abutment are given in Figures 3.6 to 3.22, where  $x/D$  stands for the dimensionless coordinate through the flow direction taking abutment axis as origin and  $z/D$  stands for the dimensionless changes in the bed bathymetry while zero being the original bed level, below zero corresponds to the scouring and above zero corresponds to the deposition regions. The change in  $z/D$  is demonstrated by contour lines and colored scaling. The scoured areas are shown with dashed contour lines, while the deposition regions are shown with full lines.

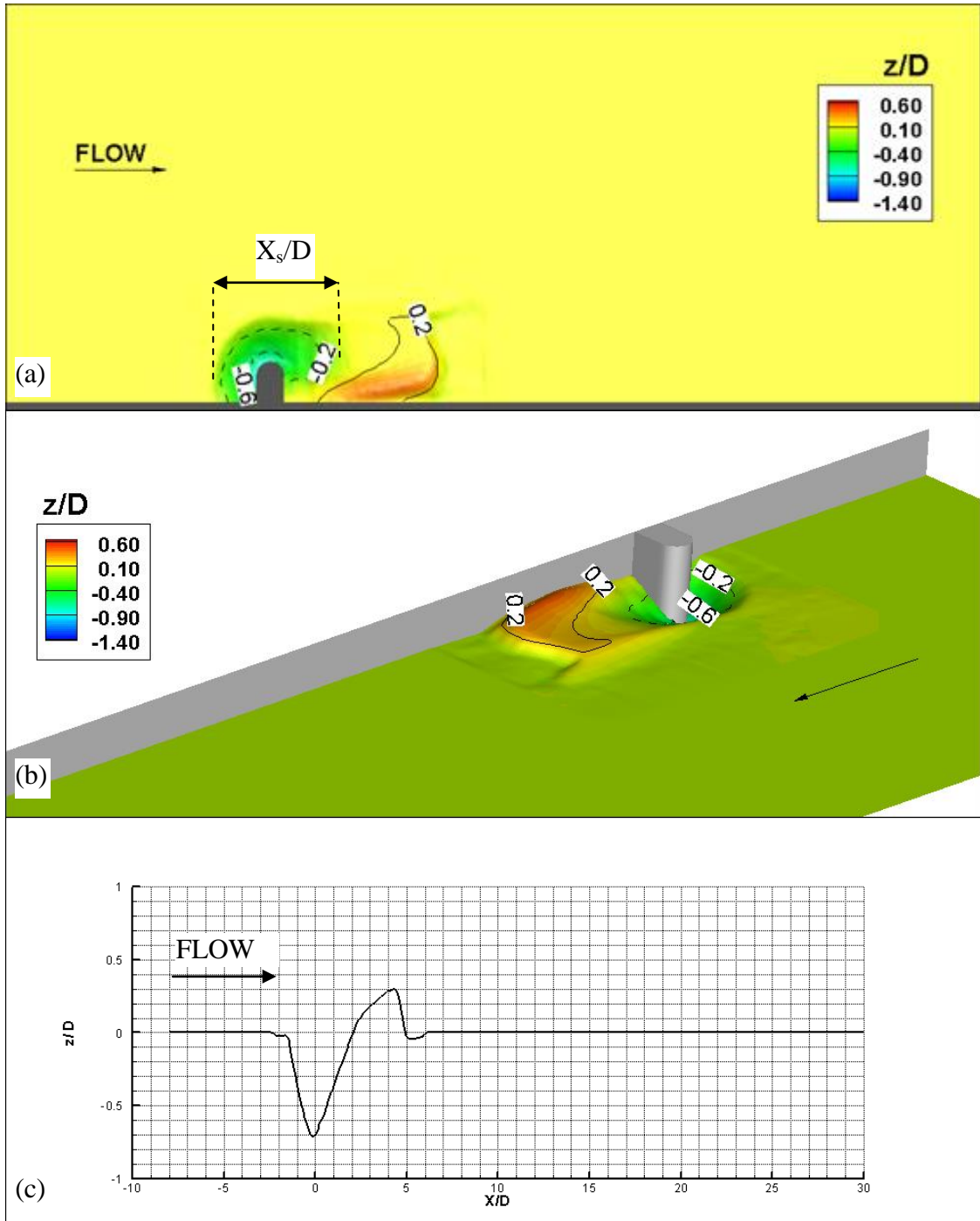


Figure 3.6 Scour and deposition pattern after a 2 hours test duration for the abutment length,  $L=15$  cm: a) top view; b) 3-D view; c) 1-D section view which is tangent to the tip of the abutment

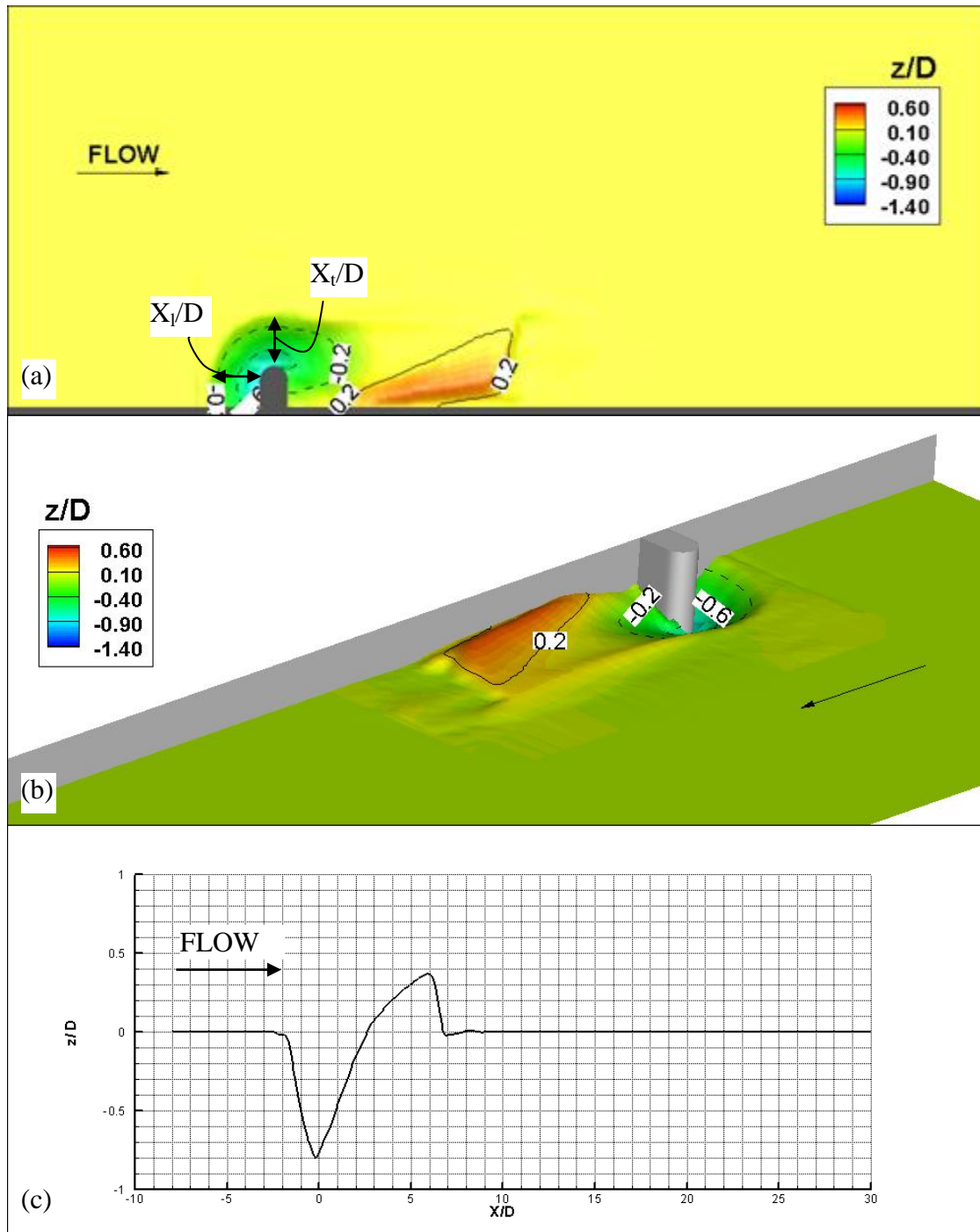


Figure 3.7 Scour and deposition pattern after a 4 hours test duration for the abutment length,  $L=15$  cm: a) top view; b) 3-D view; c) 1-D section view which is tangent to the tip of the abutment

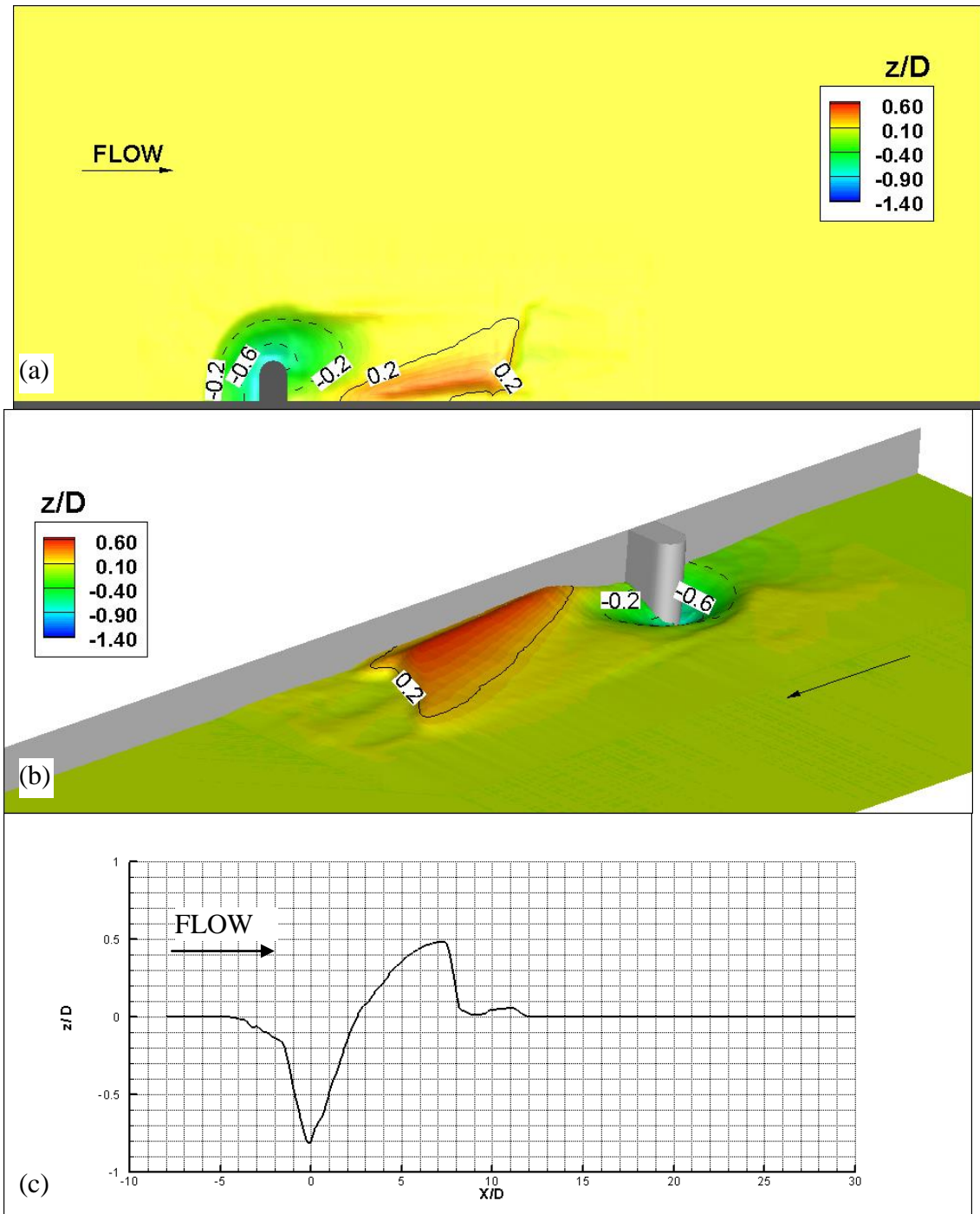


Figure 3.8 Scour and deposition pattern after an 8 hours test duration for the abutment length,  $L=15$  cm: a) top view; b) 3-D view; c) 1-D section view which is tangent to the tip of the abutment

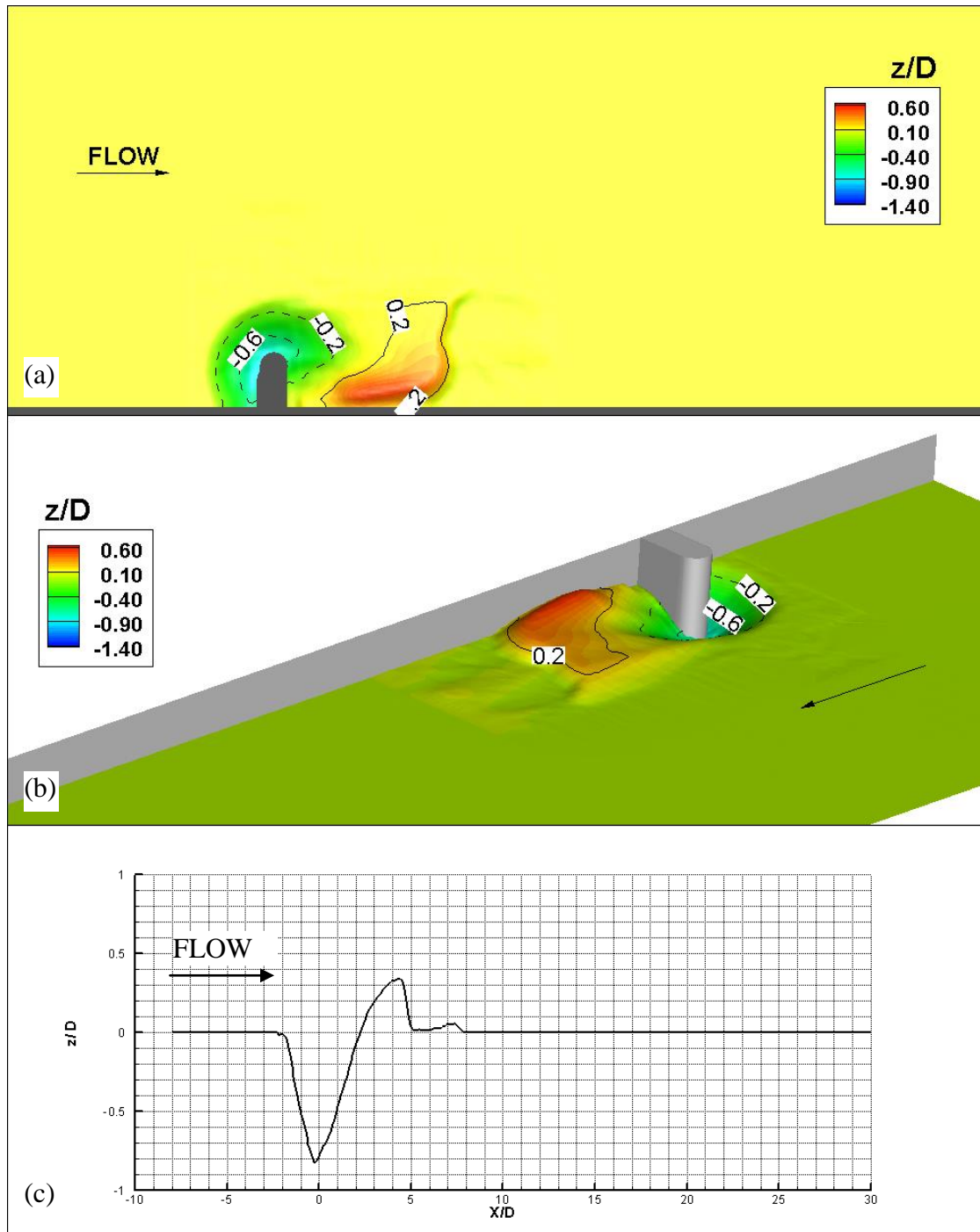


Figure 3.9 Scour and deposition pattern after a 2 hours test duration for the abutment length,  $L=20$  cm: a) top view; b) 3-D view; c) 1-D section view which is tangent to the tip of the abutment

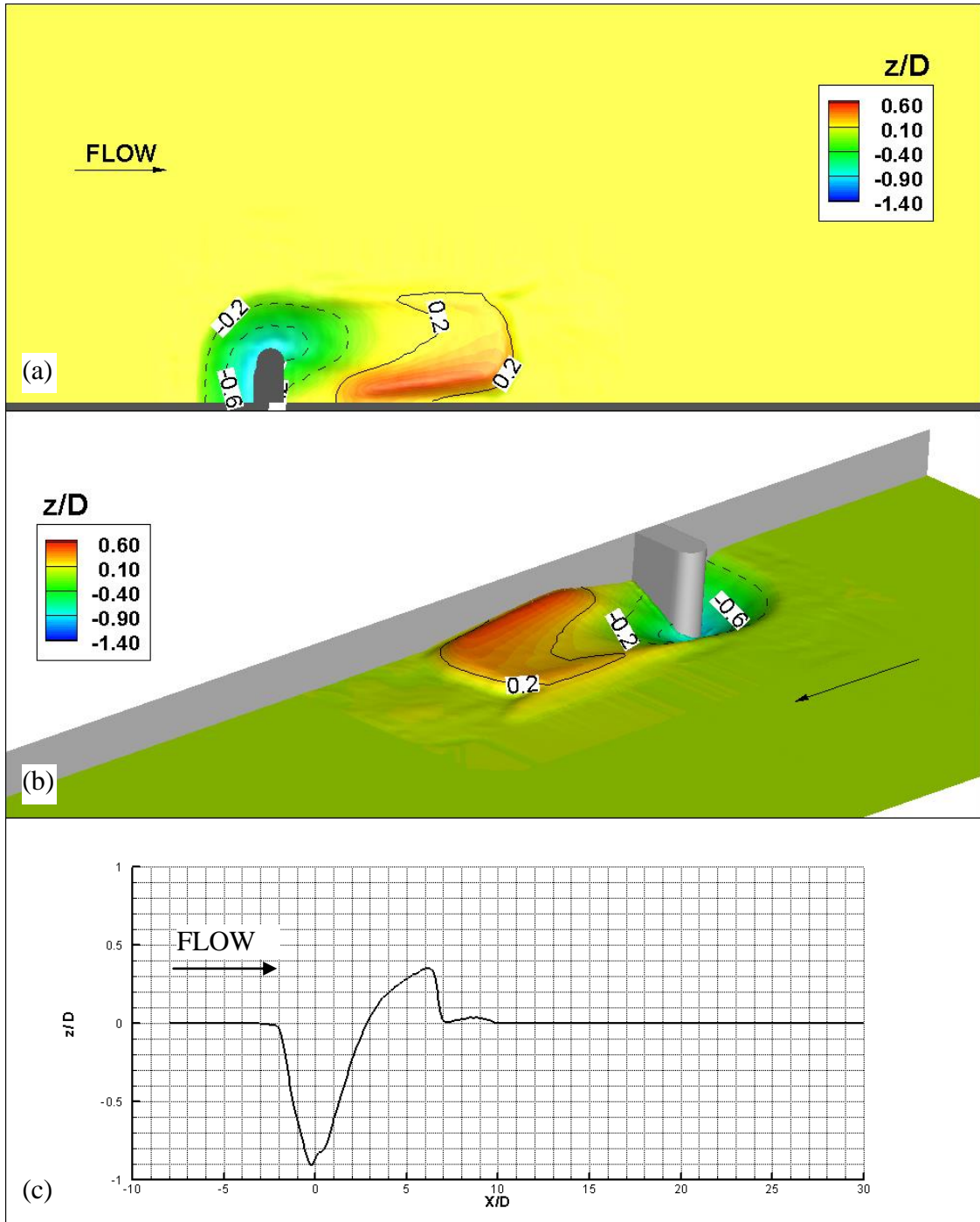


Figure 3.10 Scour and deposition pattern after a 4 hours test duration for the abutment length,  $L=20$  cm: a) top view; b) 3-D view; c) 1-D section view which is tangent to the tip of the abutment

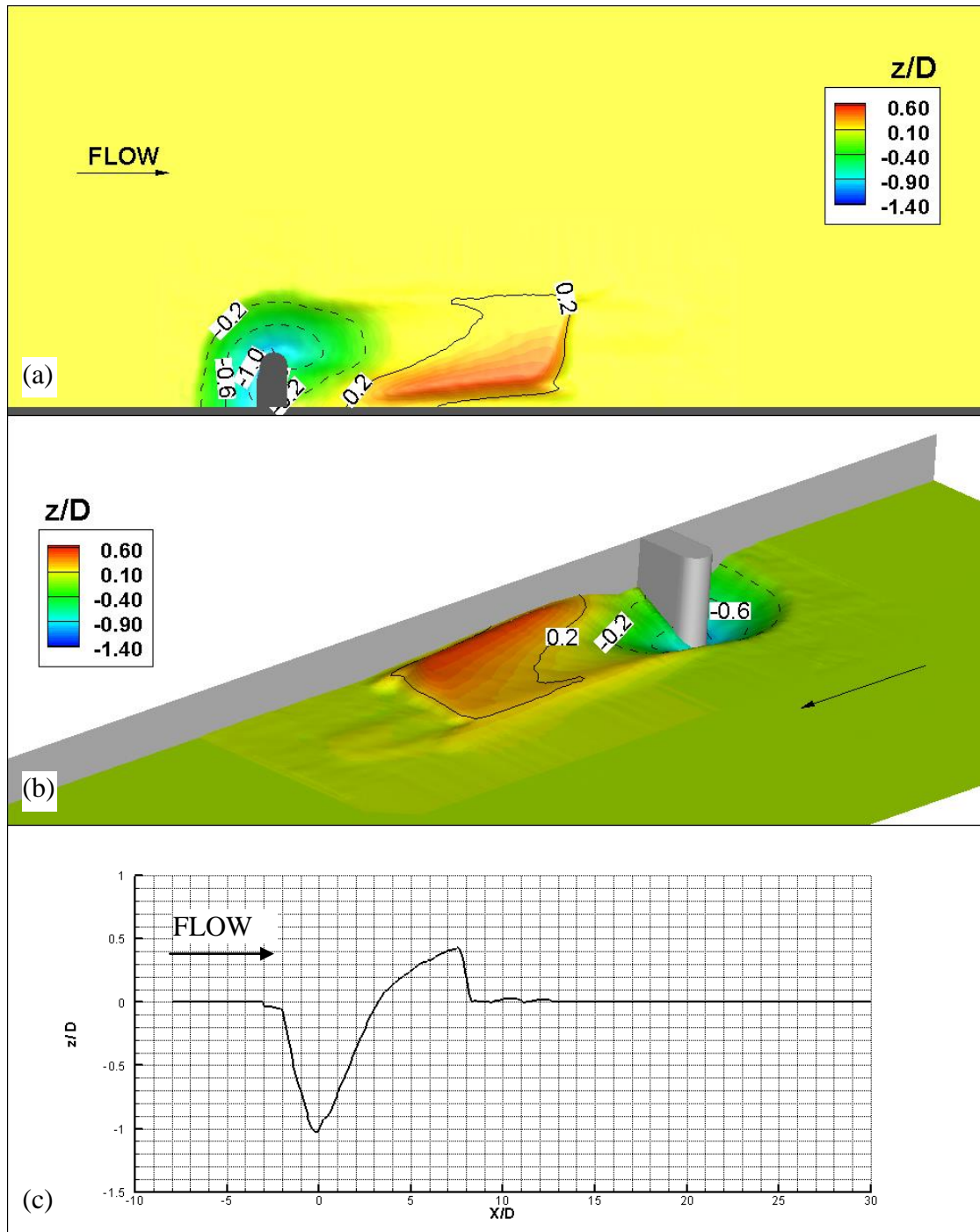


Figure 3.11 Scour and deposition pattern after an 8 hours test duration for the abutment length,  $L=20$  cm: a) top view; b) 3-D view; c) 1-D section view which is tangent to the tip of the abutment

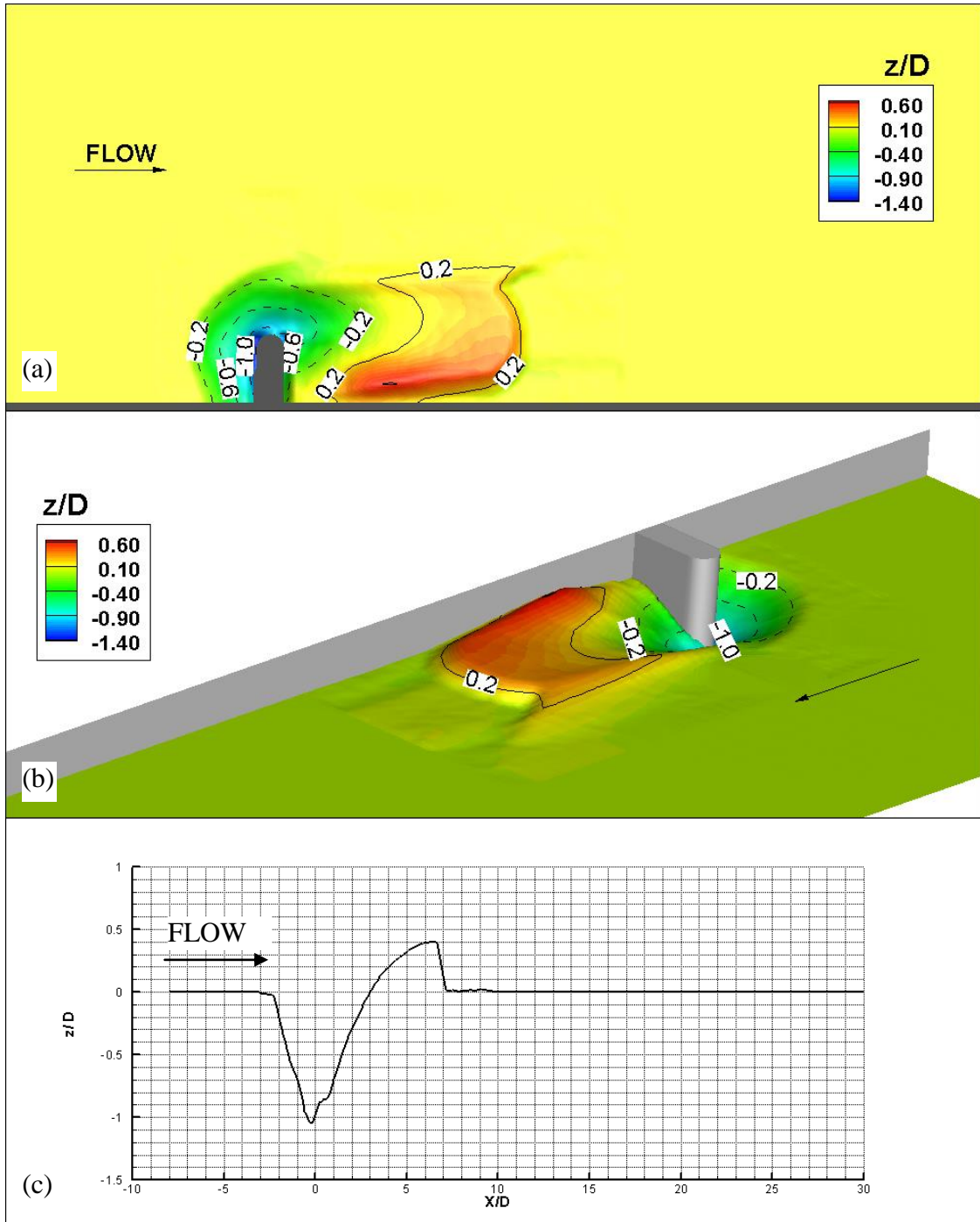


Figure 3.12 Scour and deposition pattern after a 2 hours test duration for the abutment length,  $L=25$  cm: a) top view; b) 3-D view; c) 1-D section view which is tangent to the tip of the abutment

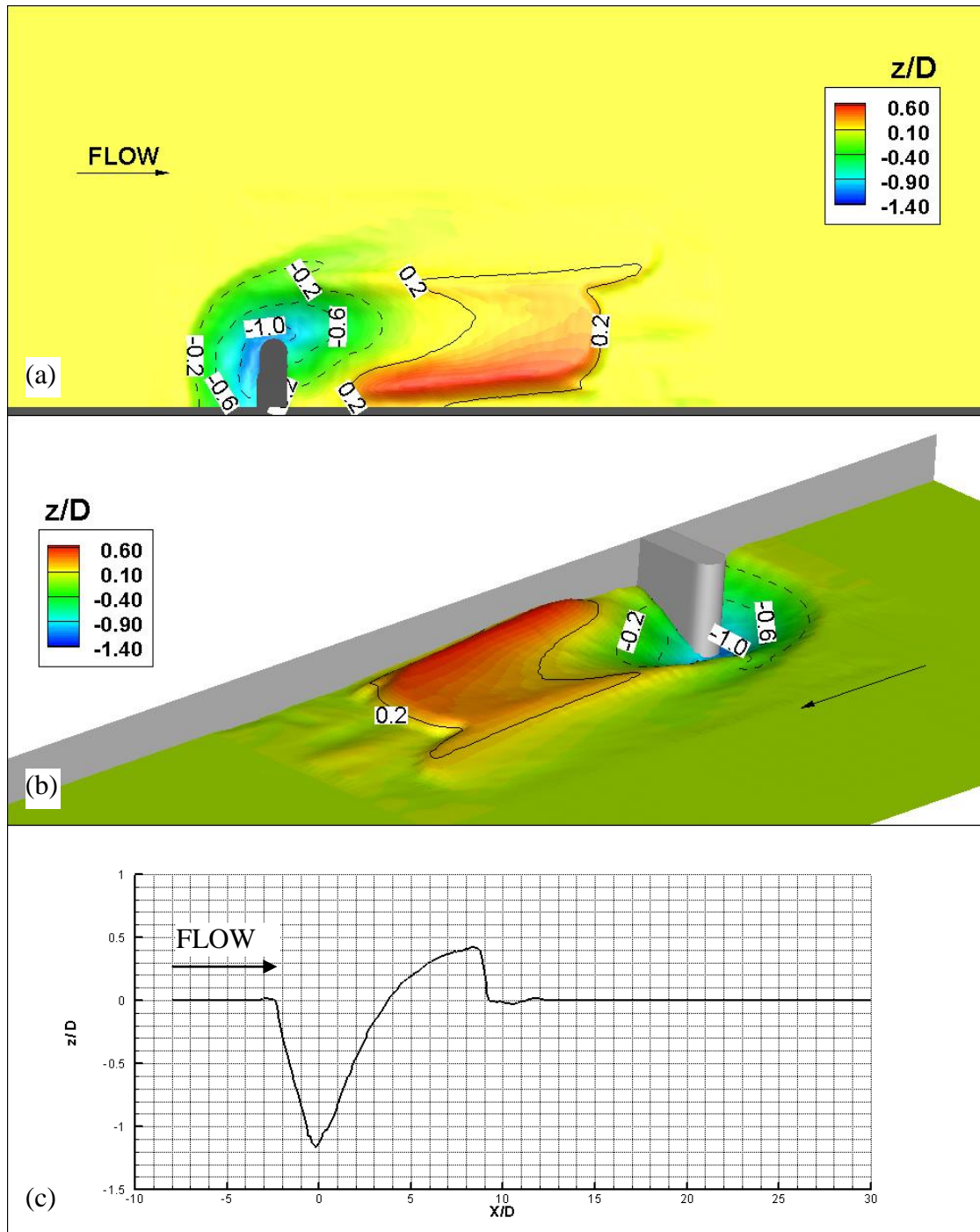


Figure 3.13 Scour and deposition pattern after a 4 hours test duration for the abutment length,  $L=25$  cm: a) top view; b) 3-D view; c) 1-D section view which is tangent to the tip of the abutment

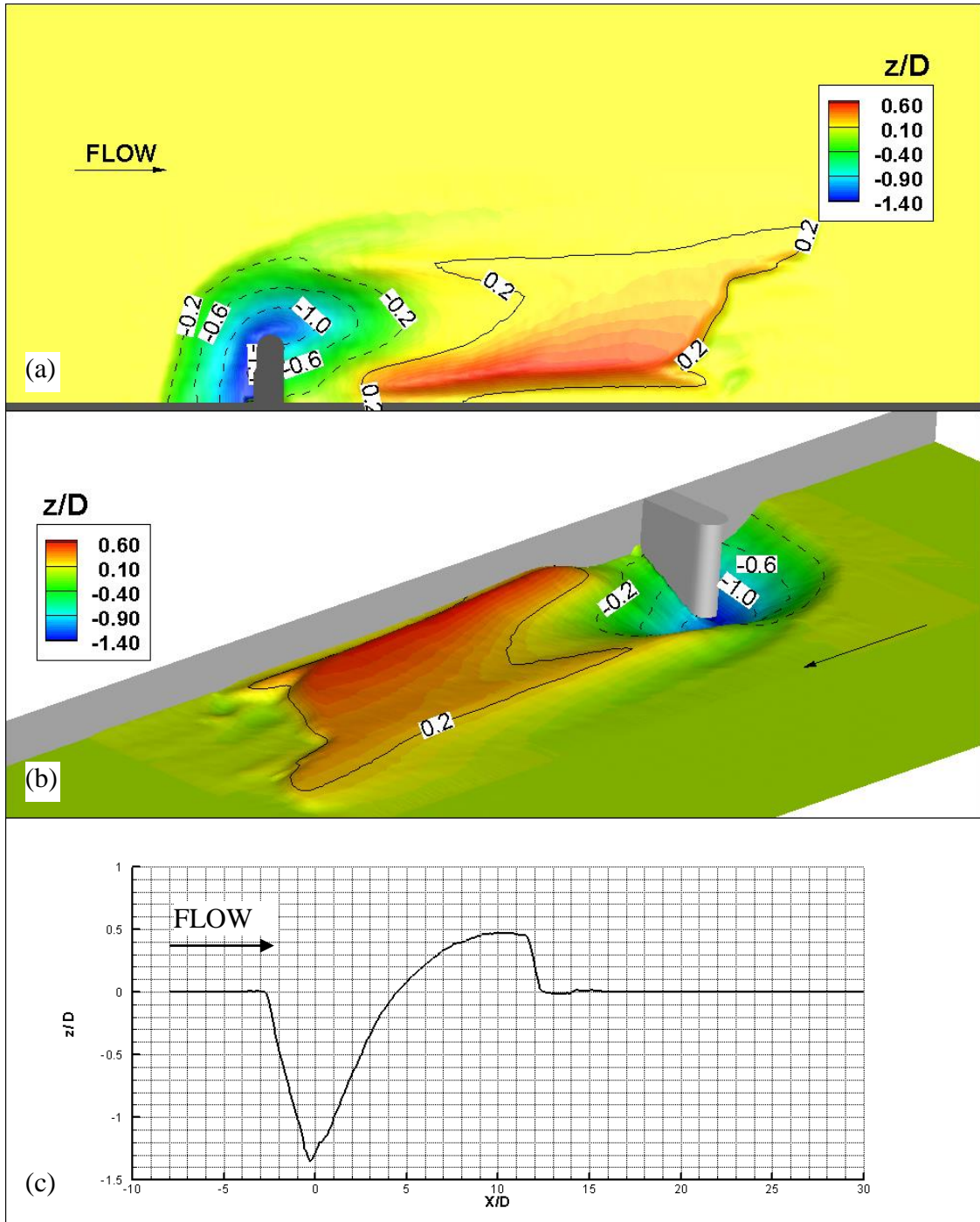


Figure 3.14 Scour and deposition pattern after an 8 hours test duration for the abutment length,  $L=25$  cm: a) top view; b) 3-D view; c) 1-D section view which is tangent to the tip of the abutment

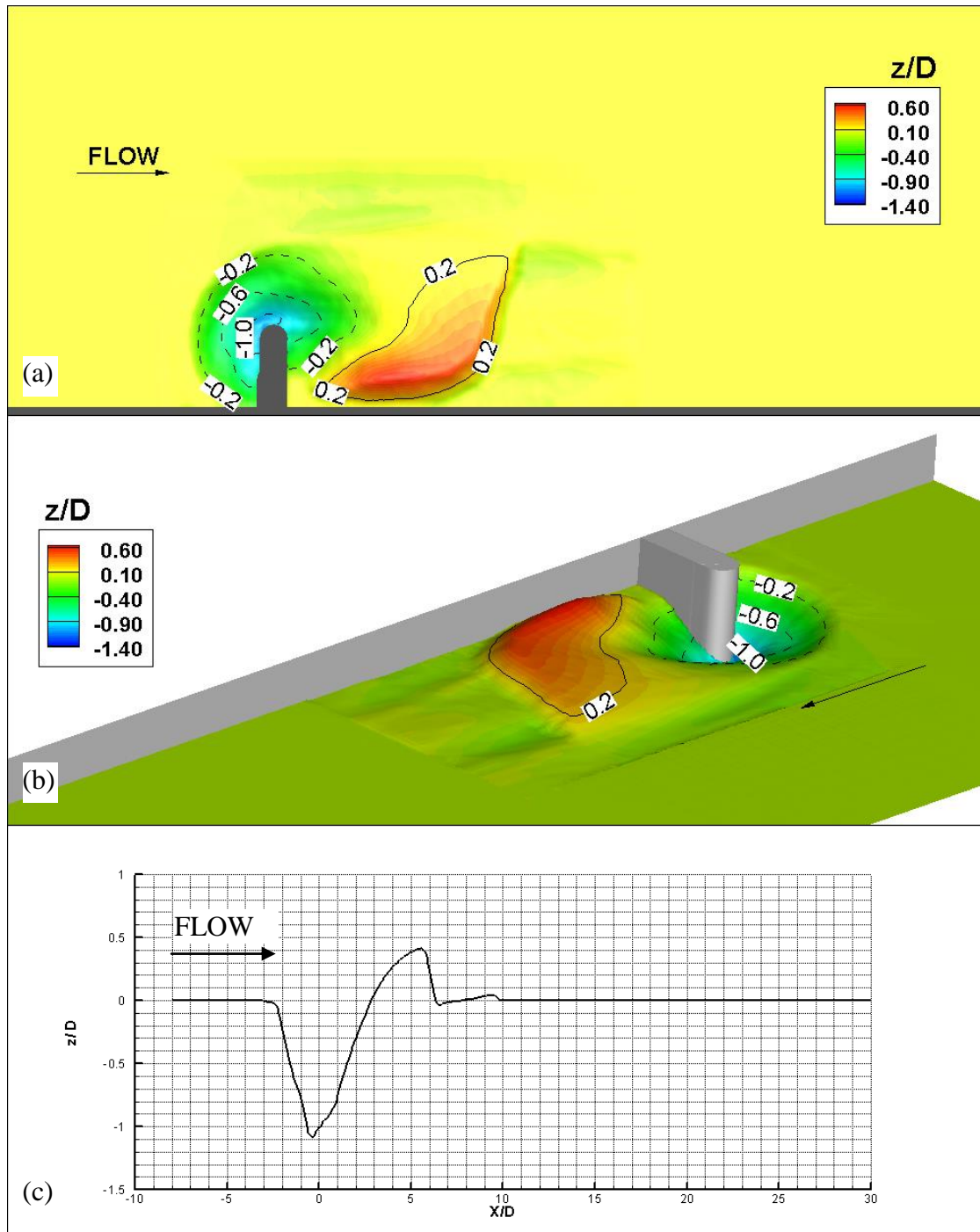


Figure 3.15 Scour and deposition pattern after a 2 hours test duration for the abutment length,  $L=30$  cm: a) top view; b) 3-D view; c) 1-D section view which is tangent to the tip of the abutment

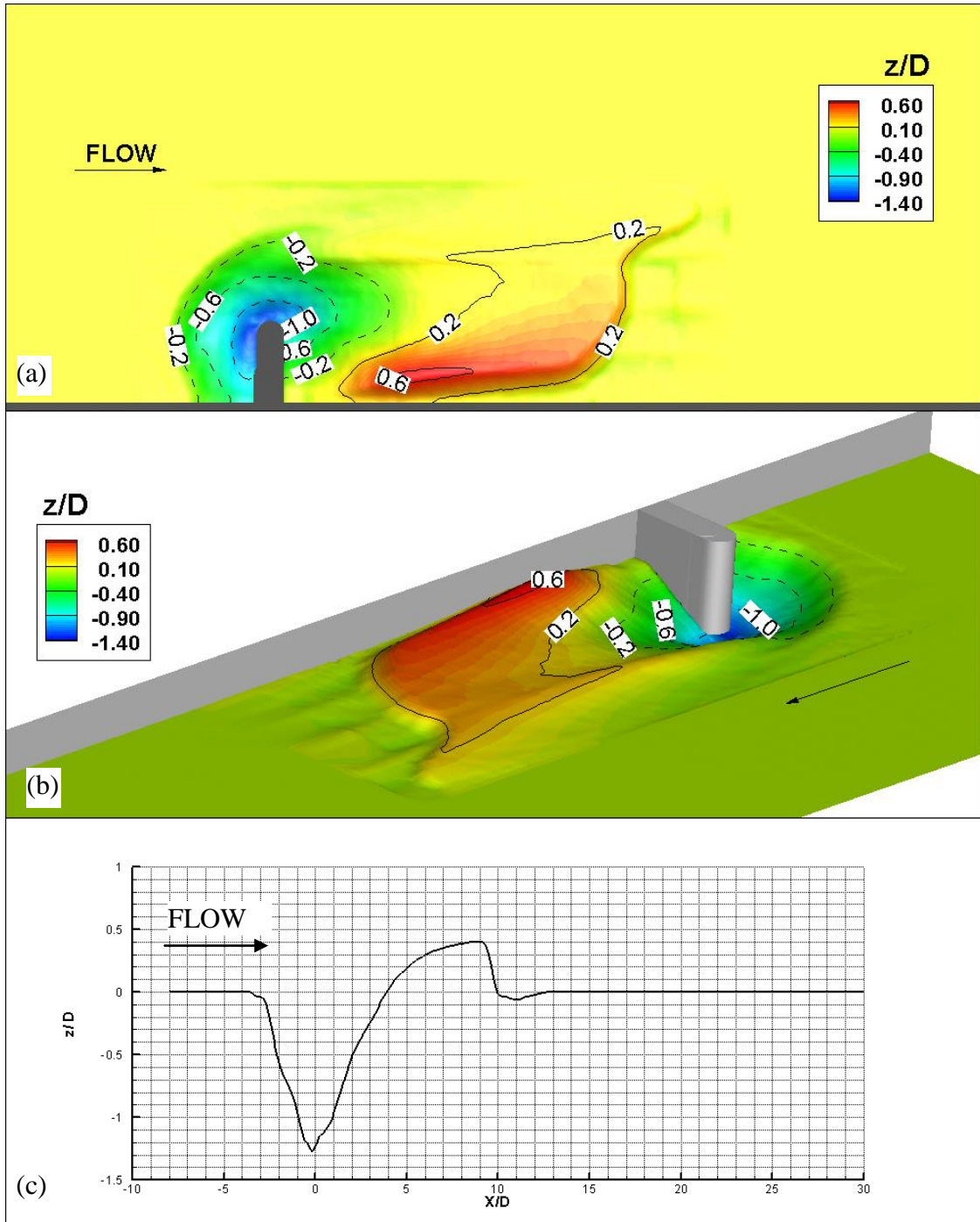


Figure 3.16 Scour and deposition pattern after a 4 hours test duration for the abutment length,  $L=30$  cm: a) top view; b) 3-D view; c) 1-D section view which is tangent to the tip of the abutment

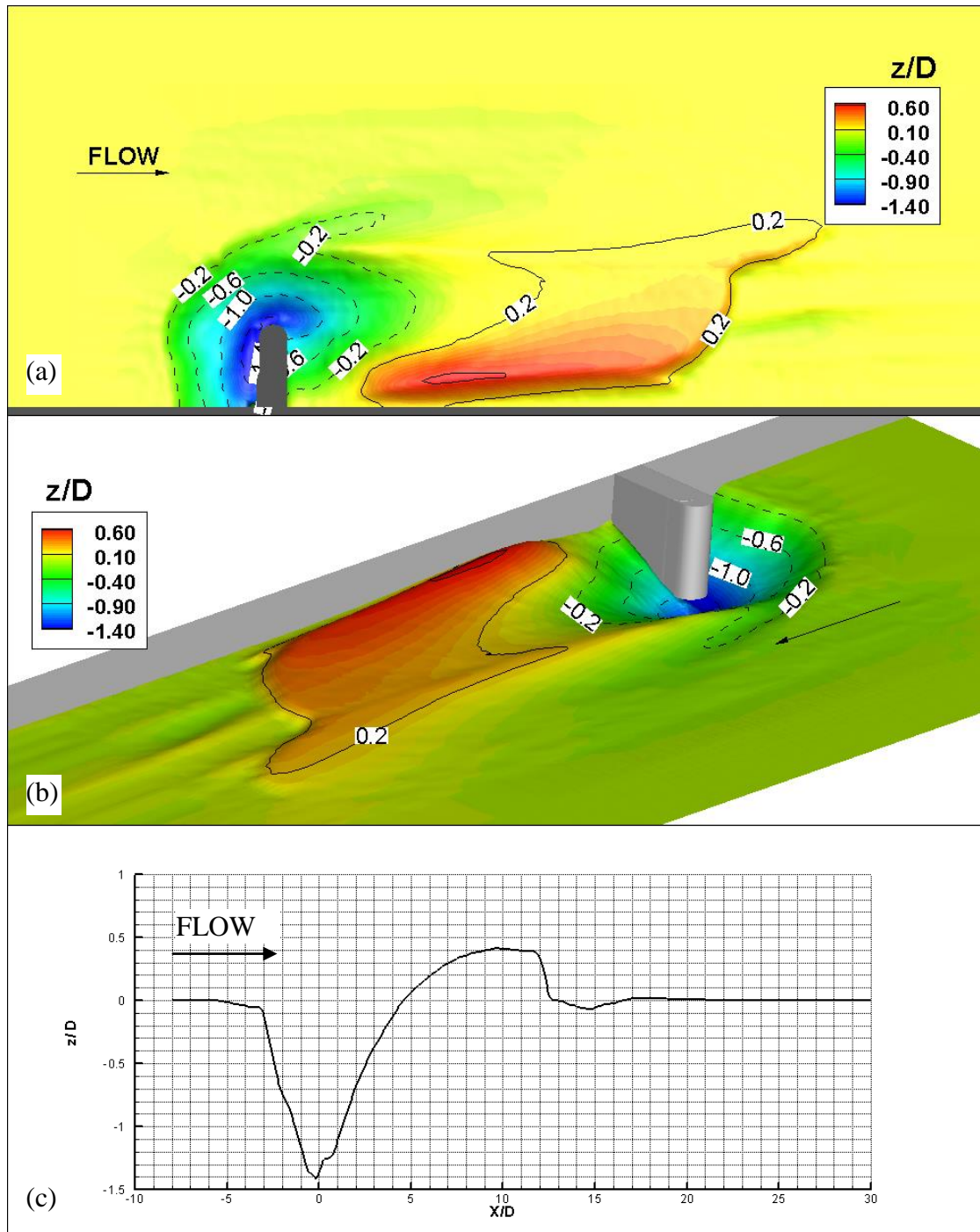


Figure 3.17 Scour and deposition pattern after an 8 hours test duration for the abutment length,  $L=30$  cm: a) top view; b) 3-D view; c) 1-D section view which is tangent to the tip of the abutment

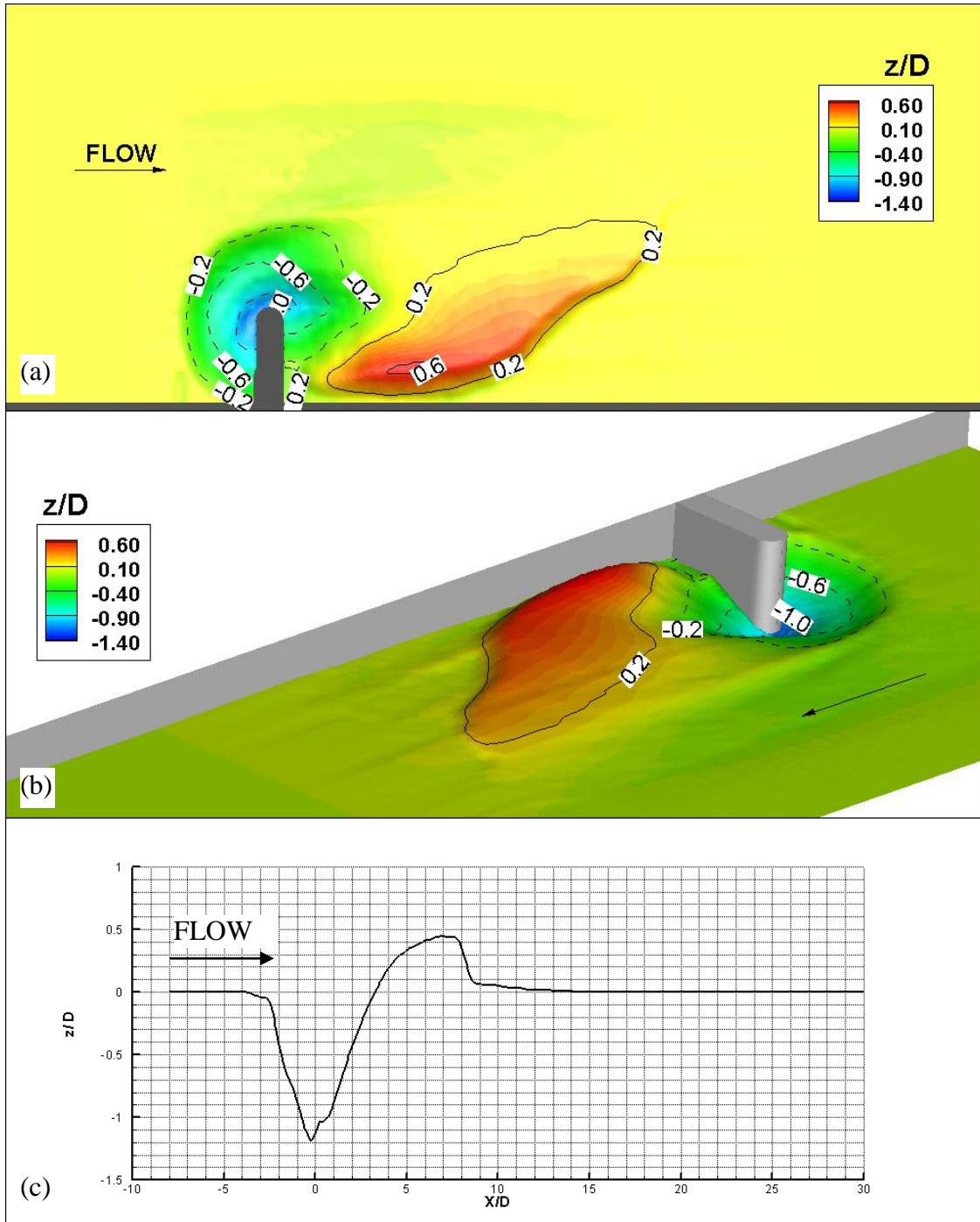


Figure 3.18 Scour and deposition pattern after a 2 hours test duration for the abutment length,  $L=35$  cm: a) top view; b) 3-D view; c) 1-D section view which is tangent to the tip of the abutment

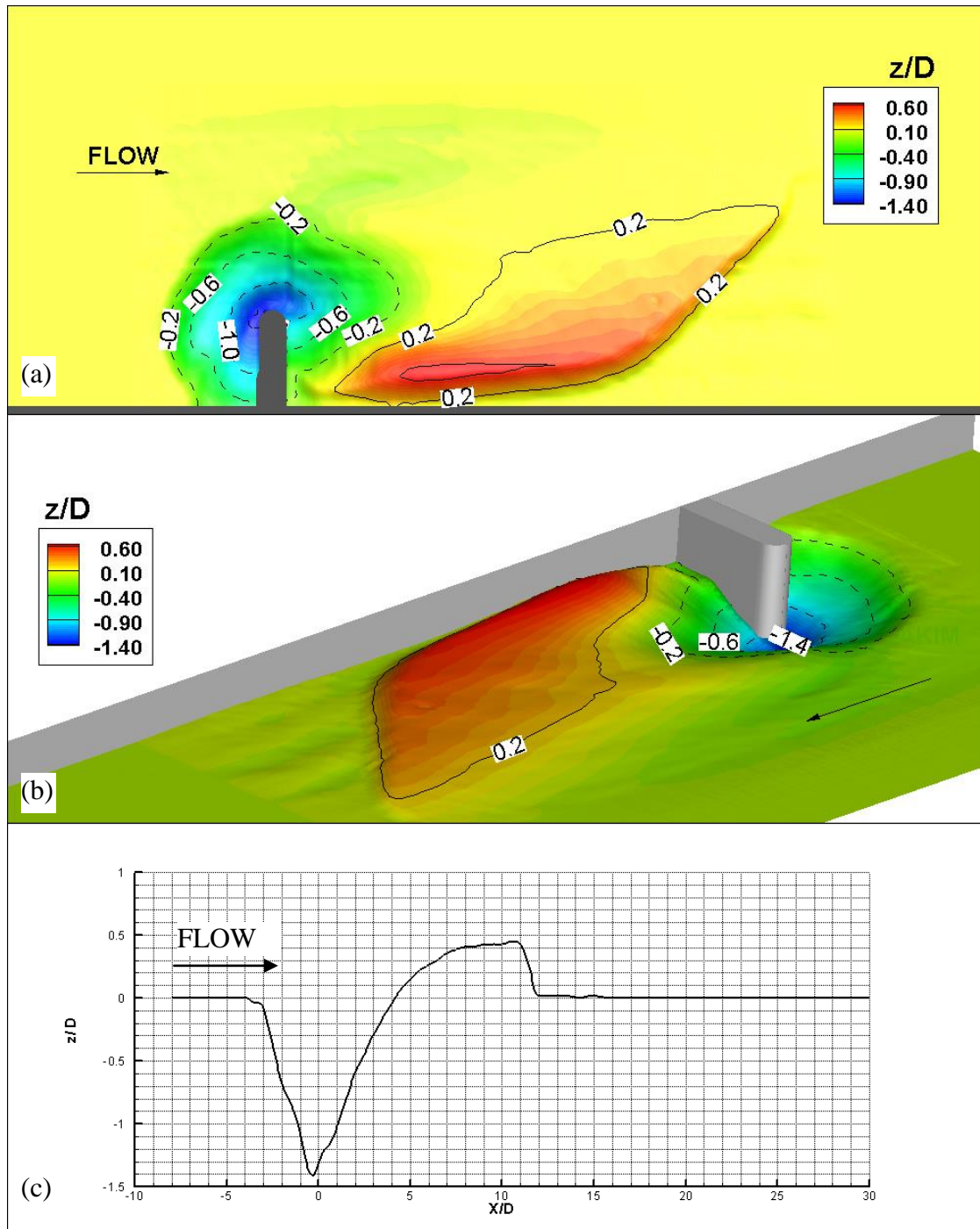


Figure 3.19 Scour and deposition pattern after a 4 hours test duration for the abutment length,  $L=35$  cm: a) top view; b) 3-D view; c) 1-D section view which is tangent to the tip of the abutment

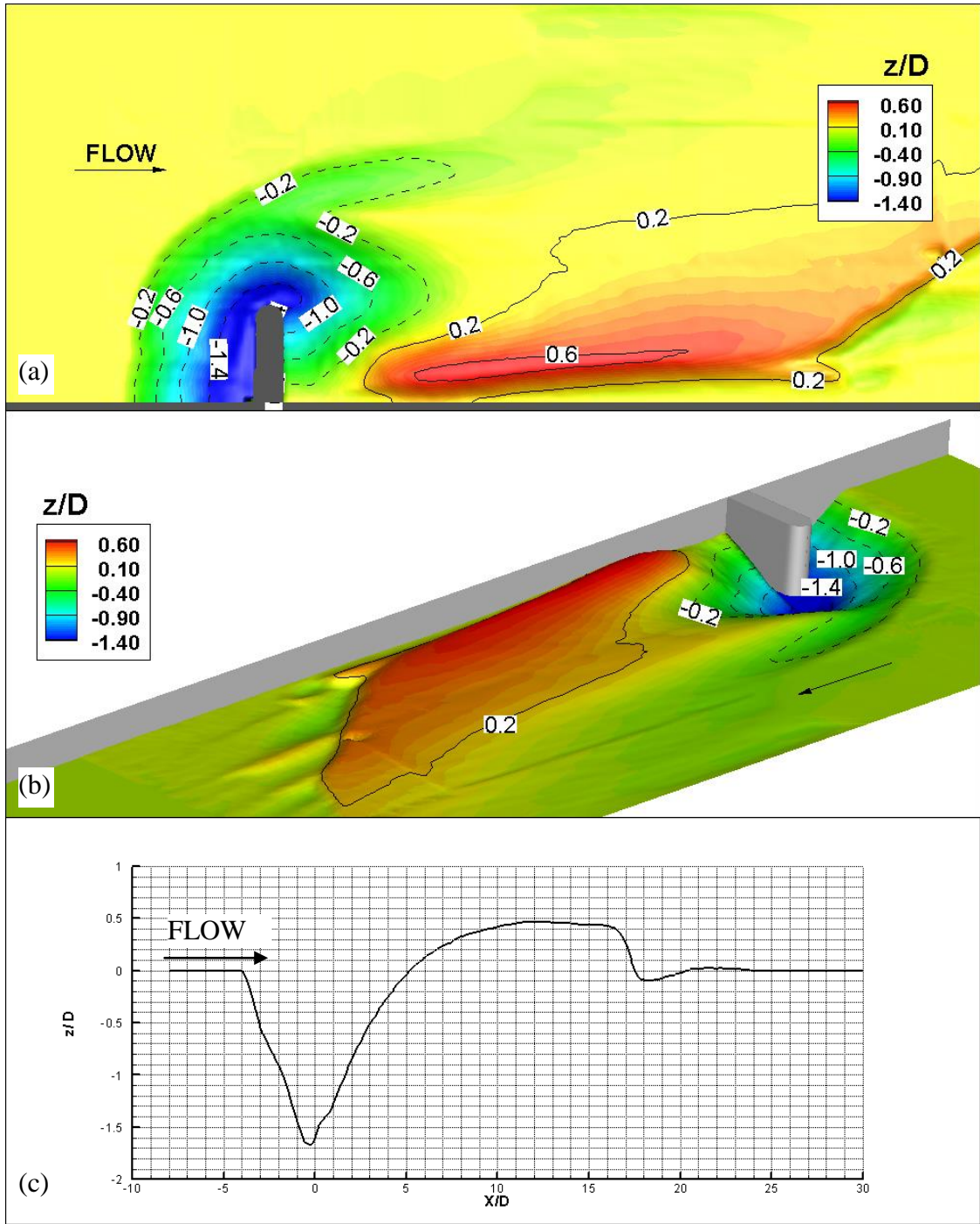


Figure 3.20 Scour and deposition pattern after an 8 hours test duration for the abutment length,  $L=35$  cm: a) top view; b) 3-D view; c) 1-D section view which is tangent to the tip of the abutment

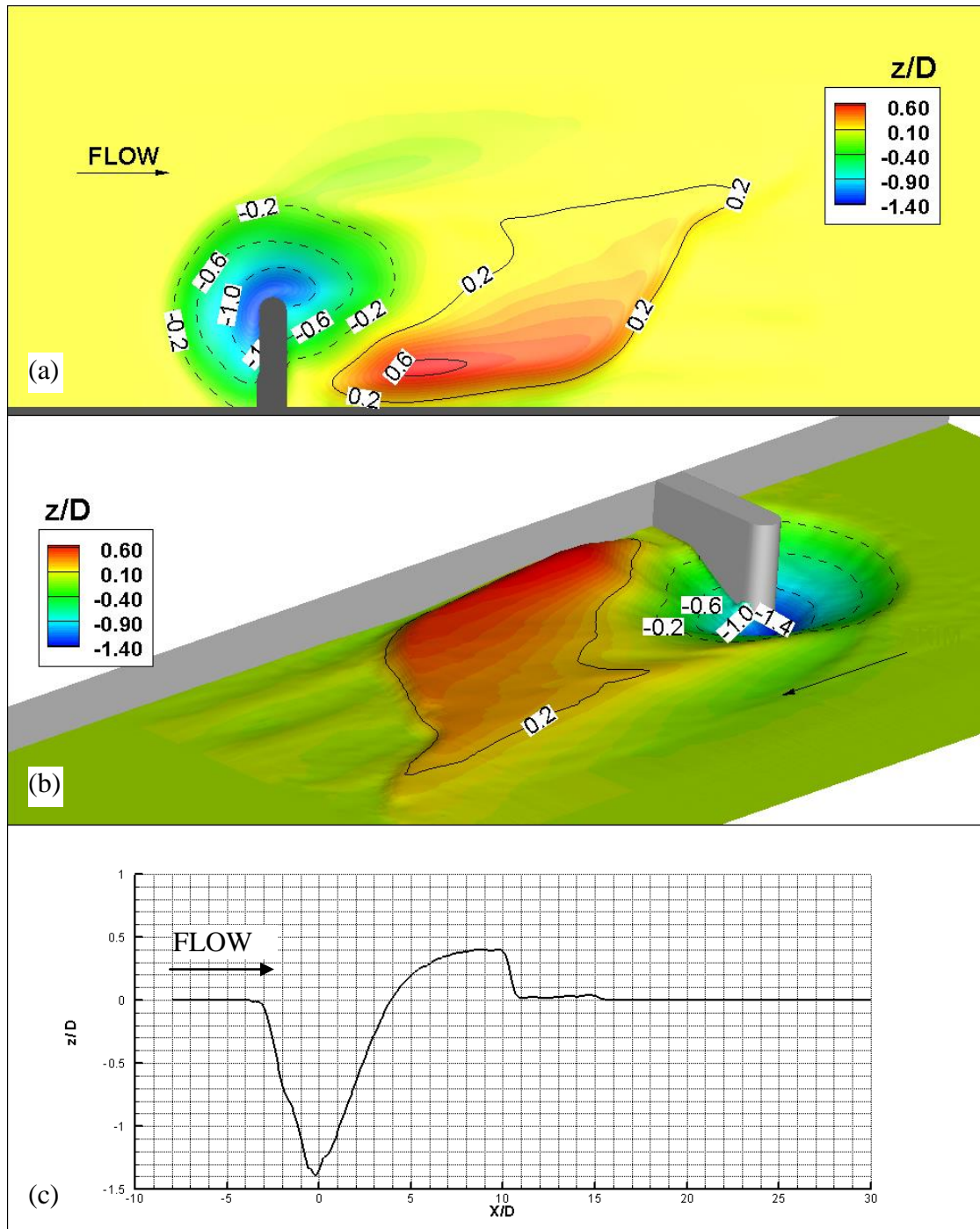


Figure 3.21 Scour and deposition pattern after a 2 hours test duration for the abutment length,  $L=40$  cm: a) top view; b) 3-D view; c) 1-D section view which is tangent to the tip of the abutment

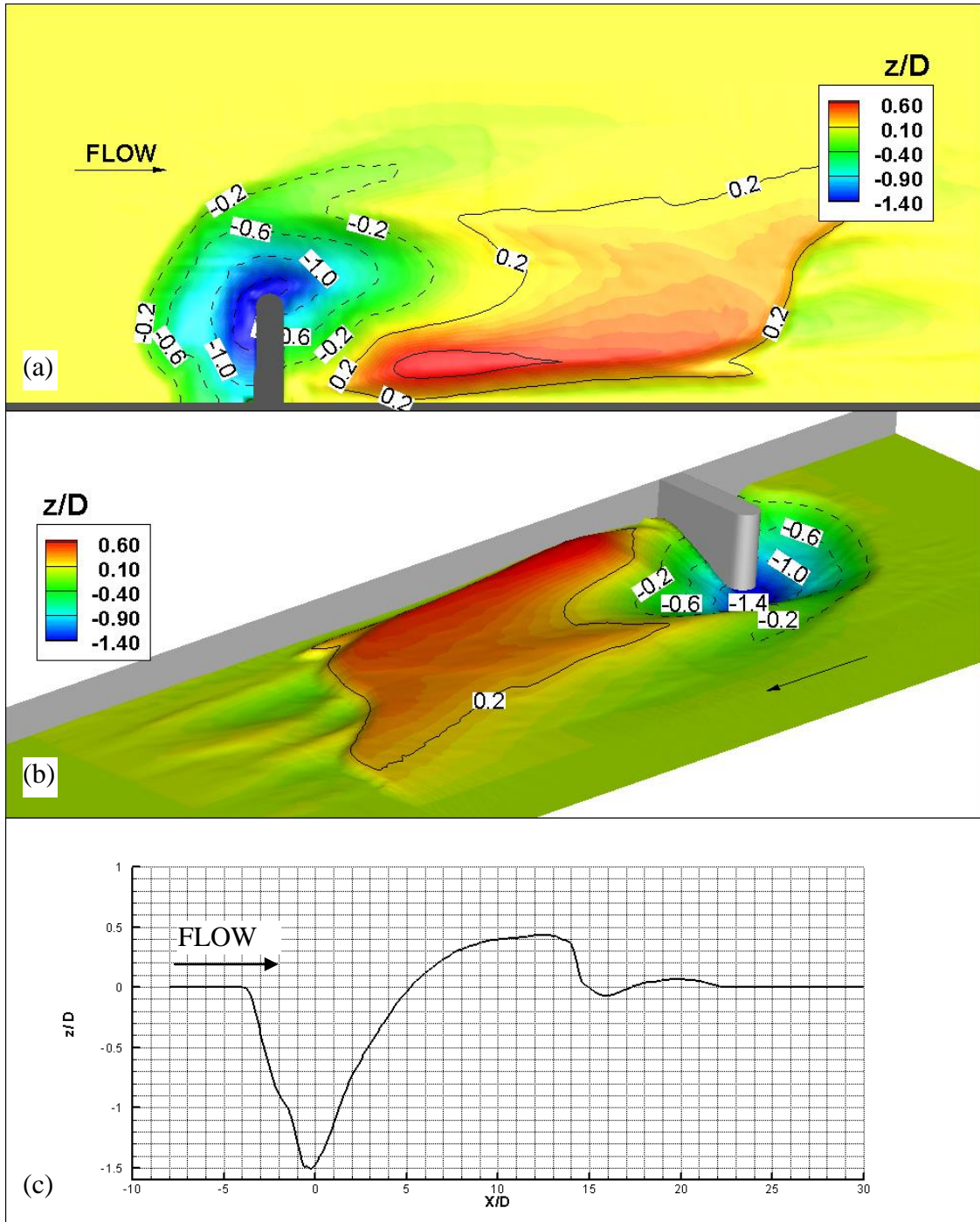


Figure 3.22 Scour and deposition pattern after a 4 hours test duration for the abutment length,  $L=40$  cm: a) top view; b) 3-D view; c) 1-D section view which is tangent to the tip of the abutment

From (a) and (b) frames of Figures 3.6 to 3.22, the development of scour hole by abutment length and test duration can be observed by the help of contour lines and the colored scaling used in the 3-D view and top view of the area around the abutment. Frame (c) of Figures 3.6 to 3.22 was produced to demonstrate the 1-D scour profile of one of the most critical sections, tangent to the abutment tip, around the abutment. During the scouring process, the maximum scour depth and the top point of the deposition hill occurs on this section or very close to this section.

In Table 3.2, experimental findings regarding the scour pattern are given.  $d_s/D$  stands for the dimensionless maximum scour depth measured for each experiment.  $X_s/D$  is the dimensionless scour hole length in the flow direction. Scour hole length was measured by taking the difference of the most upstream and most downstream streamwise coordinates of the scour hole, as shown in Figure 3.6 (a), for each data set. Afterwards,  $X_u/D$  and  $X_d/D$  were defined as shown in Figure 3.7 (a). These two parameters were introduced regarding their importance in scour counter measures, especially for riprap protection.

Moreover, to define the position of the maximum scour depth, two new parameters were defined standing for the radius and the angle in the polar coordinate system. Origin of the coordinate system for defining these parameters was taken as the cross point of the abutment axis and flume side wall. The angles were defined positive in clockwise direction. In this manner,  $r/D$  and  $\alpha$  stand for the dimensionless radius and the angle, respectively. Figure 3.23 demonstrates the definitions of these two new defined parameters.

The scour hole volume is given in non-dimensional form ( $V_s/D^3$ ) after dividing the volume values to the cube of the flow depth. The scour volume values were calculated from the 3-D figures of the scour hole by numerical integration techniques.

The analyses of these results will be done in the following part of the Results section.

Table 3.2 Parameters obtained from the experiments

Set Nr.	$L/D$	$t$ (hrs.)	$d_s/D$	$X_s/D$	$X_l/D$	$X_t/D$	$r/D$	$\alpha$ (deg.)	$V_s/D^3$
1	1.11	2	0.65	3.23	0.97	1.15	0.76	50.91	2.58
2		4	0.82	3.78	1.25	1.36	1.07	66.98	3.56
3		8	0.98	4.66	1.58	1.45	1.07	84.61	3.84
4	1.48	2	0.87	3.98	1.40	1.39	1.13	66.80	4.13
5		4	1.00	4.85	1.52	1.48	0.99	63.43	5.60
6		8	1.09	5.20	1.69	1.56	1.01	53.97	7.16
7	1.85	2	1.08	5.30	1.78	1.83	1.48	72.47	7.80
8		4	1.21	6.80	1.99	2.17	1.39	64.80	10.92
9		8	1.42	7.56	2.54	2.34	1.13	58.39	15.77
10	2.22	2	1.12	5.14	1.82	2.20	2.11	79.88	10.27
11		4	1.33	6.80	2.34	2.46	1.94	72.26	14.53
12		8	1.53	7.84	2.68	2.68	1.80	70.82	23.62
13	2.59	2	1.22	5.65	2.16	2.26	2.23	74.58	14.88
14		4	1.44	7.25	2.64	2.74	2.61	83.48	20.63
15		8	1.82	9.54	3.37	3.34	1.56	64.65	38.55
16	2.96	2	1.45	7.20	2.51	2.76	3.05	85.82	20.18
17		4	1.63	9.26	3.25	3.23	2.47	81.38	29.67

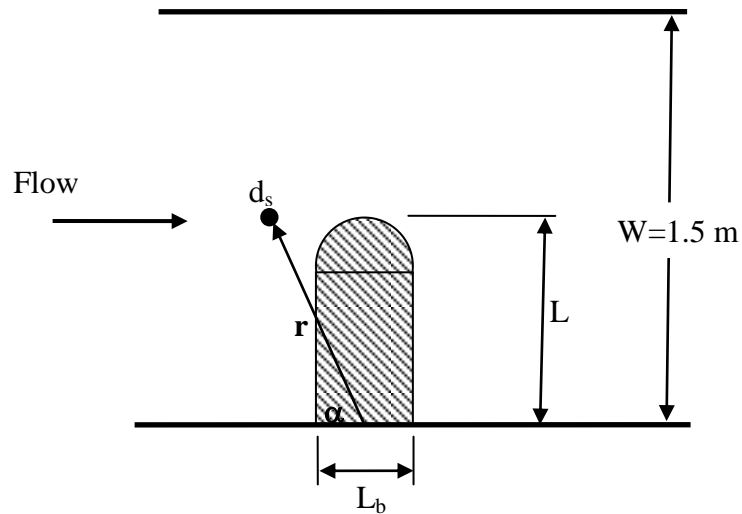


Figure 3.23 Position of the maximum scour depth in terms of  $r$  and  $\alpha$

### 3.2.2.1 Discussion of Results

After obtaining the digitalized bathymetry data and the values of the parameters regarding the scour pattern, the relations of the parameters relating to the scour pattern and the abutment length for various test durations have been investigated.

Figure 3.24 shows the variation of the dimensionless maximum scour depth,  $d_s/D$ , with the dimensionless abutment length,  $L/D$ , for various test durations. From this figure it is seen that, for any tested abutment length,  $d_s/D$  increases with the increase in time. Also, for a given period,  $d_s/D$  increases linearly with increase in  $L/D$ . The related linear equations with high correlation coefficients are given on the figure. The flow characteristics around abutments change significantly with the change in abutment length where there are variations in the structure of the vortices forming around the abutments. This brings an increase in the bed shear stress values observed and hence larger areas are exposed to the scour process where the depth of the scour hole also increases. Using the curves given in Figure 3.24, maximum dimensionless scour depths for an abutment with a dimensionless length,  $L/D$ , of 1.0 to 3.0 can be determined within a time period of two to eight hours for the experimental conditions of the present study.

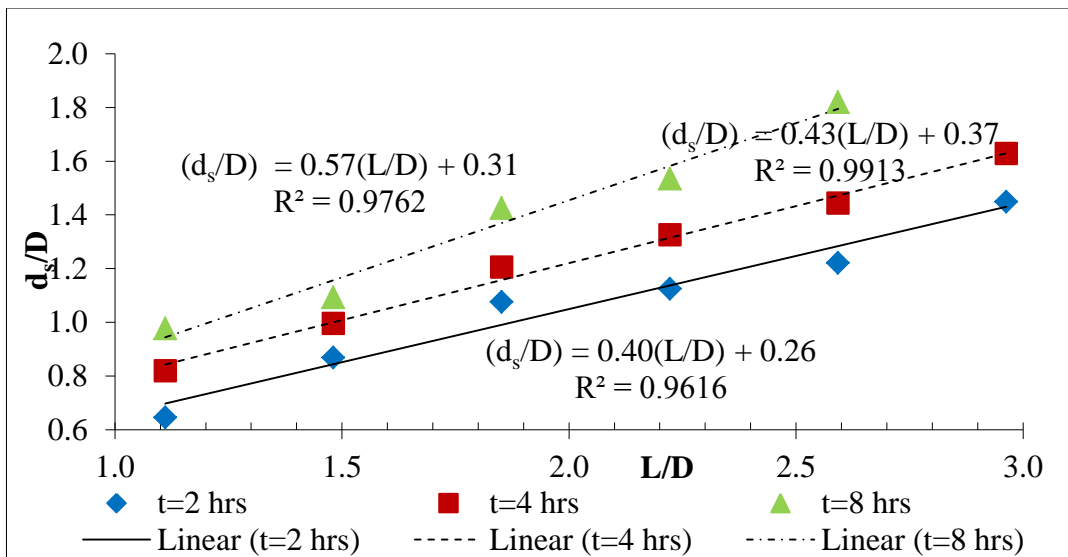


Figure 3.24 Variation of the dimensionless maximum scour depth with the dimensionless abutment length for 2, 4 and 8 hours

In Figure 3.25, the variation of dimensionless length of the scour hole in flow direction,  $X_s/D$  with  $L/D$  is shown. For each abutment length,  $X_s/D$  value increases with time and for a given period of time,  $X_s/D$  value increases linearly with the increase in  $L/D$ . The linear equations fitted for the relations are given in the figure with high correlation coefficients.

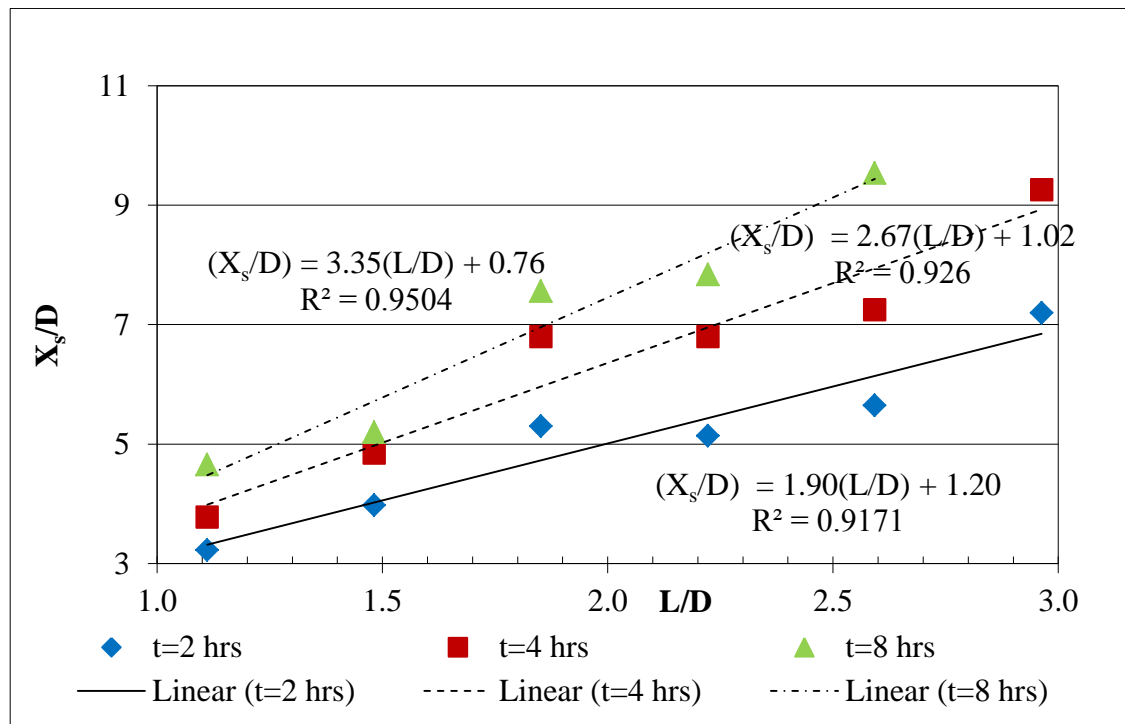


Figure 3.25 Variation of the dimensionless scour hole length with the dimensionless abutment length for 2, 4 and 8 hours

In Figures 3.26 and 3.27, the variations of  $X_i/D$  and  $X_f/D$  with the dimensionless abutment length for various test durations are shown, respectively. The dimensionless length terms,  $X_i/D$  and  $X_f/D$ , were demonstrated within Figure 3.7 (a). As can be seen from Figures 3.26 and 3.27, the variation of the parameters with the dimensionless abutment length shows linear behavior with high correlation ratios. Moreover, these parameters always increase with the increase in time. The relation of these parameters

with each other is also important in choosing the dominant side in case of riprap protection. To observe this situation clearly, Figure 3.28 shows the variation of  $X_1/D$  and  $X_2/D$  with set number. As can be seen from the figure, there exists a random relation between each parameter and it can be stated that, one side does not have a dominance over other.

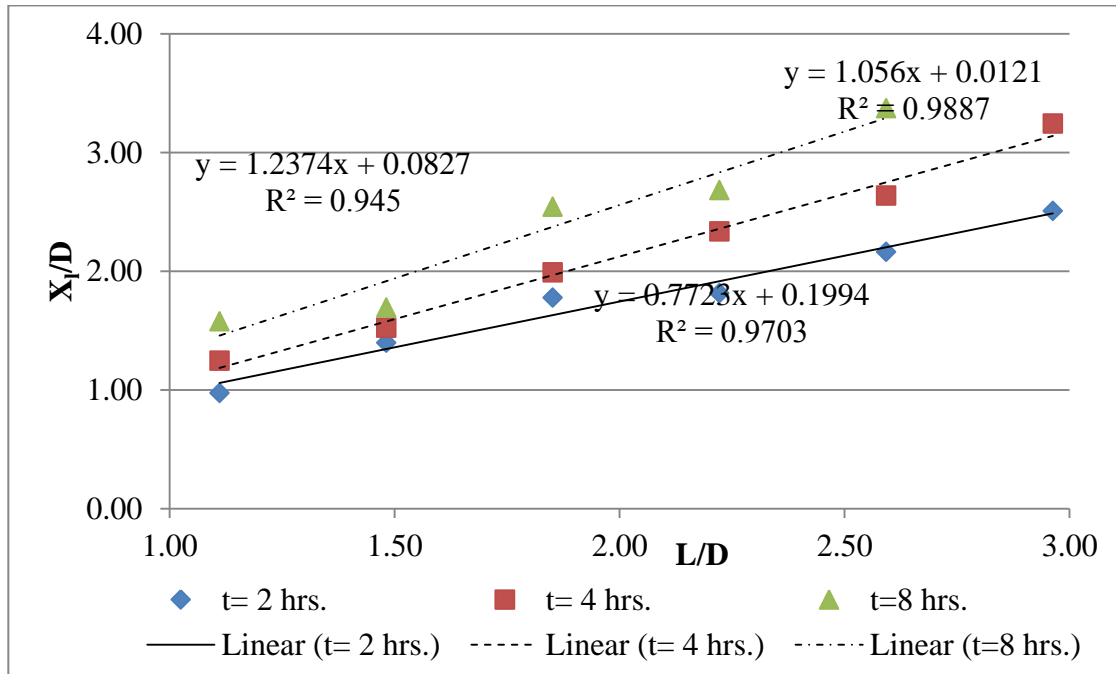


Figure 3.26 Variation of  $X_1/D$  with the dimensionless abutment length for 2, 4 and 8 hours

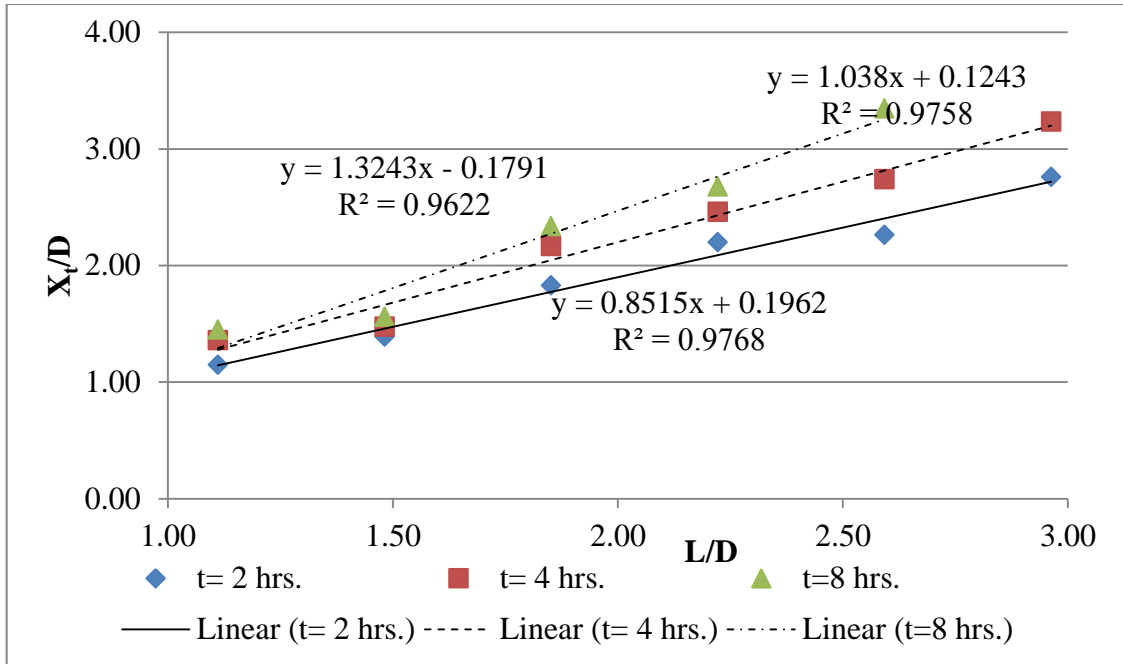


Figure 3.27 Variation of  $X_t/D$  with the dimensionless abutment length for 2, 4 and 8 hours

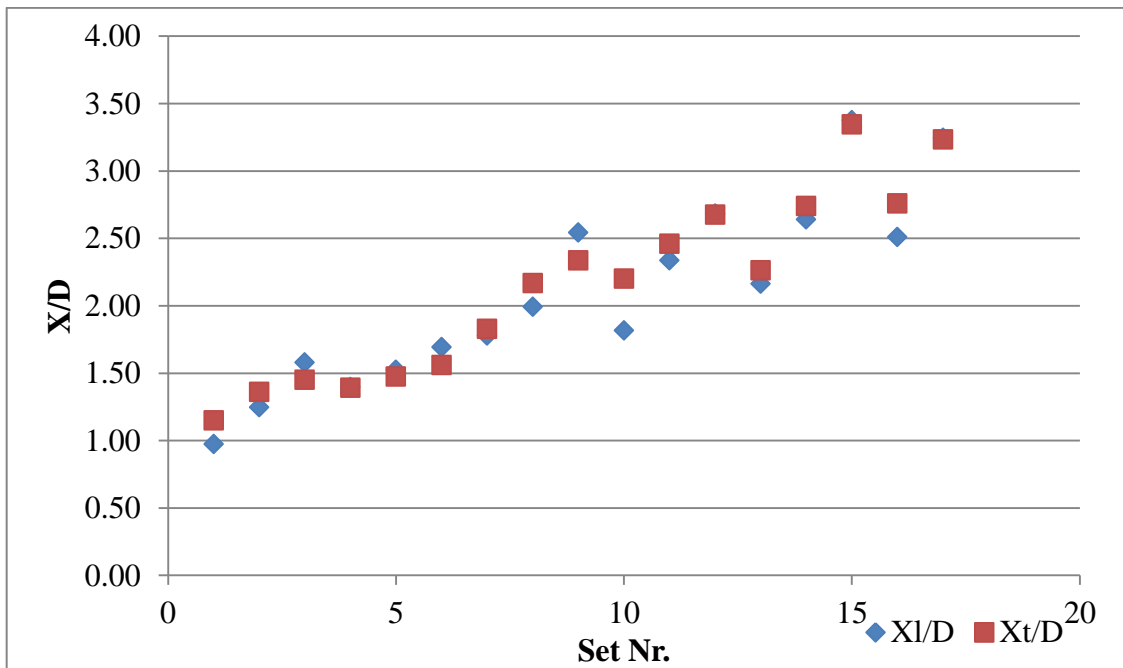


Figure 3.28 Comparison of the values of  $X_l/D$  and  $X_t/D$  for the entire data

The change of dimensionless parameters  $r/D$  and  $\alpha$ , which show the polar coordinates of the location of the maximum scour depth point, with the dimensionless abutment length  $L/D$  are shown in Figures 3.29 and 3.30. From short to long, for the first four abutment lengths, variation of  $r/D$  with time is very limited, but for the remaining two abutment lengths,  $L/D=2.59$  and  $2.96$ ,  $r/D$  differs significantly at the later stages of the scour. There is no significant relation between  $r/D$  and experiment duration. Therefore, a new relation between  $r/D$  and  $L/D$ , which is independent of time, was searched. Covering all the experimental data, it can be seen from Figure 3.29,  $r/D$  increases almost linearly with increase in  $L/D$ . The relation of  $\alpha$  and  $L/D$  is shown in Figure 3.30. The figure prevails that, generally the value of  $\alpha$  increases with the increase in  $L/D$ . For these data sets, presence of a linear relationship is not investigated as the variation is random. To sum up, one can say that,  $r/D$  increases with  $L/D$  linearly and  $\alpha$  is always smaller than 90 degree, where its variation with  $L/D$  is random. The location of the position of the maximum scour depth always exists at the upstream side of the abutment and close to the abutment tip.

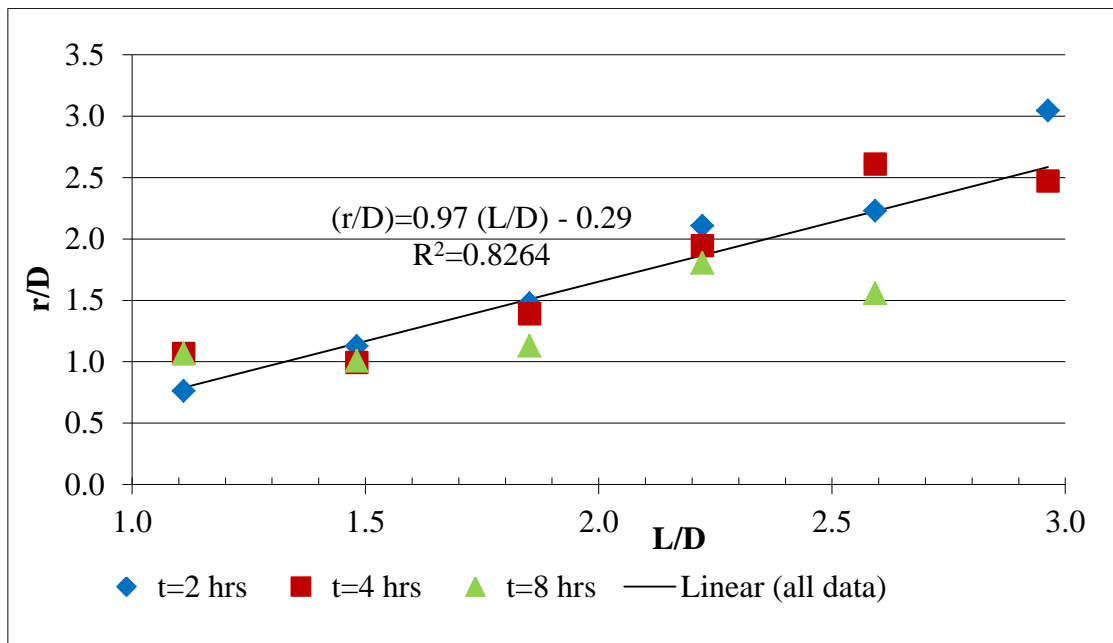


Figure 3.29 Variation of the radius of the position of the maximum scour depth with the dimensionless abutment length for 2, 4 and 8 hours

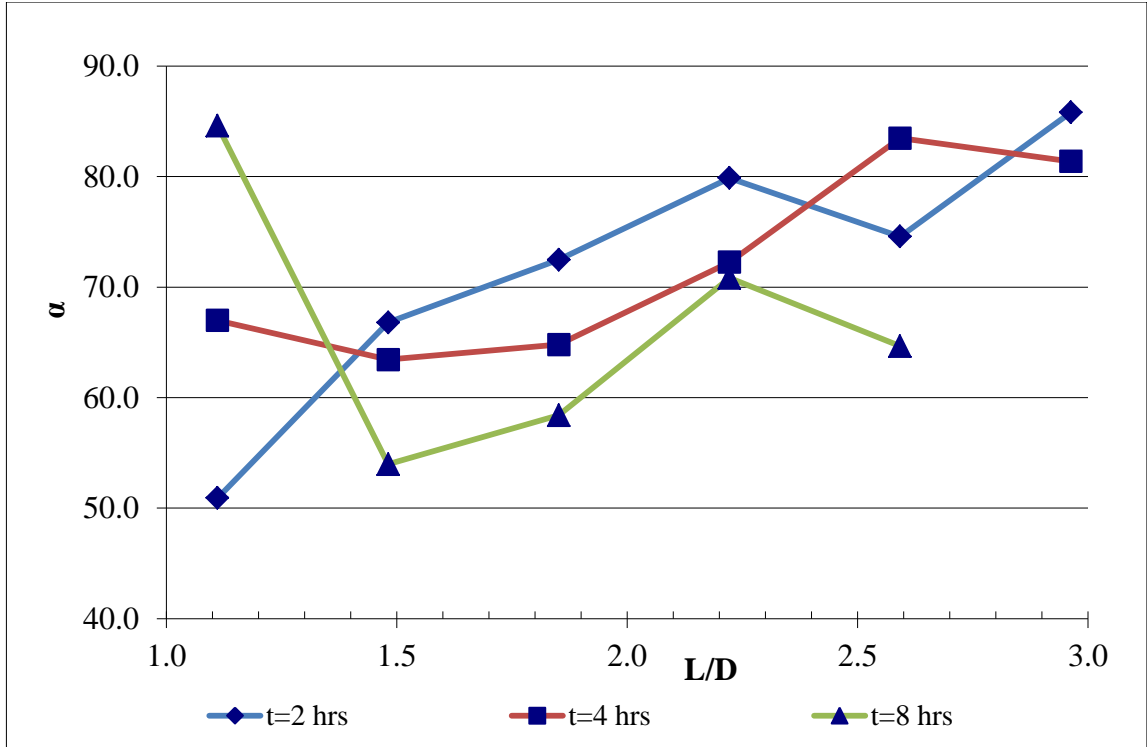


Figure 3.30 Variation of the angle of the position of the maximum scour depth with the dimensionless abutment length for 2, 4 and 8 hours

Figure 3.31 shows that, the  $L/D$  vs  $V_s/D^3$  relation fits almost perfectly with power functions for any given test duration. Besides, for any  $L/D$ ,  $V_s/D^3$  increases with increase in experiment duration. The time parameter was inserted into the obtained equation by using the dimensionless time parameter offered by Yanmaz and Altinbilek (1991);

$$T_s = \frac{tD_{50}(\Delta g D_{50})^{0.5}}{L^2} \quad (3.1)$$

The following time dependent volumetric equation was obtained covering all the data obtained in this set;

$$\left( \frac{V_s}{D^3} \right) = 0.061(T_s)^{0.68} (L/D)^{3.83} \quad (3.2)$$

This equation has fitted to the data set with a correlation coefficient of  $R^2=0.98$ .

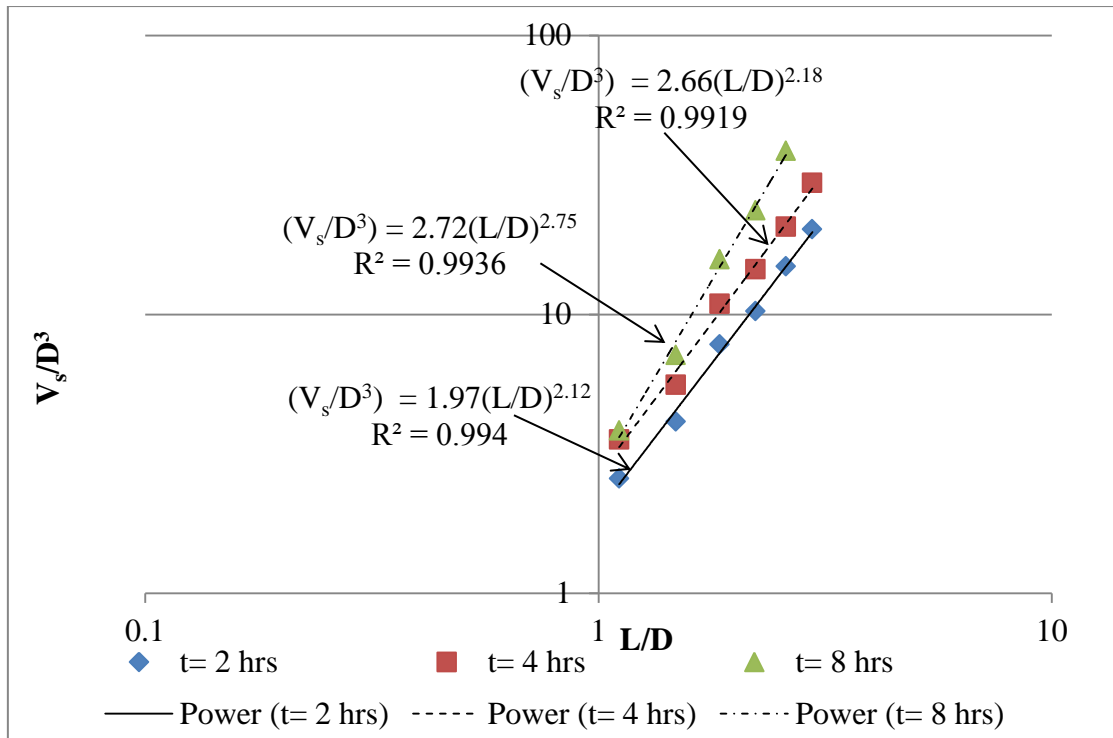


Figure 3.31 Variation of the dimensionless scour hole volume with the dimensionless abutment length for 2, 4 and 8 hours

In literature, the variation of scour hole volume with scour depth was investigated to write scour hole volume in terms of scour depth in semi-empirical model studies (Dey and Barbhuiya, 2005; Yanmaz and Kose, 2009). In these studies, the shape of the scour hole has been approximated to similar geometries. By the help of measured scour hole volume data within this study, an analysis on this issue was accomplished. In Figure 3.32, the variation of dimensionless scour hole volume with dimensionless maximum scour depth is demonstrated. It can be seen from the figure that, regardless of the abutment length and the experimental duration, all data of the experiment set was fit with a power function with a high correlation ratio. This equation can be used to write scour hole volume in terms of scour hole depth. This verifies the deduction of Ballio and Orsi (2001) that, the volume of scour hole depends only on the maximum scour hole depth. Additionally, it should be stated that, the volume of the scour hole depends also on the abutment model base area and the angle of repose of the sediment. It is known

that, the side slopes of the scour hole are very close to the angle of repose of the sediment. Therefore, it can be stated that Equation 3.3 is valid for abutments with base width,  $L_b = 10$  cm and bed material with an angle of repose equals to  $30^\circ$ .

$$\left( V_s / D^3 \right) = 6.51 \left( d_s / D \right)^{2.91} \quad (3.3)$$

This discussion will be extended further in Chapter 4 with the addition of new data.

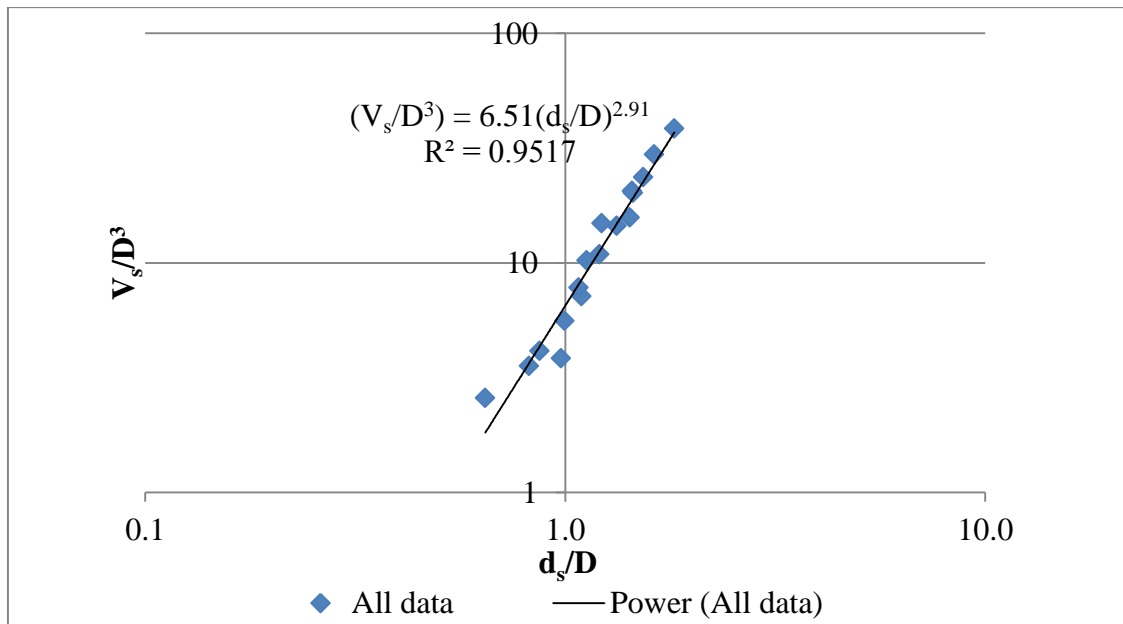


Figure 3.32 Variation of the dimensionless scour hole volume with the dimensionless maximum scour depth

### 3.2.2.2 Comparison of Results with the Results of Similar Studies in Literature

In literature, there exist not so many studies using SCE abutment. Melville (1992) used this type of abutments and modeled the equilibrium scour depth. This study was further developed by Coleman et al. (2003) by counting for the temporal development of the

scour. The comparison of the findings with Coleman et al. (2003) will be done at Section 3.3.3 with the addition of data set on temporal development of the scour.

Moreover, findings of this study were compared with the results of two studies using similar abutment types. The first study (Garde et al., 1961) was dealt with spur dikes having rectangular cross section and four different lengths. The experiments were done in a rectangular channel with 60 cm width. Durations of the experiments in this study were varied with three to five hours and the channel contraction coefficients,  $\beta = L/W$ , are used as 0.10, 0.165, 0.333 and 0.470, where  $W$  is the channel width. The experiments were done for four different bed materials with  $d_{50} = 0.20$  mm, 0.45 mm, 1 mm and 2.25 mm and the results are represented with the equation given below.

$$\frac{D+d_s}{D} = \frac{4}{(1-\beta)} (Fr)^{(2/3)} \quad (3.4)$$

The comparison of the above equation and the data of the present study are given in Figure 3.33 for experimental periods of two, four and eight hours. It is seen that, the results of two and four hour experiments are compatible with the results of Garde et al (1961), but the eight hour experiments give larger results than those of Garde et al. (1961). In general, the distribution of the data is correlated with each other. Although Garde et al. (1961) used spurs with rectangular cross section; in this study, SCE abutments were used, and this creates different flow patterns around the abutment. Therefore, it is expected to have such variations.

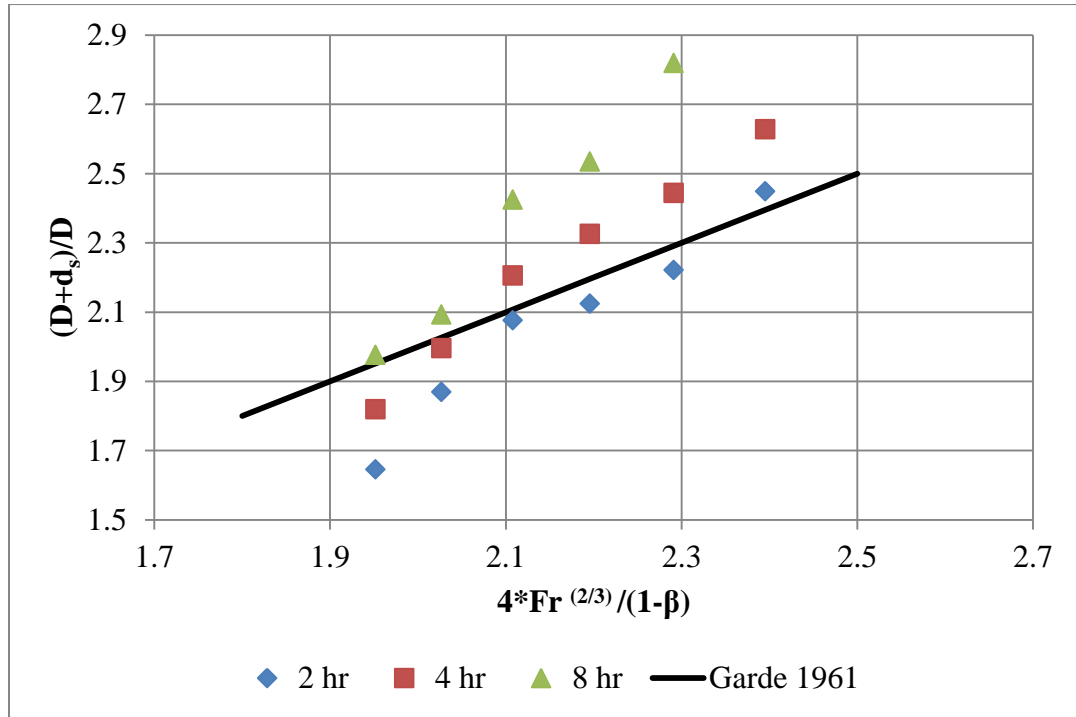


Figure 3.33 Comparison of the experimental data with Garde's (1961)

In the second study (Kayatürk, 2005), abutments with rectangular cross section, width,  $L_b$ , of 5 cm and varying lengths of  $L = 10$  cm, 15 cm, 20 cm and 25 cm were used. The experiments were done in a rectangular channel 1.50 m wide and 30 m long. A uniform bed material is used with  $d_{50} = 1.48$  mm. The experiments were done for flow depths of  $D = 10$  cm ( $Fr = 0.34$ ),  $D = 12$  cm ( $Fr = 0.26$ ) and  $D = 14$  cm ( $Fr = 0.20$ ) for a time period of 6 hours and the below equation for the dimensionless maximum scour depth,  $d_s/D$ , was obtained.

$$\frac{d_s}{D} = \left(\frac{L}{D}\right)^{1.4} (Fr)^{1.76} \left(\frac{L}{L_b}\right)^{0.12} \left(\frac{L}{W}\right)^{-0.66} \quad (3.5)$$

The comparison of the above equation and the data of the present study for the experimental periods of two, four and eight hours are shown in Figure 3.34. It can be said that, the experiments lasting two hours and four hours give results compatible with Kayatürk (2005), but the correlation of the results of the experiment lasting eight hours is less. The most important differences to be mentioned here are the different abutment

geometries, the difference in Froude numbers and the different experimental durations of studies. Therefore, the differences observed in these results are acceptable.

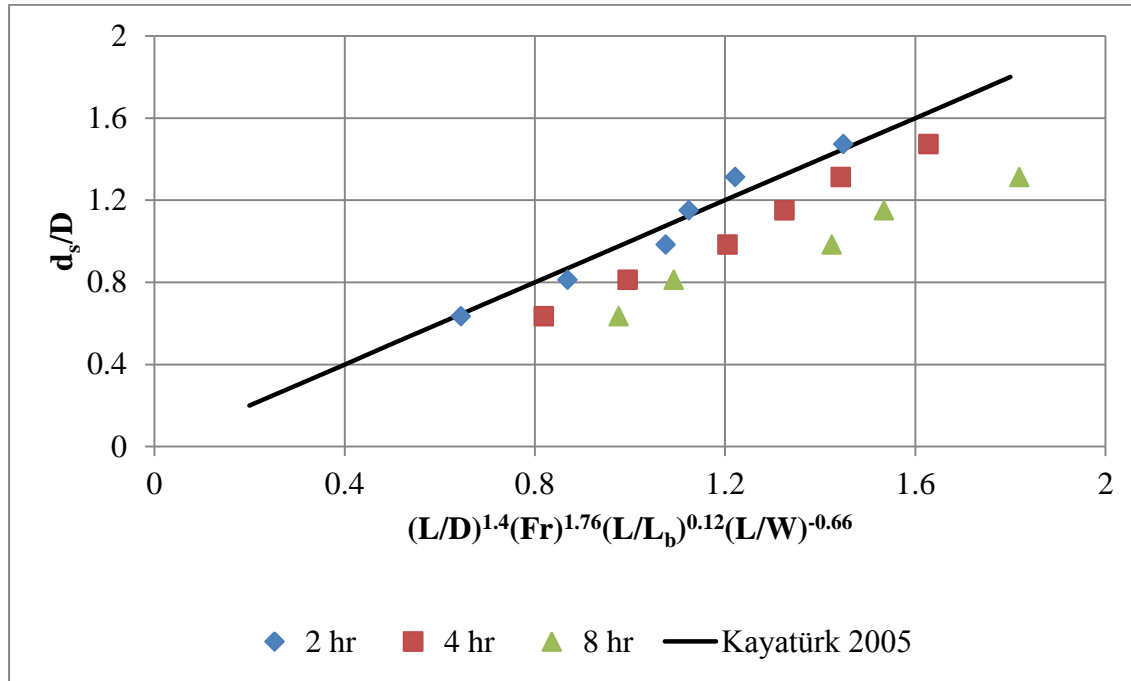


Figure 3.34 Comparison of the experimental data with Kayatürk's (2005)

### 3.3 Temporal Scour Measurements

Temporal development of scour was investigated by simultaneous recording of the scour data while experiments were running. Bed profiles around the abutment were measured at several sections. By using the Ultrasonic Ranging System (Figure 3.4), the data were recorded with short time intervals. The experiments were repeated for two abutment lengths and for five sections around the abutment for each abutment length.

This section will be covered by two subsections namely; "Experimental Equipment and Procedure" and "Results". The subsections will be discussed below with details.

### 3.3.1 Experimental Equipment and Procedure

The experiments were conducted for two abutment lengths;  $L= 15$  cm (short abutment) and  $L= 35$  cm (long abutment). In this experimental set, 10 experiments were conducted with eight hours of experimental duration to obtain the bed profiles at five sections for each abutment length. The sections were selected as follows; the first one at the upstream of the abutment, located vertically to the flow direction cutting through the scour hole, the second one at the tip of the abutment located vertically to the flow direction, the third one at the downstream of the abutment, located vertically to the flow direction cutting through the deposition region, the fourth one at the tip of the abutment located parallel to the flow direction and the last one was obtained by distributing the transducers around the abutment. Figures 3.35 (a) and (b) demonstrate the positions of these sections for the abutments of  $L=15$  cm and  $L=35$  cm, respectively.

The experimental procedure applied here is similar to the procedure discussed in Section 3.2.1. Apart from it, in this type of experiments the measurements were taken simultaneously while the experiments were running and the transducers were stayed submerged during the experiments. The data were recorded with one minute intervals during the experiments. For most of the experiments, 26 transducers were used for recording but for the fifth measurement for the abutment of  $L= 15$  cm, only the individual transducers were used for practical reasons therefore; 10 transducers were installed for these recordings.

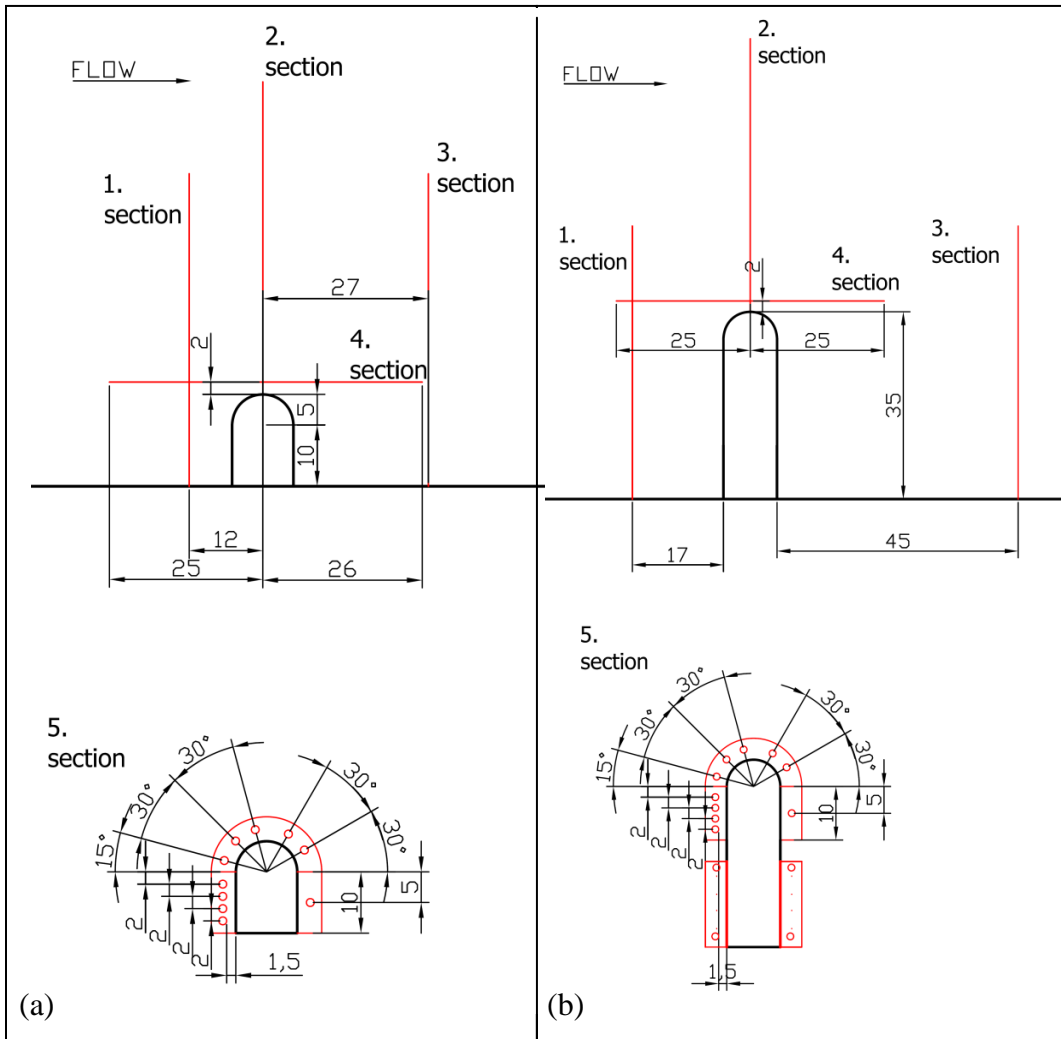


Figure 3.35 Positions of the measurement sections for the abutments of (a)  $L= 15$  cm (b)  $L= 35$  cm (dimensions are in cm, red drawings stand for the transducers)

### 3.3.2 Results

After recording the data, the bed profiles were obtained for each section. In Figures 3.36 to 3.45, the bed profiles are given for each section separately starting at  $t= 0.5$  hour and  $t= 1$  hour, and then increased with 1 hour increments till  $t= 8$  hours. In the figures, while  $x/D$ ,  $y/D$  and  $s/D$  stands for the dimensionless coordinates,  $z/D$  stands for the bed elevation changes, while zero being the original bed level, below zero and above zero correspond to the scouring and deposition regions, respectively. Besides, in the legend of each figure, the numbers with letter P stands for the transducer numbers.

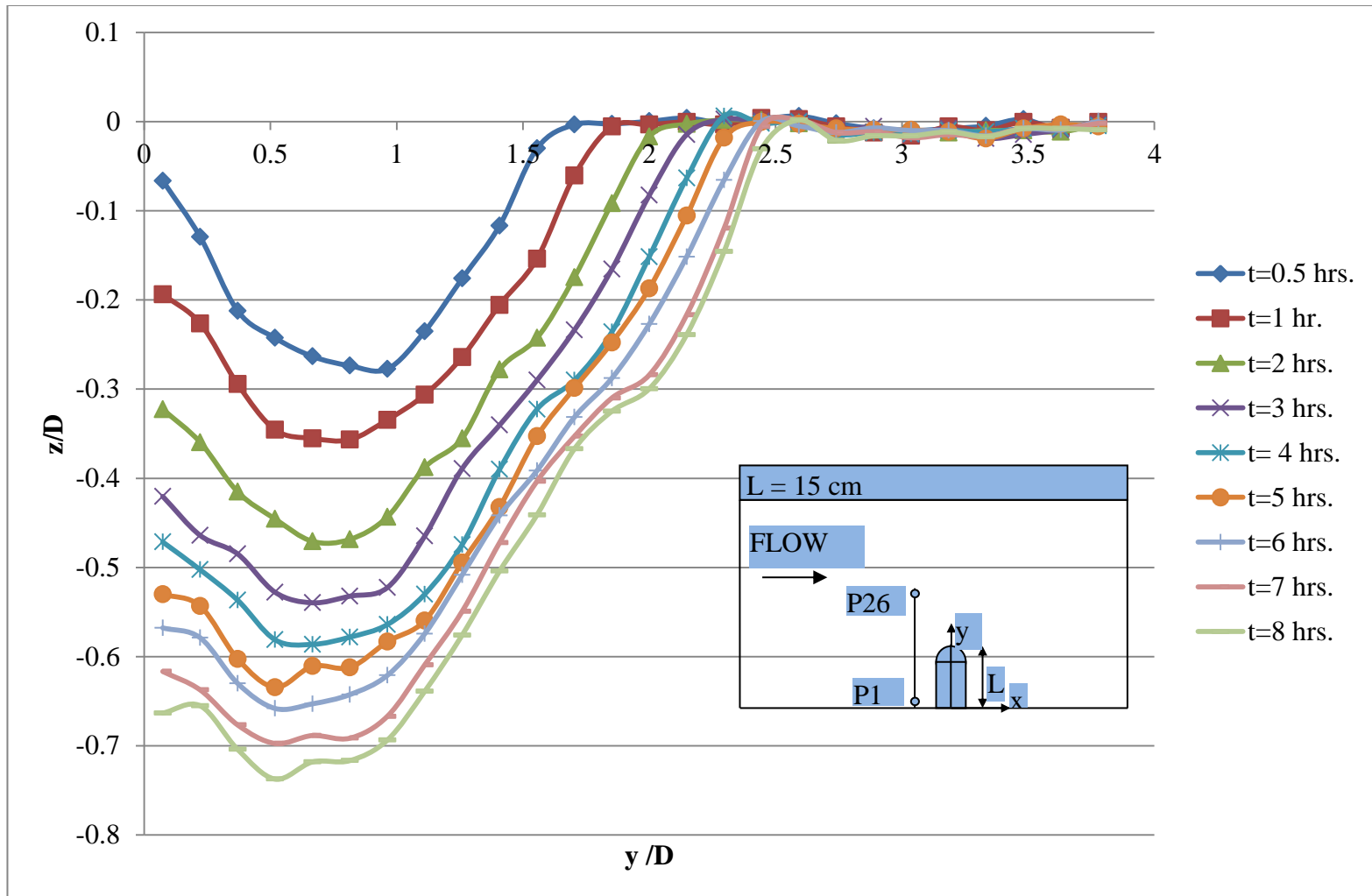


Figure 3.36 Temporal changes of bed profiles at Section #1 for the abutment of  $L = 15$  cm

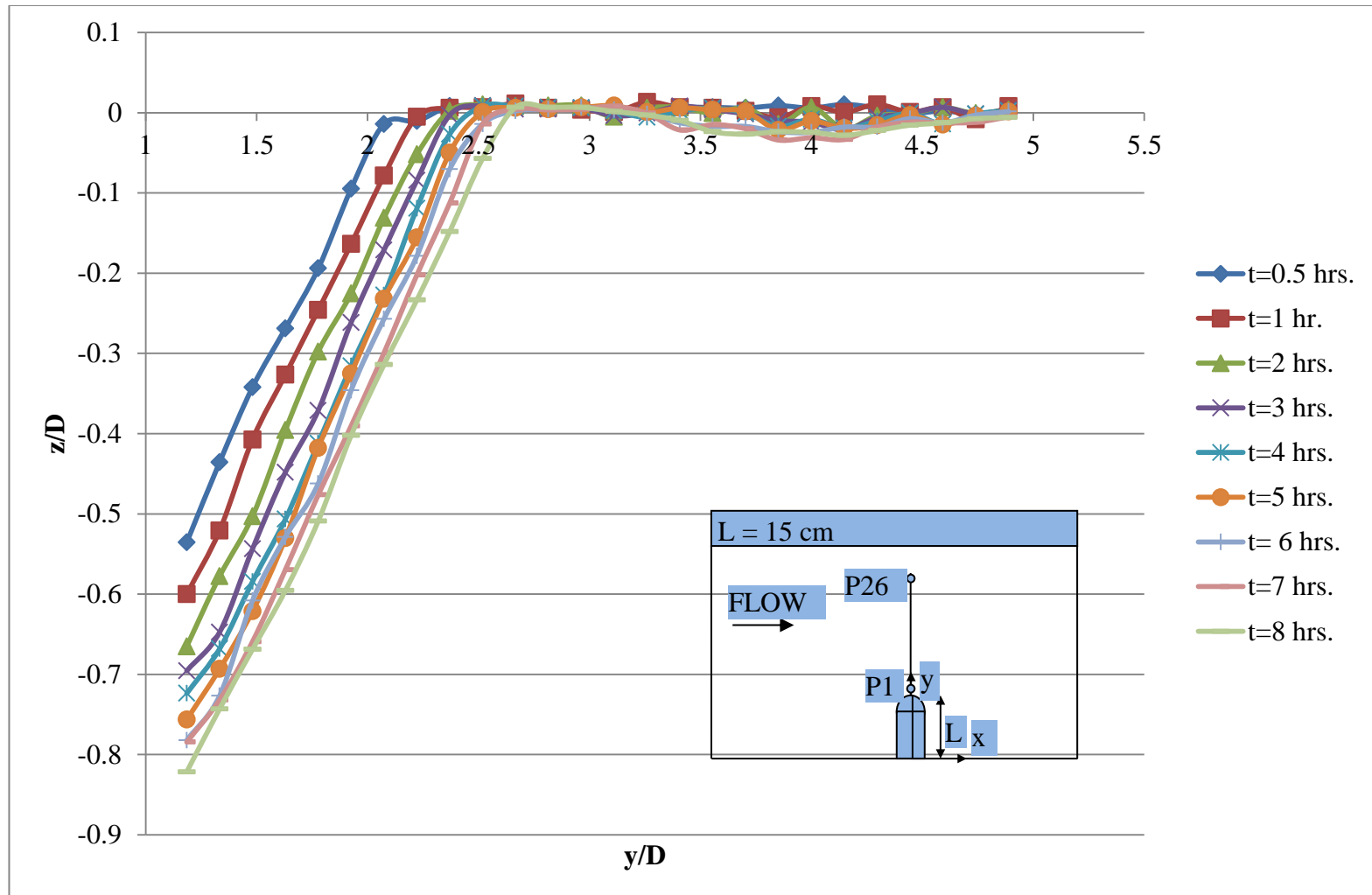


Figure 3.37 Temporal changes of bed profiles at Section #2 for the abutment of  $L=15$  cm

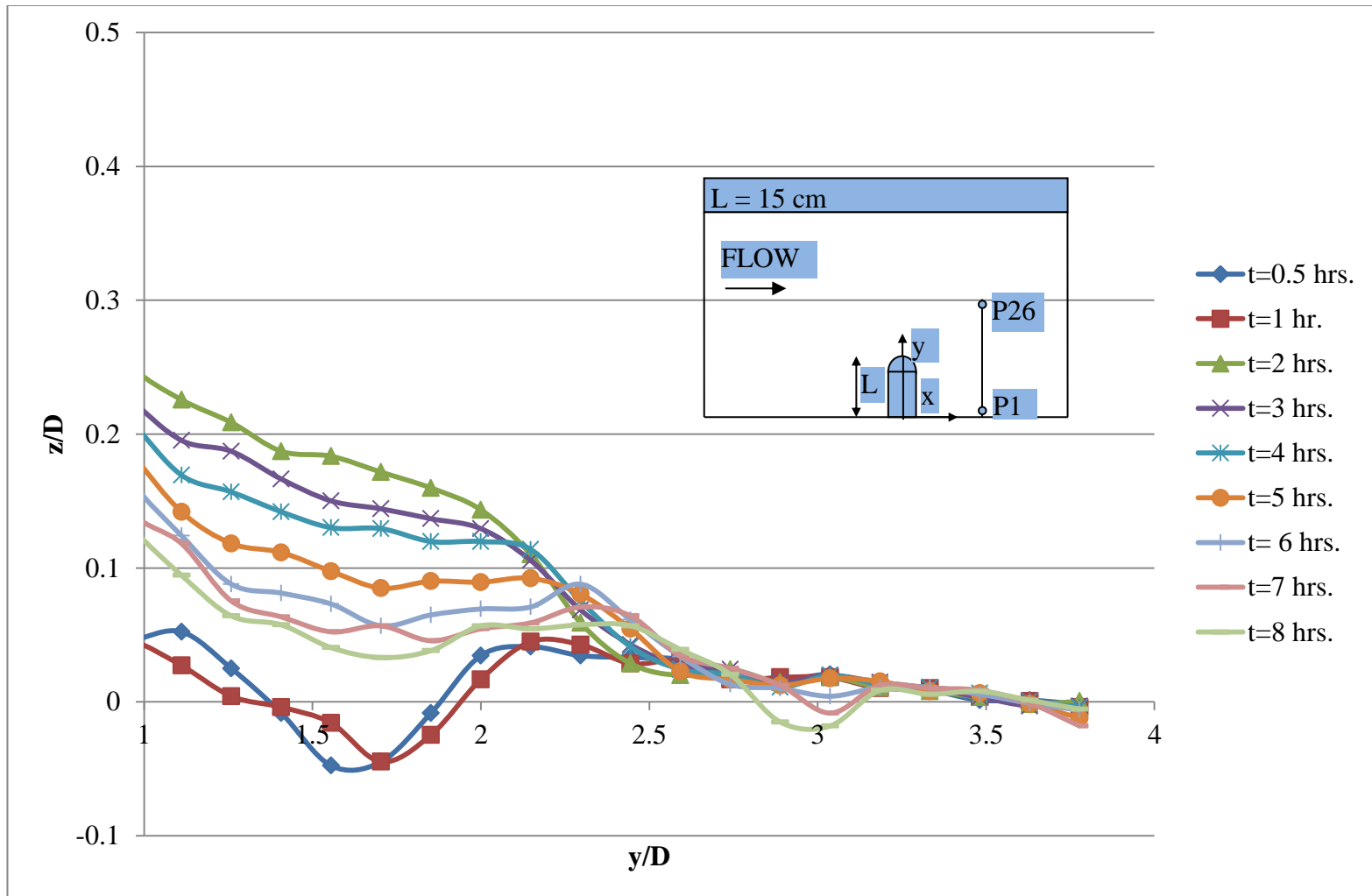


Figure 3.38 Temporal changes of bed profiles at Section #3 for the abutment of  $L = 15$  cm

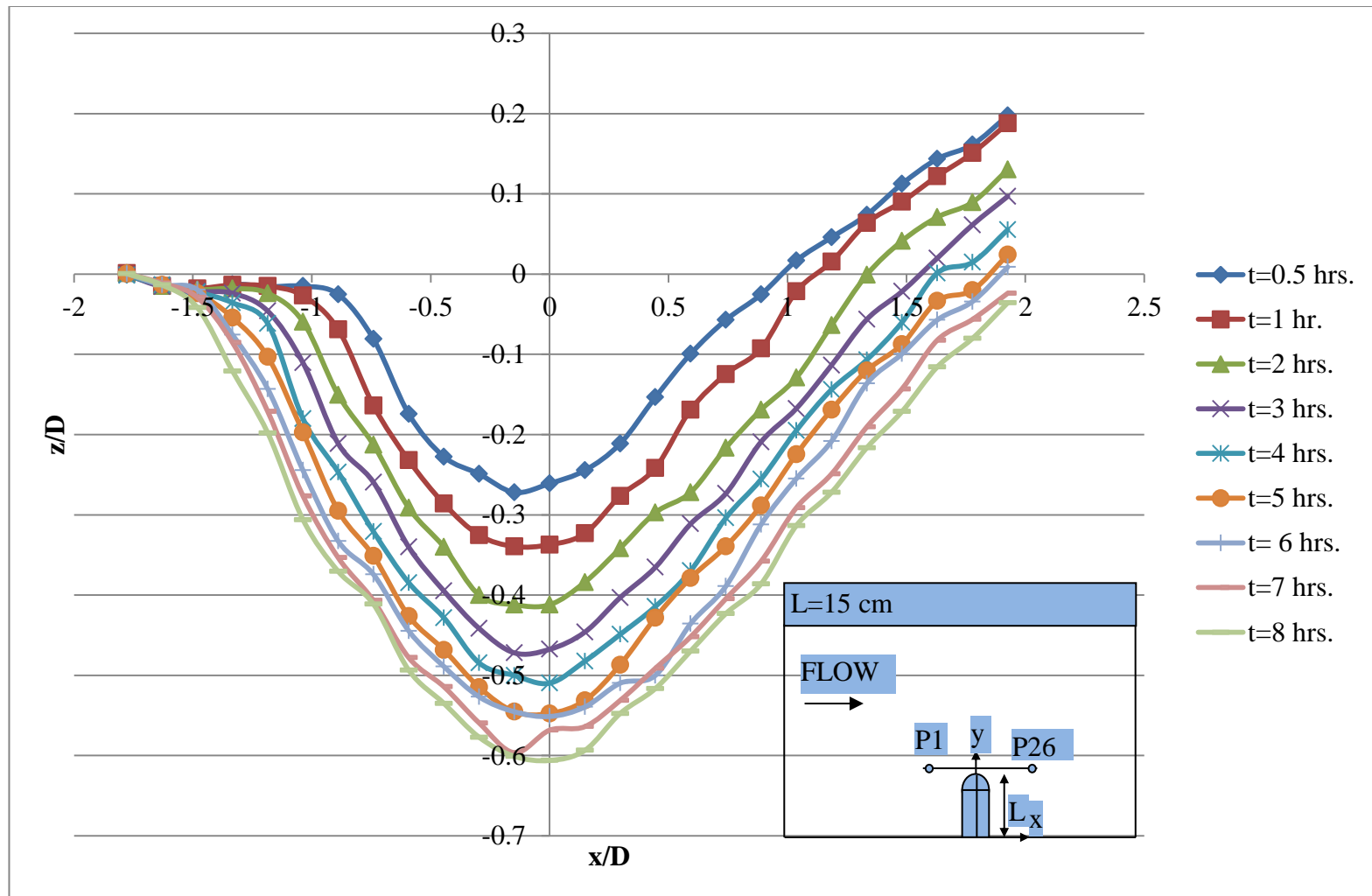


Figure 3.39 Temporal changes of bed profiles at Section #4 for the abutment of  $L = 15$  cm

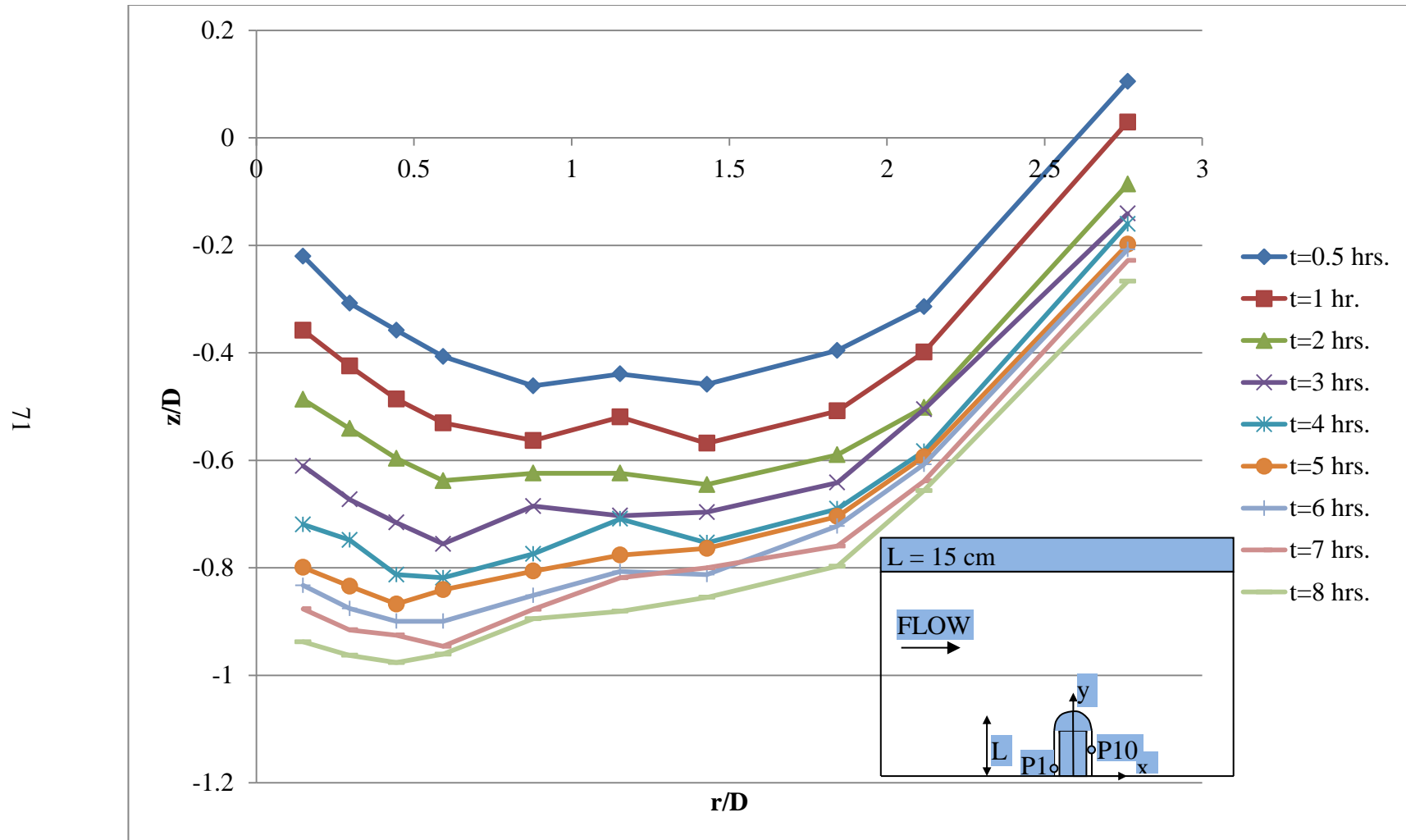


Figure 3.40 Temporal changes of bed profiles at Section #5 for the abutment of  $L = 15$  cm

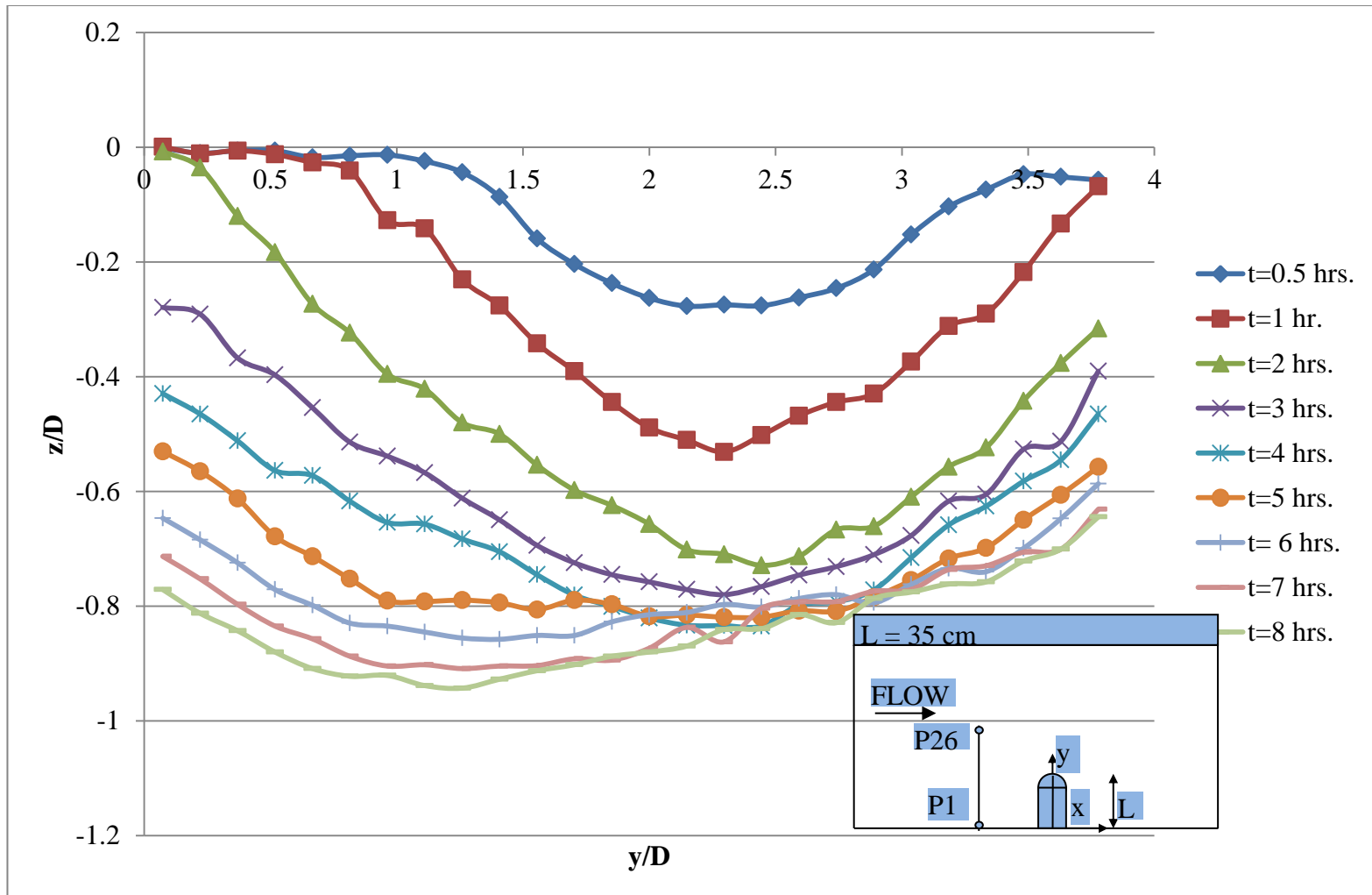


Figure 3.41 Temporal changes of bed profiles at Section #1 for the abutment of  $L = 35$  cm

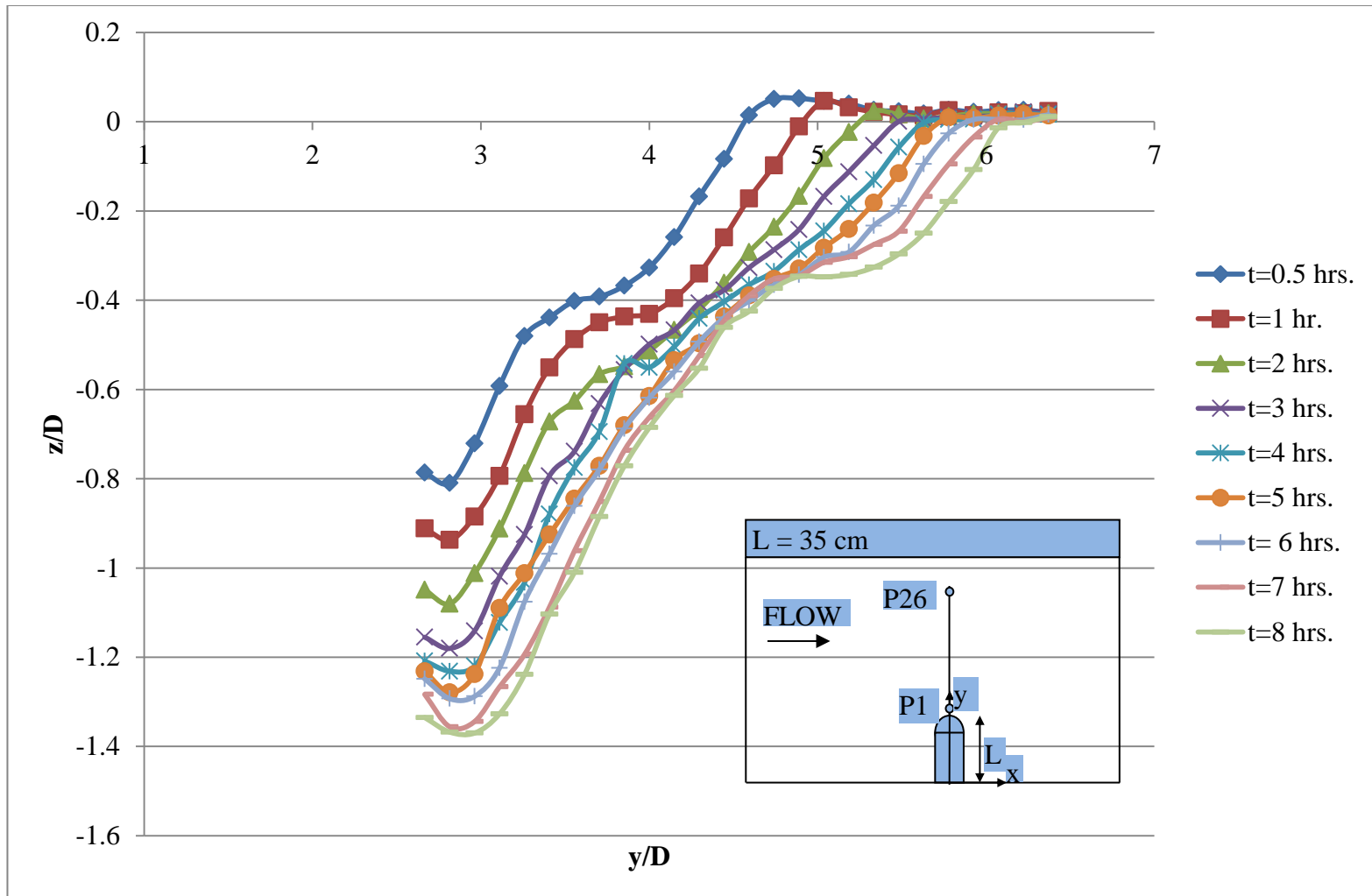


Figure 3.42 Temporal changes of bed profiles at Section #2 for the abutment of  $L = 35$  cm

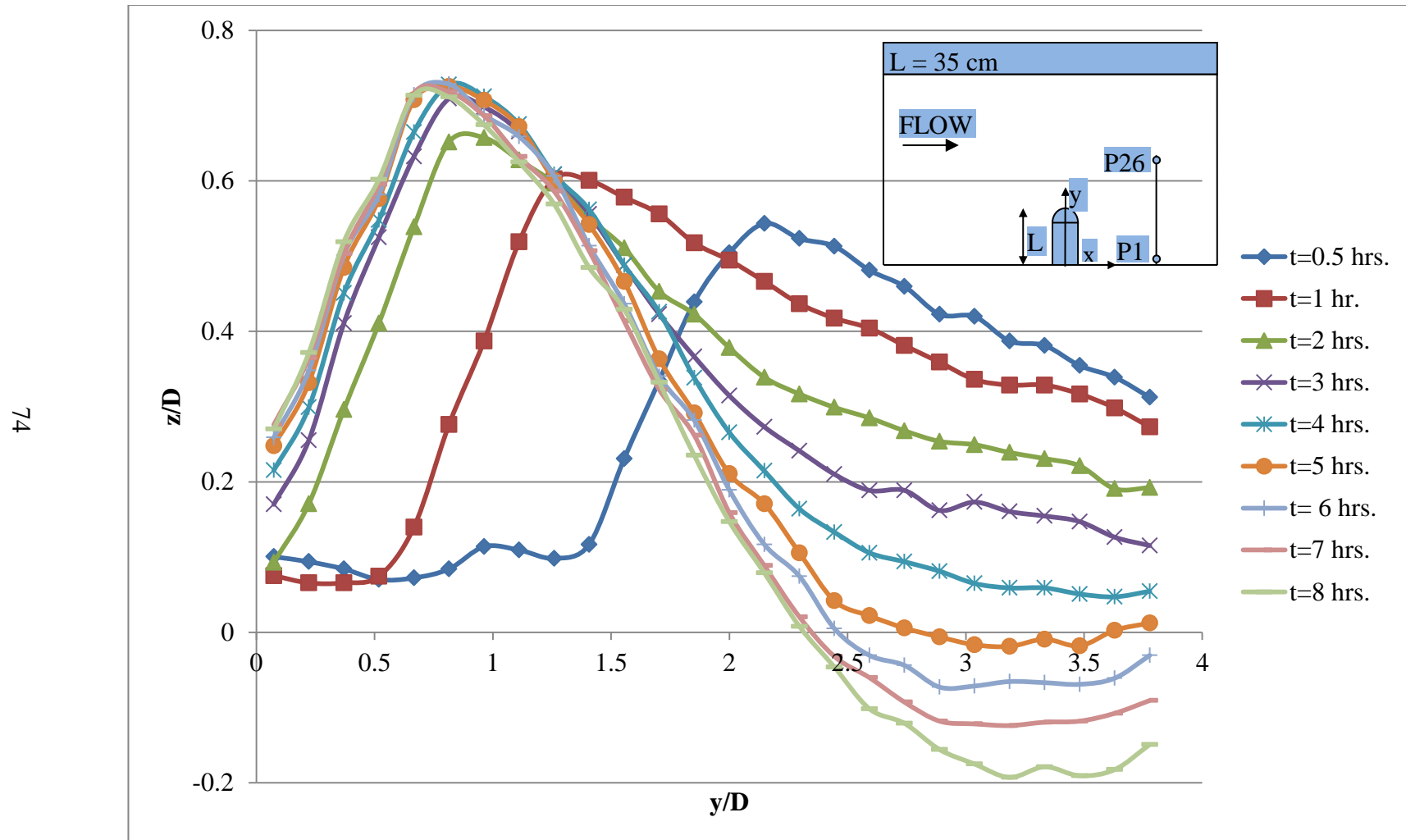


Figure 3.43 Temporal changes of bed profiles at Section #3 for the abutment of  $L= 35$  cm

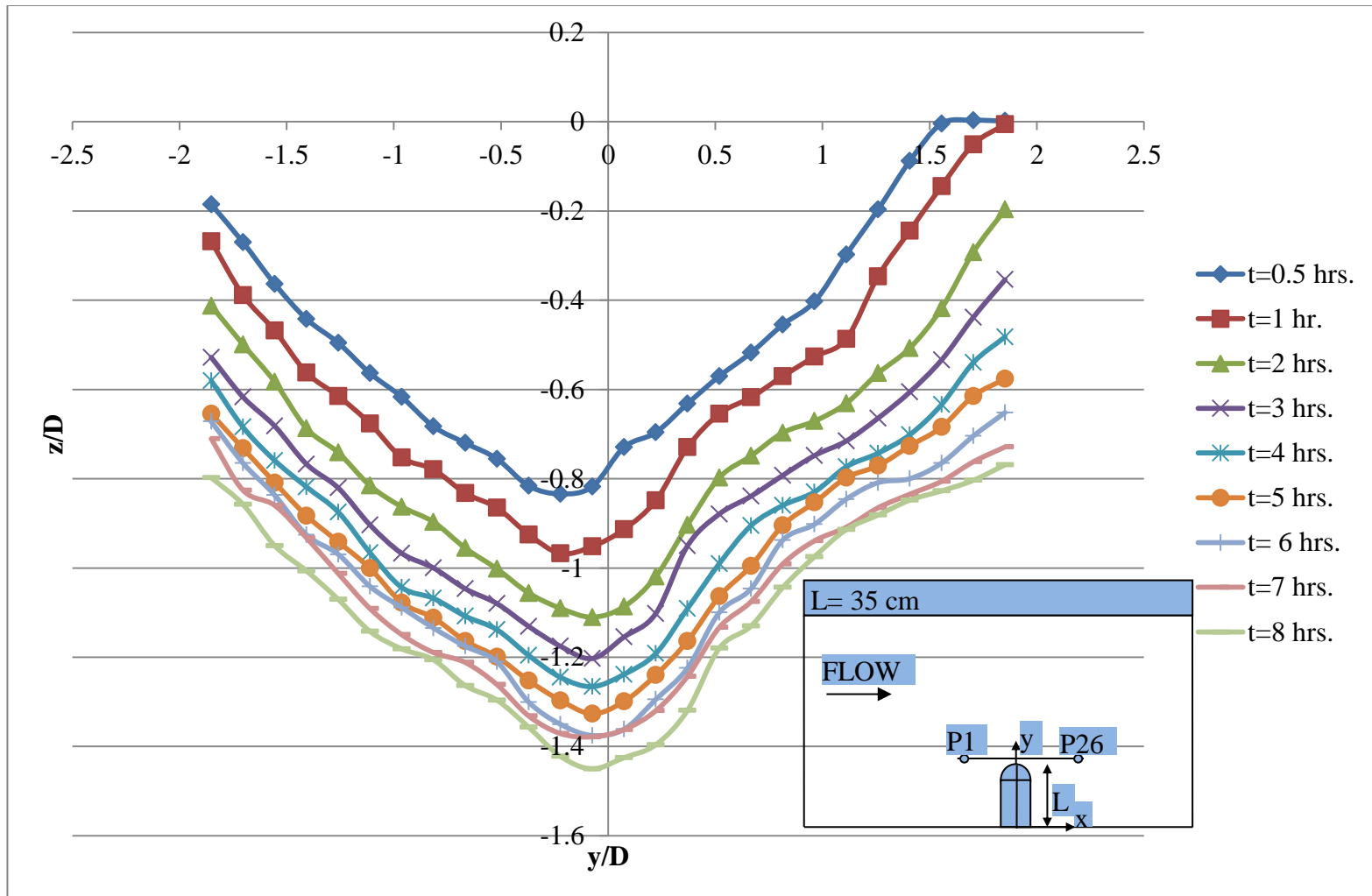


Figure 3.44 Temporal changes of bed profiles at Section #4 for the abutment of  $L=35$  cm

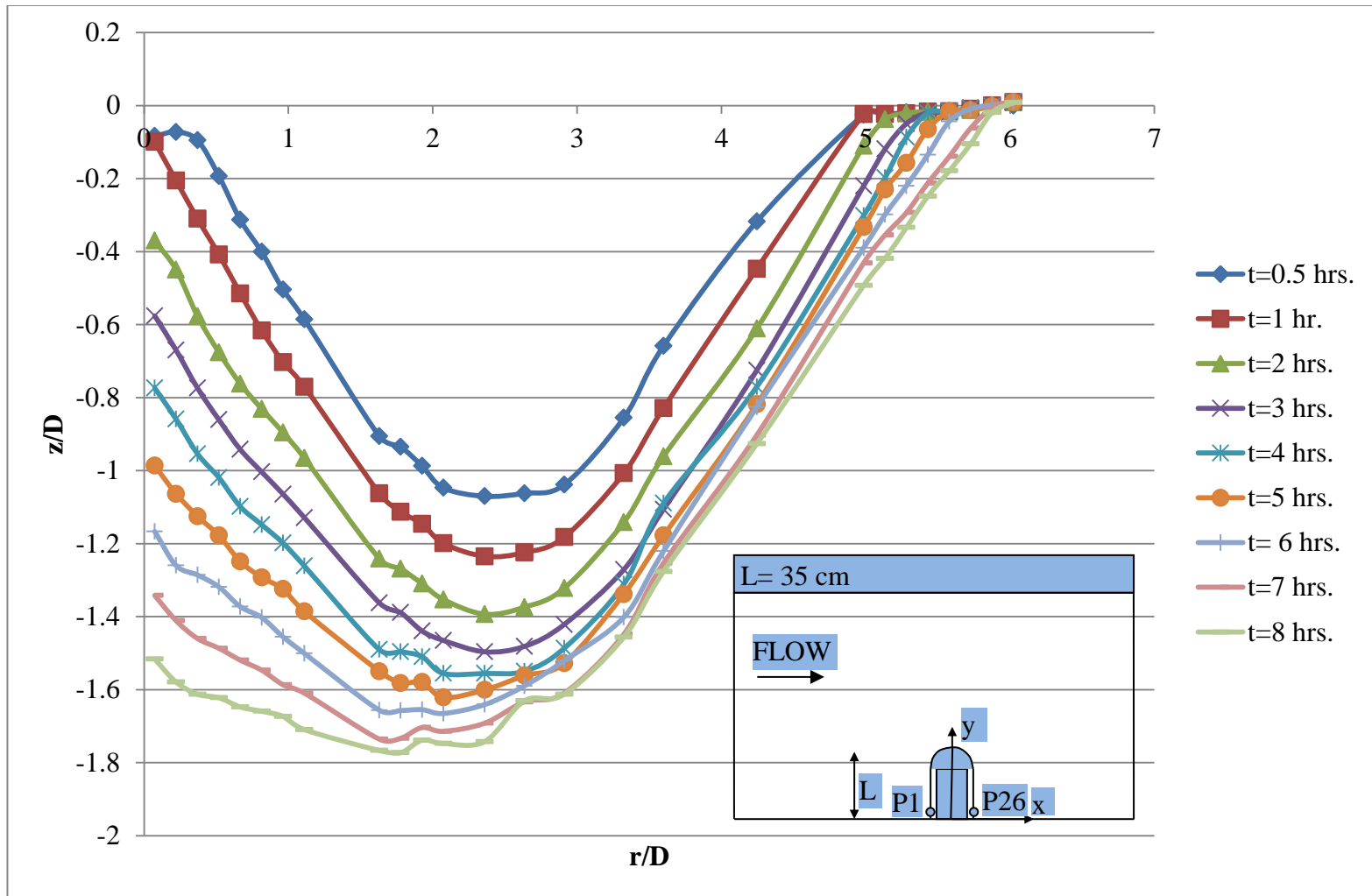


Figure 3.45 Temporal changes of bed profiles at Section #5 for the abutment of  $L = 35$  cm

### 3.3.2.1 Discussion of Results

As can be seen from Figures 3.36 to 3.45, the scour hole grows with time. The scour hole mostly maintains its shape while the rate of change of growth decreases with time, which is one of the main characteristics of the scouring mechanism.

The side slopes of the scour hole at the main channel side were measured as equal to the tangent of the angle of repose of the bed material. However, the side slopes at the flume wall side could not maintain the natural shape as the scour hole elongates till the side wall of the flume and deforms with the effect of integrating with the wall. The figures giving the bed profiles obtained from Section 2 demonstrates the parallel side slopes clearly (Figures 3.37 and 3.42).

From Figure 3.42, the initiation of the formation of a secondary step in the scour hole is observable from the 0.5<sup>th</sup> hour of the experiment for the long abutment. The formation keeps its shape throughout the test duration. A similar formation is not present for the short abutment until the 7<sup>th</sup> hour of the experiment (Figure 3.36).

Figure 3.43 shows development of the deposition region at the downstream of the long abutment. It can be seen from this figure that, the deposition hill forms away from the flume side wall at the first hour of the experiment and it starts to move towards to the side wall of the flume as the time passes. This motion becomes very slow after the third hour and stops at the fifth hour of the experiment. The slope on the flume wall side remains constant at all times throughout the experiment. However, the slope on the main channel side varies throughout the experiment with the effect of the deposited material transported from the scour hole through downstream. After fifth hour while the scour hole still grows, the height of the deposition hill remains unchanged. It is also important to note that on both sides of the deposition hill, slopes remain constant after this time.

The maximum scour depths were obtained at the fifth section for both abutment lengths. The maximum depths were obtained at the upstream side of the abutment tip. Temporal development of the scour depths at these points where maximum scour

depth is obtained for the short and the long abutments are given in Figures 3.46 and 3.47, respectively. These points were corresponding to the maximum scour locations as the locations and the scour depth values of them are consistent with the ones obtained from bathymetry measurements.

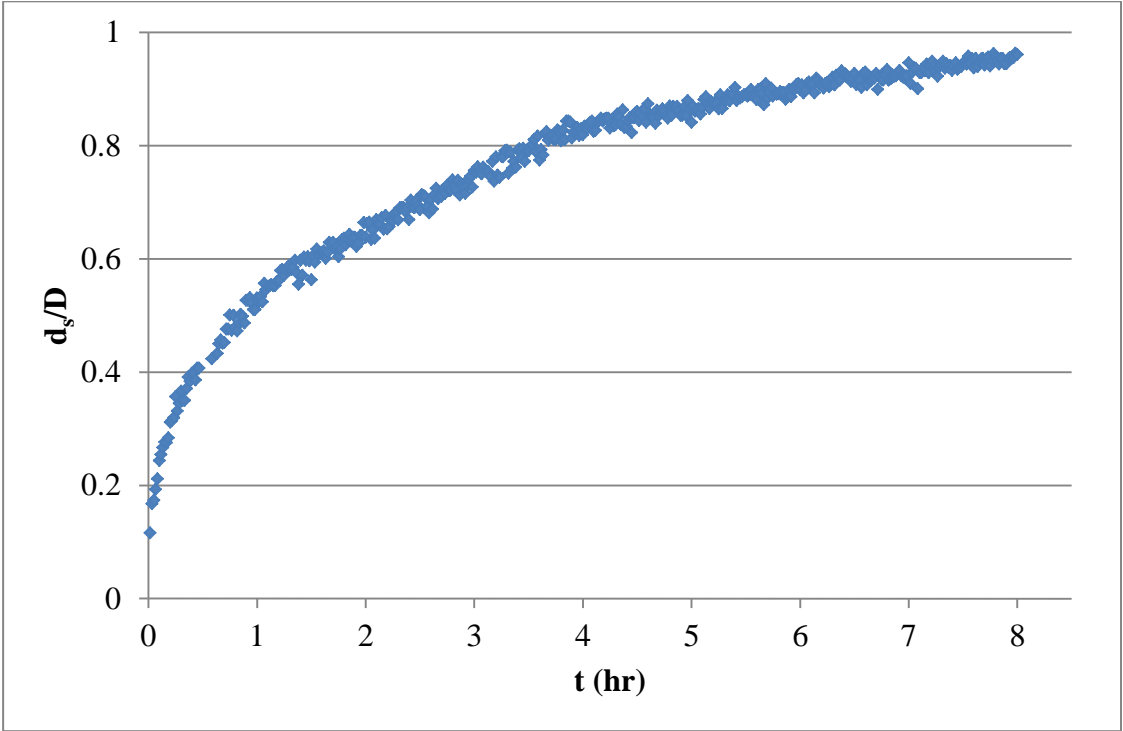


Figure 3.46 Temporal development of scour depth for  $L= 15$  cm

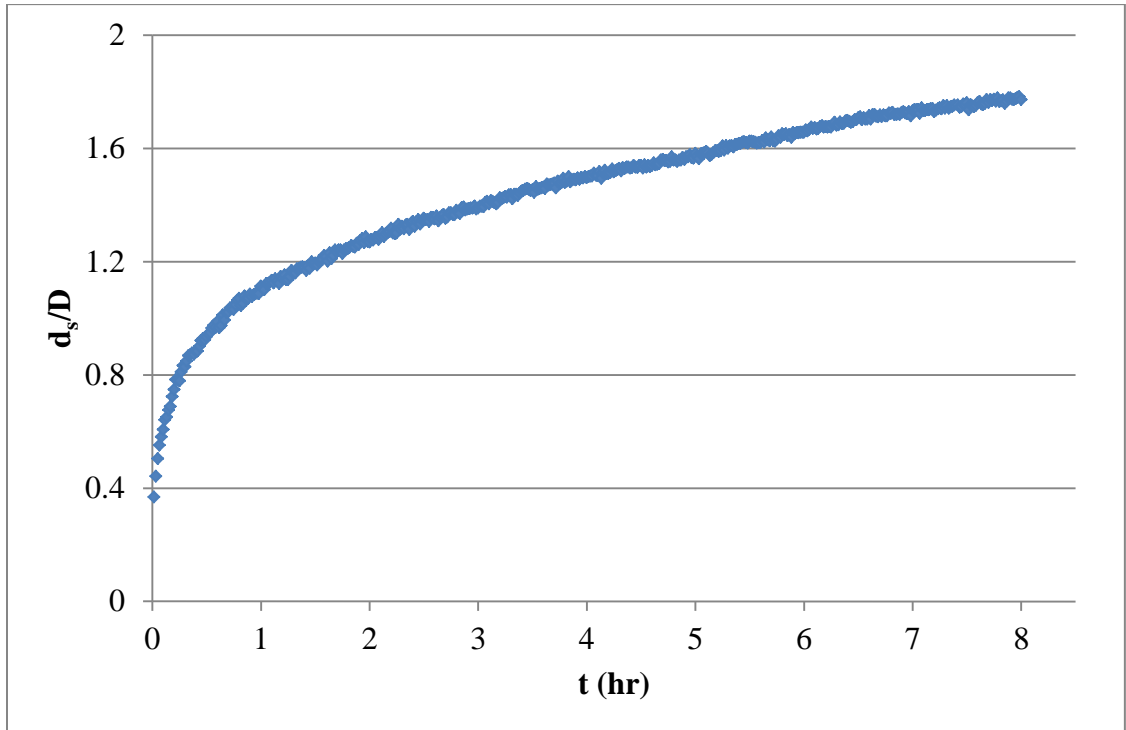


Figure 3.47 Temporal development of scour depth for  $L= 35$  cm

It can be seen from both figures that, the scour development is very fast in the early stages of the experiments. Then, the rate of change of increase in the scour depth decreases gradually with time. For short abutment case, the rate of change of increase in scour depth is smaller than that of long abutment case at time,  $t= 8$  hours. Therefore, it can be concluded that, the scouring for short abutment case is closer to the equilibrium phase than the scouring for long abutment case at the end of the experiment duration. Hence, it can be expected that the scouring would reach to equilibrium phase faster for short abutment case rather than the long abutment case.

It can also be concluded from Figure 3.47 that, 50% of the final scour depth was reached after the 1/16 of the total experiment duration passes ( $t=0.5$  hour,  $T_s = 3.43$ ) for long abutment. This ratio is the 1/8 of the total experiment duration ( $t=1$  hour,  $T_s = 37.39$ ) for the short abutment (Figure 3.46).

### 3.3.2.2 Comparison of Results with the Results of Similar Studies in Literature

The temporal variations of the bed profiles around the abutments were measured by Ballio and Orsi (2001) for various sections taken around the abutment. In the present study, the general observations on the scour pattern was experienced similar to the one obtained by Ballio and Orsi (2001). However, as the positions of the sections were not compatible with the positions of the sections on the present study, no further comparison would be accomplished. That study is the only one found in literature analyzing the temporal development of bed profiles around the abutments.

However, the temporal development of maximum scour depth was studied previously by many researchers (Coleman et al., 2003; Oliveto and Hager, 2002 and 2005; Yanmaz and Kose, 2007). Among these studies the latter three were developed models for limited abutment types which do not cover the SCE abutments. Therefore, the findings of the experimental set were only compared with the results of the model developed by Coleman et al. (2003).

To apply the method offered by Coleman et al. (2003), the present problem is modeled for the methodology given by that study, which is given below;

$$d_{se} = K_{yl}K_IK_dK_sK_\theta K_G \quad (3.6)$$

where, the coefficients  $K_{yl}$ ,  $K_I$ ,  $K_d$ ,  $K_s$ ,  $K_\theta$  and  $K_G$  stands for the effects of flow depth-abutment length, flow intensity, sediment size, abutment shape, foundation alignment and approach channel alignment, respectively.

The model coefficients (K-coefficients) are selected as given in Table 3.3 for the present study. As the experiments of the present study were conducted in rectangular flume with no alignment in flow and abutment direction by using fine sediment particles as bed material, the coefficients  $K_d$ ,  $K_\theta$  and  $K_G$  were remained as 1.  $K_{yl}$  was defined as  $2*L$  for short abutments (the shortest abutment case in the present study) and  $2*(DL)^{0.5}$  for intermediate abutments (the remaining cases).  $K_I$  was defined as

equals to flow intensity value for the clear-water scour and  $K_s$  was defined as 0.75 for SCE abutments.

Table 3.3 Parameters used in modeling the problem with Coleman et al. (2003)

	$L= 15$ cm	$L= 35$ cm
$K_{yl}$	0.285	0.435
$K_I$	0.9	0.9
$K_d$	1	1
$K_s$	0.75	0.75
$K_\theta$	1	1
$K_G$	1	1

The timely variation of the maximum scour depth was defined with the given equation below at Coleman et al. (2003);

$$\frac{d_s}{d_{se}} = \exp \left[ -0.07 \left( \frac{U}{U_c} \right)^{-1} \left| \ln \left( \frac{t}{t_e} \right) \right|^{1.5} \right] \quad (3.7)$$

In the same study, for  $D/L < 1$  and  $L/d_{50} > 60$ , which is the case of the both abutment lengths investigated in this study ( $L= 15$  cm and  $L= 35$  cm),  $t_e$  was defined as;

$$t_e = 10^6 \left( \frac{L}{U} \right) \left( \frac{U}{U_c} \right)^3 \left( \frac{D}{L} \right) \left\{ 3 - \left[ 1.2 \left( \frac{D}{L} \right) \right] \right\} \quad (3.8)$$

The comparison graphs are given in Figures 3.48 and 3.49 for short and long abutments, respectively. In these figures, the temporal development data of the scour depth of the present study were compared with the results obtained from the models offered in the aforementioned studies. Instead of  $L/D$ ,  $\beta$ , which is the contraction ratio and equals to  $L/W$  for the isolated abutment case, was used to define the length effect. I was used to make a comparison with the results of the following chapter.

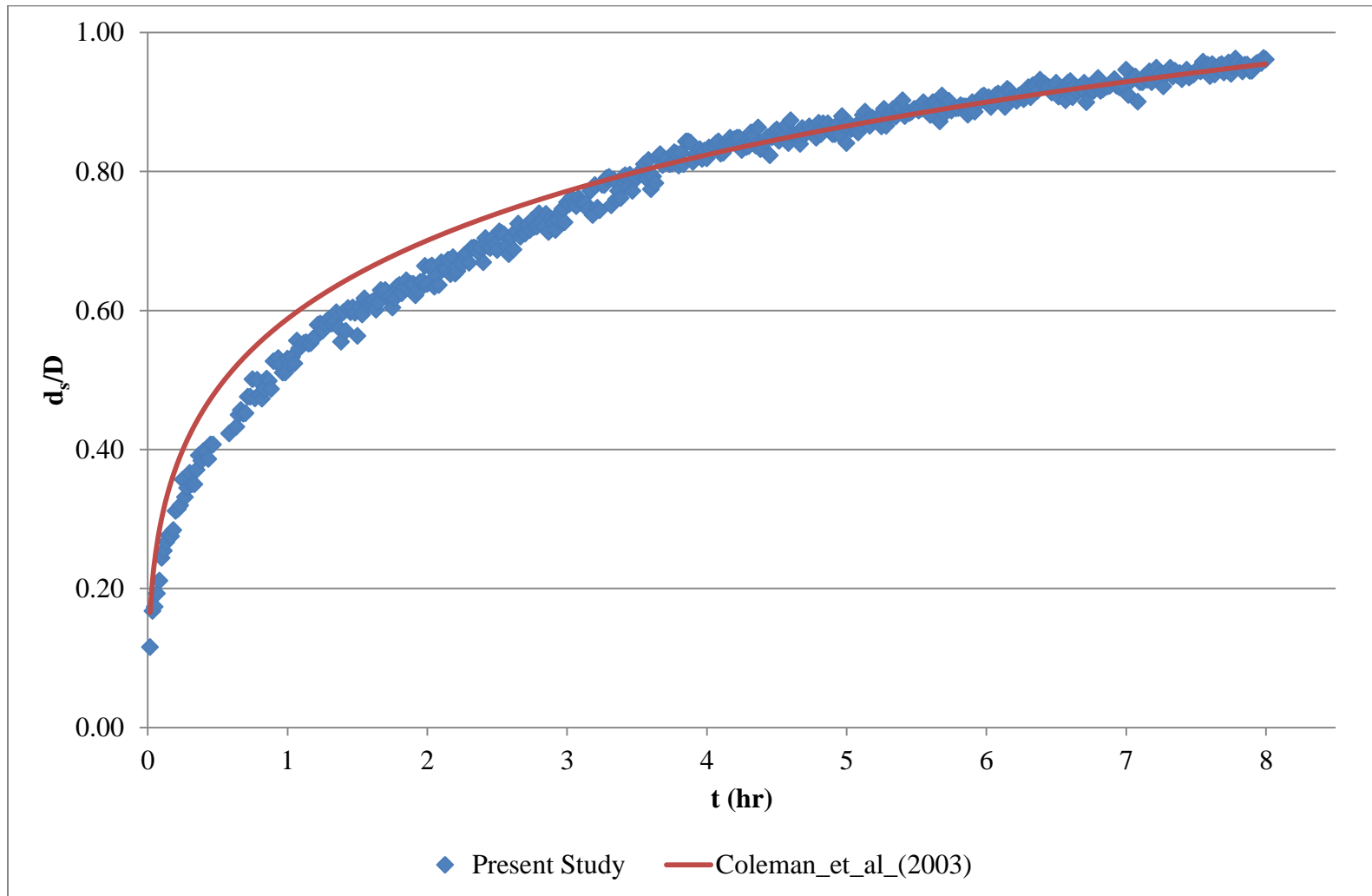


Figure 3.48 Comparison of experimental findings with Coleman et al. (2003) for  $\beta=0.10$

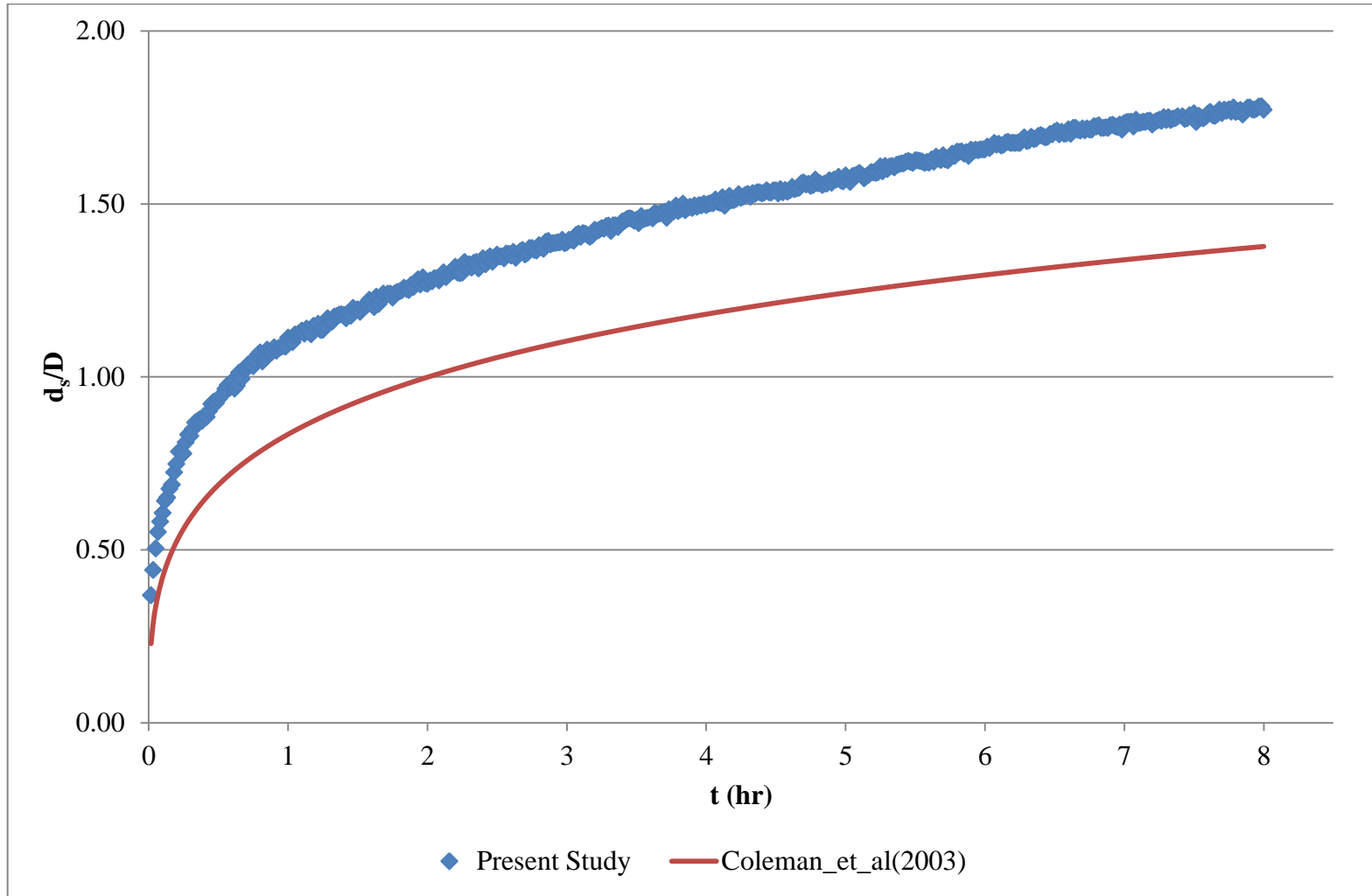


Figure 3.49 Comparison of experimental findings with Coleman et al. (2003) for  $\beta=0.23$

It can be seen from Figure 3.48 that, for short abutment, the results of the method offered by Coleman et al. (2003) overestimates the result slightly for the the initial stages ( $t < 3$  hours) and then fits almost perfectly to the data for the rest of the experiment time ( $t > 3$  hours).

From Figure 3.49, for the long abutment it can be seen clearly that, the results of the model offered by Coleman et al. (2003) underestimates the scour depth. It should be noted that, the model was developed for the time development of scour depth created by local scour only. For the case of long abutment, the contraction ratio is higher ( $\beta = 0.23$ ) compared with the case of short abutment ( $\beta = 0.10$ ). Therefore, the difference observed between the result of the model and the data of the long abutment case would be because of the significant amount of contraction introduced for this case.

To investigate the effect of contraction, additional analyses were done. For this purpose, the data obtained from the bathymetry measurements for various abutment lengths and various test durations were compared with the result of the method offered by Coleman et al (2003). From previous figures one can see that, the model of Coleman et al. (2003) fitted almost perfectly with the data of the short abutment and it showed similar behavior with the data of the long abutment case. Figures 3.50, 3.51 and 3.52 demonstrate the variation in  $d_s/D$  values with the change in contraction ratios for two, four and eight hours of test durations, respectively. It can be seen from each figure that, for the small values of contraction ratio, the data of the present study agreed well with the method. However, by the increase in contraction ratio, the rate of change of increase in  $d_s/D$  is higher for the experiment data rather than the offered method and the data diverges from the model slightly. By comparing the contraction ratios at the divergence points for Figures 3.50 to 3.52,  $\beta = 0.15$  can be stated as the critical ratio of contraction above which the divergence begins with the experimental data of the present study and the result of the model offered by Coleman et al. (2003). Hence, it can be stated that, the effect of flume contraction on local scour is observable over  $\beta = 0.15$  for this experimental set based on the comparisons with Coleman et al. (2003). The discussion of this topic will be extended further in Chapter 4 after the analysis of the experimental data covered in that chapter.

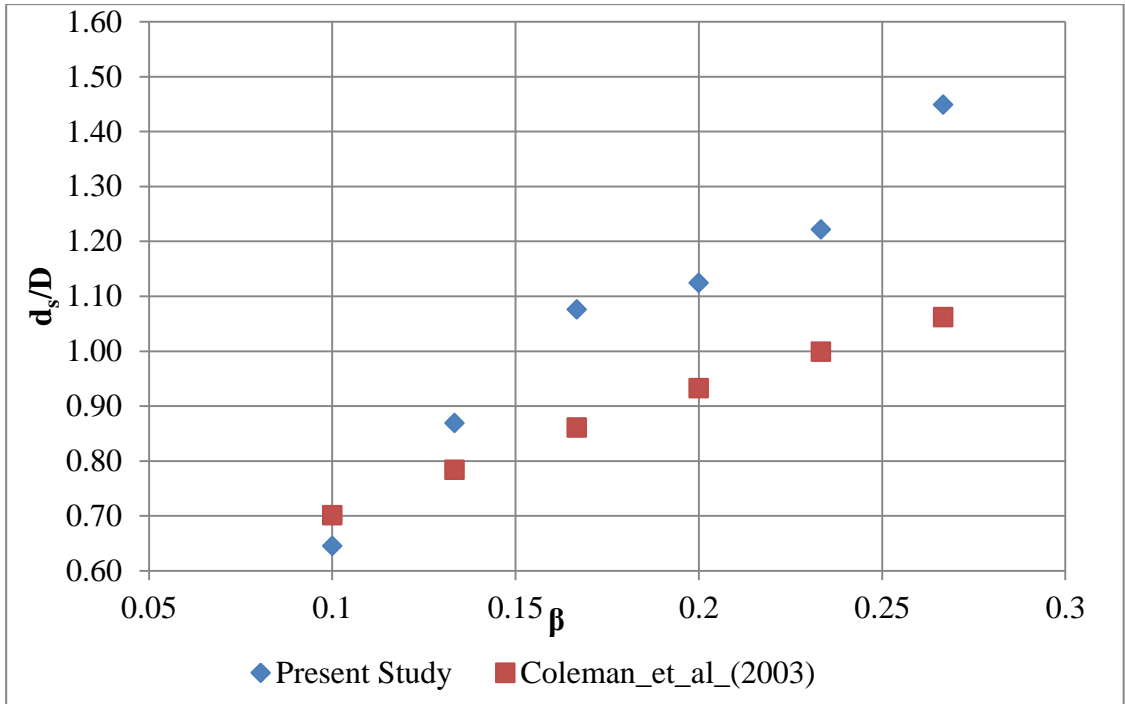


Figure 3.50 Comparison of bathymetry data with Coleman et al. (2003) for  $t= 2$  hours

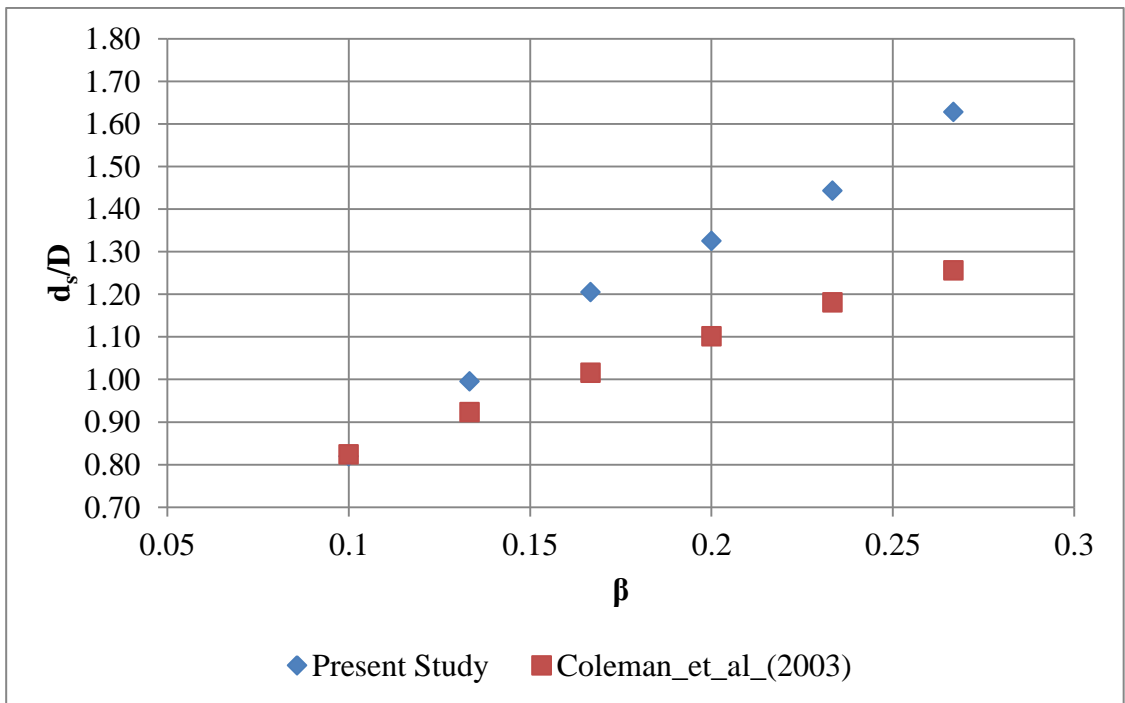


Figure 3.51 Comparison of Bathymetry Data with Coleman et al. (2003) for  $t= 4$  hours

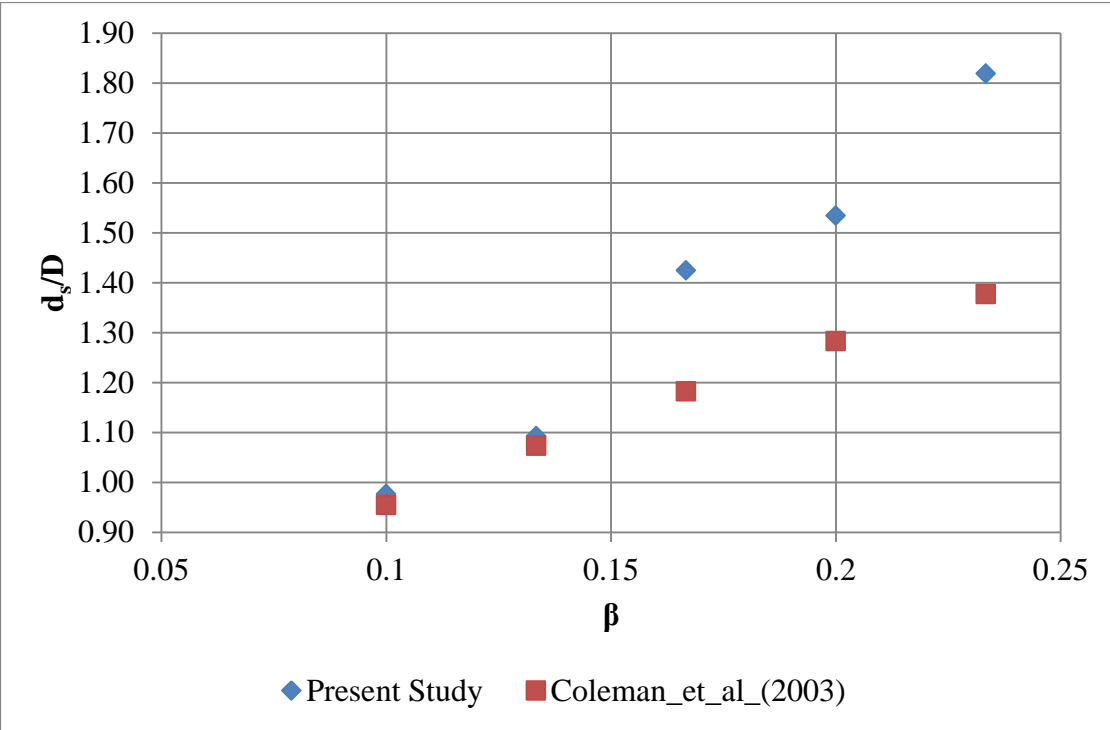


Figure 3.52 Comparison of bathymetry data with Coleman et al. (2003) for  $t= 8$  hours

## CHAPTER 4

### MORPHOLOGICAL CHANGES ON RIVER BED AROUND A PAIR OF BRIDGE ABUTMENTS AT CONTRACTED SECTIONS

The channel contraction caused by the presence of bridge abutments in the bridge crossings has an essential effect on the development of scour around these structures. Although, the interaction of the contraction and local scour mechanisms should be handled with great attention in order to estimate the scour pattern accurately, very limited number of studies was considered the effect of contraction on local scour in the literature. For this reason, the effect of contraction on local scour was investigated within this chapter.

The effect of contraction on local scour has been analyzed experimentally by obtaining large contraction ratios up to 0.452, by placing two abutment models in the sediment storage part of the flume. In the experiments, spill-through abutment models with sharp corners were used. The methodology in the experiments was followed as it has been done for the experiment sets covered in Chapter 3. First, bathymetry measurements were taken for various contraction ratios and test durations. Then, the measurements were taken while the experiment was running to obtain the temporal changes in the bed profiles around the abutment.

As the general experimental conditions were discussed in Chapter 3 with details, this Chapter will be covered only by two headings as; Bathymetry Measurements and Temporal Scour Measurements.

#### **4.1 Bathymetry Measurements**

To investigate the effect of contraction on scour pattern, the bathymetries of the eroded beds were measured. The measurements were taken after the experiments were conducted for various experiment durations.

The contraction in the flume was obtained by placing two spill-through abutment models facing one another, in the sediment storage part of the flume. Analyses of the scour pattern were made for each case after taking bathymetry measurements. By this manner the relations of the scour pattern parameters with varying contraction ratios and time were obtained.

This section includes the “Experimental Equipment and Procedure” and “Results” parts, which are given in detail below.

#### **4.1.1 Experimental Equipment and Procedure**

In the experiments, spill-through type abutment models were used which are produced from plexiglass. Sidewalls of the abutments had  $60^\circ$  angle with the horizontal direction. The corners of the abutments on the bridge crossing side of the flume were produced with sharp corners due to practical reasons in the laboratory production medium. Due to this sharpness, the models used in this study would be expected to result with slightly more scour depths than the scour depths resulted with the classical spill-through abutments with round corners. Abutments had a fixed base width of  $L_b = 25.6$  cm buried in the sand where lengths of the abutments were variable. Figure 4.1 shows the dimensions of the shortest abutment model. The other abutment models are obtained by increasing the length with five cm portions at each experiment set. In the calculations, the lengths of the spill through abutments are taken as the corresponding length at the mid depth of the flow (Melville, 1997). Therefore, while the base length ( $L_a$ ) of the shortest abutment is 12.8 cm, in the study its length ( $L$ ) is used as 8.9 cm. Similarly, the lengths of the remaining abutment models are given in Table 4.1. As can be seen from the table, in the present set, 18 experiments were conducted for six contraction ratios and three different experimental durations for each contraction ratio. The experiment durations were selected as two, four and eight hours. The reason of choosing these durations were discussed in Chapter 3.

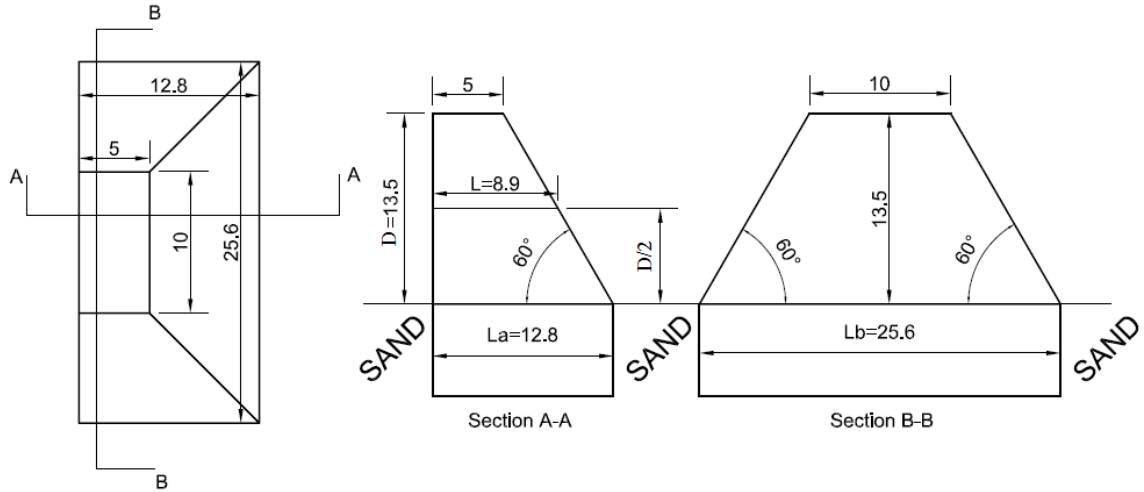


Figure 4.1 Dimensions of the shortest abutment model (in cm)

Table 4.1 Test Conditions

Set Nr.	L (cm)	L <sub>a</sub> (cm)	t (hrs.)	D (cm)	d <sub>50</sub> (mm)	β	L/L <sub>b</sub>
1	8.9	12.8	2	13.5	1.50	0.119	0.35
2	8.9	12.8	4	13.5	1.50	0.119	0.35
3	8.9	12.8	8	13.5	1.50	0.119	0.35
4	13.9	17.8	2	13.5	1.50	0.185	0.54
5	13.9	17.8	4	13.5	1.50	0.185	0.54
6	13.9	17.8	8	13.5	1.50	0.185	0.54
7	18.9	22.8	2	13.5	1.50	0.252	0.74
8	18.9	22.8	4	13.5	1.50	0.252	0.74
9	18.9	22.8	8	13.5	1.50	0.252	0.74
10	23.9	27.8	2	13.5	1.50	0.319	0.93
11	23.9	27.8	4	13.5	1.50	0.319	0.93
12	23.9	27.8	8	13.5	1.50	0.319	0.93
13	28.9	32.8	2	13.5	1.50	0.385	1.13
14	28.9	32.8	4	13.5	1.50	0.385	1.13
15	28.9	32.8	8	13.5	1.50	0.385	1.13
16	33.9	37.8	2	13.5	1.50	0.452	1.32
17	33.9	37.8	4	13.5	1.50	0.452	1.32
18	33.9	37.8	8	13.5	1.50	0.452	1.32

During the experiments, two identical abutment models were placed on the opposite walls of the flume within the sediment storage portion as seen in Figure 4.2. By this manner, the flume width is contracted with a ratio of  $\beta = 2L/W$ , while  $\beta$  denotes the contraction ratio and  $W$  stands for the flume width. The bed material properties were

discussed in Chapter 3 with details. The measurements were taken only around one abutment as the geometry in the flume was obtained as symmetrical about the flume axis in the flow direction and the bathymetries around both abutments were obtained almost identical. The 3-D bathymetry measurements of the scoured region were taken with SeaTek 5 MHz ultrasonic ranging system. The bathymetry measurements were taken by scanning the eroded bed with minimum 1 cm of intervals by the help of mobile carrier of the transducers after the experiments have finished. The transducers scanning interval was taken finer around the abutments to obtain the bathymetry of the area close to the location of the maximum scour depth with more accuracy. The top view of the illustration of the scour hole is given in Figure 4.3 to identify the parameters used in the further sections of this chapter.



Figure 4.2 A view of the flume and scour pattern when  $\beta= 0.452$  and  $t= 2$  hrs

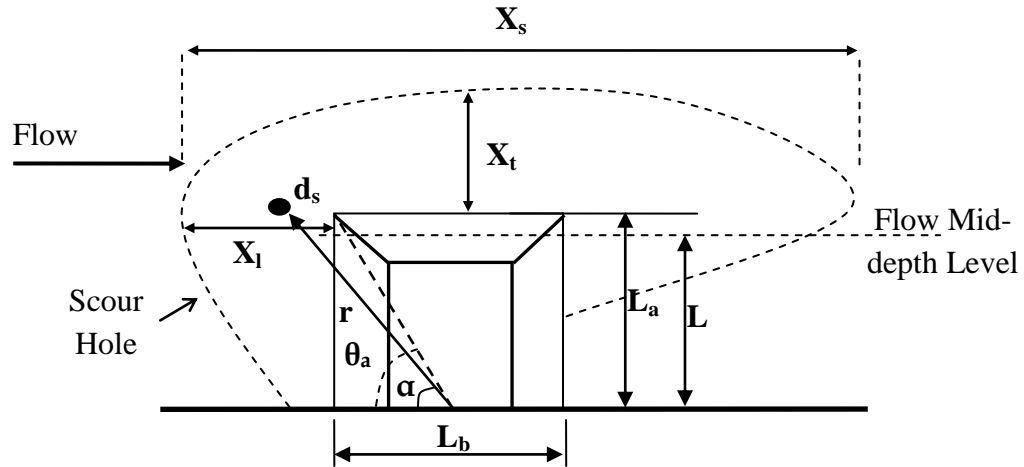


Figure 4.3 Top view of the illustration of scour hole

#### 4.1.2 Results

The processing of the experimental data covered in this section is similar to the processing of the bathymetry measurements data covered in Chapter 3. First, the data has been digitalized and the 3-D data of the eroded bathymetries for each set were obtained. Figures 4.4 to 4.21 show the 3-D bathymetry views, top views of the scour pattern and the longitudinal sections taken tangent to the toe of the abutment for each set.

In these figures,  $x/D$  stands for the dimensionless coordinate through the flow direction taking abutment axis as origin and  $z/D$  stands for the dimensionless scour depth and deposition height in  $z$  direction while zero being the original bed level, below zero corresponds to the scouring and above zero corresponds to the deposition regions.

It can be seen from the 3-D schemas of the scour patterns that, for small contraction ratios, the scour hole dimensions are very small and the scour hole expands with the increase in contraction ratio and also with the increase in time. For contraction ratios bigger than 0.319; the deposition region extends by passing the flume axis and the two deposition regions of the two abutments meet at the mid portion of the flume. The extension of scour holes through the flume axis is seen for contraction ratios bigger than

0.385. Although, at contraction ratio equals to 0.319, minor erosion is observed at the flume axis, the interaction of the two scour holes is noticed for the contraction ratios bigger than 0.385. Moreover, from the (c) frame Figures 4.4 to 4.21, the development of the scour hole and the deposition region can be seen with the help of 1-D graph showing the bed profile taken tangent to the toe of the abutment.

In Table 4.2, experimental findings regarding to the scour pattern are given. The parameters regarding to the scour pattern were used in dimensionless forms by rationalizing with the flow depth.  $d_s/D$  stands for the dimensionless maximum scour depth measured for each experiment.  $X_s/D$  is the dimensionless scour hole length in the flow direction. Scour hole length was measured as discussed in Section 3.2.2. Afterwards,  $X_l/D$  and  $X_r/D$  were measured for each set as discussed in Section 3.2.2. As for the experiment sets 13-18, the two scour holes coincide at the flume axis, the measurement of  $X_l/D$  could not be accomplished due to this physical situation. Two parameters,  $r/D$  and  $\alpha$ , were introduced to define the position of the maximum scour depth location. Figure 4.3 can be referred in defining these parameters.

The scour hole volume is given in non-dimensional form  $(V_s/D^3)$  after dividing the volume values to the cube of the flow depth. The scour volume values were calculated from the 3-D figures of the scour hole by numerical integration techniques.

The analyses of these results will be done in the following part of the Results section.

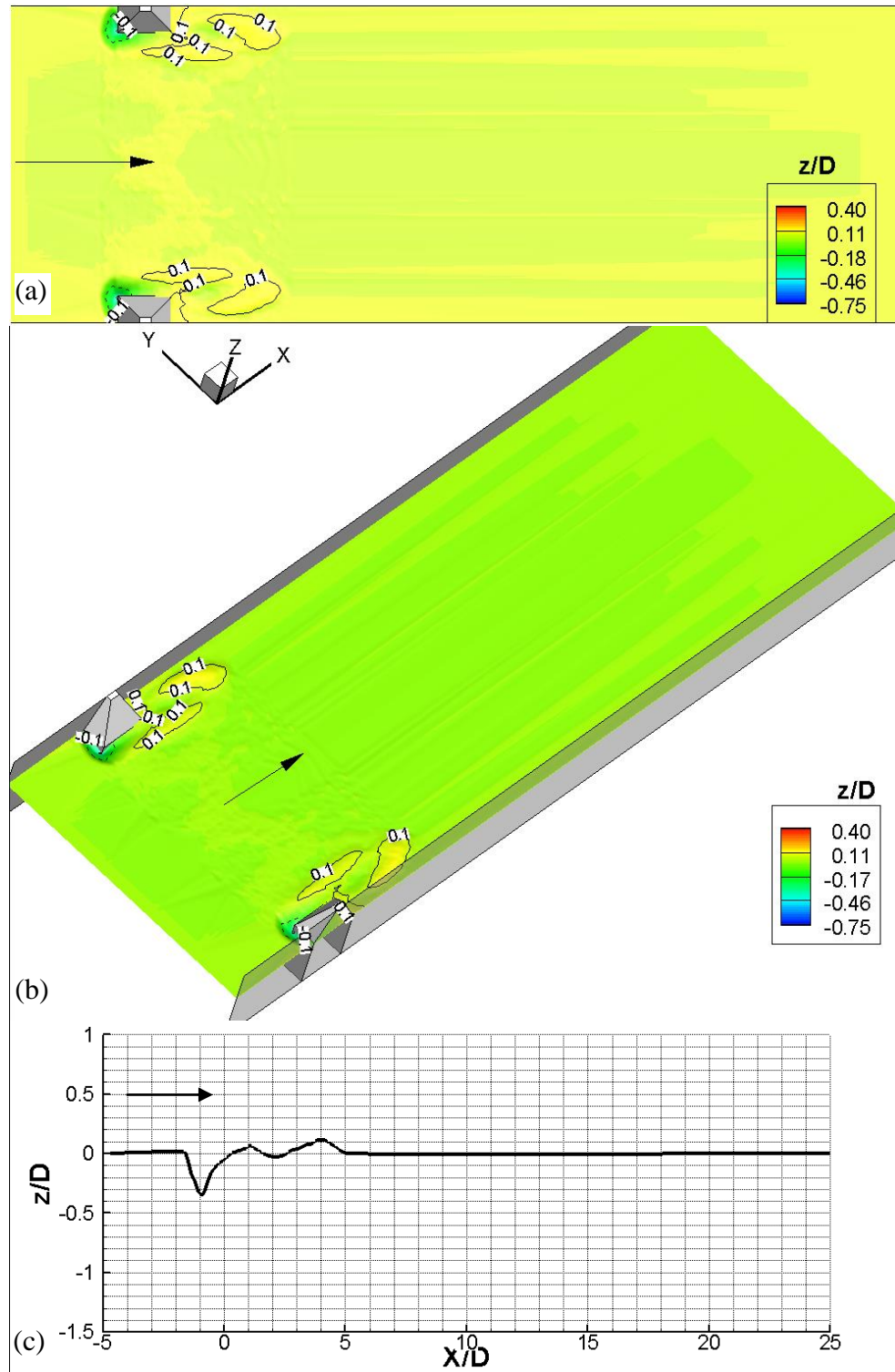


Figure 4.4 Scour pattern after a 2 hrs period experiment for the contraction ratio  $\beta=0.119$ : a) top view; b) 3-D view; c) longitudinal section view which is taken tangent to the toe of the abutment

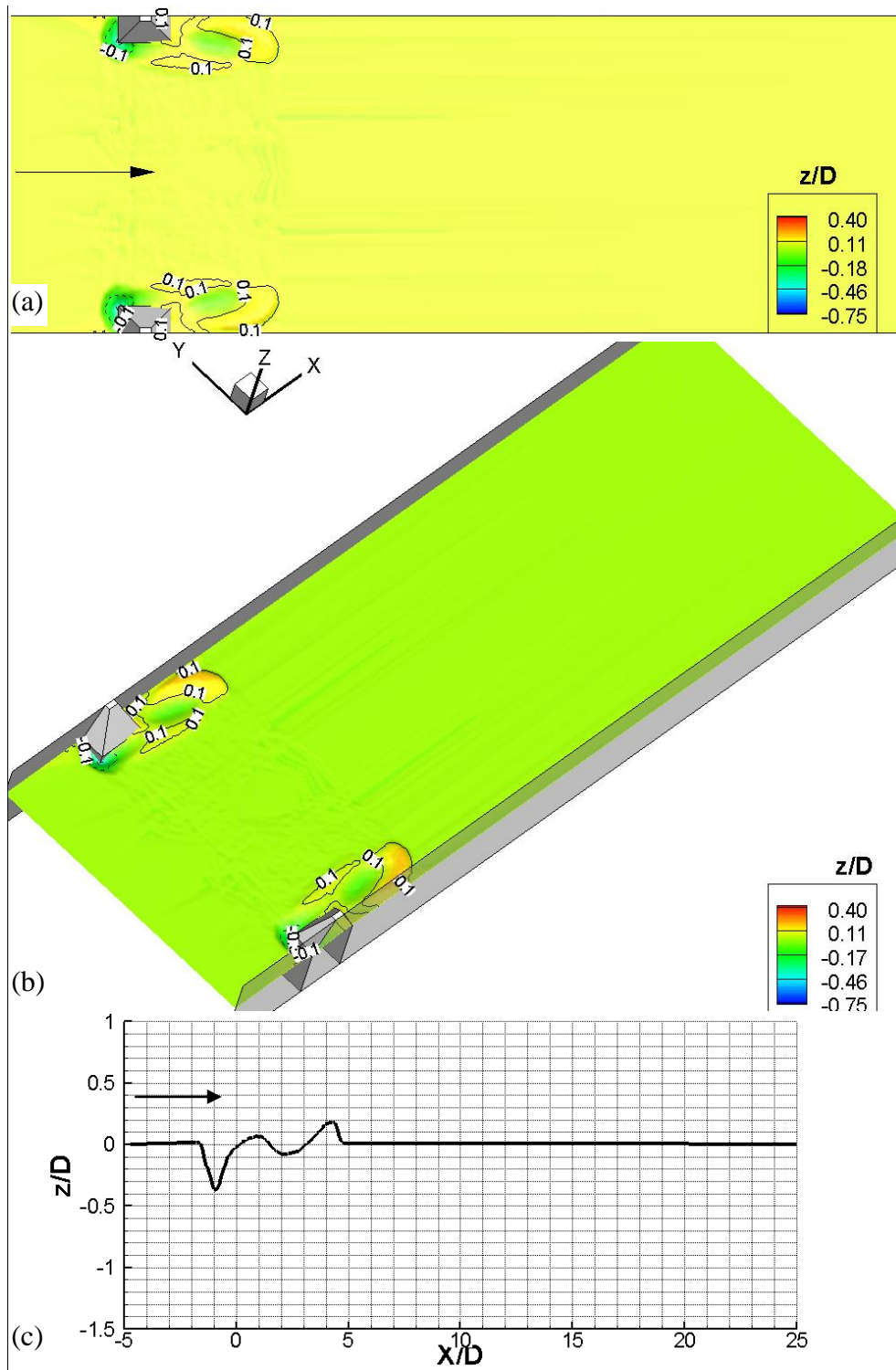


Figure 4.5 Scour pattern after a 4 hrs period experiment for the contraction ratio  $\beta=0.119$ : a) top view; b) 3-D view; c) longitudinal section view which is taken tangent to the toe of the abutment

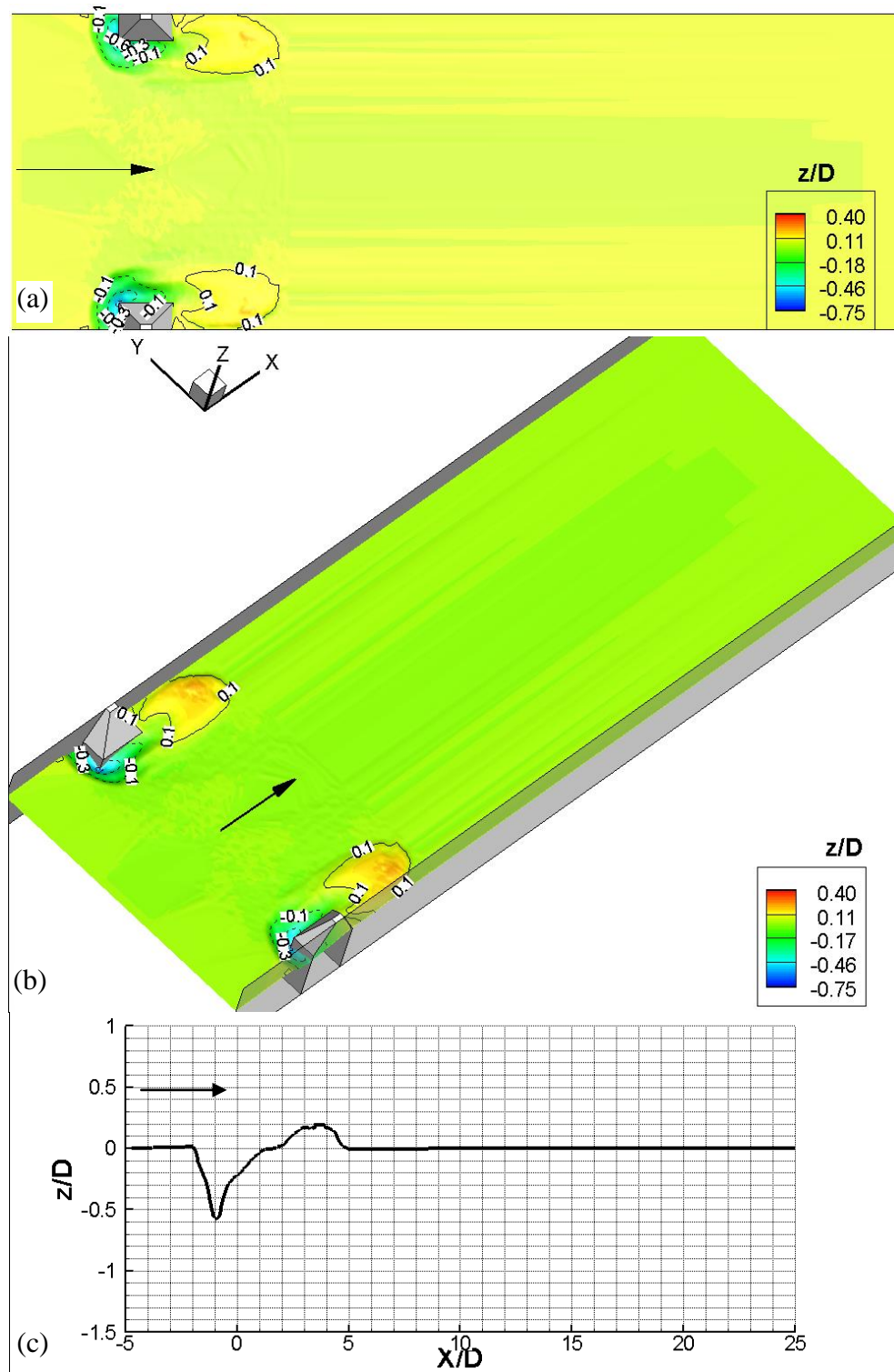


Figure 4.6 Scour pattern after a 8 hrs period experiment for the contraction ratio  $\beta = 0.119$ : a) top view; b) 3-D view; c) longitudinal section view which is taken tangent to the toe of the abutment

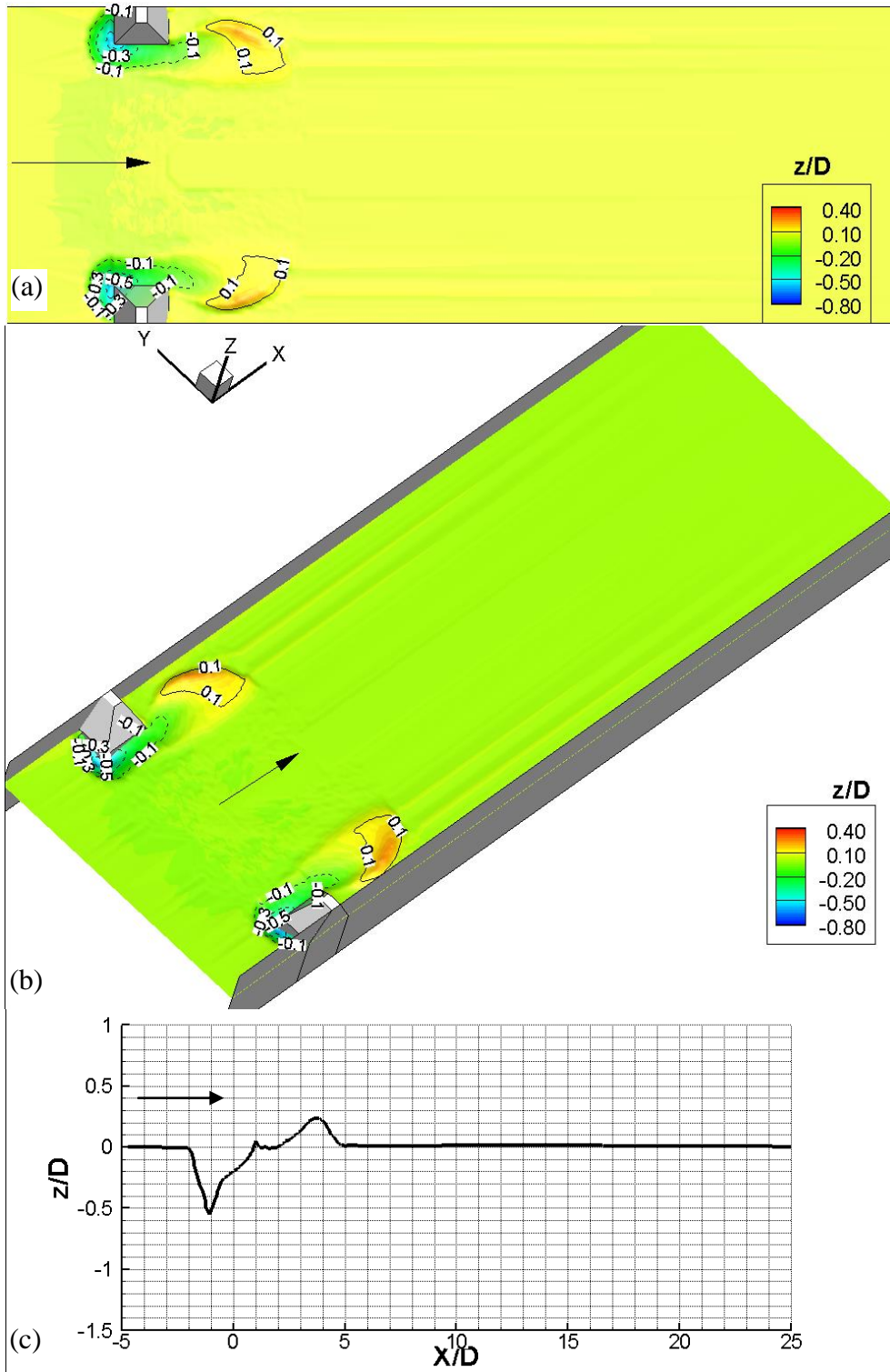


Figure 4.7 Scour pattern after a 2 hrs period experiment for the contraction ratio  $\beta = 0.185$ : a) top view; b) 3-D view; c) longitudinal section view which is taken tangent to the toe of the abutment

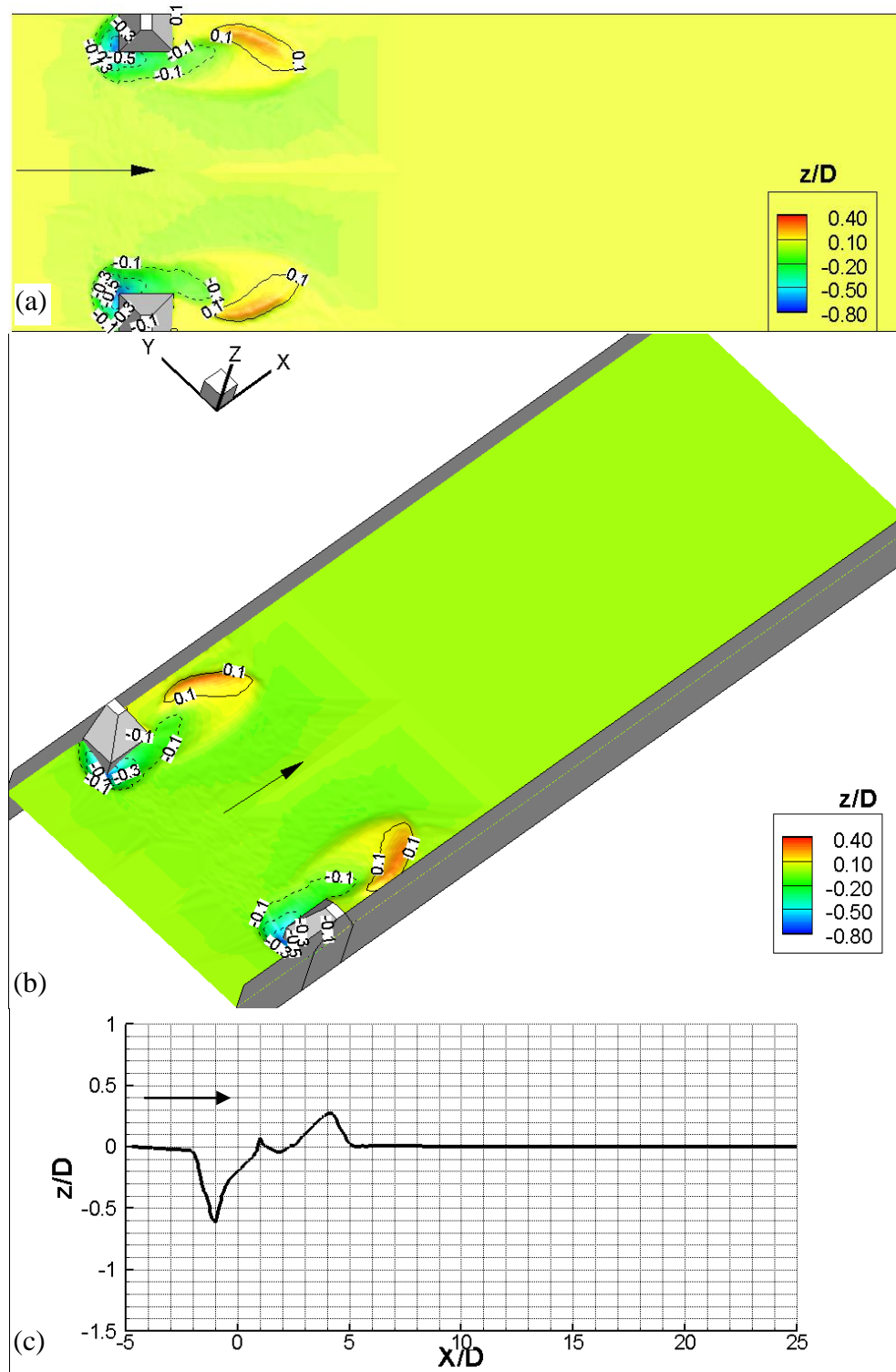


Figure 4.8 Scour pattern after a 4 hrs period experiment for the contraction ratio  $\beta = 0.185$ : a) top view; b) 3-D view; c) longitudinal section view which is taken tangent to the toe of the abutment

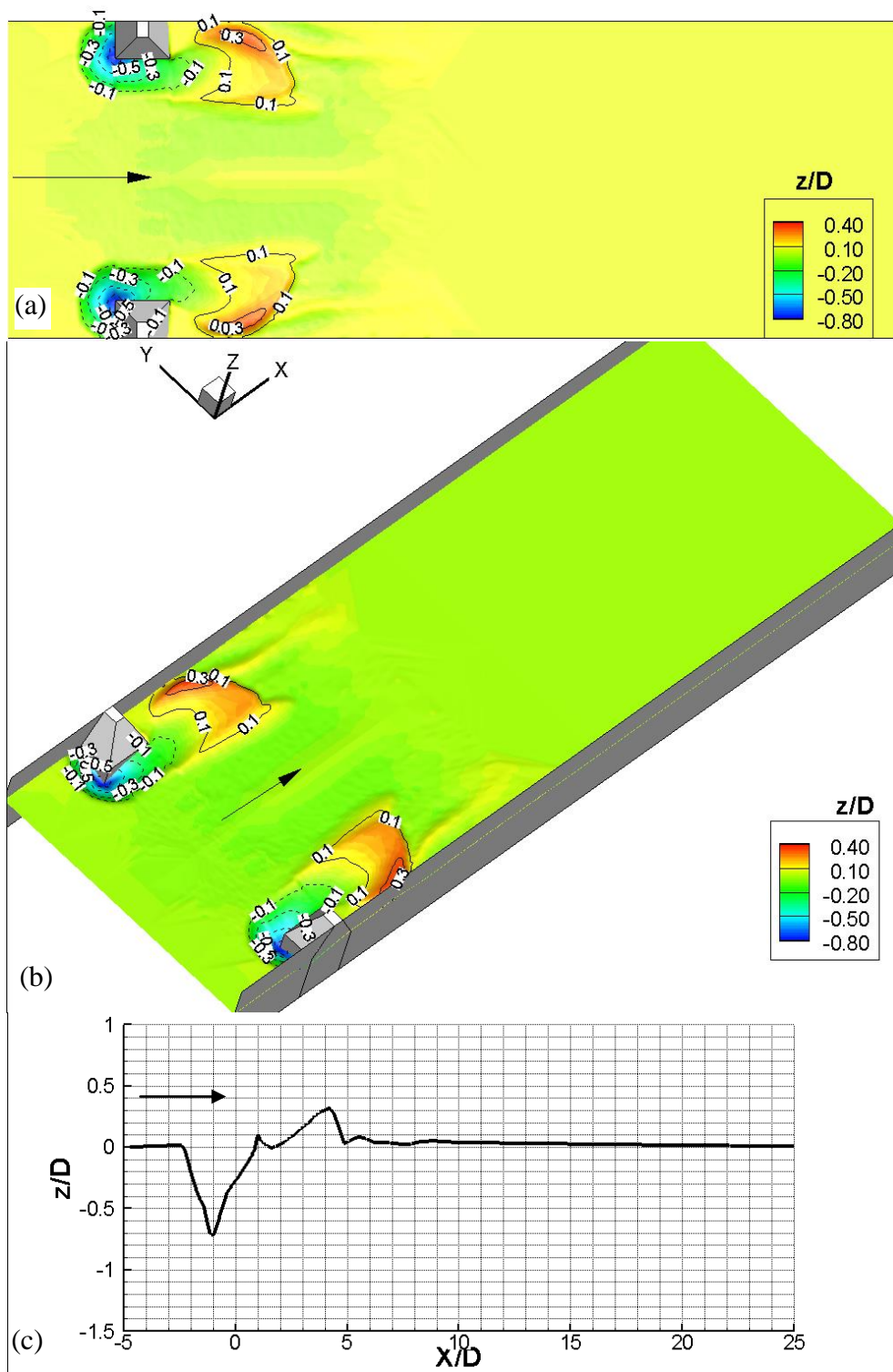


Figure 4.9 Scour pattern after a 8 hrs period experiment for the contraction ratio  $\beta = 0.185$ : a) top view; b) 3-D view; c) longitudinal section view which is taken tangent to the toe of the abutment

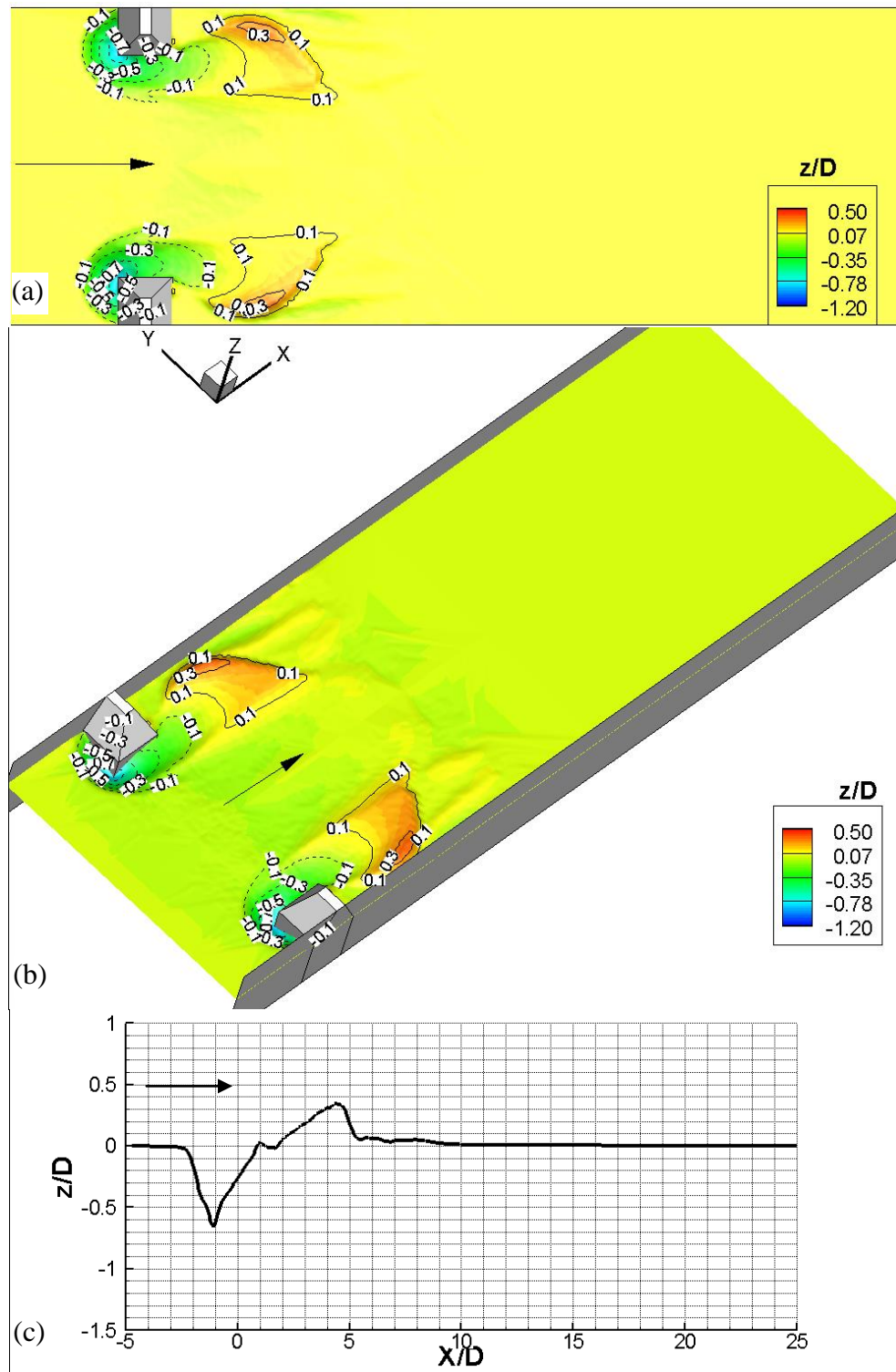


Figure 4.10 Scour pattern after a 2 hrs period experiment for the contraction ratio  $\beta = 0.252$ : a) top view; b) 3-D view; c) longitudinal section view which is taken tangent to the toe of the abutment

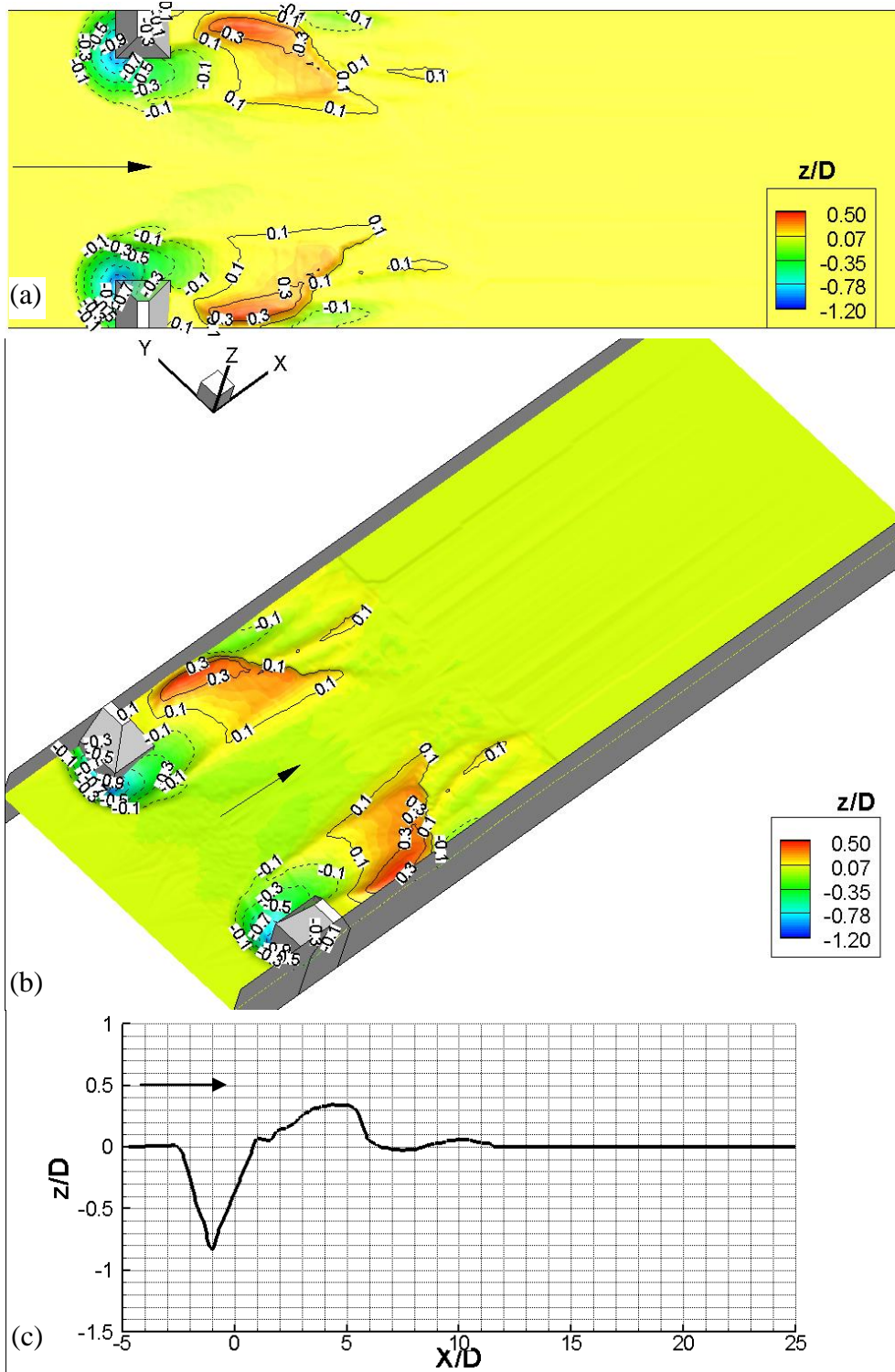


Figure 4.11 Scour pattern after a 4 hrs period experiment for the contraction ratio  $\beta = 0.252$ : a) top view; b) 3-D view; c) longitudinal section view which is taken tangent to the toe of the abutment

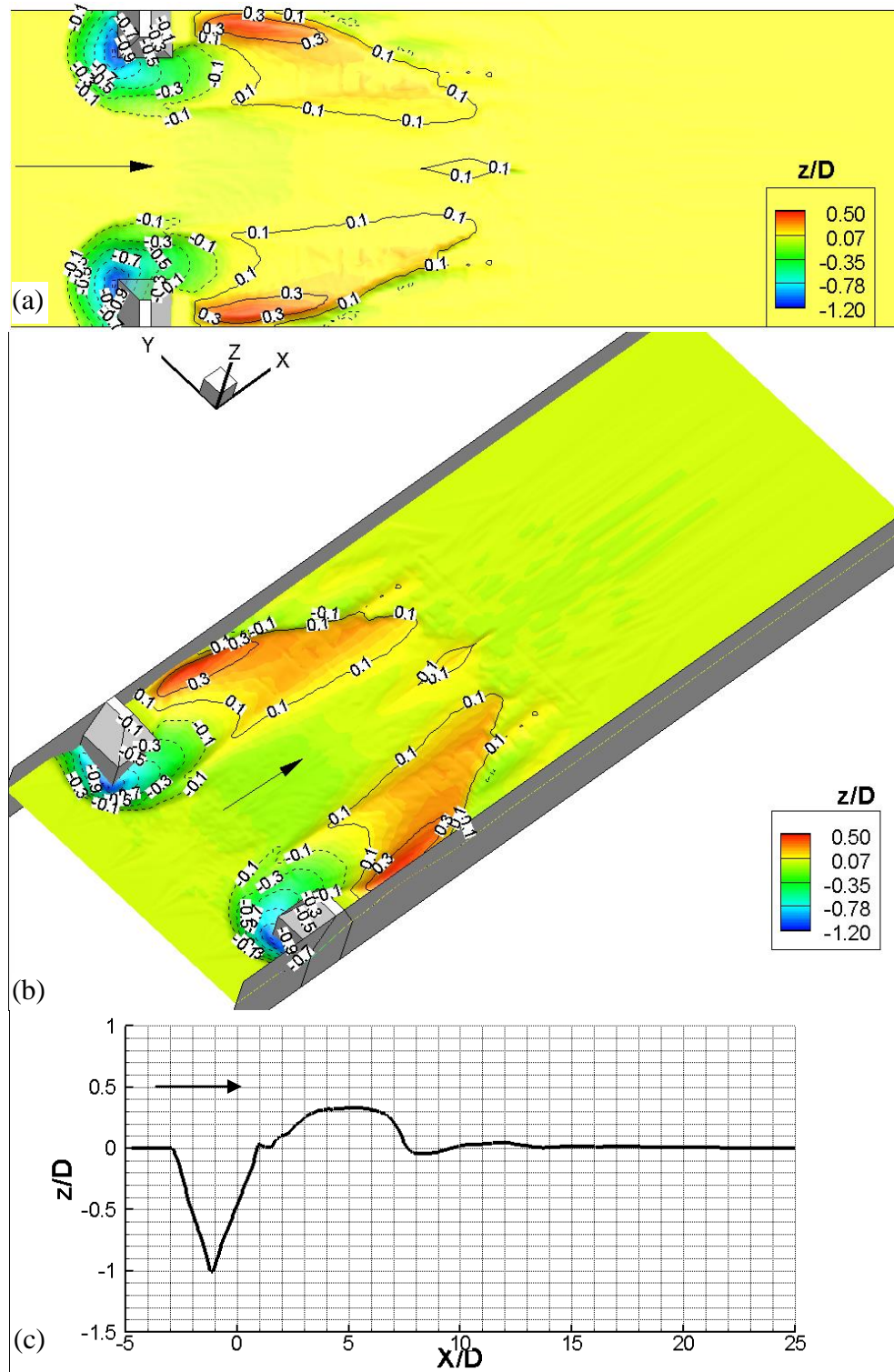


Figure 4.12 Scour pattern after a 8 hrs period experiment for the contraction ratio  $\beta = 0.252$ : a) top view; b) 3-D view; c) longitudinal section view which is taken tangent to the toe of the abutment

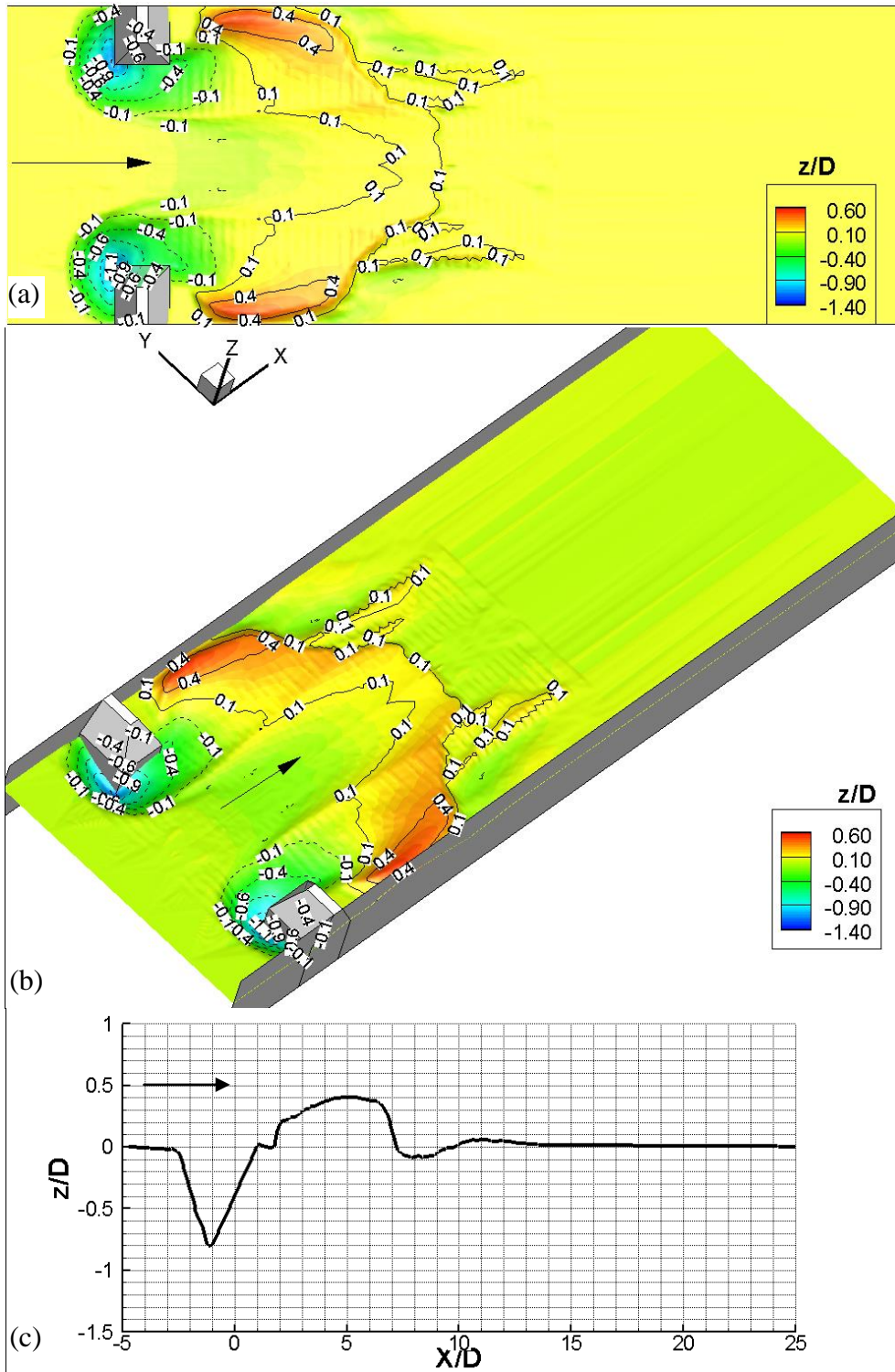


Figure 4.13 Scour pattern after a 2 hrs period experiment for the contraction ratio  $\beta = 0.319$ : a) top view; b) 3-D view; c) longitudinal section view which is taken tangent to the toe of the abutment

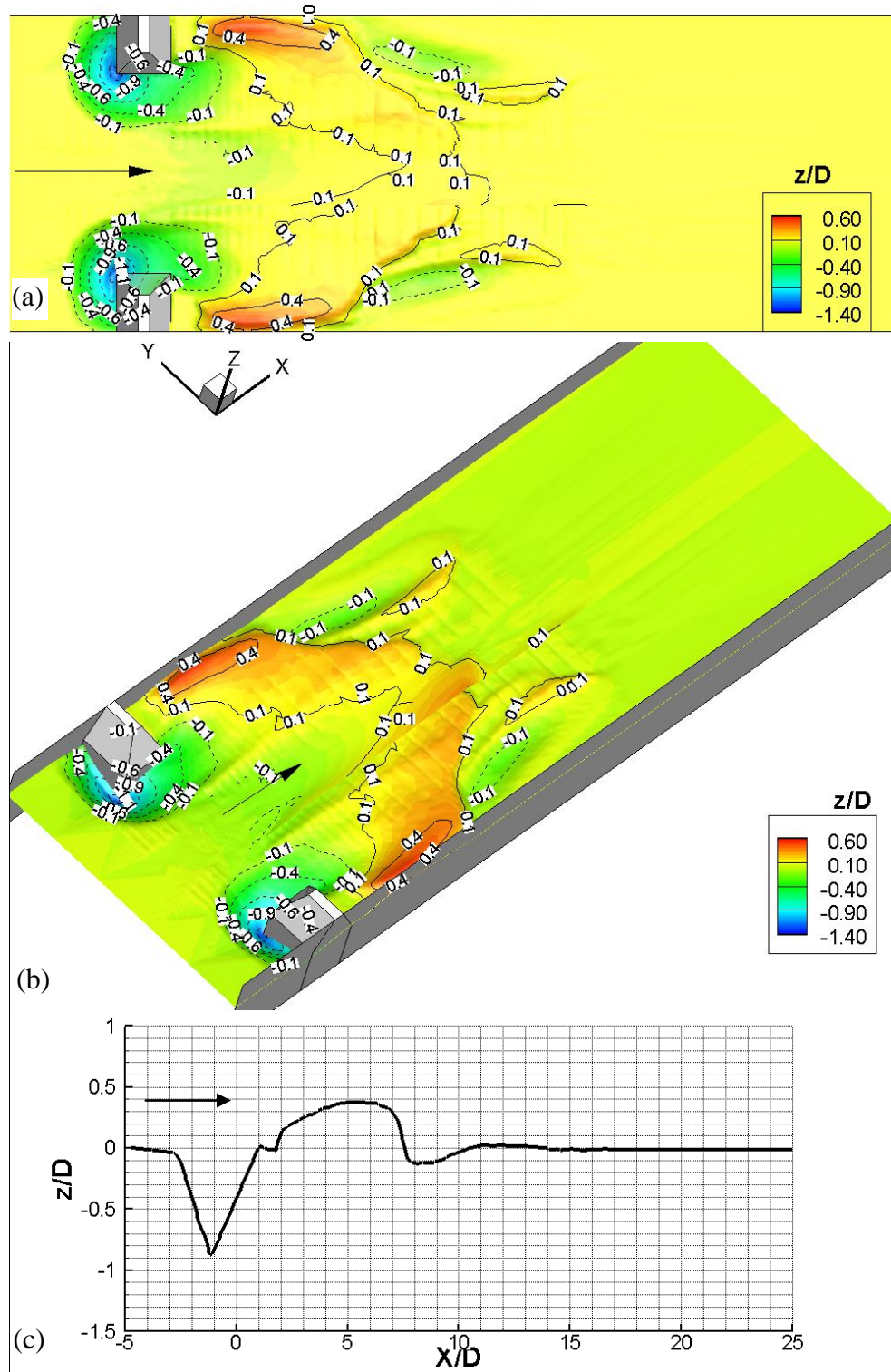


Figure 4.14 Scour pattern after a 4 hrs period experiment for the contraction ratio  $\beta=0.319$ : a) top view; b) 3-D view; c) longitudinal section view which is taken tangent to the toe of the abutment

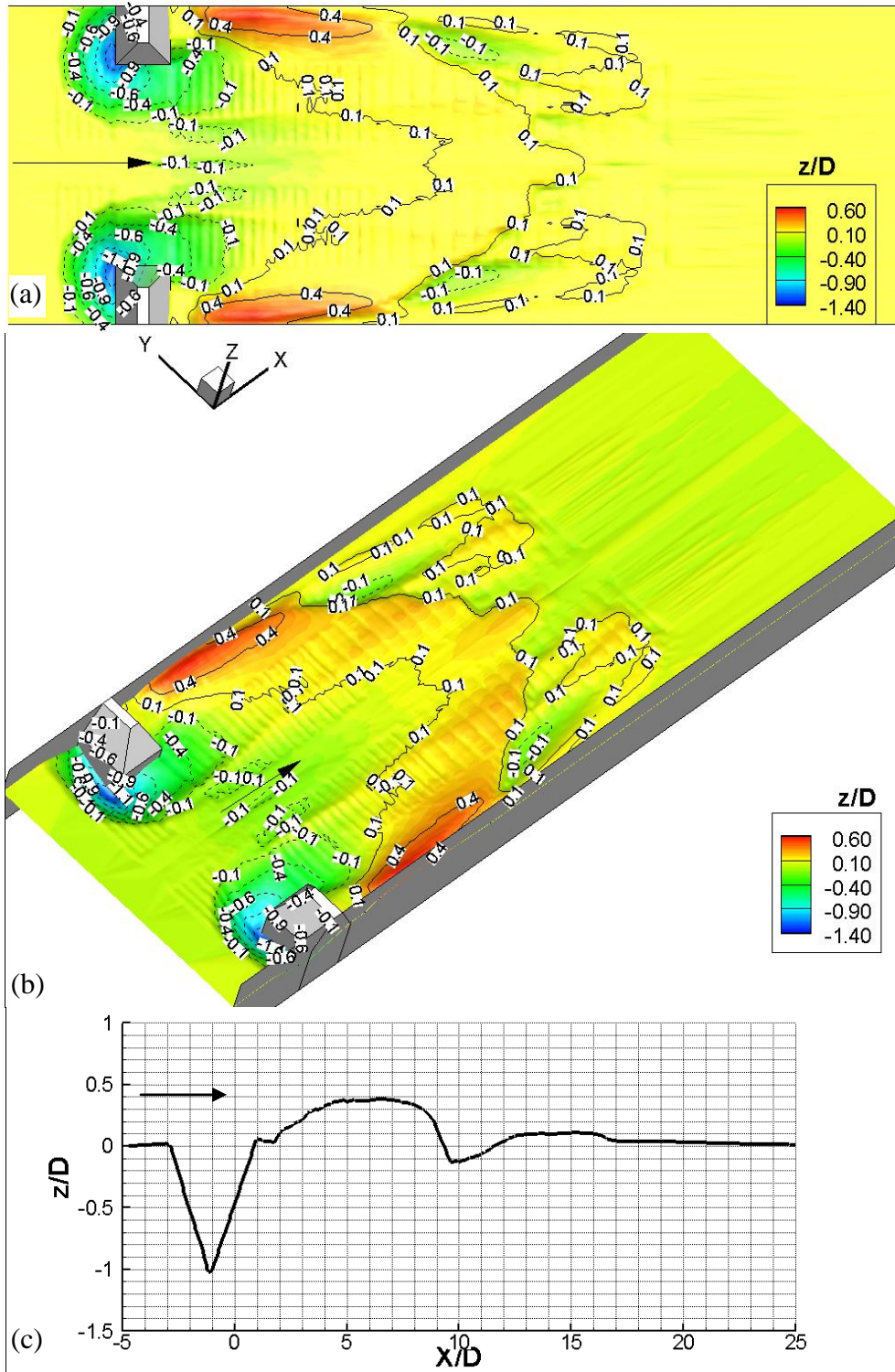


Figure 4.15 Scour pattern after a 8 hrs period experiment for the contraction ratio  $\beta = 0.319$ : a) top view; b) 3-D view; c) longitudinal section view which is taken tangent to the toe of the abutment

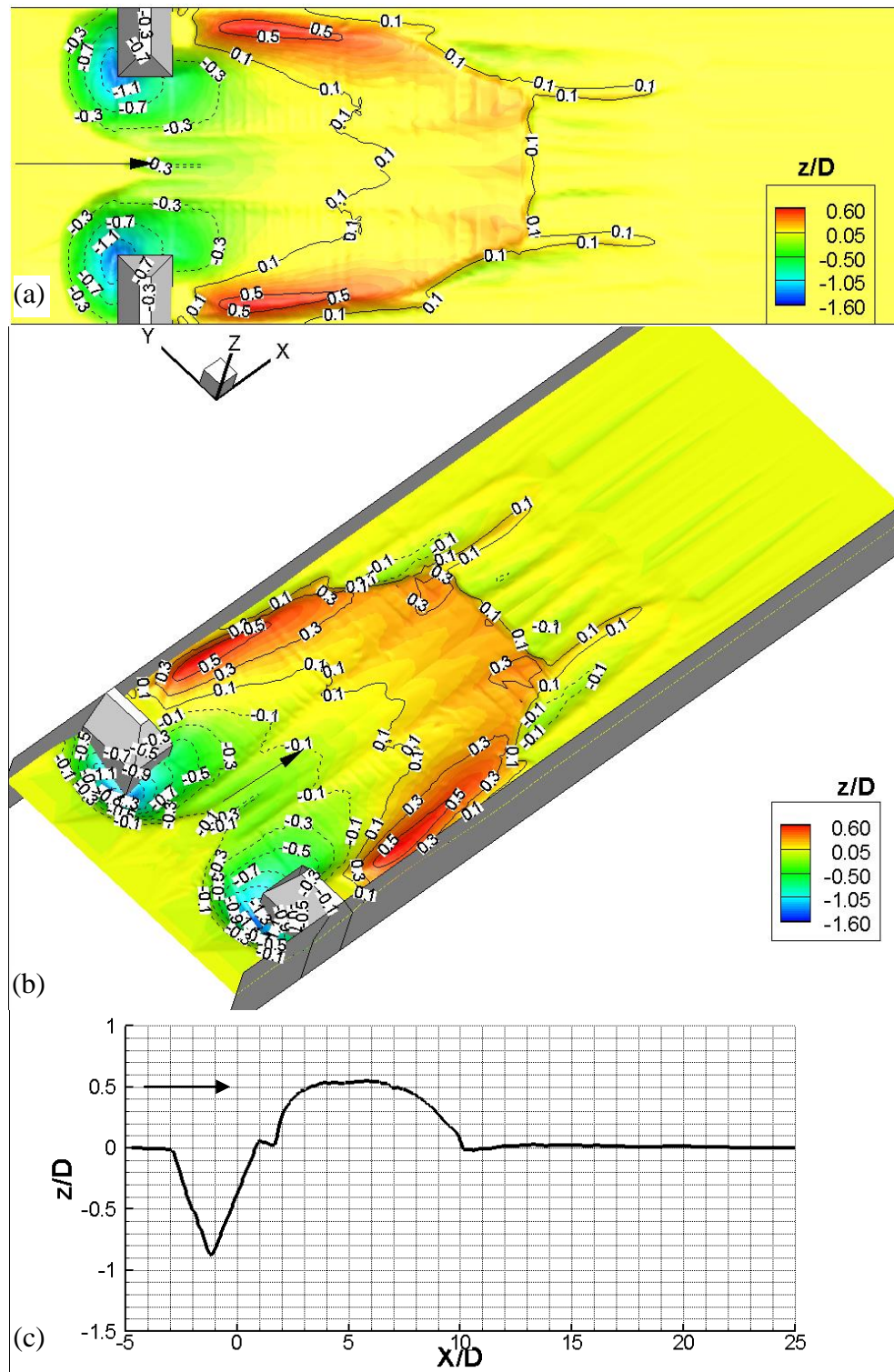


Figure 4.16 Scour pattern after a 2 hrs period experiment for the contraction ratio  $\beta=0.385$ : a) top view; b) 3-D view; c) longitudinal section view which is taken tangent to the toe of the abutment

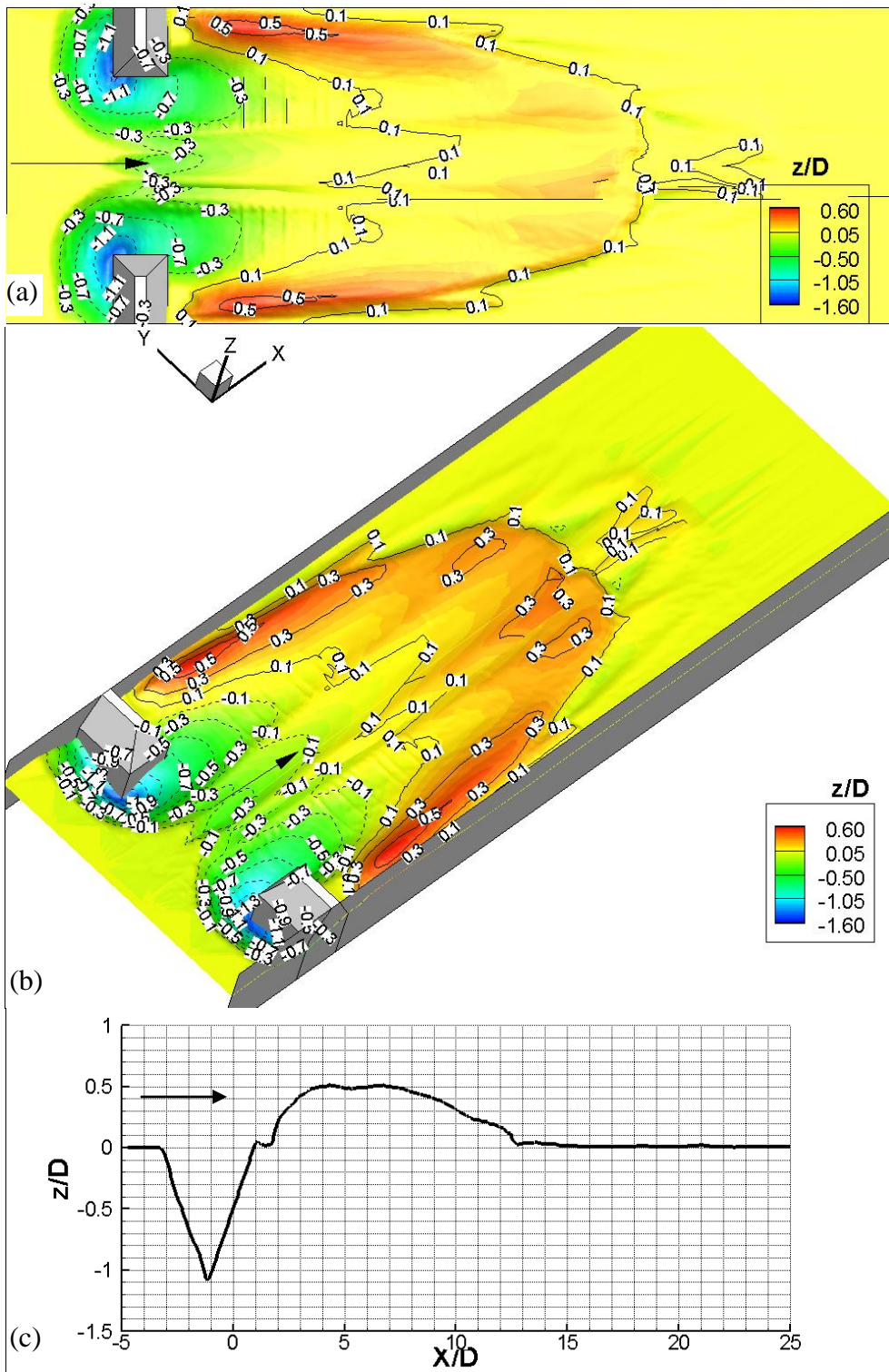


Figure 4.17 Scour pattern after a 4 hrs period experiment for the contraction ratio  $\beta = 0.385$ : a) top view; b) 3-D view; c) longitudinal section view which is taken tangent to the toe of the abutment

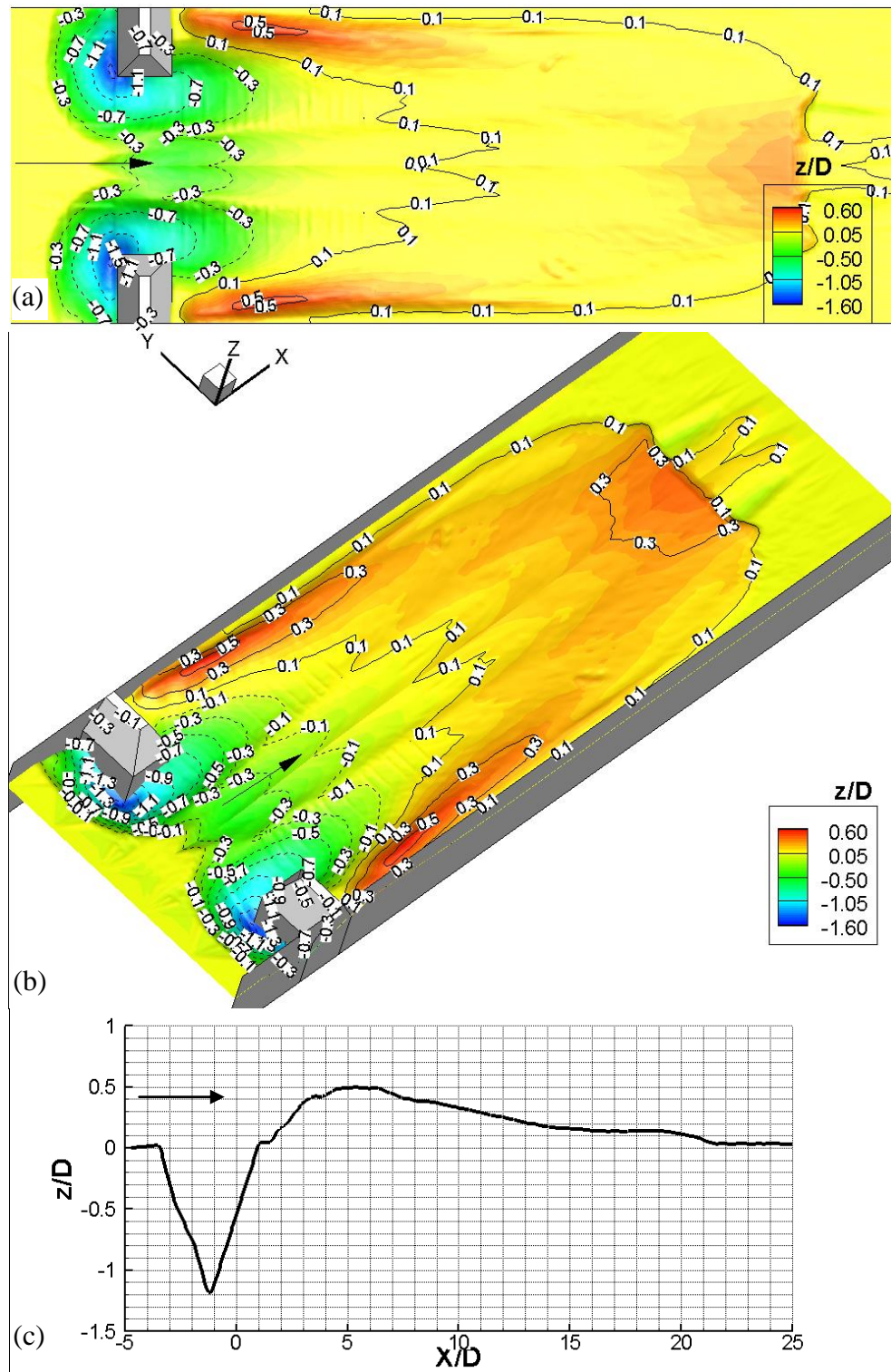


Figure 4.18 Scour pattern after a 8 hrs period experiment for the contraction ratio  $\beta = 0.385$ : a) top view; b) 3-D view; c) longitudinal section view which is taken tangent to the toe of the abutment

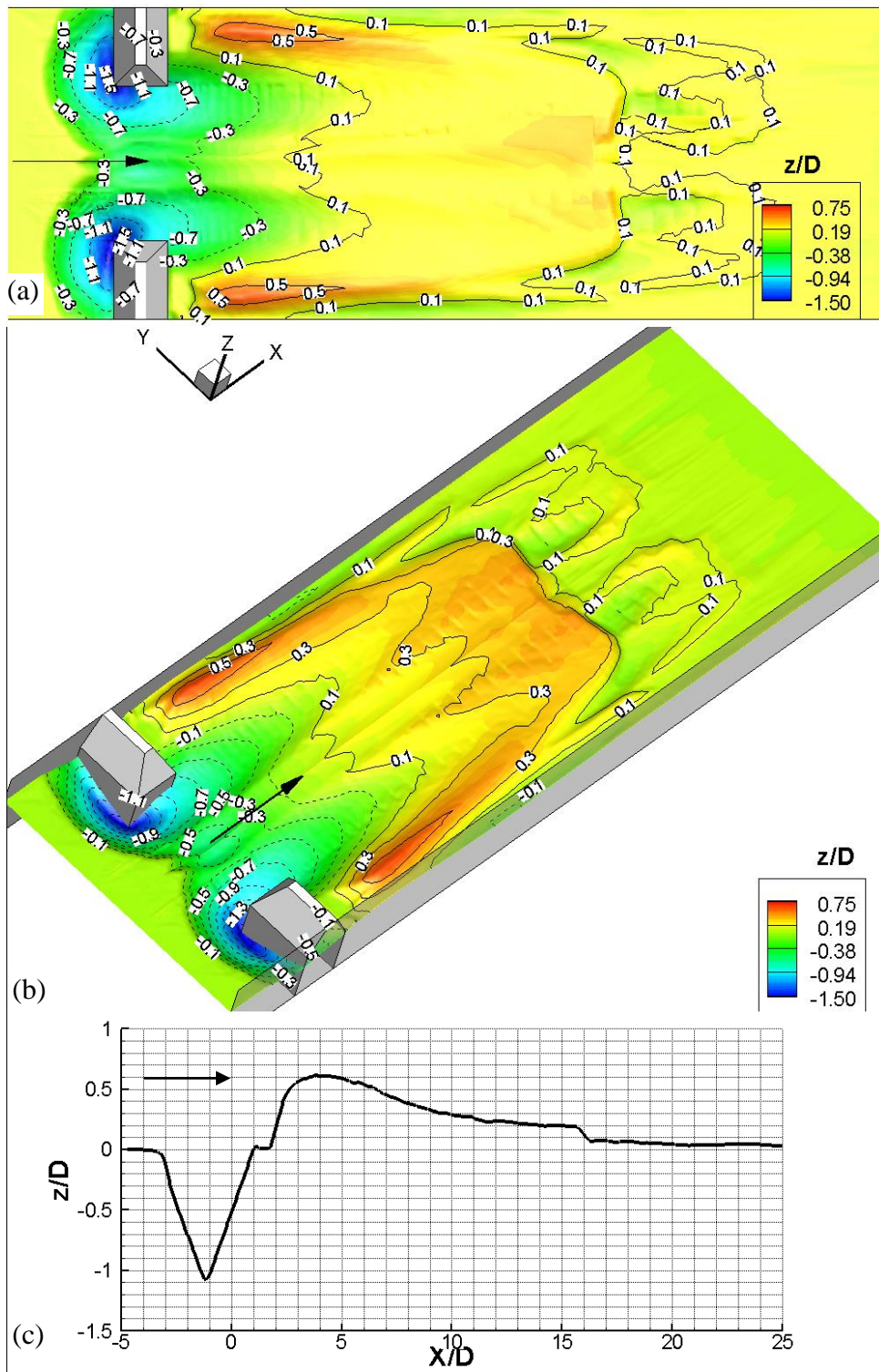


Figure 4.19 Scour pattern after a 2 hrs period experiment for the contraction ratio  $\beta=0.452$ : a) top view; b) 3-D view; c) longitudinal section view which is taken tangent to the toe of the abutment

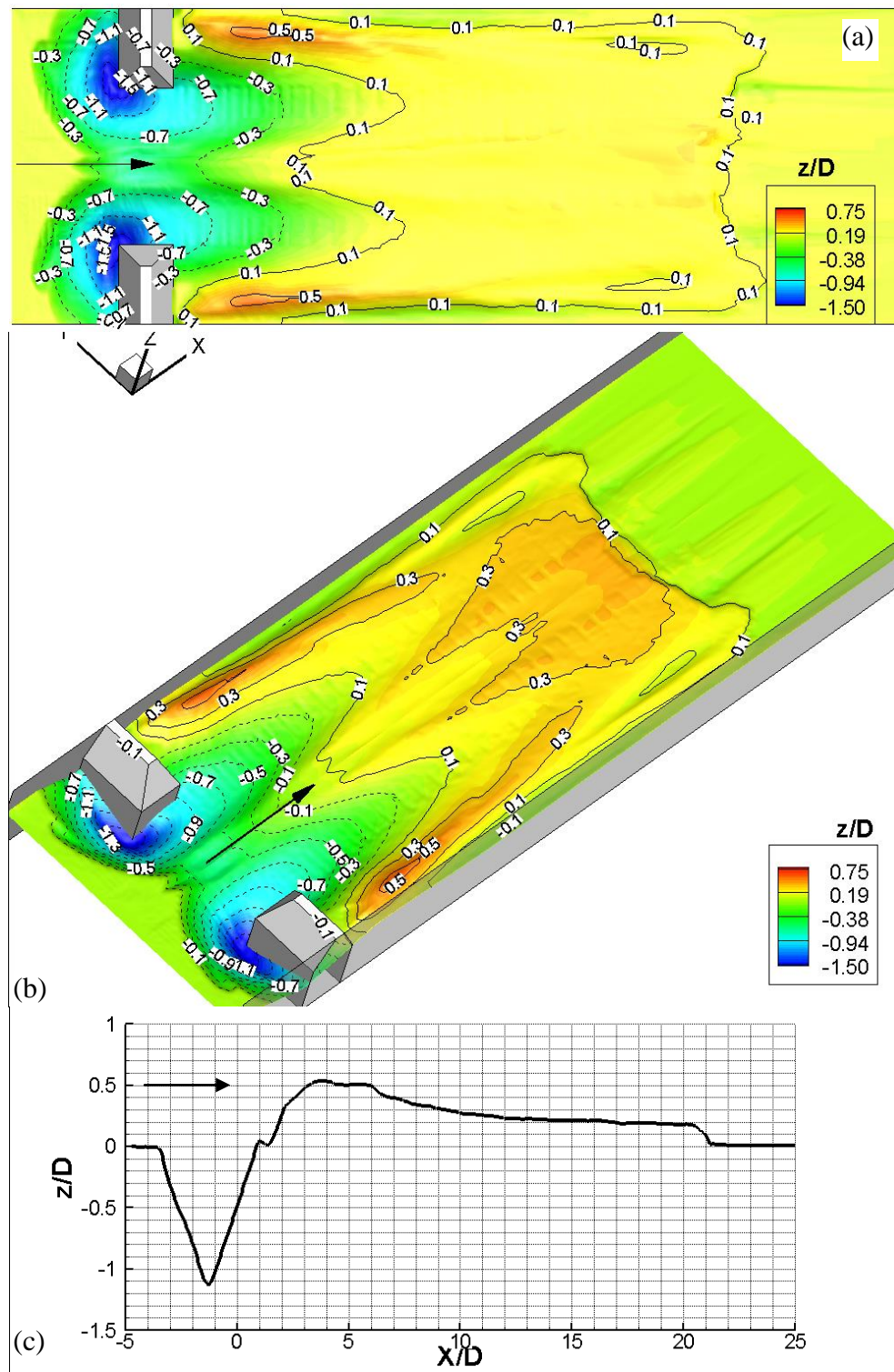


Figure 4.20 Scour pattern after a 4 hrs period experiment for the contraction ratio  $\beta = 0.452$ : a) top view; b) 3-D view; c) longitudinal section view which is taken tangent to the toe of the abutment

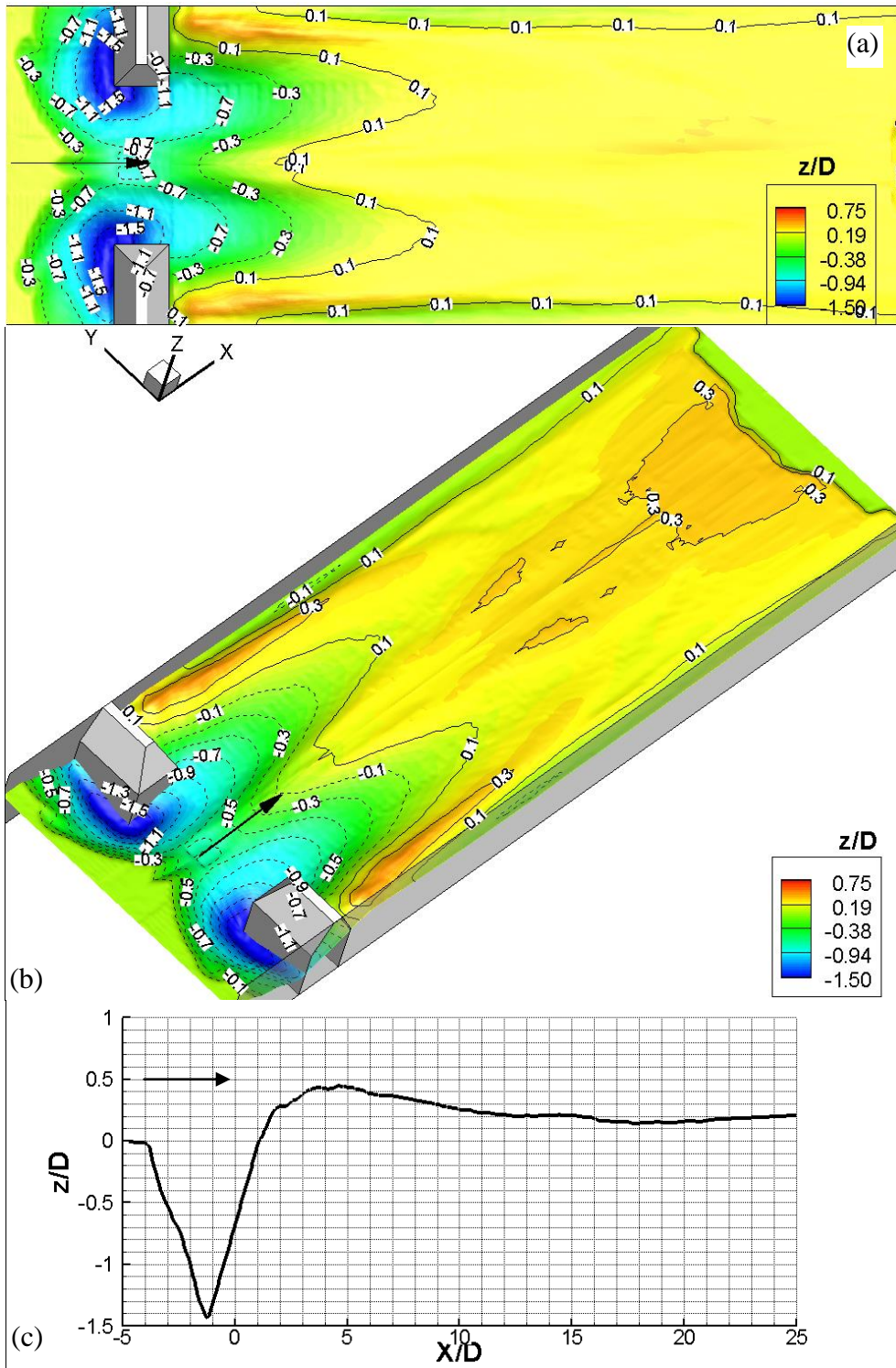


Figure 4.21 Scour pattern after a 8 hrs period experiment for the contraction ratio  $\beta=0.452$ : a) top view; b) 3-D view; c) longitudinal section view which is taken tangent to the toe of the abutment

Table 4.2 Parameters obtained from the experiments

Set Nr.	$\beta$	t (hrs.)	$d_s/D$	$X_s/D$	$X_l/D$	$X_t/D$	r/D	$\alpha$	$V_s/D^3$
1	0.119	2	0.377	1.88	0.65	0.68	1.311	47.291	0.213
2	0.119	4	0.386	1.83	0.66	0.78	1.336	46.123	0.276
3	0.119	8	0.587	3.29	0.97	1.20	1.362	45.000	0.938
4	0.185	2	0.621	4.51	1.00	1.12	1.655	49.538	1.185
5	0.185	4	0.707	4.94	1.08	1.25	1.608	51.546	1.607
6	0.185	8	0.806	4.63	1.37	1.46	1.655	49.538	2.325
7	0.252	2	0.882	5.02	1.30	1.70	1.870	56.310	3.331
8	0.252	4	1.008	5.07	1.62	1.88	1.829	58.241	4.652
9	0.252	8	1.114	5.89	2.01	2.19	1.793	51.710	6.658
10	0.319	2	1.181	5.82	1.83	2.08	2.253	62.592	7.622
11	0.319	4	1.272	6.22	2.02	2.19	2.287	65.095	8.816
12	0.319	8	1.292	6.77	2.08	2.31	2.253	62.592	10.210
13	0.385	2	1.433	8.44	2.24	NA	2.655	67.011	12.926
14	0.385	4	1.467	8.78	2.27	NA	2.601	70.017	15.740
15	0.385	8	1.541	9.24	2.61	NA	2.551	64.179	18.746
16	0.452	2	1.607	10.00	2.57	NA	2.952	72.474	18.956
17	0.452	4	1.684	11.18	3.09	NA	2.986	66.615	23.665
18	0.452	8	1.788	12.42	3.50	NA	2.972	67.270	29.001

#### 4.1.2.1 Discussion of Results

Investigating the 3-D scour patterns, important parameters of abutment scour pattern were obtained. The dimensionless maximum scour depth ( $d_s/D$ ), dimensionless radius ( $r/D$ ) and angle ( $\alpha$ ) to identify the position of the point where the maximum scour depth occurs, dimensionless length of the scour hole in the flow direction ( $X_s/D$ ), the distance of the extension of the scour hole in upstream direction from the abutment wall ( $X_l/D$ ), the distance of the extension of the scour hole in lateral direction from the abutment wall ( $X_t/D$ ) and dimensionless scour hole volume ( $V_s/D^3$ ) were taken as the important parameters of the problem (Table 4.2). Variation of these parameters with the contraction ratio ( $\beta$ ) were investigated and shown in Figures 4.22 to 4.25. Also, variation of the dimensionless scour hole volume ( $V_s/D^3$ ) with the dimensionless maximum scour depth ( $d_s/D$ ) is analyzed and shown in Figure 4.31.

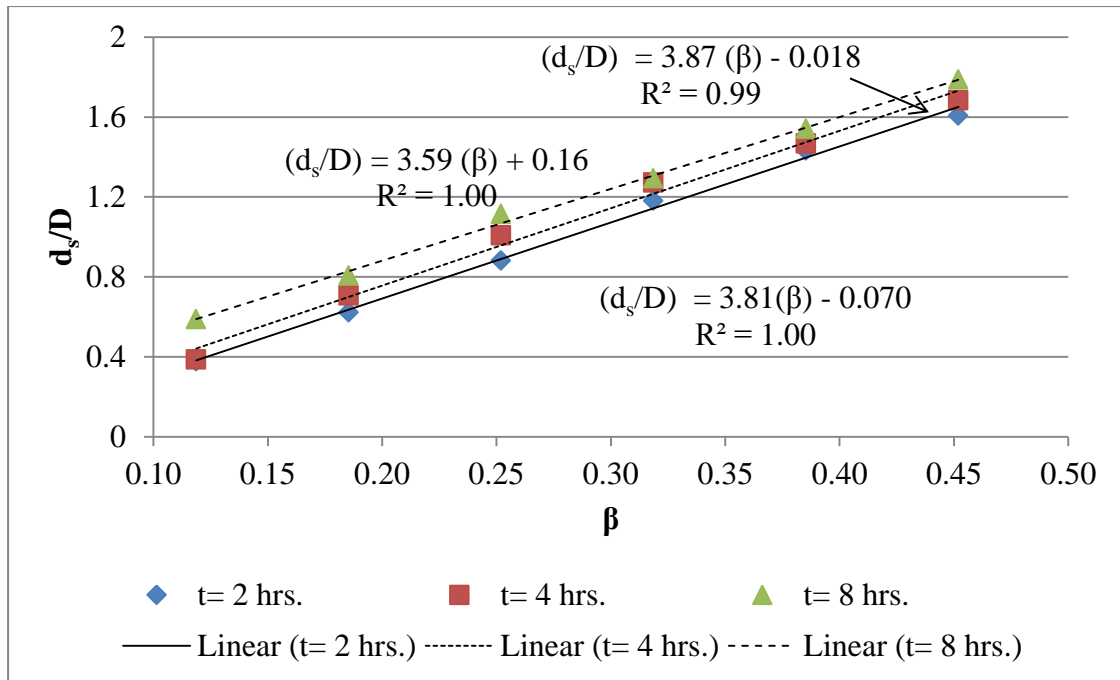


Figure 4.22 Variation of the dimensionless maximum scour depth with the contraction ratio for various experiment times

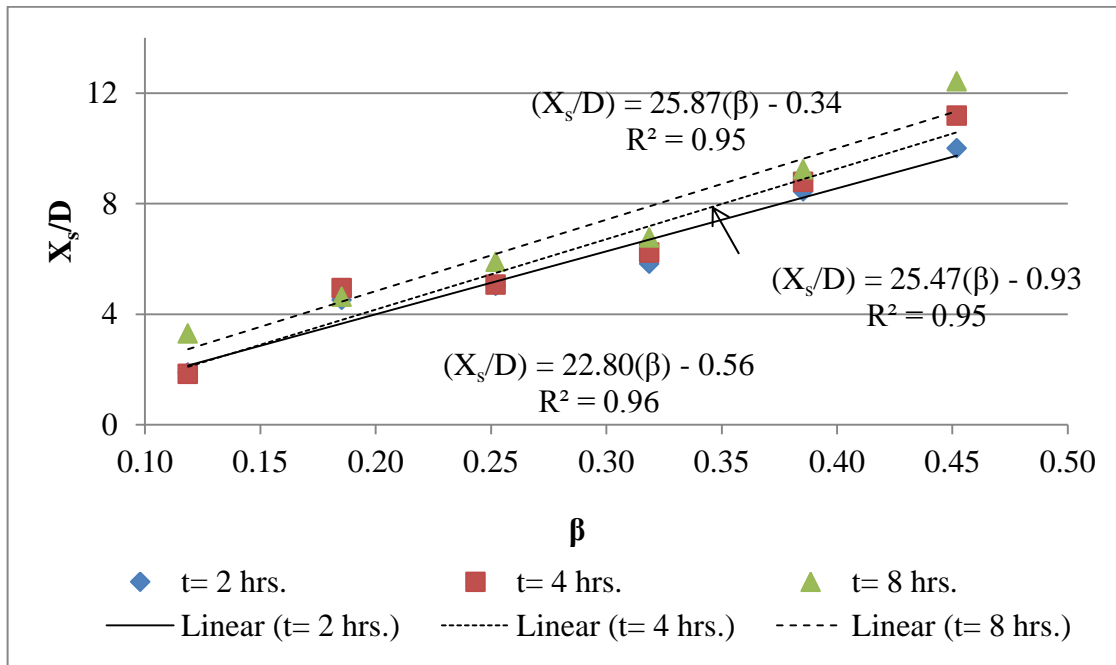


Figure 4.23 Variation of the dimensionless scour hole length with the contraction ratio for various experiment times

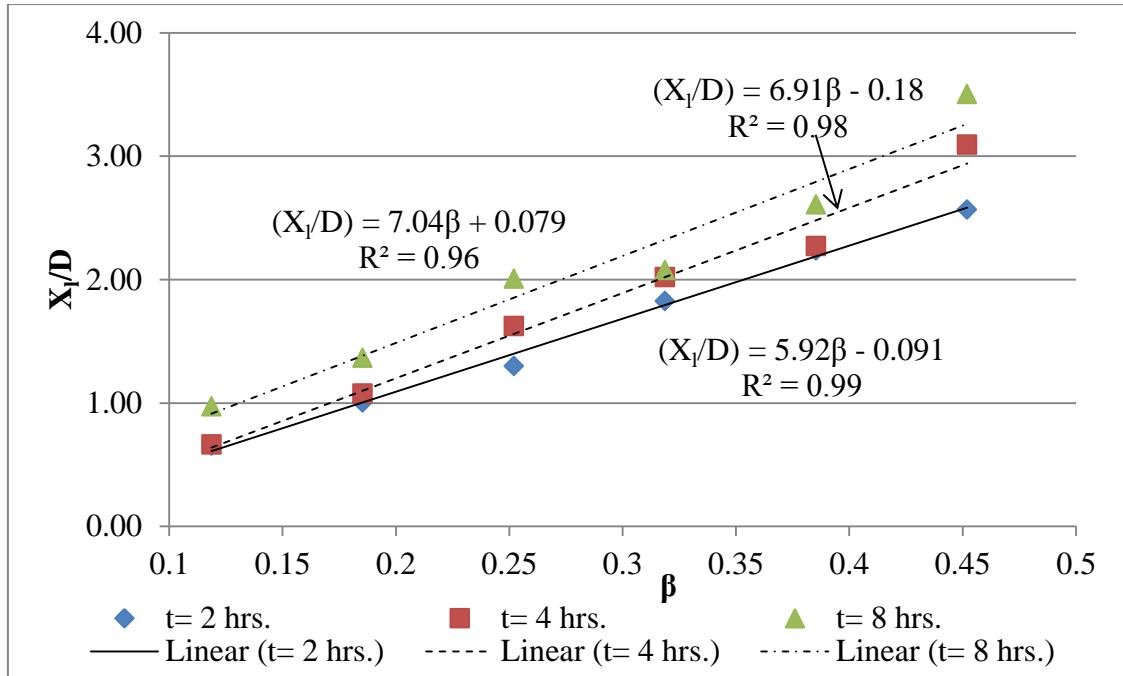


Figure 4.24 Variation of  $X_t/D$  with the contraction ratio for 2, 4 and 8 hours

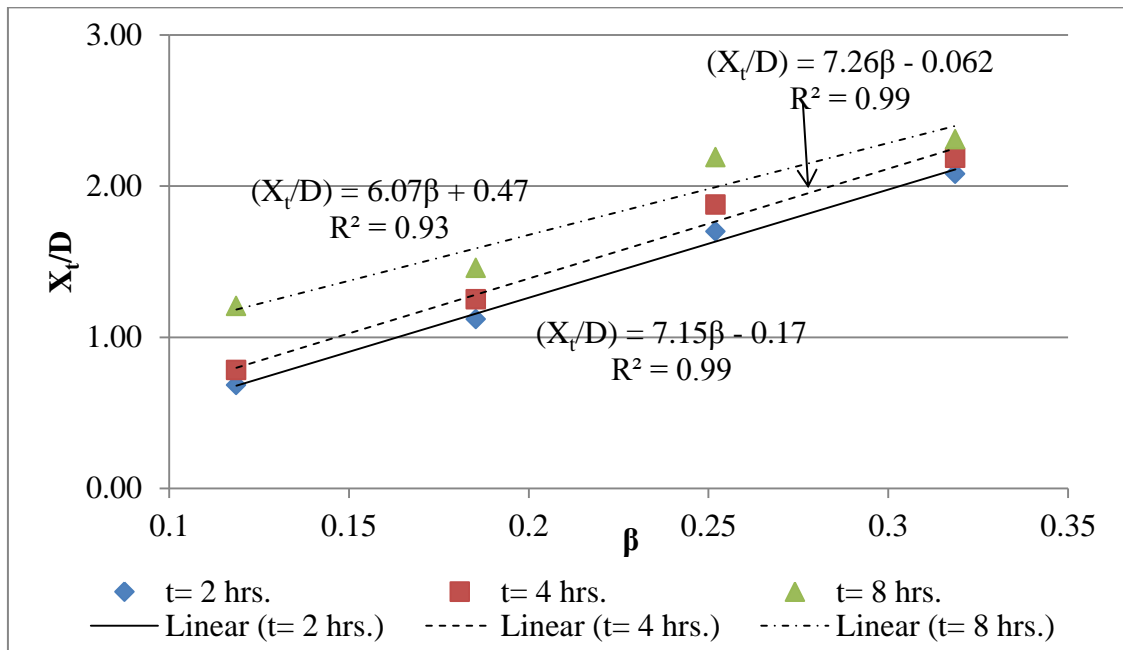


Figure 4.25 Variation of  $X_t/D$  with the contraction ratio for 2, 4 and 8 hours

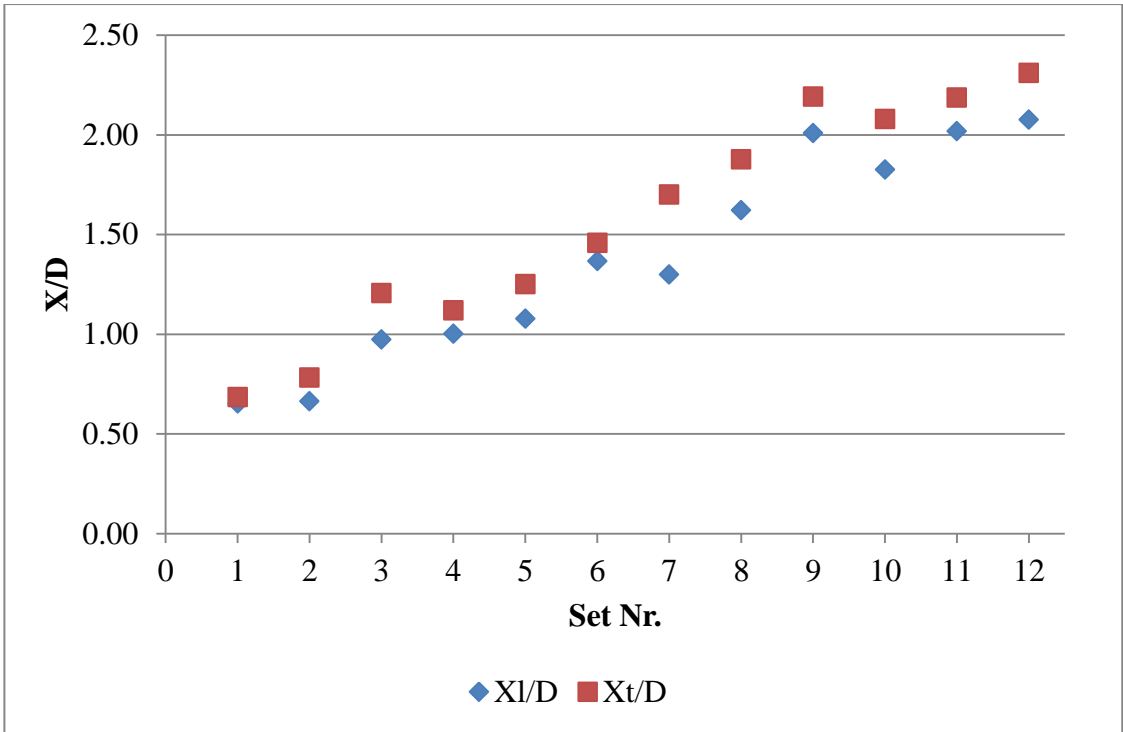


Figure 4.26 Comparison of the values of  $X_I/D$  and  $X_t/D$  for the entire data

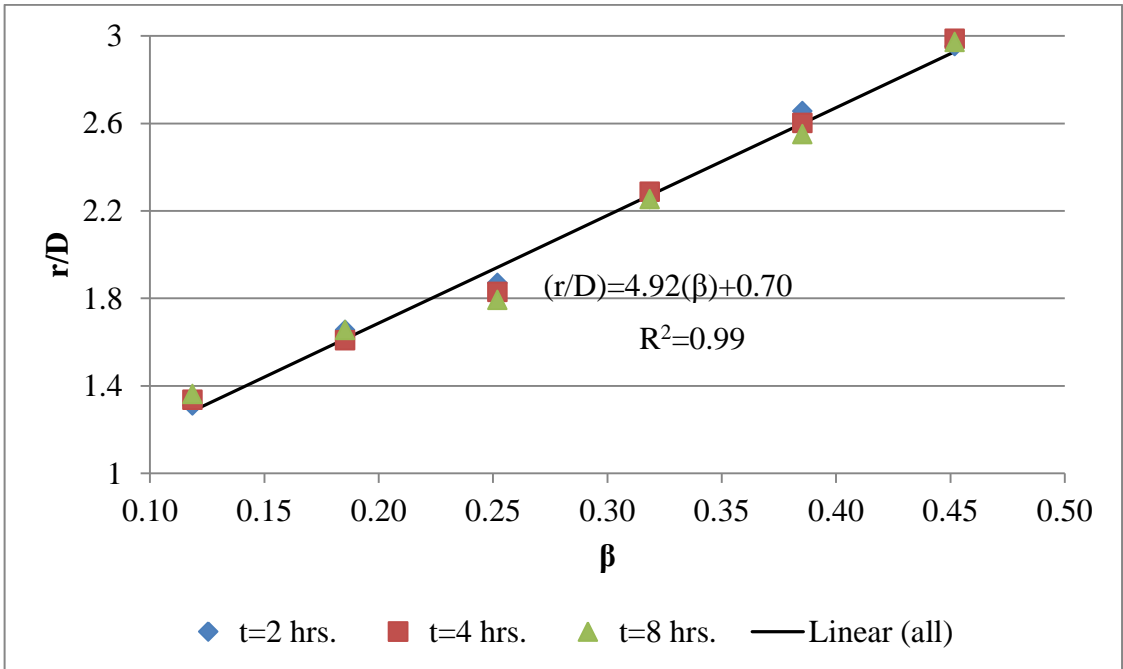


Figure 4.27 Variation of the dimensionless radius with the contraction ratio

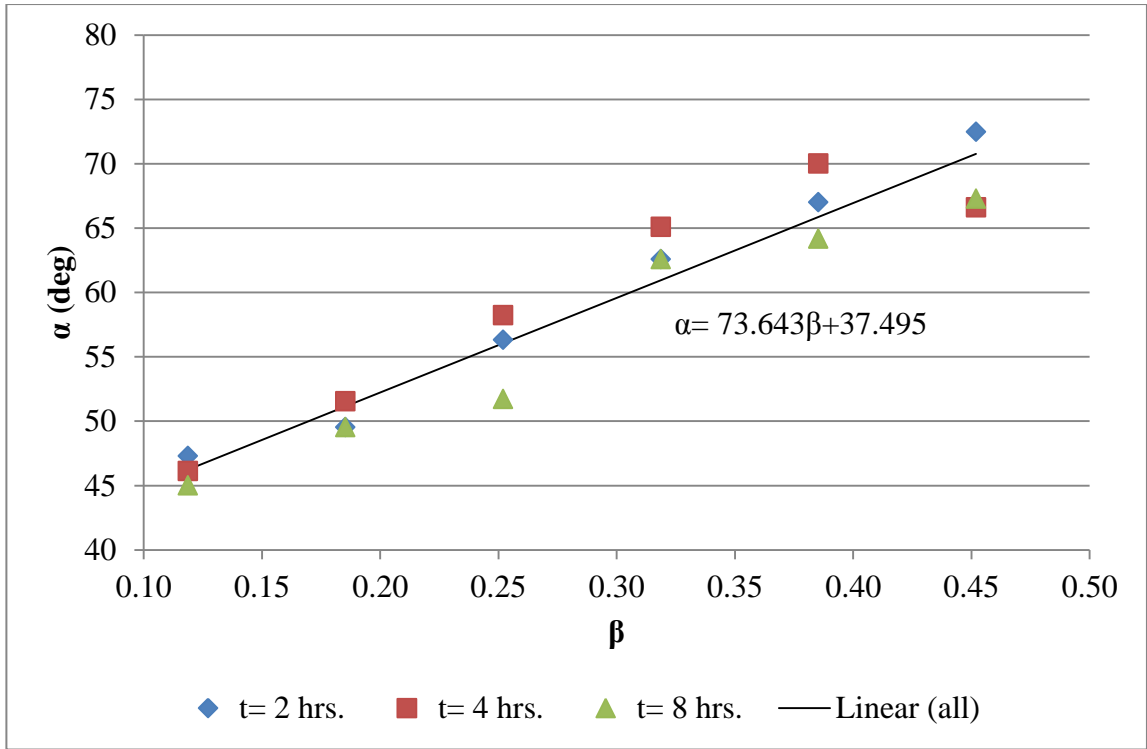


Figure 4.28 Variation of  $\alpha$  with the contraction ratio

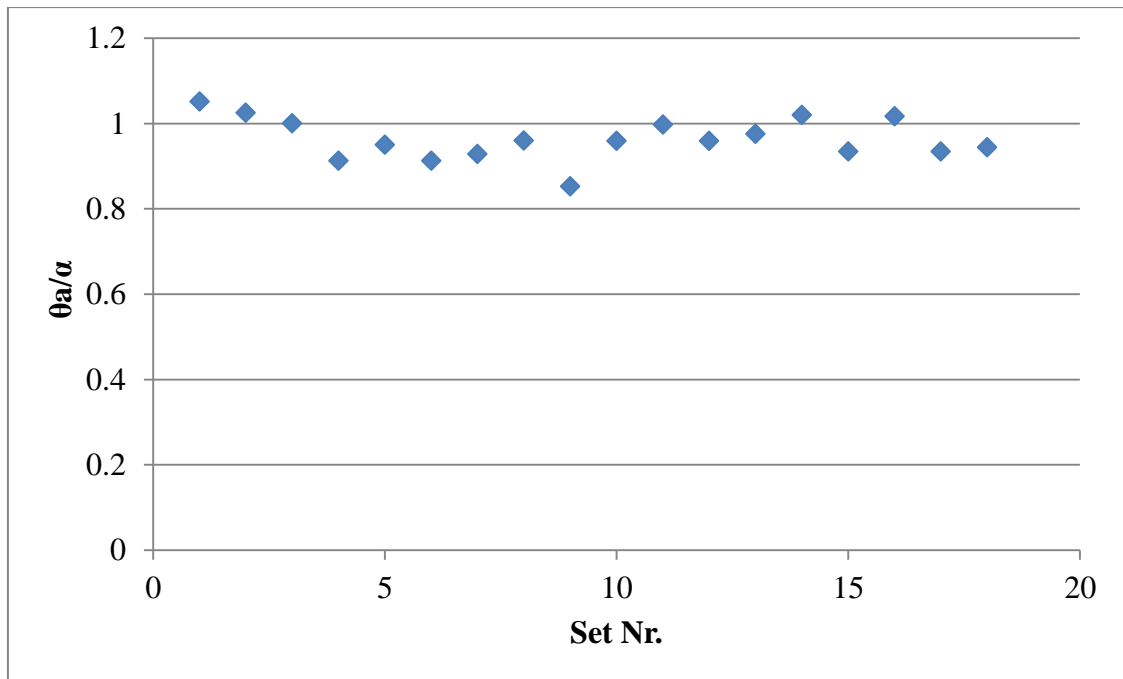


Figure 4.29 Variation of  $\theta_a/\alpha$  ratio for all experimental sets

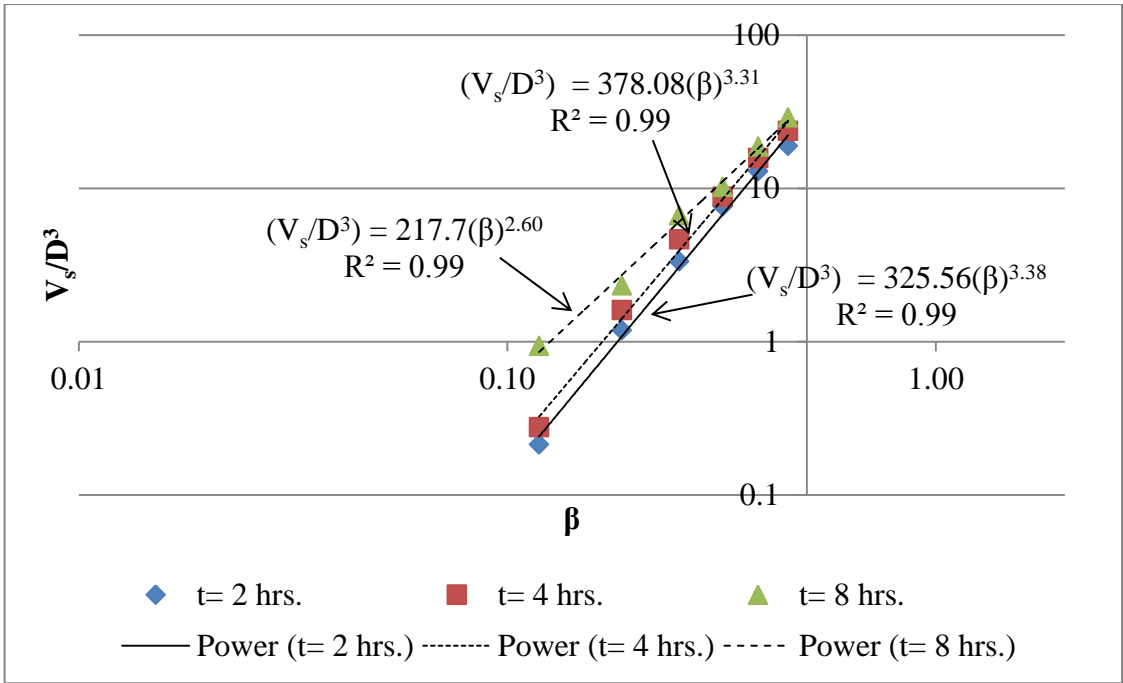


Figure 4.30 Variation of the dimensionless scour hole volume with the contraction ratio for various experiment times

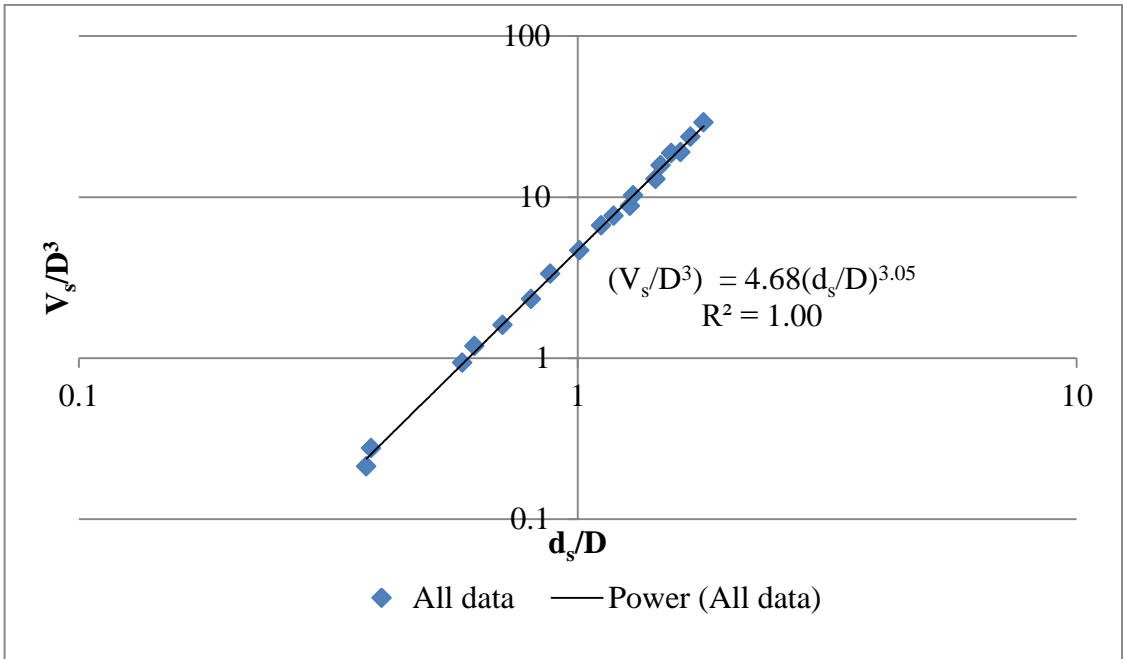


Figure 4.31 Variation of the dimensionless scour hole volume with the dimensionless maximum scour depth

Figure 4.22 shows the variation of  $d_s/D$  with the contraction ratio for various experiment durations. It can be seen that, for a fixed contraction ratio,  $d_s/D$  always increases with time. Also, the figure shows that, for each experiment duration,  $d_s/D$  changes with  $\beta$  linearly fitted almost perfectly (correlation coefficient,  $R^2 > 0.99$  for all cases). The linear equations, showing the relation between these two parameters are given within the figure.

Figure 4.23 shows the variation of the dimensionless length of the scour hole in the flow direction ( $X_s/D$ ) with the contraction ratio for various experiment durations. The length of the scour hole is calculated by taking the difference of the most upstream and most downstream coordinates of the scour hole for each data set.  $X_s/D$  mostly increases with experiment duration except small contraction ratios ( $\beta < 0.2$ ). Moreover, it can be added that the upstream border of the scour hole always shifts towards upstream with the increase in time and the downstream border of the scour hole generally moves in the downstream direction with the increase in time but for some contraction values it shifts back towards upstream direction with the effect of motion of the transported material from the scour hole. Besides, for all the experiment durations the dimensionless length of the scour hole increases almost linearly with increasing contraction ratio. The equation of the relation and the corresponding correlation coefficients are shown in the figure.

In Figures 4.24 and 4.25, the variations of  $X_l/D$  and  $X_r/D$  with the contraction ratio for various test durations are shown, respectively. Although Figure 4.25 lacks the data of experiment sets 13-18 due to physical situations, it can be seen from Figures 4.24 and 4.25 that, the variation of these parameters with the contraction ratio shows linear behavior with high correlation ratios. Moreover, these parameters always increase with the increase in time. The relation of these parameters with each other is also important in choosing the dominant side in case of riprap protection. To observe this situation clearly, Figure 4.26 was developed showing the variation of  $X_l/D$  and  $X_r/D$  for each useable data. As can be seen from the figure, unlike the results obtained in Chapter 3 for this relation,  $X_r/D$  values are always larger than the  $X_l/D$  values within the data set. This means the lateral extension of the scour hole is larger than the extension of the scour hole through

upstream direction. This result shows that, the lateral direction is more critical in a possible riprap protection around the abutment.

Figures 4.27 and 4.28 show the variation of  $r/D$  and  $\alpha$  with the contraction ratio, respectively. In Figure 4.27, the variation of  $r/D$  with  $\beta$  is given. Analyzing the data, it can be seen that for a fixed contraction ratio,  $r/D$  does not have much variation with the experiment duration. Therefore, the relation is obtained by using all the data values and is independent of time. As can be seen from Figure 4.27, the relation between  $r/D$  and  $\beta$ , which is presented in the figure, is almost linear ( $R^2 > 0.99$ ). In Figure 4.28, the variation of  $\alpha$  with  $\beta$  is given. Similarly, after analyzing the data, it can be seen that for a fixed contraction ratio,  $\alpha$  does not have much variation with the experiment duration. Therefore, the relation is obtained by using all the data values and is independent of time. It is seen that,  $\alpha$  never exceeds 90 degrees, which means the maximum scour depth location never occurs at the downstream side of the abutment. Another observation here is that  $\alpha$  increases linearly with  $\beta$ . The equation of this linear relation is given in the figure. Actually, the reason for this increase is because of the increase in the angle between the diagonal line starting from the abutment axis through abutment upstream corner, and flume side wall axis ( $\theta_a$  in Figure 4.3) with the increase in abutment length. Figure 4.29 shows the variation of ratio of the angles  $\theta_a$  and  $\alpha$ . As it can be seen from the figure, the values of this ratio are always close to 1, which means  $\alpha$  is always close to  $\theta_a$  regardless of the contraction ratio (abutment length) or experiment duration. As a result it can be said that the relative position of the maximum scour depth with respect to upstream abutment corner does not change significantly with the change in the contraction ratio or experiment duration. It is always observed at the upstream side of the abutment tip.

Figure 4.30 shows the variation of the dimensionless scour volume ( $V_s/D^3$ ) with the contraction ratio. The scales of the graph were selected as logarithmic scale to easily visualize the power relation of the two parameters. As can be seen from the figure,  $V_s/D^3$  always increases with the increase in time and the variation of it with the contraction ratio shows parabolic behavior with very high R-squared coefficients for each experiment duration. The equations showing the power relation among the parameters

are presented in the figure. Making a similar analyses as done for an isolated abutment in Chapter 3; the equation giving the relation of  $V_s/D^3$  with  $\beta$  and the dimensionless time parameter ( $T_s$ ) was obtained and given below;

$$\left( V_s/D^3 \right) = 127.68(\beta)^{3.36}(T_s)^{0.29} \quad (4.1)$$

To make a comparison between equation (4.1) and the relation obtained in Chapter 3, equation (3.2) is redeveloped inserting contraction ratio for the dimensionless abutment length term. The equation given below is obtained for the scour hole volume around a SCE abutment;

$$\left( V_s/D^3 \right) = 585.45(\beta)^{3.84}(T_s)^{0.71} \quad (4.2)$$

By comparing these two equations, it can be seen that, although the effects of  $\beta$  and  $T_s$  on  $V_s/D^3$  are in similar fashion in both equations, there exist considerable difference in the coefficients. The comparison of these two equations will be done further within this section after comparing the two cases in details.

As discussed earlier in Chapter 3, there exists a necessity in literature to define scour hole volume in terms of scour depth for developing semi-empirical models of the problem. Figure 4.31 shows the variation of the dimensionless scour hole volume with the dimensionless scour depth by using every data of this experiment set regardless of time and experiment duration on logarithmic scales. The relation is analyzed and given in Figure 4.31. As can be seen from the figure, the relation is fitted to a power function almost perfectly with regression coefficient,  $R^2$  very close to one. The discussion of this result will be pursued further in this section by comparing the results with the ones analyzed in Chapter 3.

After analyzing the bathymetric variables of the experimental sets covered in Chapter 3 and Chapter 4 separately, the data of the two experimental sets were analyzed together to compare the results of the two data sets and also to develop the discussion of results with the additional data. To make the comparison clear and to develop the findings on

channel contraction effect on scour depth, the dimensionless term used in Chapter 3 regarding the abutment length ( $L/D$ ) is replaced by the contraction ratio,  $\beta = L/W$ . For this purpose Figures 4.32 to 4.39 were developed.

In Figure 4.32, the variation of  $d_s/D$  with the contraction ratio can be seen. It is seen that, the variation of data of SCE Abutment is in a wide range, while the data of spill through abutment is in a more narrow range. This means that, for spill through abutments, the change in scour depth between  $t = 2$  hours and  $t = 8$  hours is not as big as the one observed for SCE abutments. Besides, it is clearly comprehended that, for the same contraction ratio, SCE abutments result with a deeper scour hole compared with the spill-through abutments. After fitting linear relation equations for both sets separately, it can be seen that the slopes of these lines are very close for both sets. However, the values of  $d_s/D$  for SCE abutments are approximately 2 times of the ones observed for the spill-through abutments for small contraction ratios around  $\beta = 0.10$ . When the contraction ratio increases, the ratio of  $d_s/D$  for two abutment types decreases and it becomes approximately 1.4 for  $\beta = 0.45$ . Melville (1992) stated the equivalent scour depths ratio of SCE abutments and spill-through abutments with  $60^\circ$  side inclination angle in the same experiment conditions, to 1.30, which seems comparable to the results obtained in the present study keeping in mind that the experiments did not reach equilibrium conditions for the present case.

A similar variation with contraction ratio for two abutment types was also observed for the dimensionless scour hole length given in Figure 4.33. As can be seen from the figure, the dimensionless scour hole length for SCE abutments resulted in bigger values than the ones for spill-through abutments. Similar to Figure 4.32, the best fit lines of the relations regarding the two abutment types have close slopes to each other, however; the values for SCE abutment almost doubles the values for spill-through abutment for small contraction ratios and the ratio between two data sets decreases to 1.30 for  $\beta = 0.45$ . It is stated in previous studies that, the scour hole dimensions mainly depends on the scour hole depth (Ballio and Orsi, 2001). After these findings, one can say that, Figure 4.32 and Figure 4.33 supports the statement by showing that, the variations of scour depth and scour hole length in the flow direction has a similar behavior for various contraction

ratios and abutment types. As a further step, Figure 4.34 was developed to see the variation of  $X_s/D$  with  $d_s/D$ . It can be inferred from the figure that, the dimensionless scour hole length increases in a linear manner with the increase in dimensionless scour depth.

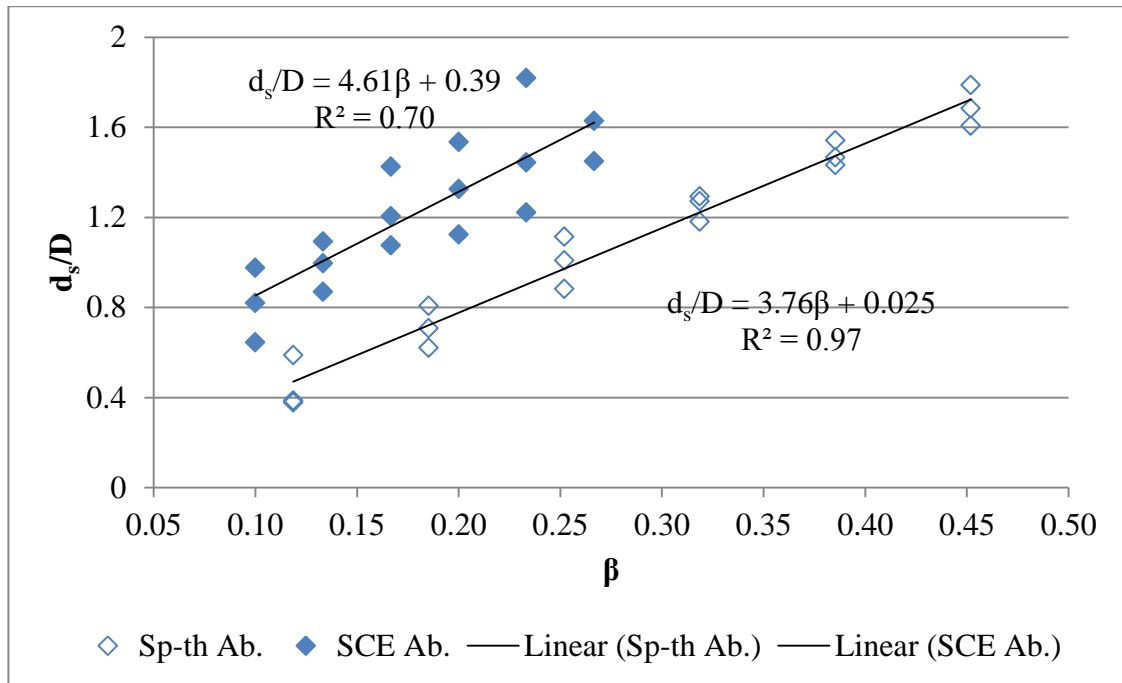


Figure 4.32 Variation of the dimensionless maximum scour depth with the contraction ratio for various abutment types

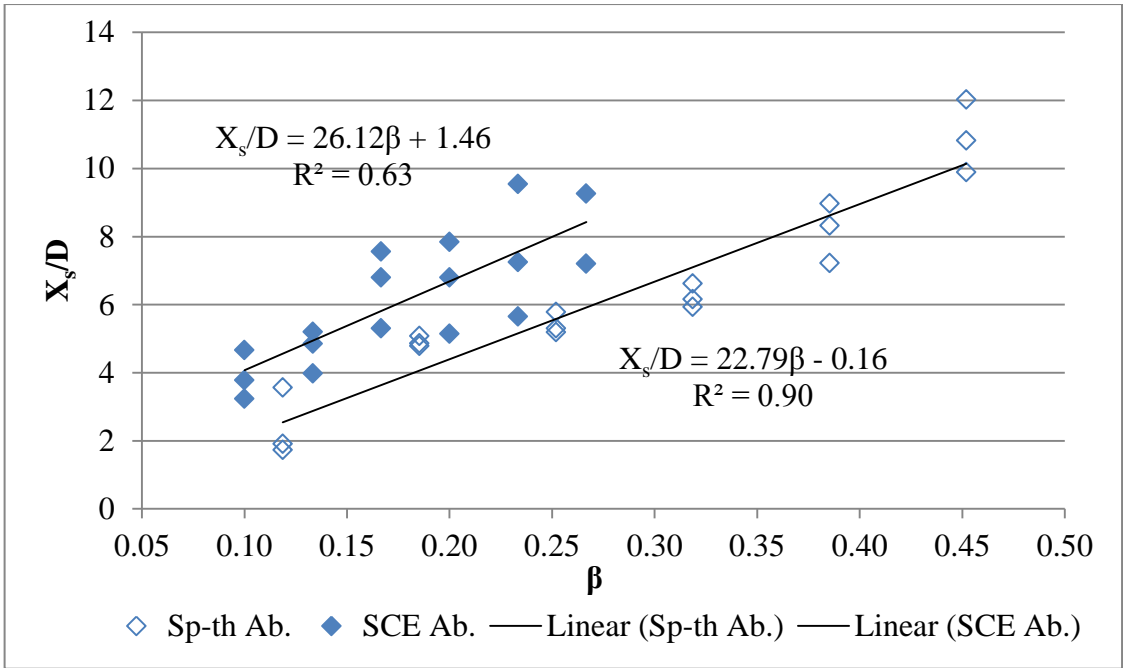


Figure 4.33 Variation of the dimensionless scour hole length with the contraction ratio for various abutment types

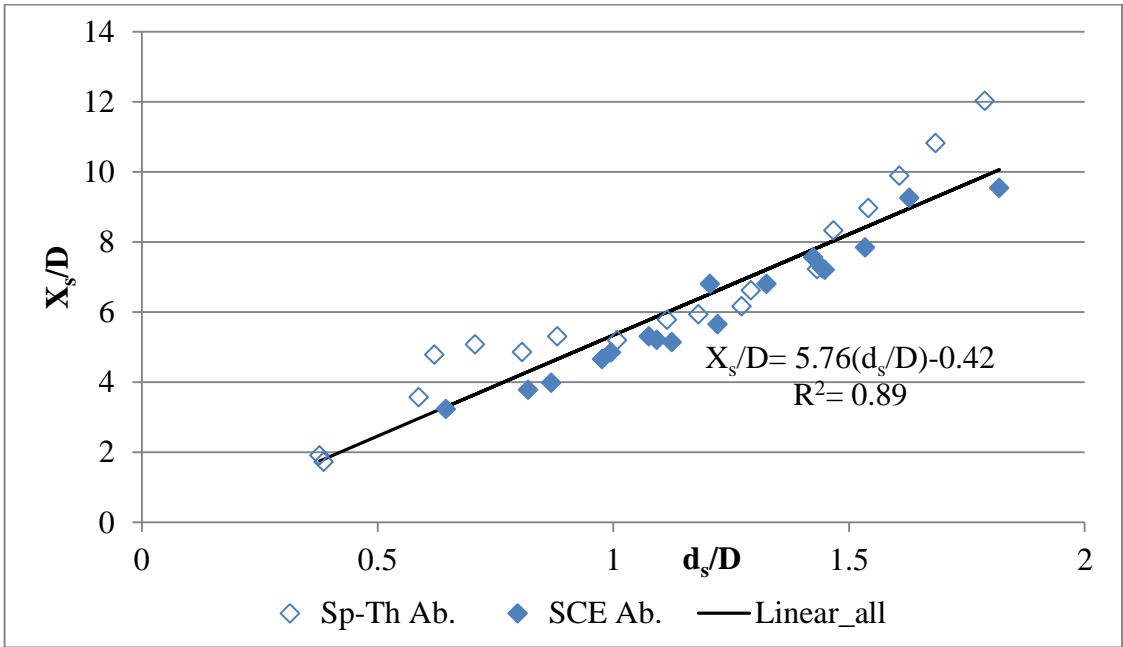


Figure 4.34 Variation of dimensionless scour hole length with the dimensionless scour depth for various abutment types

Figures 4.35 and 4.36 show the collection of the data for both abutment types of change in the parameters regarding the position of the maximum scour depth location with the contraction ratio ( $r/D$  and  $\alpha$ ). It was previously stated within the present study that, the position of the maximum scour depth always occurs at the upstream side of the abutment tip. Moreover, it can be stated that, for spill-through abutment the position of the maximum scour depth location changes with contraction ratio almost linearly where the data for the SCE abutment is more dispersed.

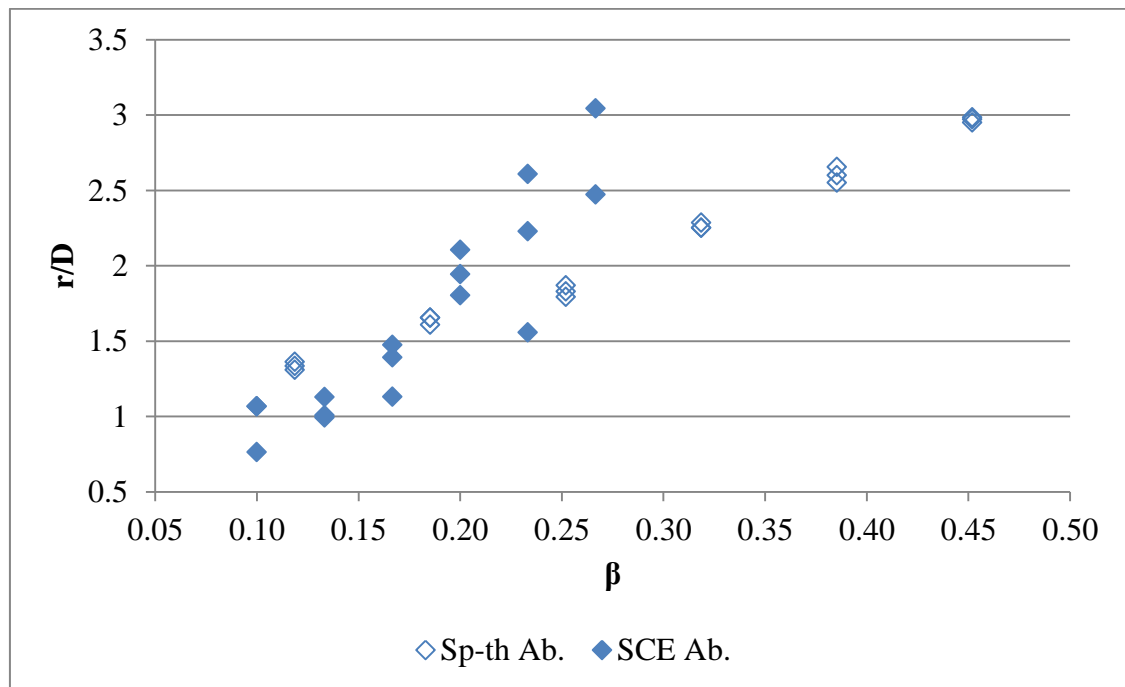


Figure 4.35 Variation of the dimensionless radius with the contraction ratio for various abutment types

From Figure 4.36, it can be stated that,  $\alpha$  values of every data are smaller than  $90^\circ$ , which means that, at all experiments the maximum scour depth occurred at the upstream side of the abutment tip. It should be noted that the contraction in the experiments with SCE abutment was created with only one abutment while it was created with two abutments for experiments with spill-through abutment, therefore; for the same

contraction ratio, the abutment lengths for the SCE abutments are twice the abutment lengths of the spill-through abutments. As the abutment length increases, the angle,  $\alpha$ , increases, in Figure 4.36, where the angles resulted for SCE abutment are always bigger than the angles resulted for spill-through abutment for the same contraction ratio.

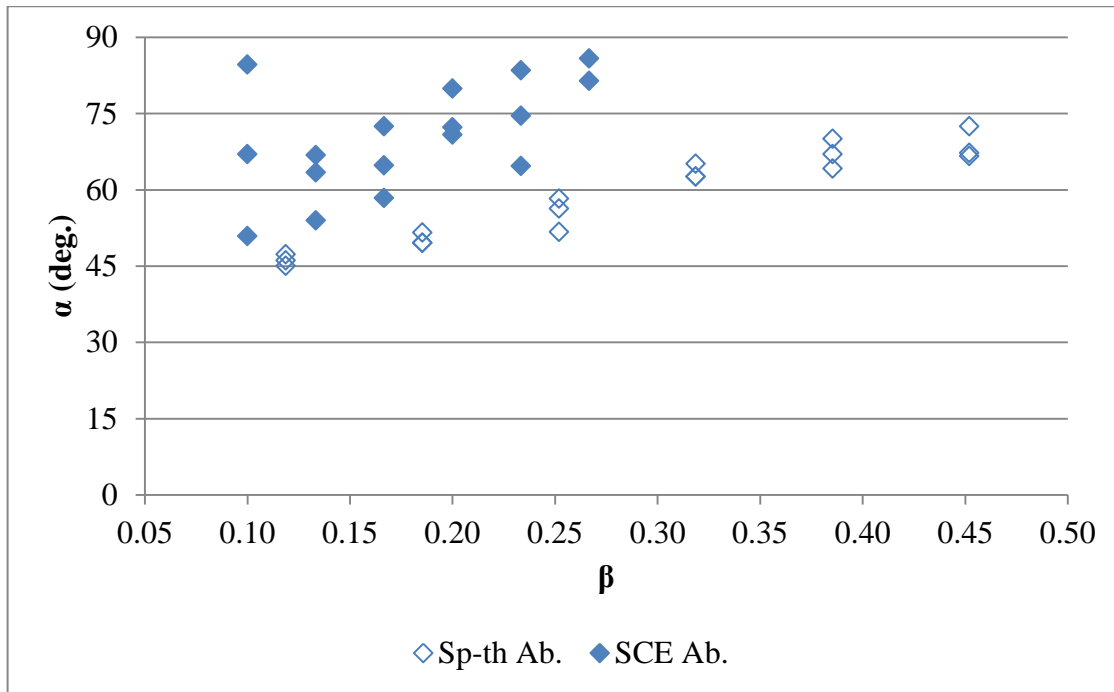


Figure 4.36 Variation of  $\alpha$  with the contraction ratio for various abutment types

Figure 4.37 shows the variation of  $V_s/D^3$  with  $\beta$  for both abutment types. The scales of the graph axes were selected as logarithmic scale to easily visualize the power relation of the two parameters. The  $V_s/D^3$  values for SCE abutments are higher than the ones for the spill-through abutment for the same contraction ratio. It is known that, the scour hole volume increase directly proportional to the increase in maximum scour depth. Therefore, as the experiments using SCE abutment resulted with more scour depths for any contraction ratio compared with the spill-through abutment, the larger values of the  $V_s/D^3$  for SCE abutments compared to the ones for the spill-through abutments for the same contraction ratio is an expected result.

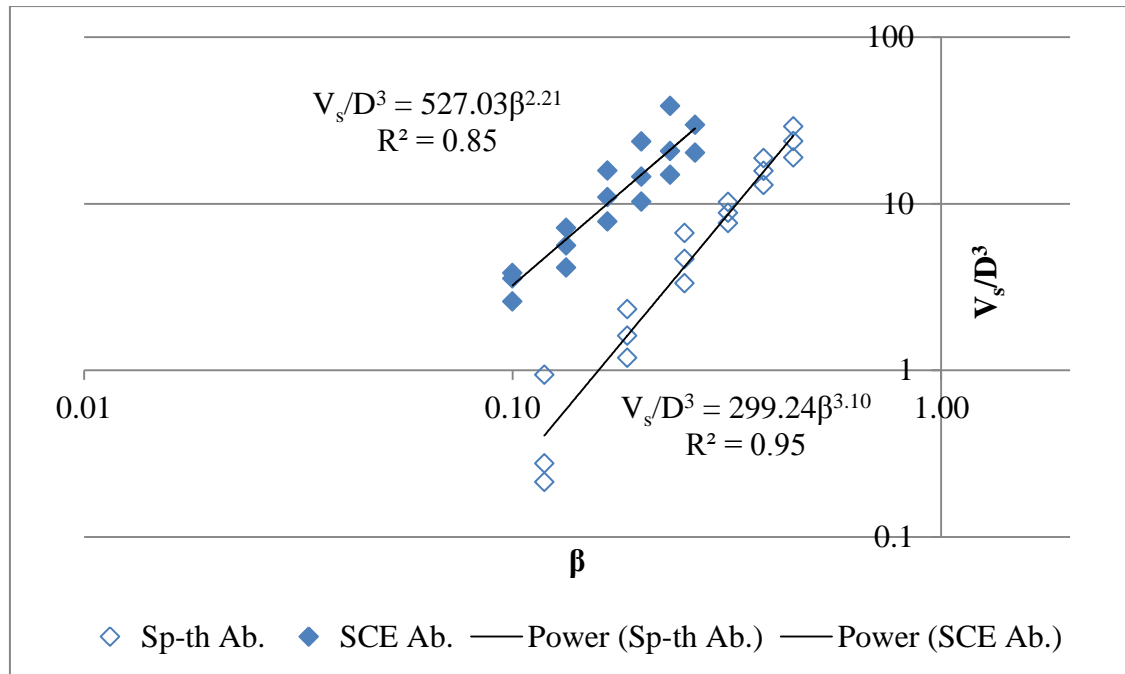


Figure 4.37 Variation of dimensionless scour hole volume with the contraction ratio for various abutment types

In Figure 4.38, the variation of the dimensionless scour hole volume with the dimensionless scour depth is demonstrated with combining the two data sets on different abutment types. The graph is created with logarithmic scales to visualize the power relation of the parameters easily. It can be seen from the figure that, regardless of the abutment type, the data of all sets can be described with a best fit line. However, after investigating the distribution of data one can say that, the  $V_s/D^3$  values for SCE abutments are slightly larger than the ones for spill-through abutments for the same contraction ratio. The reason behind this result was investigated within this study. Ballio and Orsi (2001) stated that any scour hole geometric parameter can be drawn with reasonable accuracy from the maximum scour depth value. This argument was verified in the present study. The relation of the scour hole volume with the maximum scour depth was fitted with high R-squared values for separate sets (Figure 3.32 and Figure 4.31) and the relation of the scour hole length with the maximum scour depth was fitted with high R-squared values regardless of the abutment type (Figure 4.34). The flow

conditions and the bed material properties of this two sets are identical. The only differences in these two experiment sets are the abutment type and the abutment width. The difference in abutment type leads to the difference in maximum scour depth, however; the factor affecting the relation of maximum scour depth and the scour hole volume is more like to be the abutment width. As the abutment width increases, the volume under the abutment increases and the volume deposited from the scour hole decreases. This leads a decrease in the scour hole volume with the increase in the abutment width, which is the situation presented in Figure 4.38.

It should be noted that the diversity in the base area of the abutments, such as rectangular with rounded corners or sharp corners or a semi circular end, do not change the abutment base area value significantly as the area of the concern is very small comparing with the whole abutment base area. Therefore, the diversity in the base area do not change the solid volume value of the abutment significantly and, the effect of abutment type on the abutment volume is ignored.

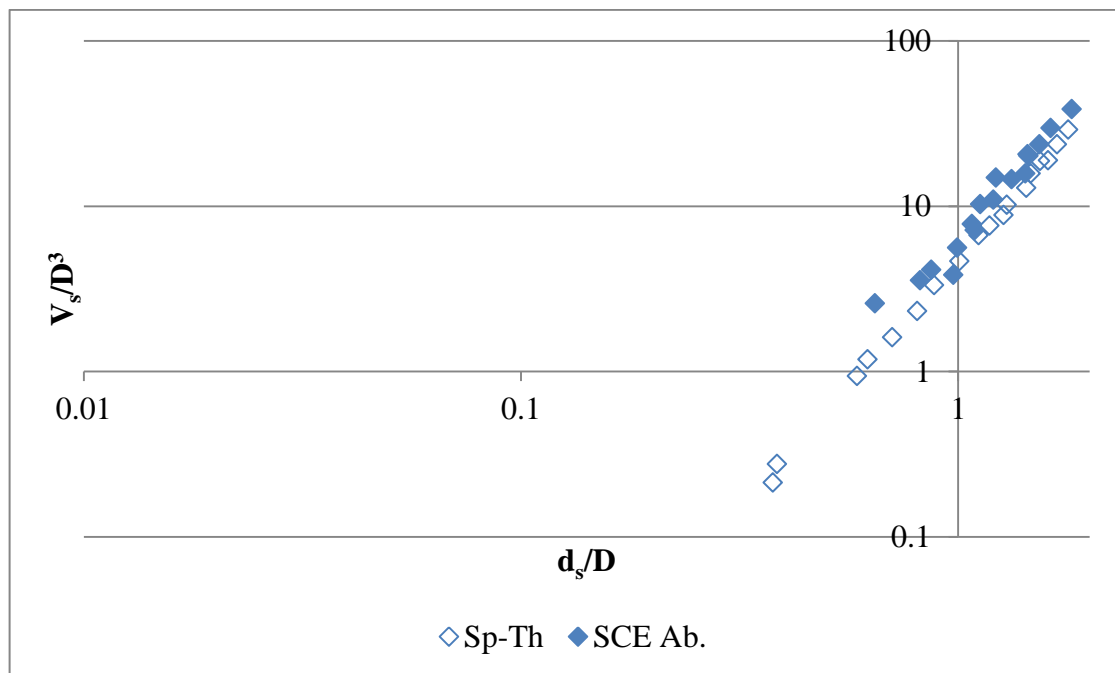


Figure 4.38 Variation of dimensionless scour hole volume with the dimensionless scour depth for various abutment types

Figure 4.39 was developed by fitting two linear relations for the two data sets separately. In doing these for spill-through abutments the data of set number: 13-18 were extracted from the data set as for those experiments the scour hole extends passing the flume axis and combines with the scour hole around the abutment model mounted at the opposite side wall. The best fit line developed previously was used for the data set of SCE abutment which is given below;

$$V_s/D^3 = 6.51 \left( d_s/D \right)^{2.91} \quad (4.3)$$

For the data set of the spill through abutments, the graph of the equation given below fitted the data well.

$$V_s/D^3 = 4.604 \left( d_s/D \right)^{2.91} \quad (4.4)$$

After fitting these two equations to the data sets one can say that, with the increase in abutment width, the scour hole volume decreases by maintaining the slope of the line in logarithmic scale. To offer a more reliable model, additional experiments should be done for various abutment widths.

It should be noted that these equations are valid for uniform sediment material with angle of repose equals to 30°. The equations may be reviewed for various bed material types also.

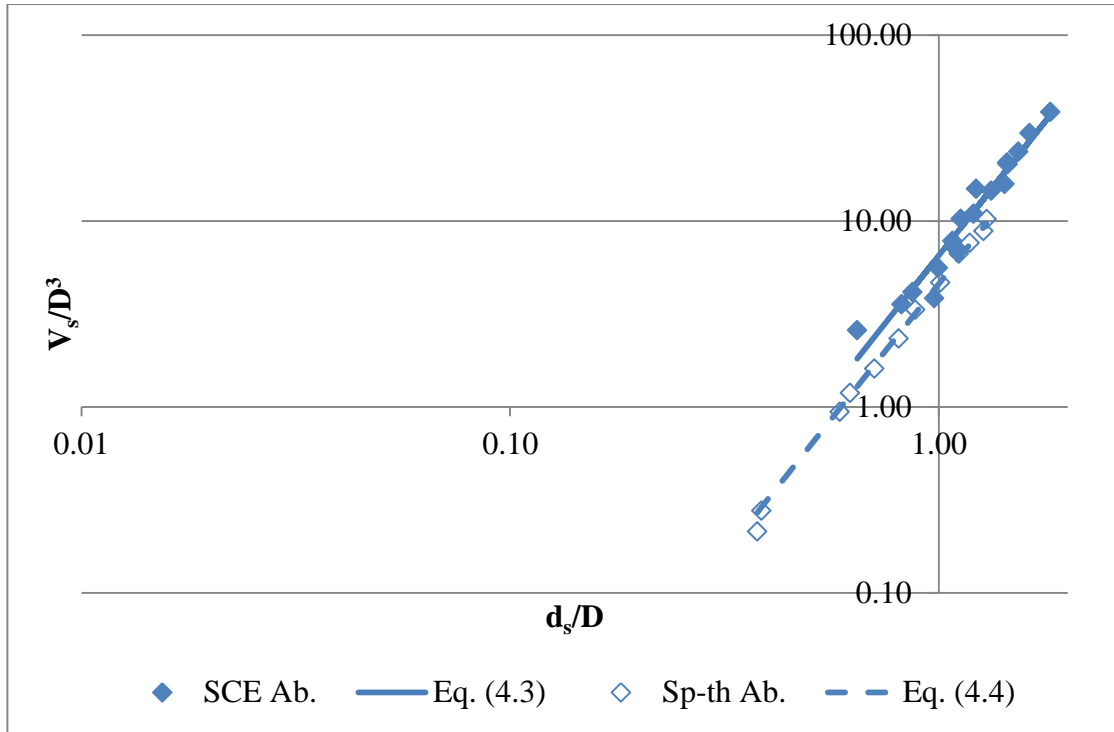


Figure 4.39 Comparison of Equations (4.3) and (4.4)

It should be seen from Equations (4.3) and (4.4) that, the exponent of the scour depth term is close to three and the following figure was developed to identify this relation clearly. Regardless of the parameters, every experimental data of the bathymetry measurements were used to develop Figure 4.40. It can be seen that the relation of  $V_s$  and  $d_s^3$  is very close to linear behavior.

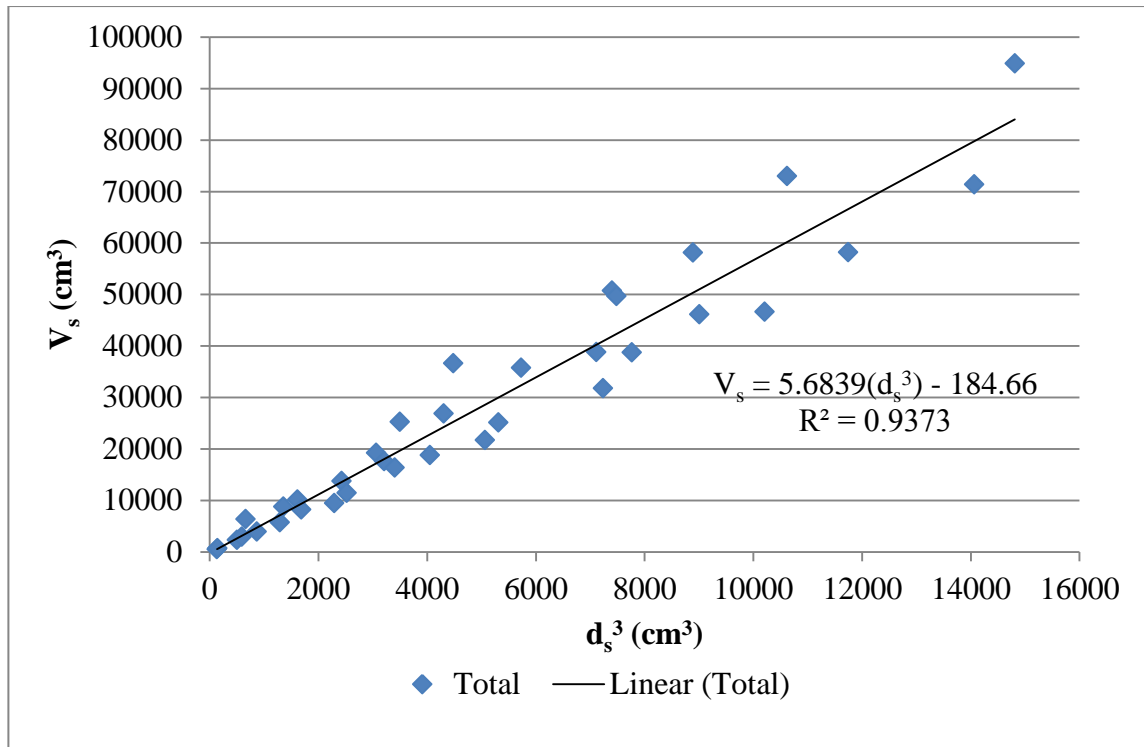


Figure 4.40 Scour hole volume vs scour depth cube relation by using every experimental data

#### 4.1.2.2 Comparison of Results with the Results of Similar Studies in Literature

There exist not many studies in literature dealing with the effect of contraction on local scour around abutments. Among these studies, some of them investigated the effect of smooth constriction on scour development, including Laursen (1963), which is recommended by FHWA Manual on Evaluating Scour at Bridges (HEC-18) for contraction scour model. This type of contraction is totally different from the contraction created by placing abutments. Ballio and Orsi (2001) studied the effect of contraction on local scour around bridge abutments. However, they only published the comparison data with and without contraction on the same laboratory flume, therefore; any data to be comparable with the present study could not be found. The contraction value, above which the effect of contraction on local scour is observed, was given as 0.33 by Ballio

and Orsi (2001). This is a relatively high value compared with the data obtained in this study, which will be analyzed at the last section of this chapter.

Moreover, a detailed analysis on scour hole geometry with the help of accurate bathymetry measurements have not been accomplished until now in the studies that exist in literature. Hence, the comparison of the equations offered in the present study (Equations (4.3) and (4.4)) with the previous studies could not be accomplished. Ballio and Orsi (2001) has analyzed the scour hole geometry by measuring bed profiles around abutments and they stated that the side slopes of the scour hole remains the same regardless of the time and they are equal to the angle of repose of the bed material. They also stated that the scour hole volume only depends on the depth of scour, which is also confirmed in the study with an additional constraint on the effect of variation in abutment width and angle of repose of the bed material.

## **4.2 Temporal Scour Measurements**

In a similar manner as the experiments covered in Section 3.3, the temporal variation of scour pattern were measured by placing two identical spill-through abutment models in the bridge crossing portion of the flume. The measurements were taken with the ultrasonic ranging system (Figure 3.3) while the experiments were running. The temporal development of the bed profiles were measured at five sections around the abutment. The experiments were repeated twice for small and large contraction ratios to obtain the effect of contraction on the temporal development of bed profiles.

Two parts will be covered within this section as; “Experimental Equipment and Procedure” and “Results”. These parts will be discussed below with details.

### **4.2.1 Experimental Equipment and Procedure**

The experiments were conducted in the same laboratory flume as the aforementioned experiments were conducted. Two identical spill-through abutment models with sharp corners were placed in the sediment storage portion of the flume on the opposite side walls by creating a contraction ratio of  $\beta = 2L/W$ .

The experiments were repeated twice for two contraction ratios. A small contraction ratio was obtained by placing the shortest abutment models in the flume and obtaining a contraction ratio of  $\beta= 0.119$ . A large contraction ratio ( $\beta= 0.452$ ) was obtained by placing the longest abutment models. The experiments were repeated five times for each contraction ratio to measure the temporal development of the bed profiles at five sections around the abutment. The sections were selected as follows; the first one at the upstream of the abutment, oriented vertically to the flow direction cutting through the scour hole, the second one at the tip of the abutment oriented vertically to the flow direction, the third one at the downstream of the abutment, oriented vertically to the flow direction cutting through the deposition region, the fourth one at the tip of the abutment located parallel to the flow direction and the last one was obtained by distributing the transducers around the abutment. Figures 4.41 (a) and (b) demonstrate the positions of these sections for  $\beta= 0.119$  and  $\beta= 0.452$ , respectively. By this manner 10 experiments were conducted in this set each lasting 8 hours.

The experiments were conducted following the procedure discussed in Section 3.1. The flow and flume characteristics were also discussed in Section 3.1. Each experiment was conducted for 8 hours and the data were recorded with 1 minute time intervals. However, some data were eliminated at the initial parts of the recording as in the sudden happening of scouring process, the suspended sediment particles in motion below the transducers caused the transducers not to record the data by acting as an obstacle between the transducers and the flume bed.

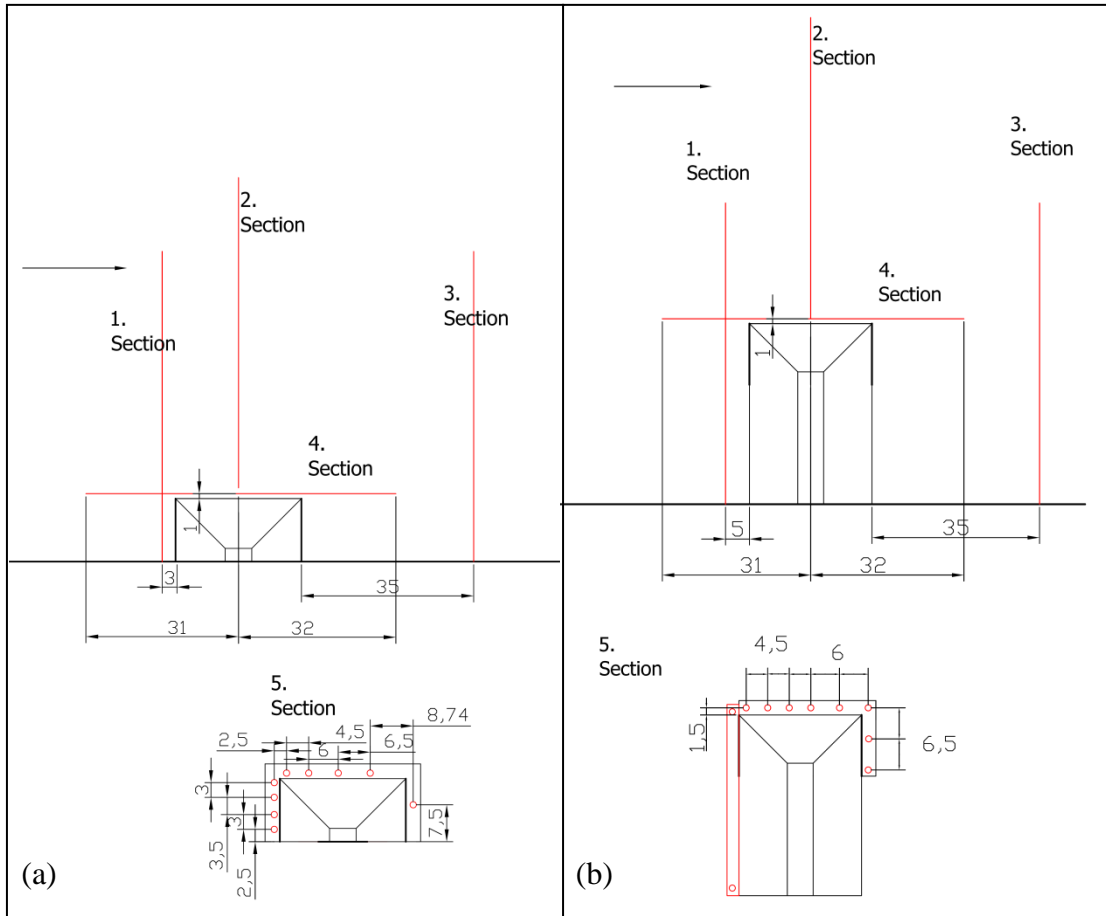


Figure 4.41 Positions of the measurement sections for (a)  $\beta= 0.119$  (b)  $\beta= 0.452$

(dimensions are in cm, red drawings stand for the transducers)

#### 4.2.2 Results

The data was recorded for each experiment within the set and the processing was done by obtaining the bed profiles for each time step. The time steps were selected as  $t= 0.5, 1, 2, 3, 4, 5, 6, 7$  and 8 hours where the bed profiles were plotted (Figures 4.42 to 4.51). The time steps used in the figures were selected to visualize the time development of the scour pattern. In the figures,  $s/D$  stands for the dimensionless distance around the abutment where transducers are located. In the legend of each figure, the numbers with letter P stands for the transducer numbers.

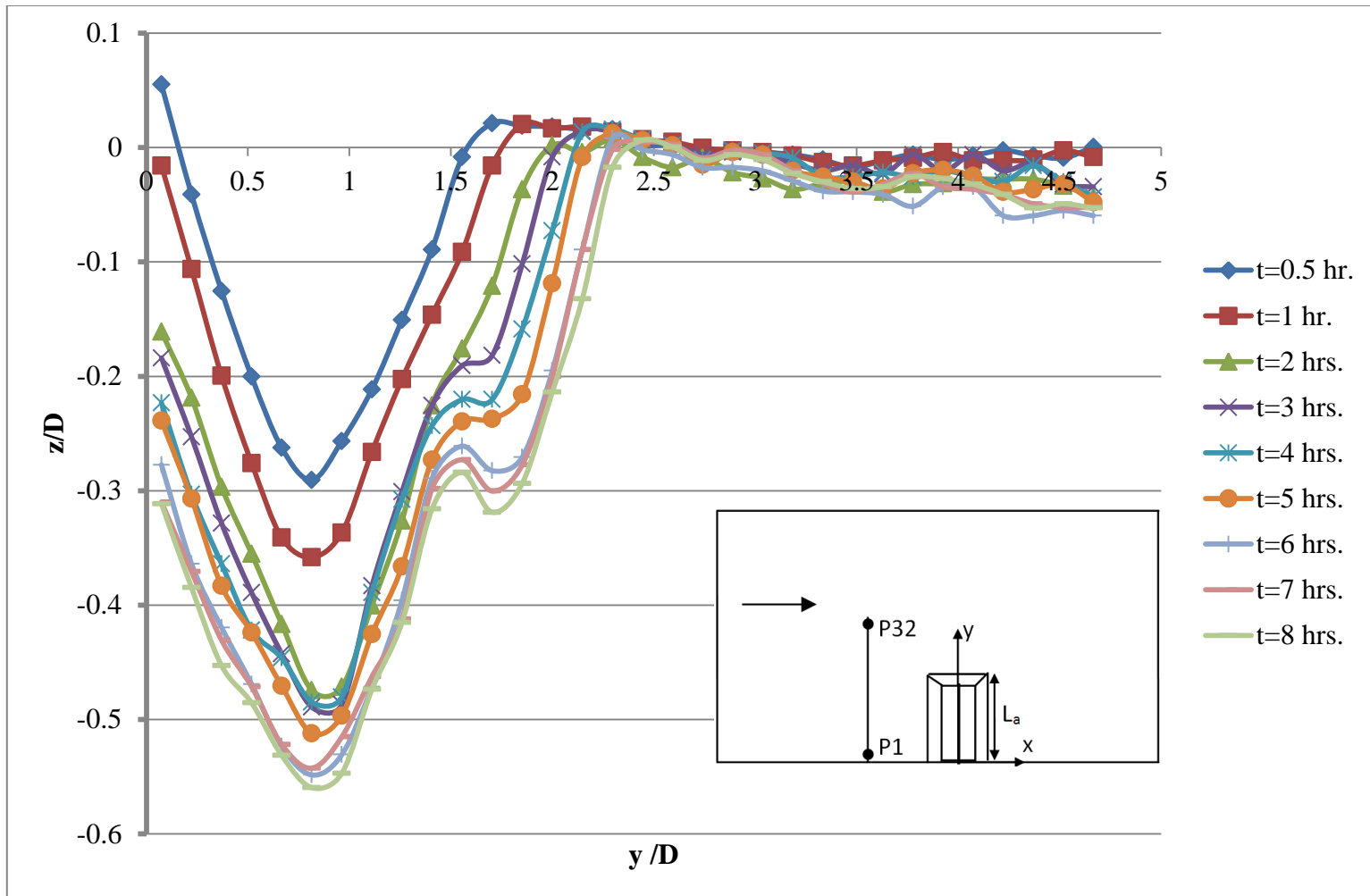


Figure 4.42 Temporal changes of bed profiles at Section #1 for  $\beta=0.119$

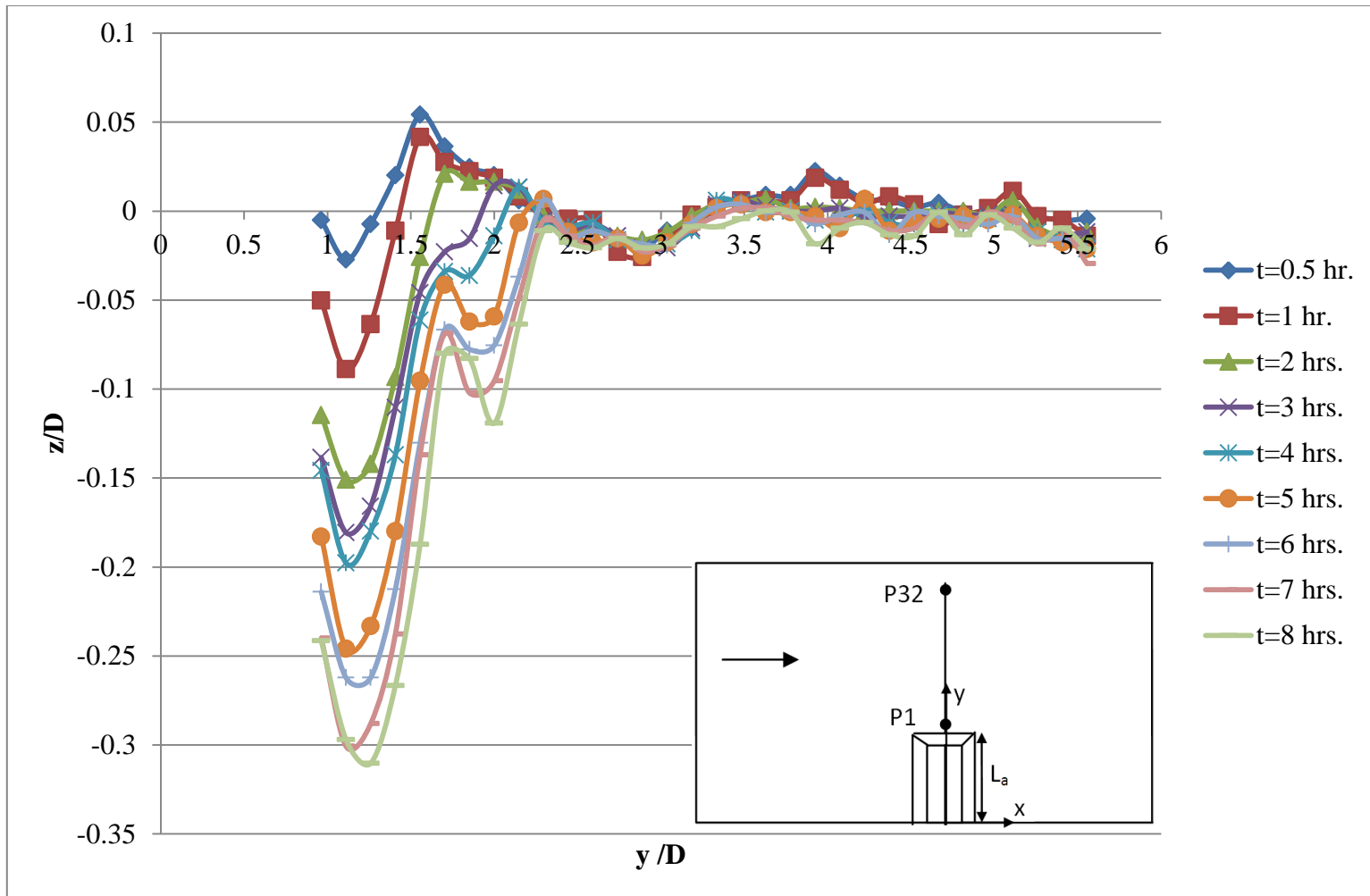


Figure 4.43 Temporal changes of bed profiles at Section #2 for  $\beta = 0.119$

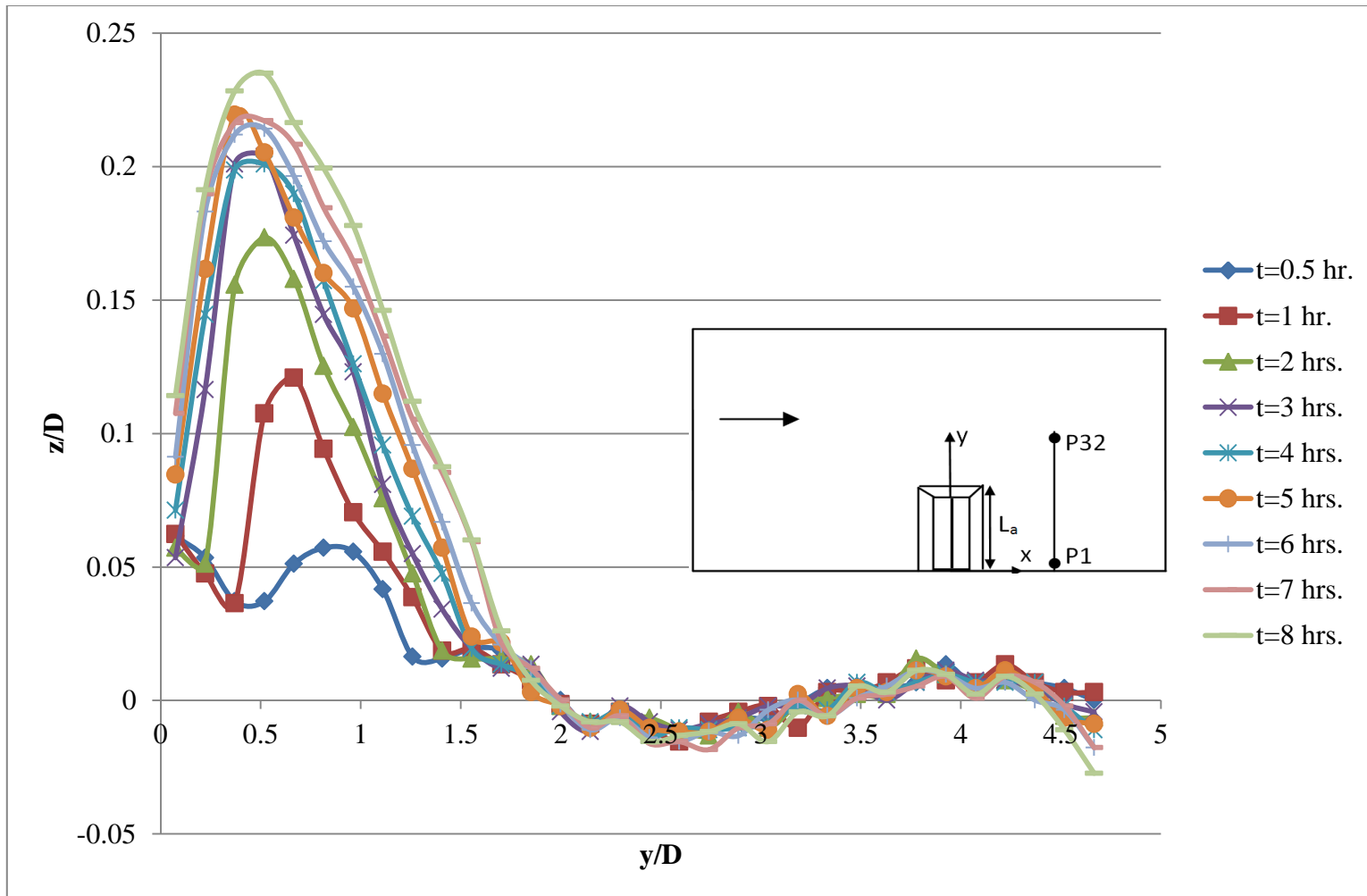


Figure 4.44 Temporal changes of bed profiles at Section #3 for  $\beta = 0.119$

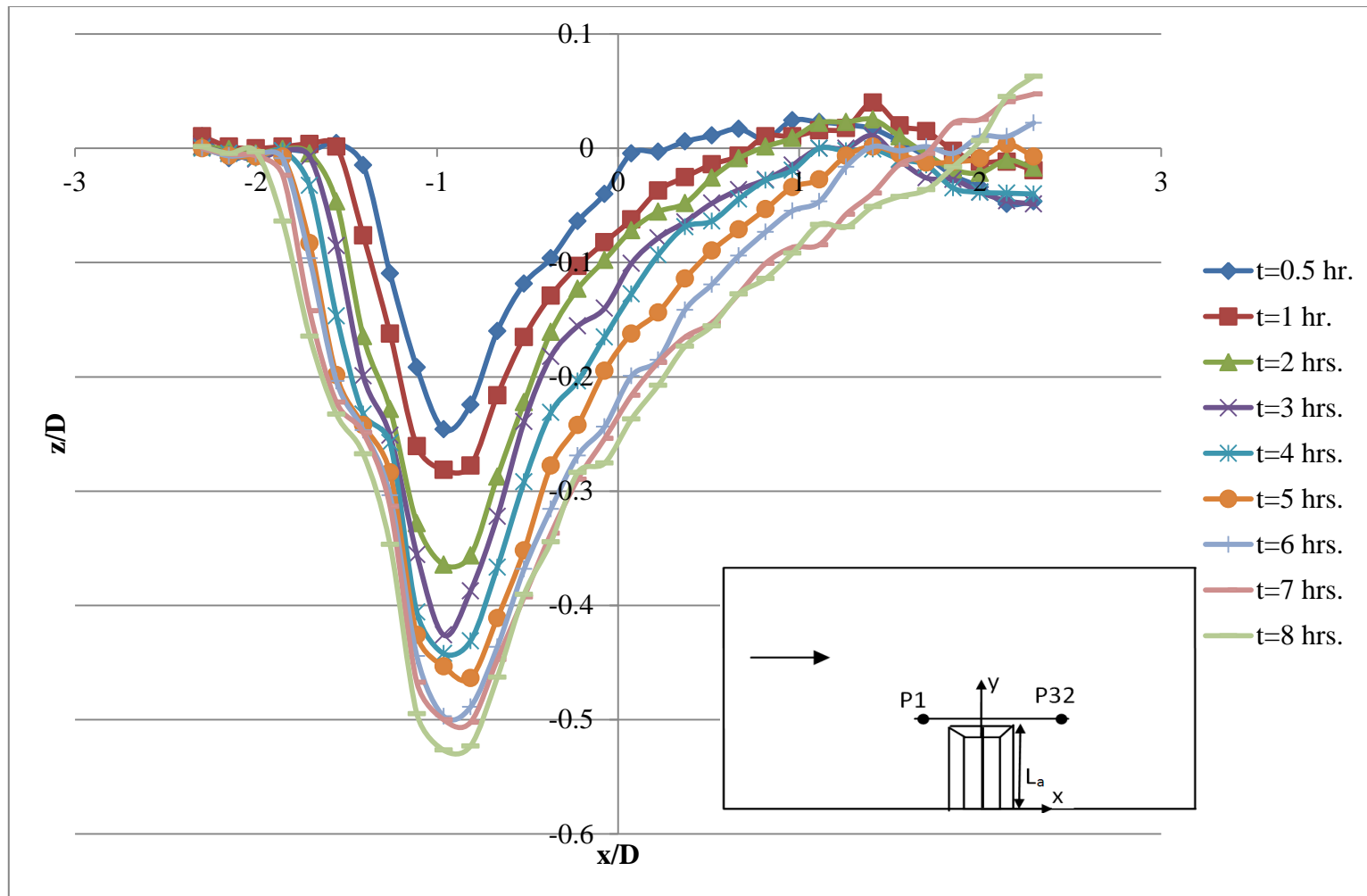


Figure 4.45 Temporal changes of bed profiles at Section #4 for  $\beta = 0.119$

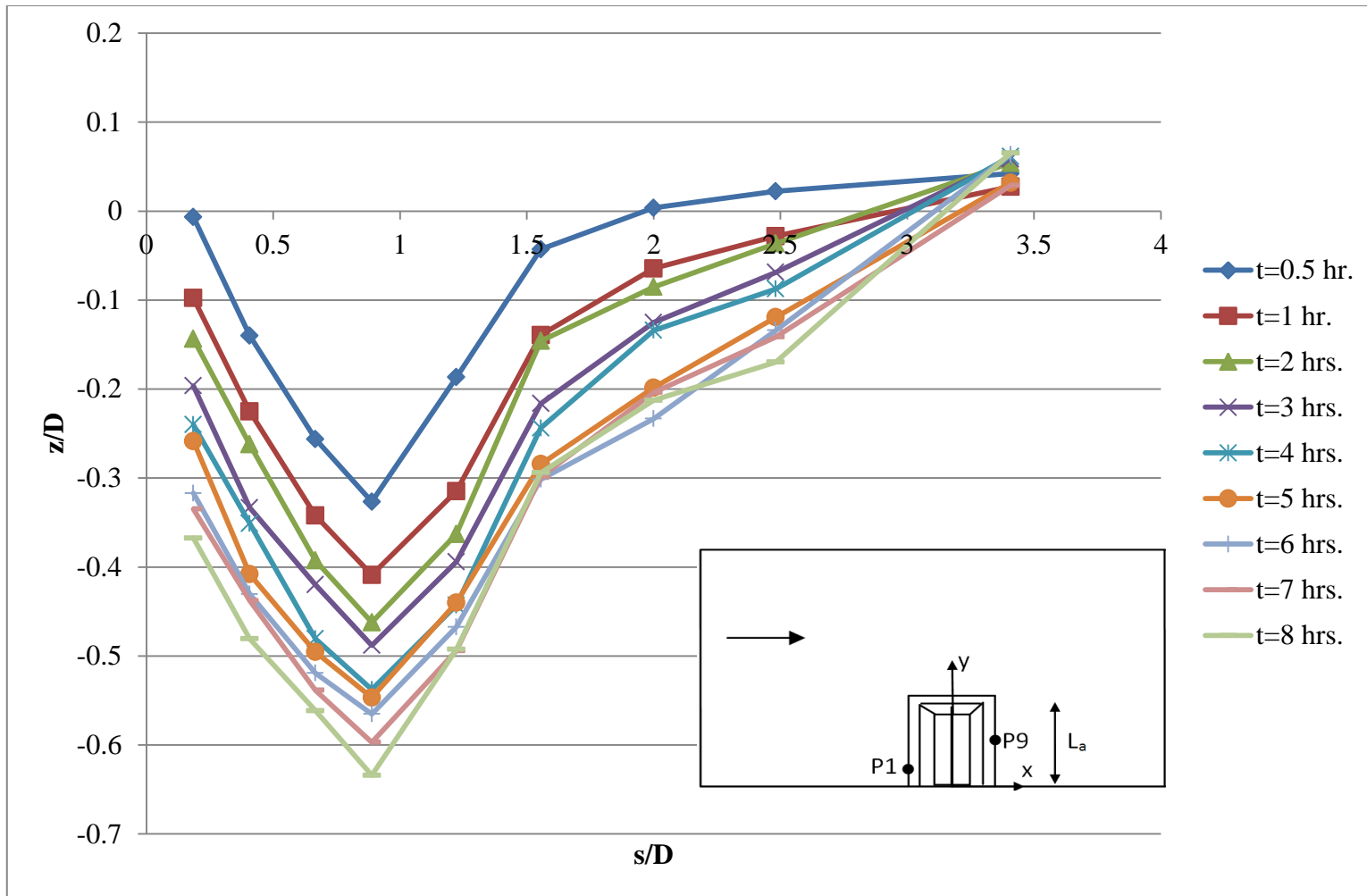


Figure 4.46 Temporal changes of bed profiles at Section #5 for  $\beta = 0.119$

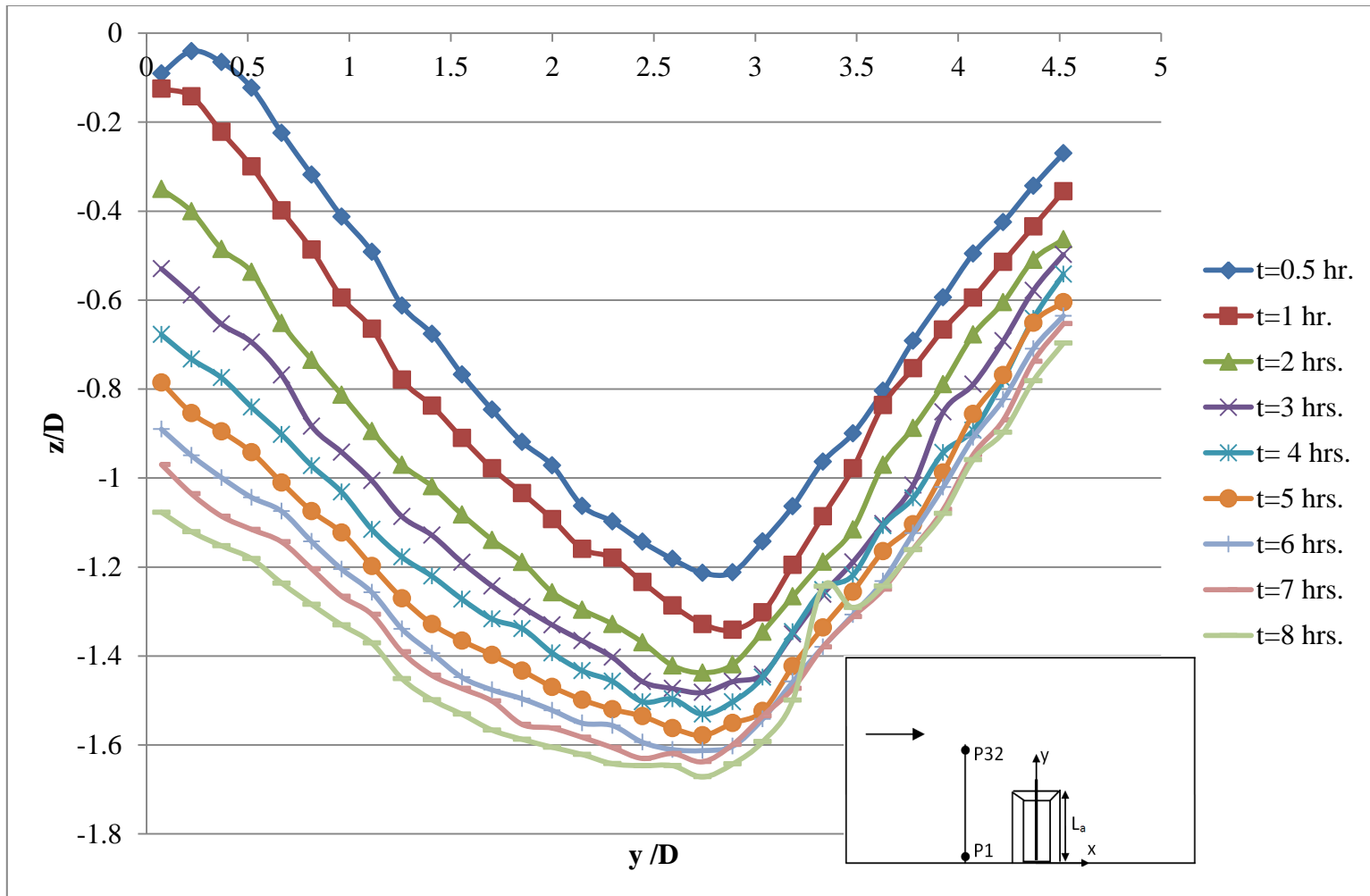


Figure 4.47 Temporal changes of bed profiles at Section #1 for  $\beta = 0.452$

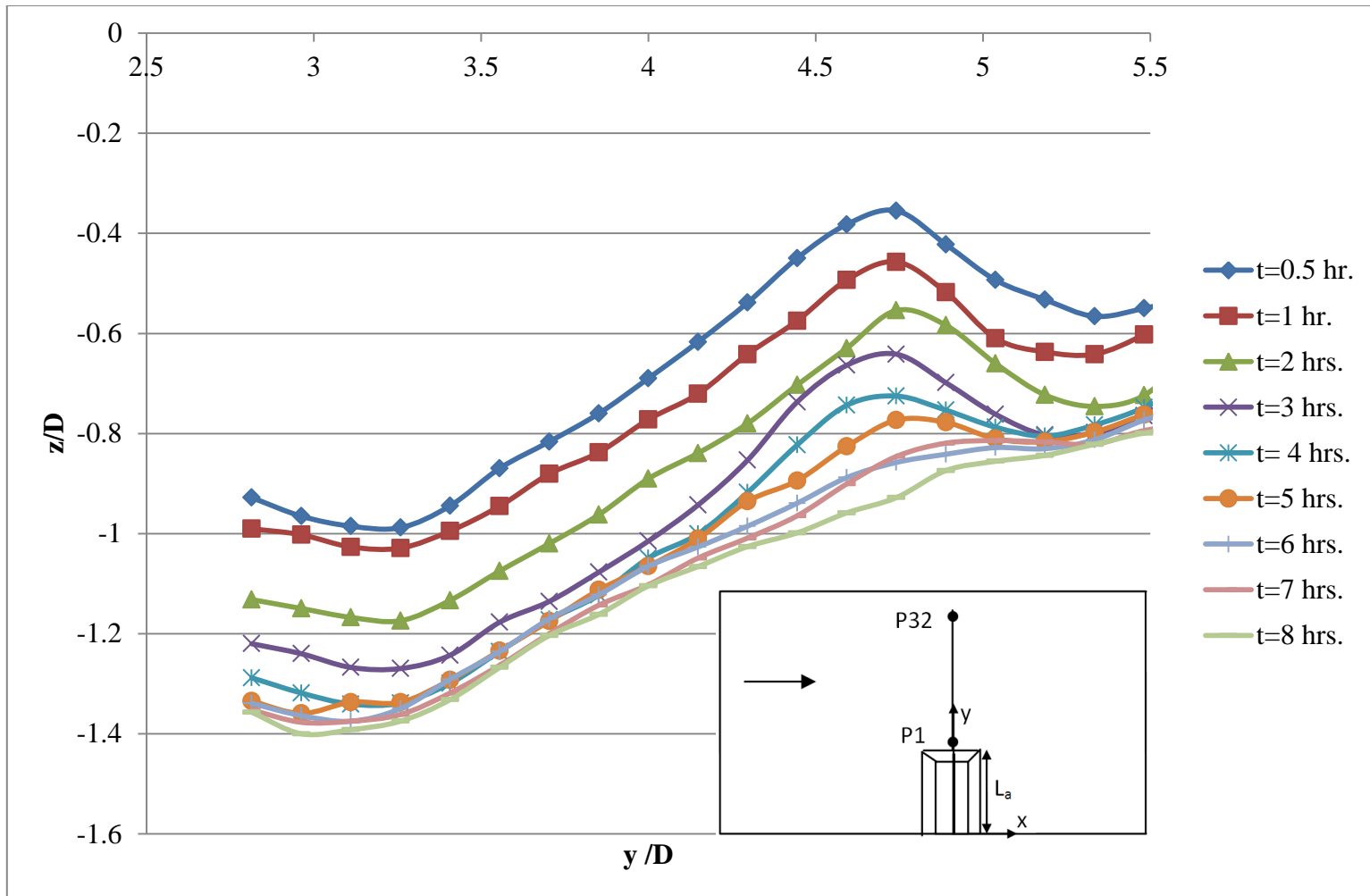


Figure 4.48 Temporal changes of bed profiles at Section #2 for  $\beta = 0.452$

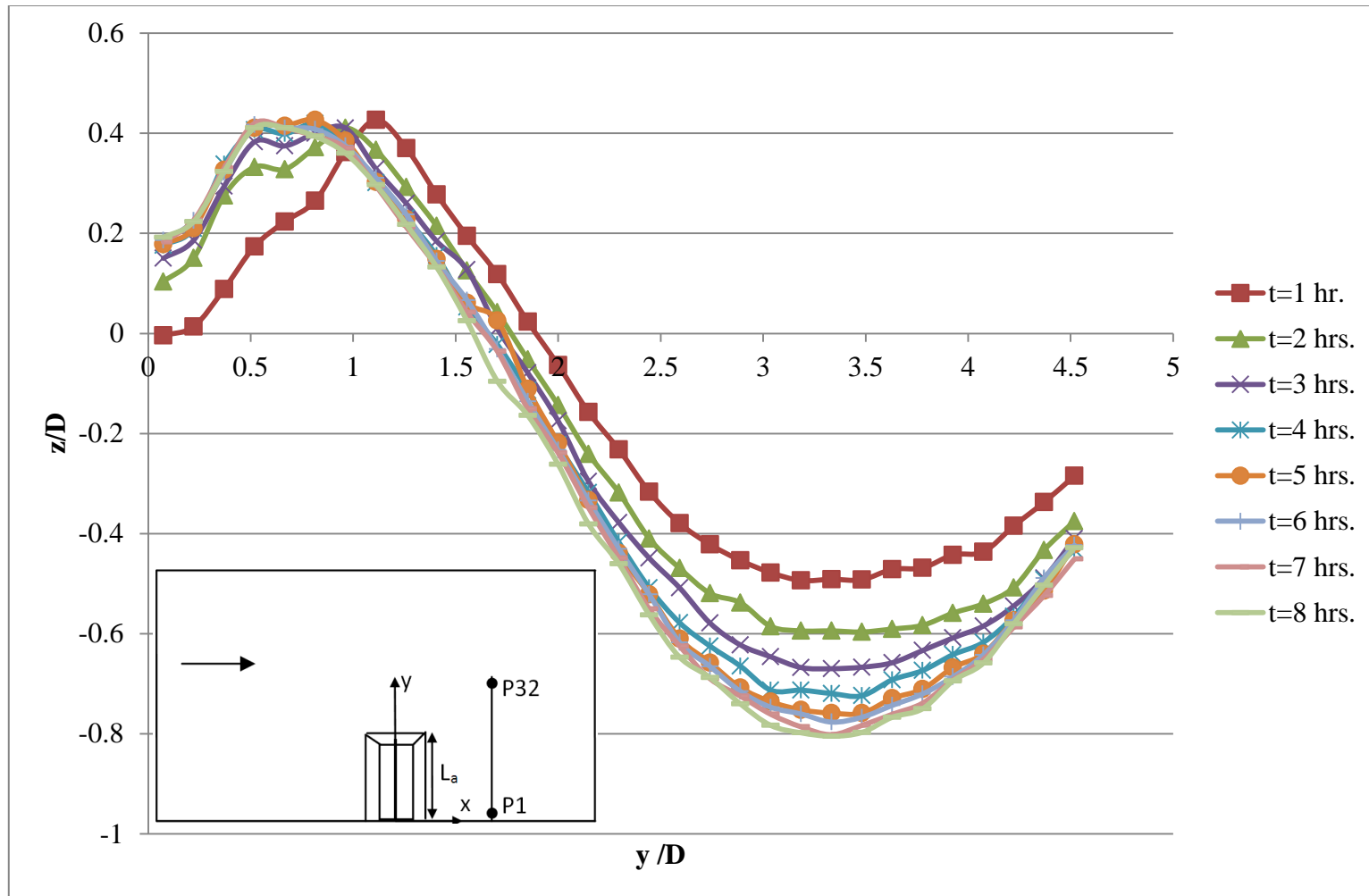


Figure 4.49 Temporal changes of bed profiles at Section #3 for  $\beta = 0.452$

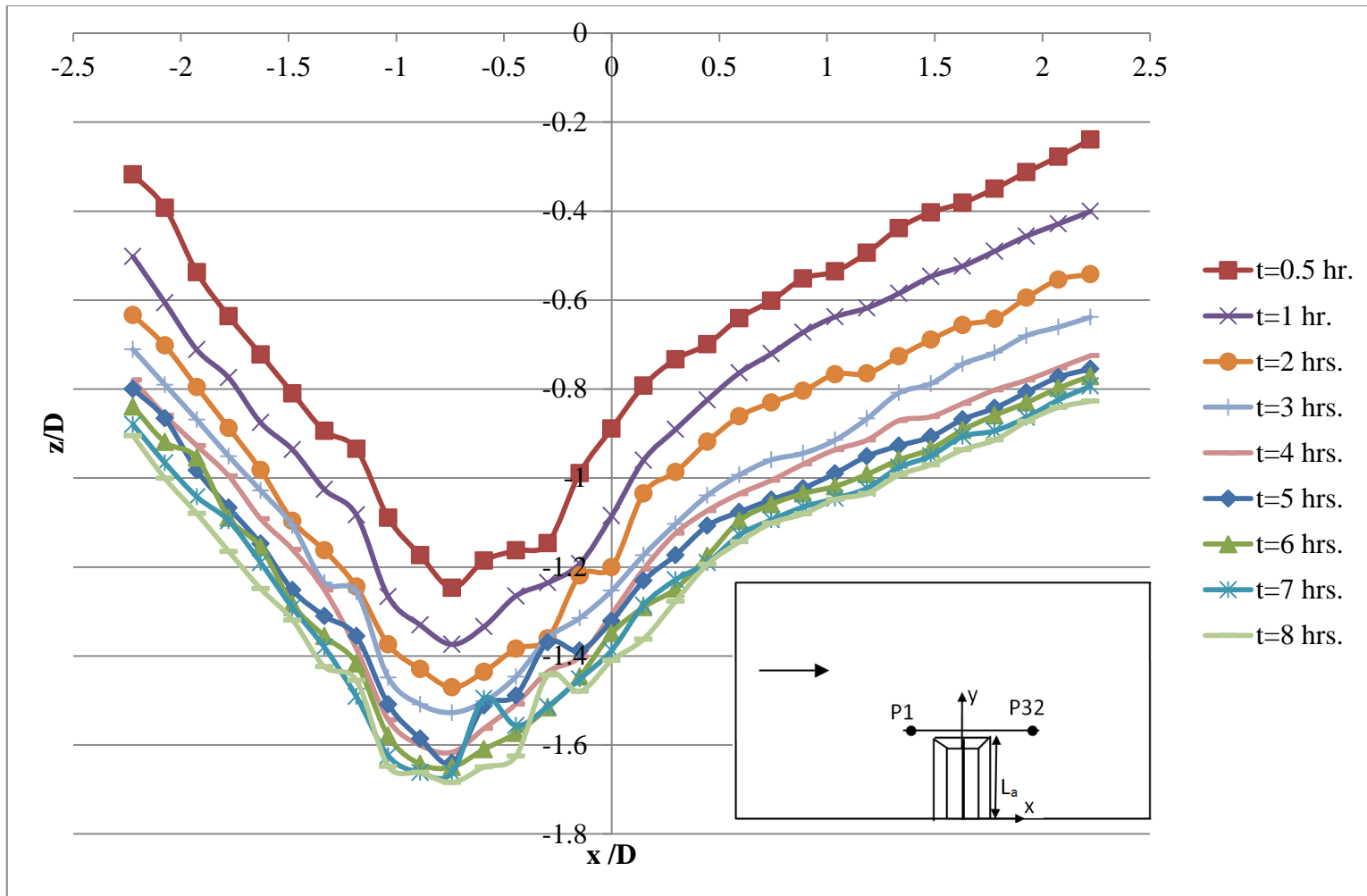


Figure 4.50 Temporal changes of bed profiles at Section #4 for  $\beta = 0.452$

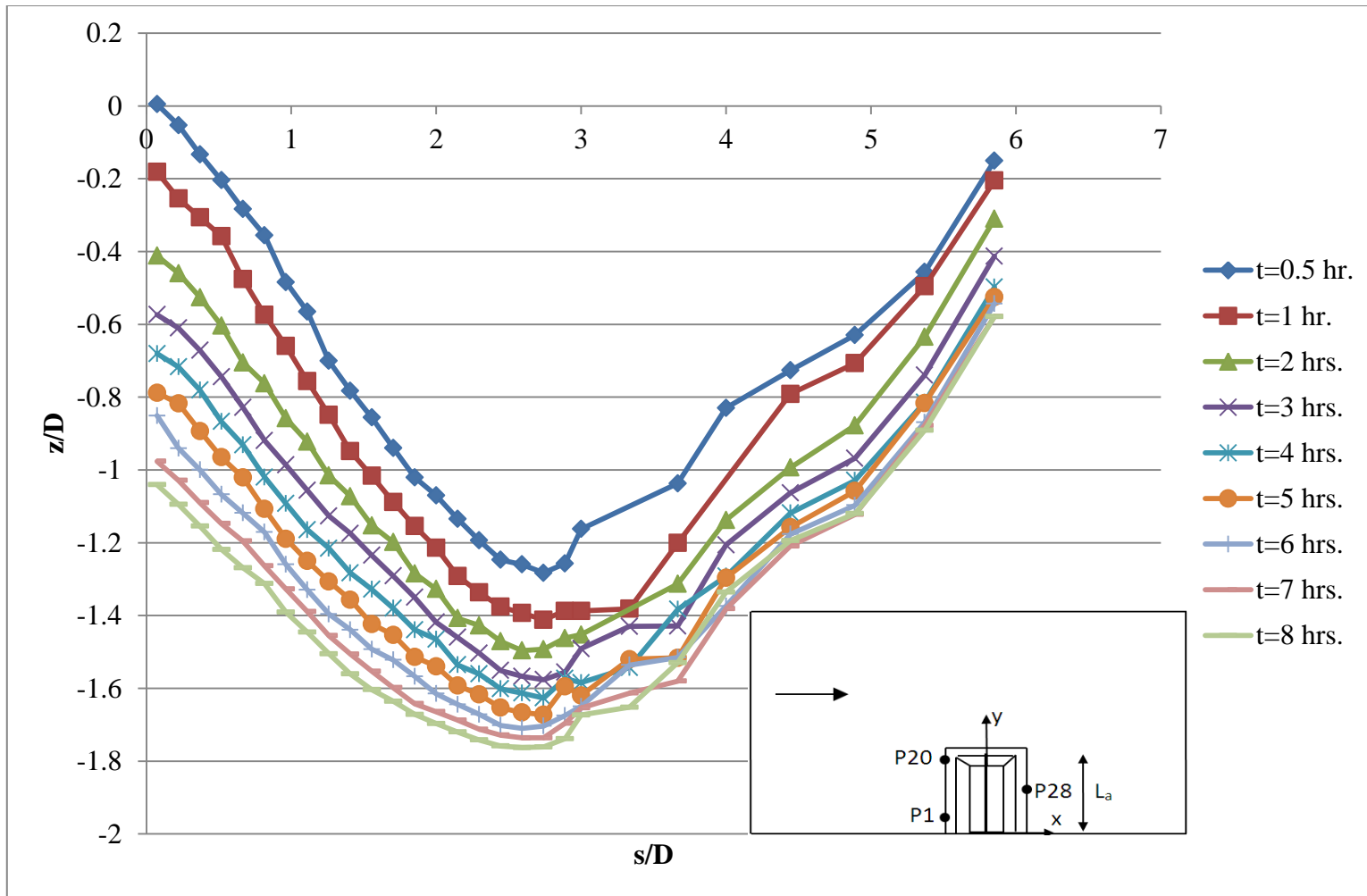


Figure 4.51 Temporal changes of bed profiles at Section #5 for  $\beta = 0.452$

#### 4.2.2.1 Discussion of Results

From the results of the temporal measurement experiments of the scoured bed profiles, it can be stated that, while the time passes throughout the experiments,  $z/D$  increases in negative direction in scour areas and it increases in positive direction in deposition areas at all the sections being investigated. This means scour hole and deposition region development continues within the experiment duration of  $t= 8$  hours for both contraction ratios and equilibrium scour depths were not reached. However, it should be noted that, the rate of increase in  $z/D$  decreases with increase in time, which can be explained with the well-known asymptotic increase of the scour depth with increase in time (Chabert and Engeldinger, 1956). Besides, from Figures 4.42 and 4.43, it can be seen for small contraction ratio that, the secondary scour region starts to develop after  $t= 3$  hours at the far end side of the main scour hole with respect to the flume side wall. This region develops further with time and it becomes a secondary scour hole after  $t= 6$  hours. This kind of formation is not observed for experiments of large contraction ratio (Figures 4.47 and 4.48). It should be noted that, as discussed in Chapter 3, a secondary scour hole formation was observed for long abutment case of the experiments with SCE abutment, while this type of formation for short abutment was weaker compared to the long abutment case.

By using every figure demonstrating the scour region, the side slopes of the scour hole were measured to be equal to the angle of repose of the bed material. This result is in agreement with the findings in Chapter 3.

Figure 4.49 shows the bed profile change taken at the deposition region downstream of the abutment for the large contraction ratio. Similar to the findings of Chapter 3, it was seen that, the deposition region shifts through the flume wall until  $t= 2$  hours and remains on the same position till the end of the experiment. The height of the deposition hill did not change considerably after the first two hours of the experiment. A similar argument was not obtained for the results of the small contraction case (Figure 4.44). From that figure it is seen that, the height of the deposition hill increases in the first four hours of the experiment considerably and then the increase do not stop

but slow down and continues till the end of the experiment. The crest of the deposition hill remains almost at the same spanwise position after  $t= 3$  hours in both cases. One other important observation is that, the side slopes of the deposition hill on the main channel side remains constant for both cases throughout the experiment. For the smaller contraction ratio, the other side slope close to the flume side wall also remains constant whereas for the larger contraction ratio, there slightly changes up to  $t= 2$  hours.

Figures 4.45 and 4.50, which are the streamwise sections tangent to the toe of the abutment, show that, the depth of scour hole at the upstream of the abutment axis is always larger than that measured at the downstream side, valid for the whole test durations regardless of the contraction ratio. In both contraction ratios, the maximum scour depth is observed at the same streamwise position throughout the experiment. In the small contraction ratio, this position is at  $x/D \approx -1$  whereas in the large contraction ratio, it shifts slightly towards the abutment and forms at  $x/D \approx -0.8$ .

Scour hole development around the abutment was measured at the fifth sections for both small and large contraction ratios (Figures 4.46 and 4.51). The maximum scour depths were obtained at the same point throughout the experiments which is at the upstream side of the abutment tip for both contraction ratios. Temporal development of the scour depth at these points for the small and the large contraction ratios are given in Figures 4.52 and 4.53, respectively with smaller time increments. These points correspond to the locations where the maximum scour depths are obtained throughout the all bathymetry.

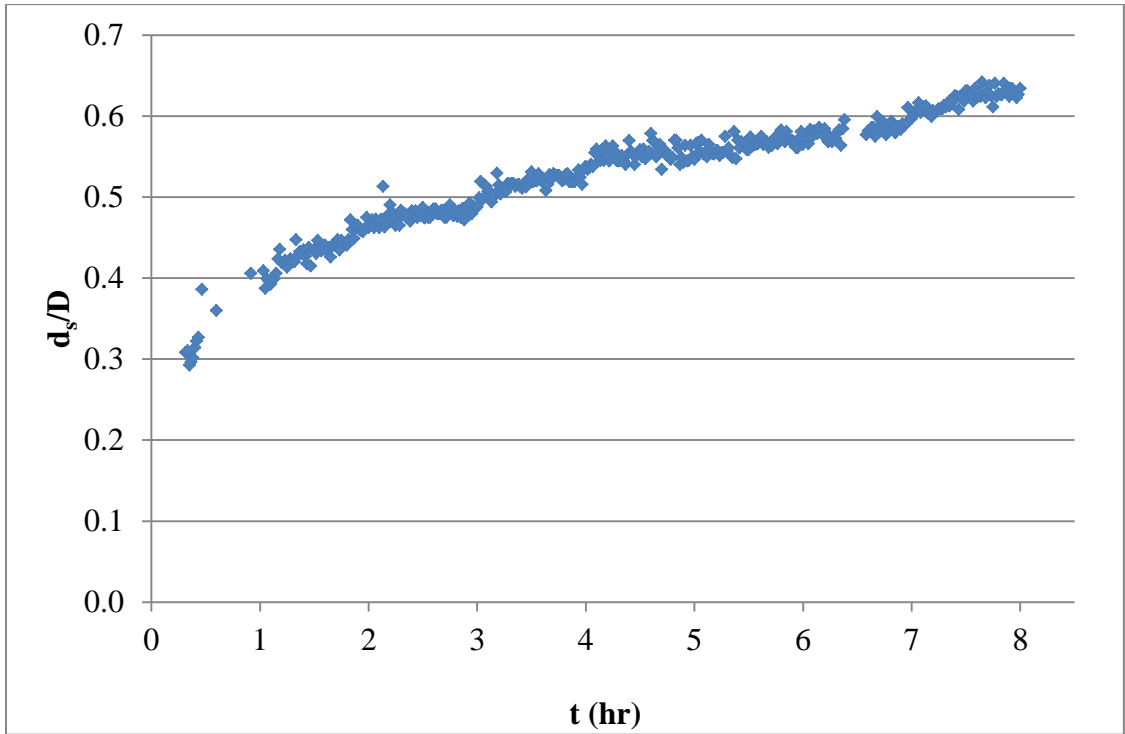


Figure 4.52 Temporal development of scour depth for  $\beta= 0.119$

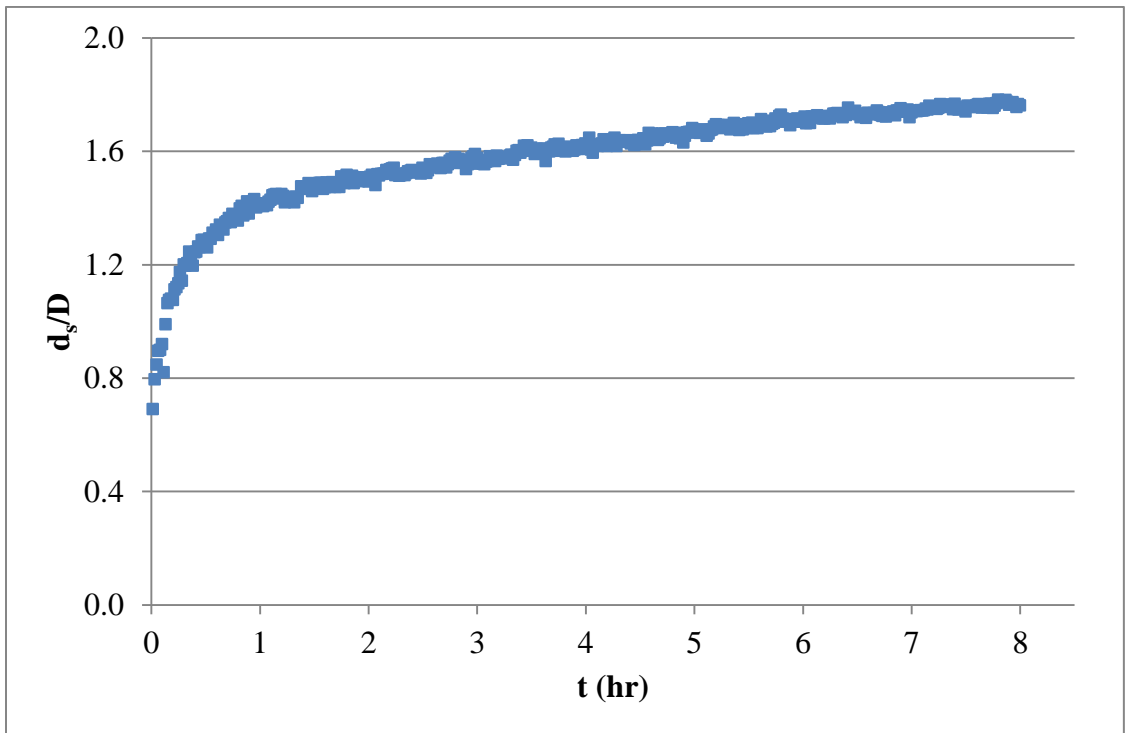


Figure 4.53 Temporal development of scour depth for  $\beta= 0.452$

After investigating Figures 4.52 and 4.53, it can be concluded that, the scour development is very fast in the early times of the experiments, then, the rate of change of increase in scour depth slow down gradually with time for both contraction ratios. It can be stated that, for large contraction case, the rate of change of increase in the scour depth is smaller than that of small contraction case at time,  $t= 8$  hours. Therefore, it can be concluded that, the scouring for large contraction case is closer to the equilibrium phase than the scouring for small contraction case at the end of the experiment duration. Hence, it can be expected that the scouring would reach to the equilibrium condition faster for large contraction case rather than the small contraction case. The similar deduction was obtained in Chapter 3 that, the scouring was seen closer to the equilibrium condition for long abutment case comparing with the short abutment case.

The comparisons of the reach time to the 50% of the scour depth obtained at  $t= 8$  hours which was accomplished in Chapter 3 for the long and short abutment cases of SCE abutment. It was obtained that, 0.5 hour and 1 hour was the reach times for long abutment and short abutment cases, respectively. After making a similar analysis to the experiment data covered in this chapter, the following reach time values were obtained:  $t= 0.1$  hour for large contraction case and  $t= 0.5$  hour for small contraction case (Figures 4.52 and 4.53). As the contraction ratios of the small contraction case of Chapter 4 and the short abutment case of Chapter 3 are close, the contraction ratio difference would not be the reason of this difference in reach times. Then, one may conclude after these findings that, the time to reach 50% of the maximum scour depth is faster for spill-through abutments comparing it with the SCE abutments of the same abutment length or contraction ratio.

#### **4.2.2.2 Comparison of Results with the Results of Similar Studies in Literature**

As discussed in Section 3.3.3.1 with details, there exists no suitable study in literature to compare the findings of this study on the temporal variations of the bed profiles. However, there exist studies in literature which are related to the temporal development of maximum scour depth. Thus, the findings of the experimental set were

compared with the results of the models developed by Coleman et al. (2003) and Oliveto and Hager (2005).

To apply the method offered by Coleman et al. (2003), the present problem is modeled for the methodology given by that study, which is presented below;

$$d_{se} = K_{yl}K_IK_dK_sK_\theta K_G \quad (4.5)$$

where the coefficients  $K_{yl}$ ,  $K_I$ ,  $K_d$ ,  $K_s$ ,  $K_\theta$  and  $K_G$  stand for the effects of flow depth-abutment length, flow intensity, sediment size, abutment shape, foundation alignment and approach channel alignment, respectively.

The model parameters (K-coefficients) are selected as given in Table 4.3 for the present study. As the experiments of the present study were conducted in rectangular flume with no alignment in flow and abutment direction by using fine sediment particles as bed material, the coefficients of  $K_d$ ,  $K_\theta$  and  $K_G$  were remained as 1.  $K_{yl}$  was defined as  $2*L$  for short abutments (the shortest abutment case in the present study) and  $2*(DL)^{0.5}$  for intermediate abutments (the remaining cases).  $K_I$  was defined as equals to the flow intensity value for the clear-water scour.

In selecting the  $K_s$  coefficient, which is a factor showing the abutment type effect, a calibration was applied as the method does not offer a value for the abutment type used in this study. The method states the use of  $K_s= 1$  for vertical wall abutments and  $K_s= 0.6, 0.5$  and  $0.45$  for spill-through abutments having  $0.5:1, 1:1$  and  $1.5:1$  H:V ratios on side walls respectively. The H:V ratio of the abutment model used in the present study is  $0.577:1$ , which corresponds to  $K_s= 0.583$  after making a parabolic interpolation using these three data. Besides, the spill-through abutment model referred in Melville (1992) is the spill-through abutment with rounded corners. In the present study, a modified version of spill-through abutment model was used with sharp corners. Hence, a correction on  $K_s$  coefficient was done in order to contain the effect of this difference. By calibrating the model with the current experimental data,  $K_s= 0.7$  was selected to be used in this section. By this selection, the model result of Coleman et al. (2003) agreed

well with the data experiments for small contraction as can be seen in Figure 4.54. As the sharp corners would lead more scour depth, this selection seems reasonable by comparing it with the one obtained after interpolation.

The timely variation of the maximum scour depth was defined with the given equation below at Coleman et al. (2003);

$$\frac{d_s}{d_{se}} = \exp \left[ -0.07 \left( \frac{U}{U_c} \right)^{-1} \left| \ln \left( \frac{t}{t_e} \right) \right|^{1.5} \right] \quad (4.6)$$

In the same study, for  $D/L < 1$  and  $L/d_{50} > 60$ ,  $t_e$  was defined as;

$$t_e = 10^6 \left( \frac{L}{U} \right) \left( \frac{U}{U_c} \right)^3 \left( \frac{D}{L} \right) \left\{ 3 - \left[ 1.2 \left( \frac{D}{L} \right) \right] \right\} \quad (4.7)$$

For  $D/L \geq 1$  and  $L/d_{50} > 60$ ,  $t_e$  was defined as;

$$t_e = 1.8 * 10^6 \left( \frac{L}{U} \right) \left( \frac{U}{U_c} \right)^3 \quad (4.8)$$

Equations (4.7) and (4.8) were used to model the timely variation of the present study for  $\beta = 0.452$  and  $\beta = 0.119$ , respectively.

Table 4.3 Parameters used in modeling the problem with Coleman et al. (2003)

	$\beta = 0.119$	$\beta = 0.452$
$K_{yl}$	0.178	0.428
$K_I$	0.9	0.9
$K_d$	1	1
$K_s$	0.7	0.7
$K_\theta$	1	1
$K_G$	1	1

The model offered by Oliveto and Hager (2005) is the developed one of the model offered by Oliveto and Hager (2002). In Oliveto and Hager (2002), a model was constructed after the experiments conducted for six different sediment types. Three of them were uniformly distributed with mean particle diameters  $d_{50} = 0.55$  mm, 3.3 mm and 4.8 mm. The other three samples were non-uniform samples with geometric standard deviation of particle size distributions,  $\sigma_g = 1.43, 1.80$  and  $2.15$  and  $d_{50} = 5.3$  mm, 1.2 mm and 3.1 mm, respectively. They used six different abutment lengths in the experiments from  $L = 0.05$  m to  $L = 0.60$  m in two laboratory channels of width  $W = 0.50$  m and  $W = 1.00$  m. The below given equation was derived to define the temporal development of the maximum scour depth around abutments;

$$d_s = 0.068 * N * \sigma_g^{-0.5} * F_d^{1.5} \log(T) \quad (4.9)$$

where  $F_d$  is the densimetric particle Froude number,  $T$  is the dimensionless time parameter and equals to  $(t/L_R) * (\Delta g d_{50})^{0.5}$ , where  $t$  is the scour duration given in seconds,  $L_R$  is the characteristic length and equals to  $L^{2/3} D^{1/3}$ ,  $g$  is the gravitational acceleration and  $\Delta$  is the relative density of sediment,  $N$  is defined as the shape factor and assigned to  $N=1$  for sloping abutments with angles between 30 and 60 degrees in Oliveto and Hager (2005).

As the method offered by Yanmaz and Kose (2007) was developed for the vertical wall abutments only, the comparison with this model with the results of the current experiments could not be achieved.

Figures 4.54 and 4.55 show the comparisons of data presented in Figures 4.52 and 4.53, respectively, with the results of the models given by Coleman et al. (2003) and Oliveto and Hager (2005). It should be noted that, the limitations of the two models developed by these studies has limitations but none of them can prevent the application of these models to the present experimental data analysis. Also, the experiments conducted at Oliveto and Hager (2005)'s study has some large contraction ratios which may create contraction scour. Besides, Coleman et al. (2003)'s experimental data has relatively less contraction ratios.

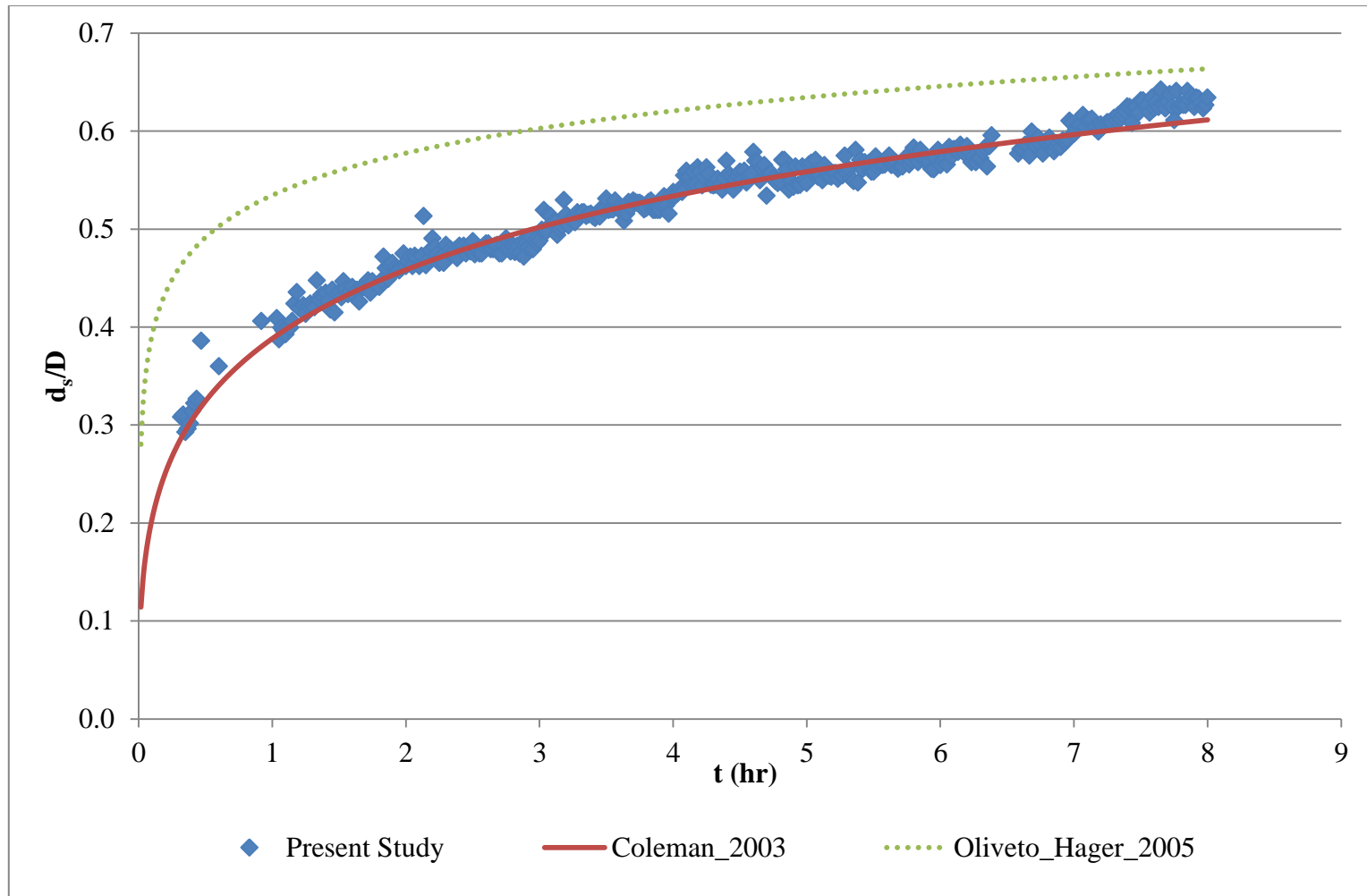


Figure 4.54 Comparison of experimental findings with the past studies for  $\beta = 0.119$

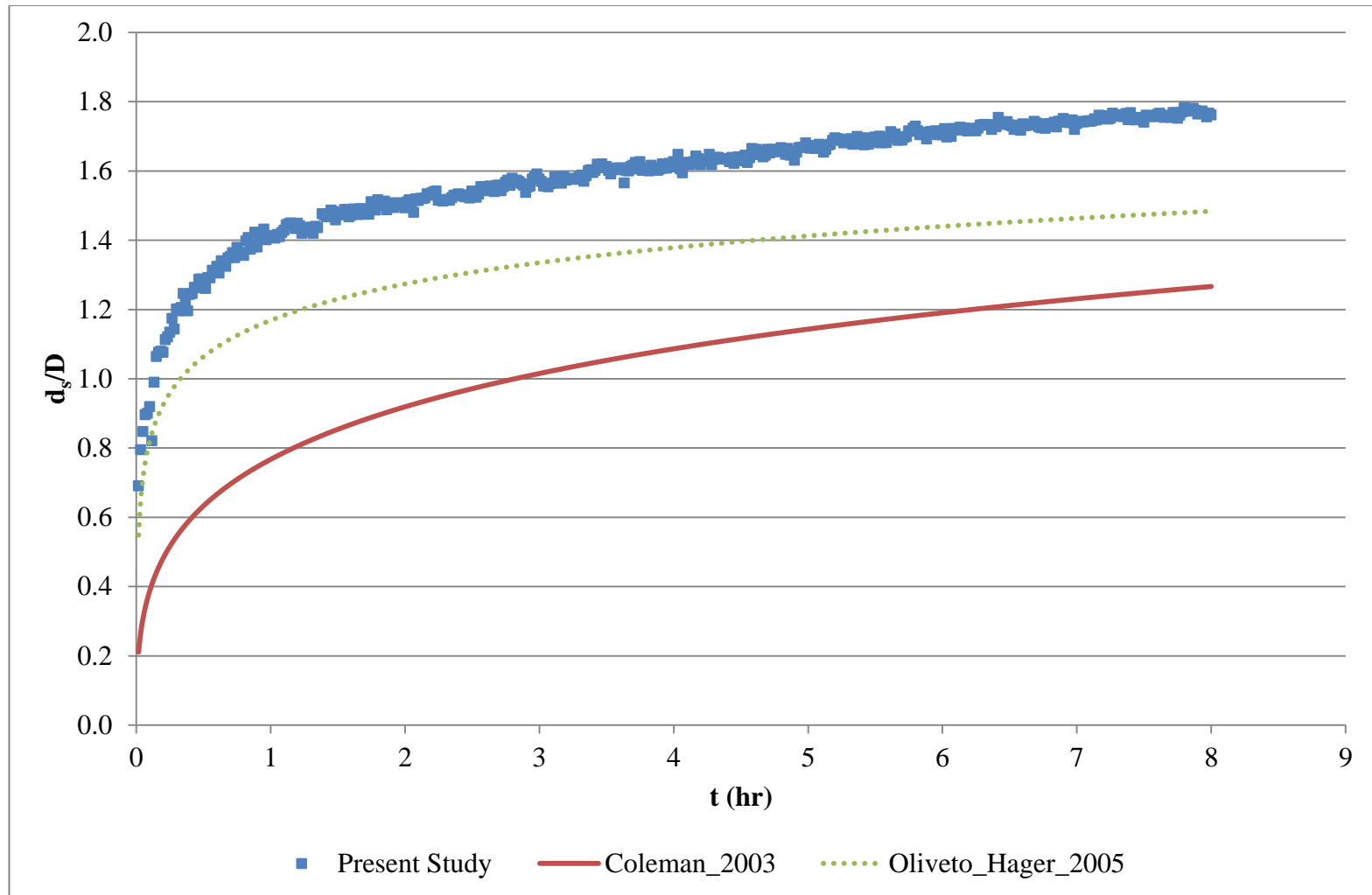


Figure 4.55 Comparison of experimental findings with the past studies for  $\beta=0.452$

As can be seen from Figure 4.54, with the help of calibration study of  $K_s$ , results of the model offered by Coleman et al. (2003) fit almost perfectly with the experiment data for the case of small contraction ratio. Besides, the model offered by Oliveto and Hager (2005) slightly overestimates the results.

As can be seen from Figure 4.55, both methods underestimate the results within the entire test duration. As can be remembered from Section 3.3.2.2 of Chapter 3, a similar result was obtained for the data of large contraction ratio, because the two mentioned models were developed for local scour only.

The scour depth values obtained from bathymetry measurements for various test durations were compared with the model offered by Coleman et al. (2003). The reason of selecting the model offered by Coleman et al. (2003) is its nearly perfect agreement with the experimental data for the small contraction ratio and the similar behavior of the result of it for the large contraction ratio. Figures 4.56 to 4.58 were developed for this purpose and show the comparison of the model offered by Coleman et al. (2003) and the data obtained in the present study in terms of scour depth values for various experiment durations.

It can be seen from Figures 4.56 to 4.58 that, the results of the model start to underestimate the experimental data for  $\beta > 0.2$ . Hence, it can be stated that, unlike the result obtained from Chapter 3 ( $\beta = 0.15$ ) the effect of flume contraction on the local scour is observable over  $\beta = 0.2$  for this experimental set. Thus, it should be stated that, further experimental studies should be conducted in future to analyze the limit of flume contraction value over which the effect of contraction is observed on local scour around abutments.

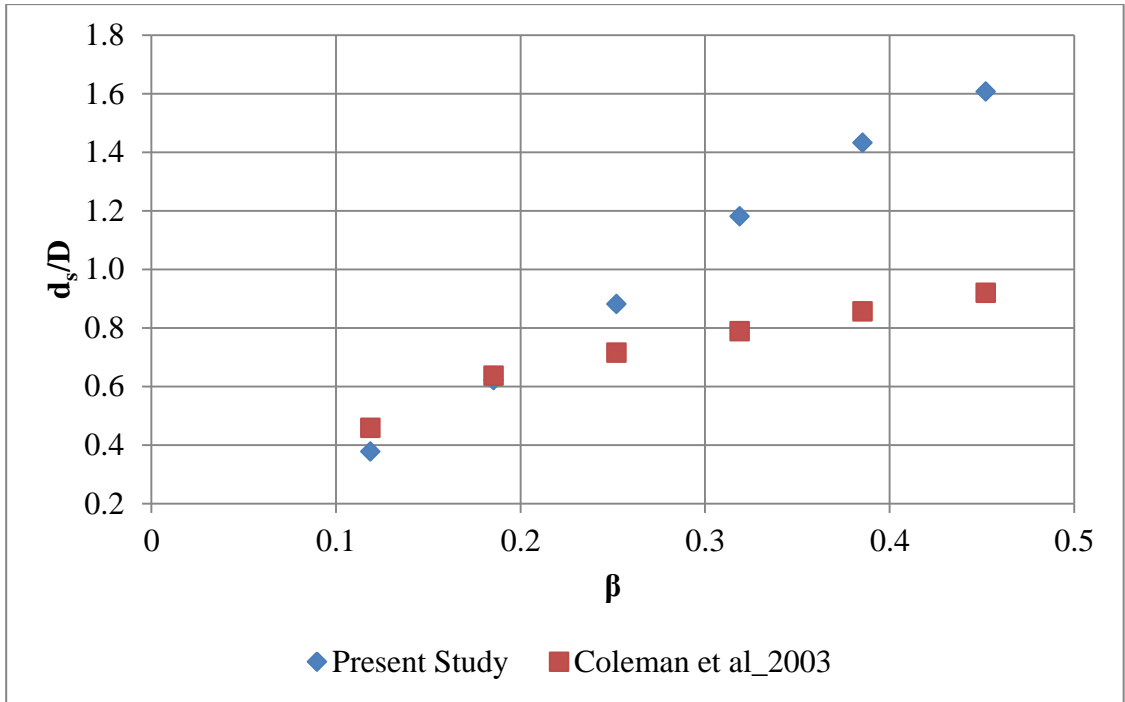


Figure 4.56 Comparison of bathymetry data with Coleman et al. (2003) for  $t=2$  hours

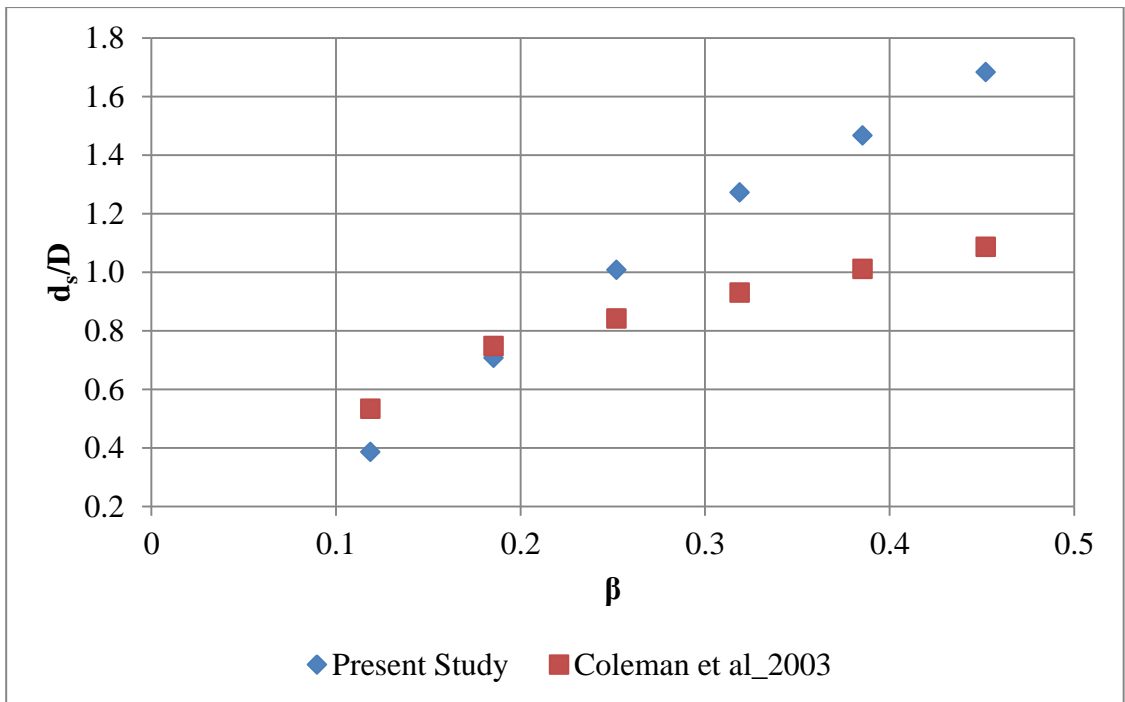


Figure 4.57 Comparison of bathymetry data with Coleman et al. (2003) for  $t=4$  hours

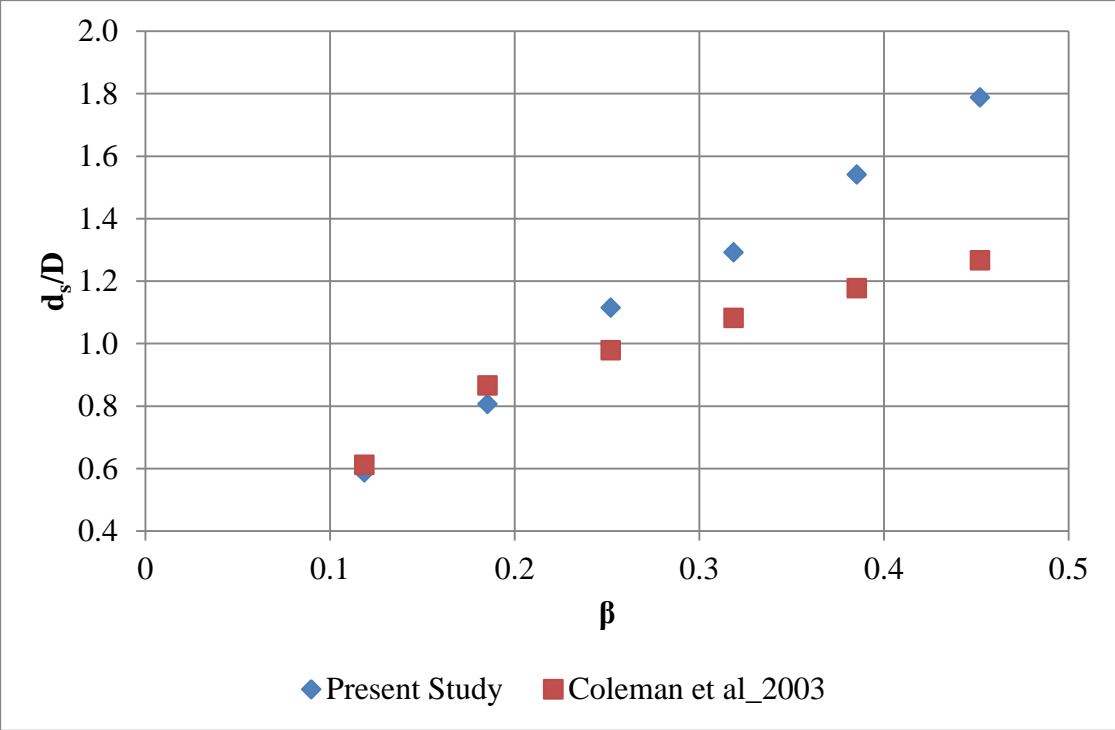


Figure 4.58 Comparison of bathymetry data with Coleman et al. (2003) for  $t= 8$  hours

## CHAPTER 5

### MEASUREMENT OF VELOCITY FIELD AROUND BRIDGE ABUTMENTS

The velocity field measurements on horizontal planes around abutments were taken by using Micro ADV Device. By this manner, the velocity field and the coherent structure around the abutments were identified at horizontal planes. In the experiments, two types of abutments, SCE and spill-through abutments, were used. This led to the comparison of flow characteristics with different abutment types. The experimental findings were also used in validating the numerical model tested within this study.

This chapter will be covered by two sections. First, the “Experimental Equipment and Procedure” section will explain the test conditions. Then the “Results” section will demonstrate the experimental data and the analyses of them.

#### 5.1 Experimental Equipment and Procedure

The velocity field experiments were conducted at the non-erodible portion of the flume discussed in Chapter 3 for the flat bed conditions. The flow conditions were kept same as discussed in Chapter 3. The measurements were taken on two horizontal planes parallel to the flume bed (Figure 5.1) with Micro ADV Device (Figure 5.2). The first plane was chosen at a depth  $D_1 = 0.1D$  above the bed, to observe the flow structures near the flume bed. These are effective in scour process. The second plane was chosen at the mid-depth of the flow ( $D_2 = 0.5D$  above the bed) to observe the average quantities of the flow. The region of recorded measurements covers a region between approximately three times of the abutment length in the upstream direction from the abutment axis to an approximately 12 times of the abutment length in the downstream direction.

The experiments were conducted by using SCE abutments and spill-through abutments, separately. A picture of SCE abutment placed at the non-erodible part of the flume is given in Figures 5.3.

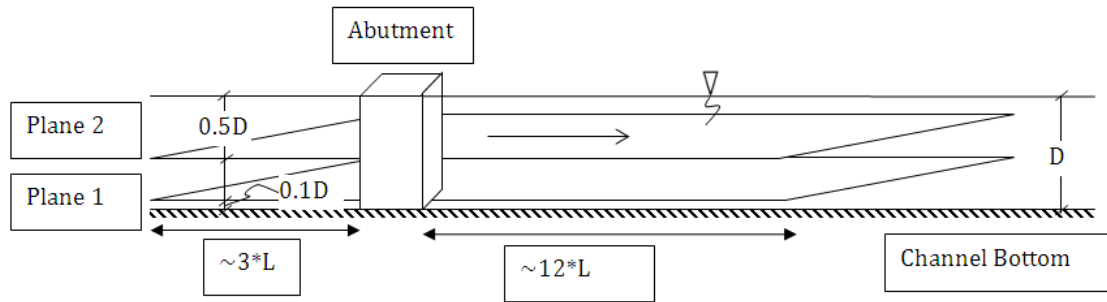


Figure 5.1 Horizontal velocity data measurement planes around abutment



Figure 5.2 SonTek Micro ADV device



Figure 5.3 Picture of a SCE abutment model at the non-erodible part of the flume

The experiments for the SCE abutments were conducted for three abutment lengths with  $L = 15, 25$  and  $35$  cm to see the abutment length effect in the flow field. In each measurement plane used for SCE abutments included 600 to 2400 recording points and the distribution of the points were refined close to the abutment to increase the resolution. The data at each point were recorded with an average duration of 30 to 60 seconds at a 50 Hz frequency by using Micro ADV. By this manner the fluctuation parts of the velocities in three Cartesian coordinates were taken into account. These values were used in computing the Reynolds Stresses.

The last sets of the velocity field measurements were conducted with the spill-through abutment model with  $L = 8.9$  cm. Two measurement planes were used at the same depths as used for SCE abutments (Figure 5.1). Approximately 700 data points were selected for each plane and the data at each point were recorded with an average duration of 150 seconds at a 50 Hz frequency.

## 5.2 Results

After the measurements were taken, the average and fluctuation parts of the velocities in three Cartesian coordinates were obtained for each data measurement points. The data points having average correlation values less than 70% were excluded from the data set. An acceleration spike filter, which was integrated in the processing software, was used to eliminate unrealistic velocity measurements. Then, by using the mean velocities on each data point, velocity contours on three directions and streamlines of the flow were obtained for each plane separately. Also, by using the fluctuation values of the velocities, turbulent kinetic energy (*tke*) values were gathered and the contours showing the variation of dimensionless *tke* were obtained. For each plane, velocity contours, streamlines and dimensionless *tke* contours of the flow were drawn. The dimensionless *tke* contours and the streamlines were shown together to highlight the *tke* increase in flow separation zones. Figures from 5.4 to 5.9 shows the outputs obtained from the experiments conducted by using SCE abutment and the Figures 5.10 and 5.11 give the results obtained from the experiments conducted by using spill-through abutment. It should be noted that, the Micro ADV device could not measure the regions that are closer than 4 cm to the vertical walls due to practical reasons. Therefore, in these

figures, those regions near the flume wall were colored manually to white to avoid any confusion. Besides, for the measurements using SCE abutment, as the abutment has vertical walls, the same problem aroused for the region 4 cm near abutment. These regions were not hidden, but it should be noted that the contour values on the regions close to SCE abutment are the interpolated values between the closest measured data and the data defined for the abutment face, which is “0” for all values. This type of problem was not been faced during the measurement for spill-through abutments due to the sloping faces of the abutments. The discussion of results will be done in the following part of this section.

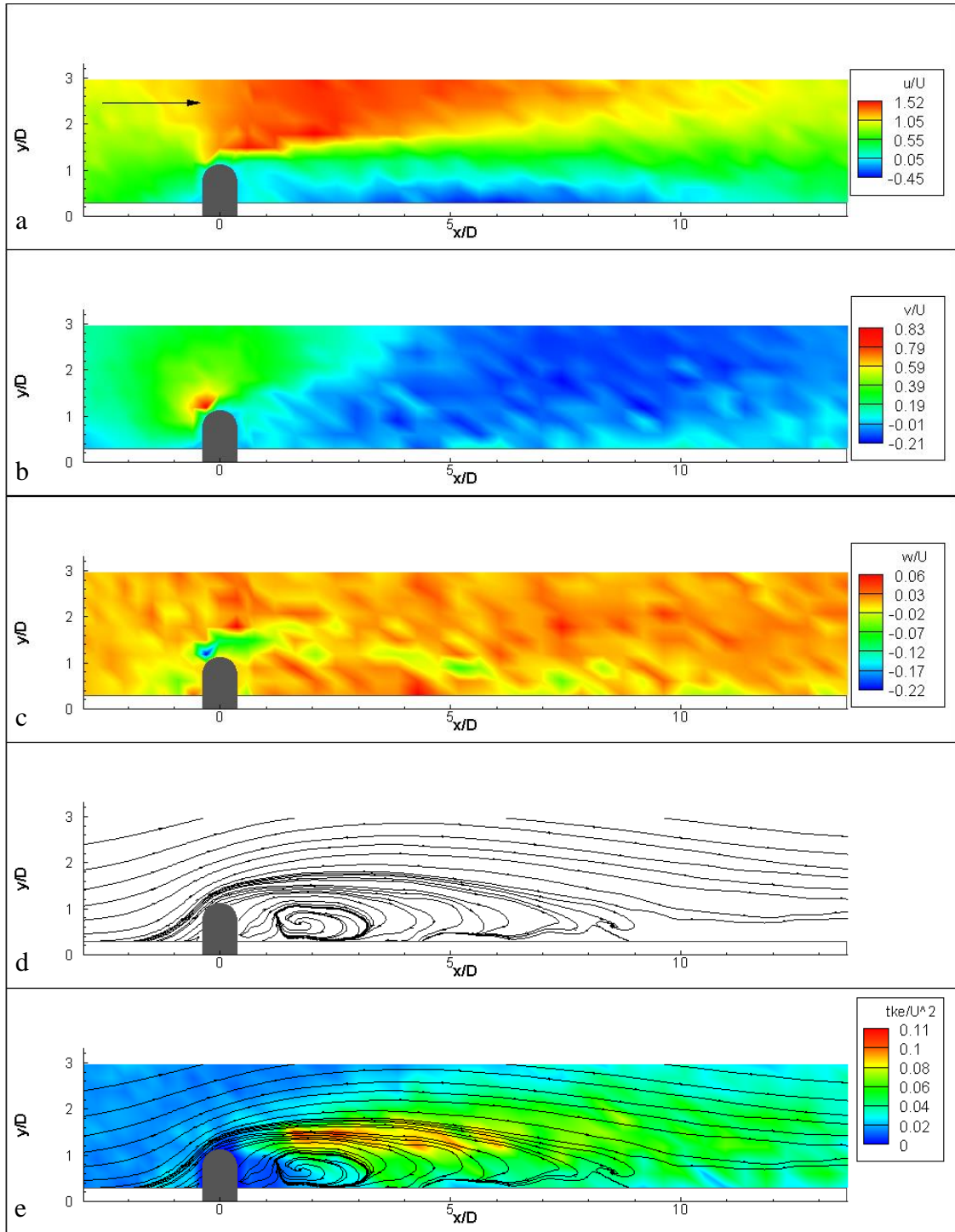


Figure 5.4 SCE abutment with abutment length,  $L=15$  cm, and at flow depth,  $D_1=0.1D$ :  
 (a) Streamwise velocity contours (b) Lateral velocity contours (c) Velocity contours in gravity direction (d) Streamlines of the flow (e)  $tke$  contours with streamlines

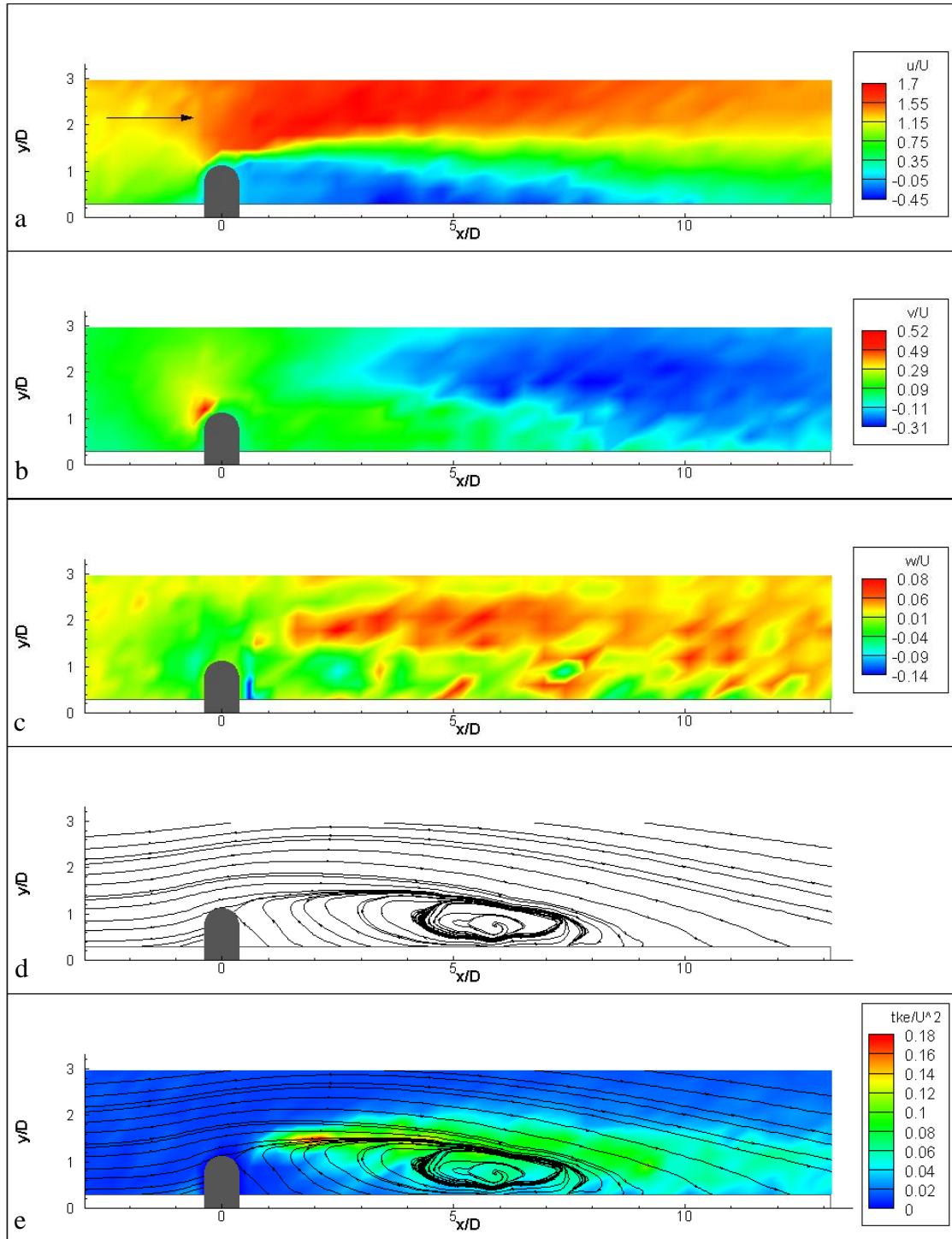


Figure 5.5 SCE abutment with abutment length,  $L=15$  cm, and at flow depth,  $D_2=0.5D$ :  
 (a) Streamwise velocity contours (b) Lateral velocity contours (c) Velocity contours in gravity direction (d) Streamlines of the flow (e)  $tke$  contours with streamlines

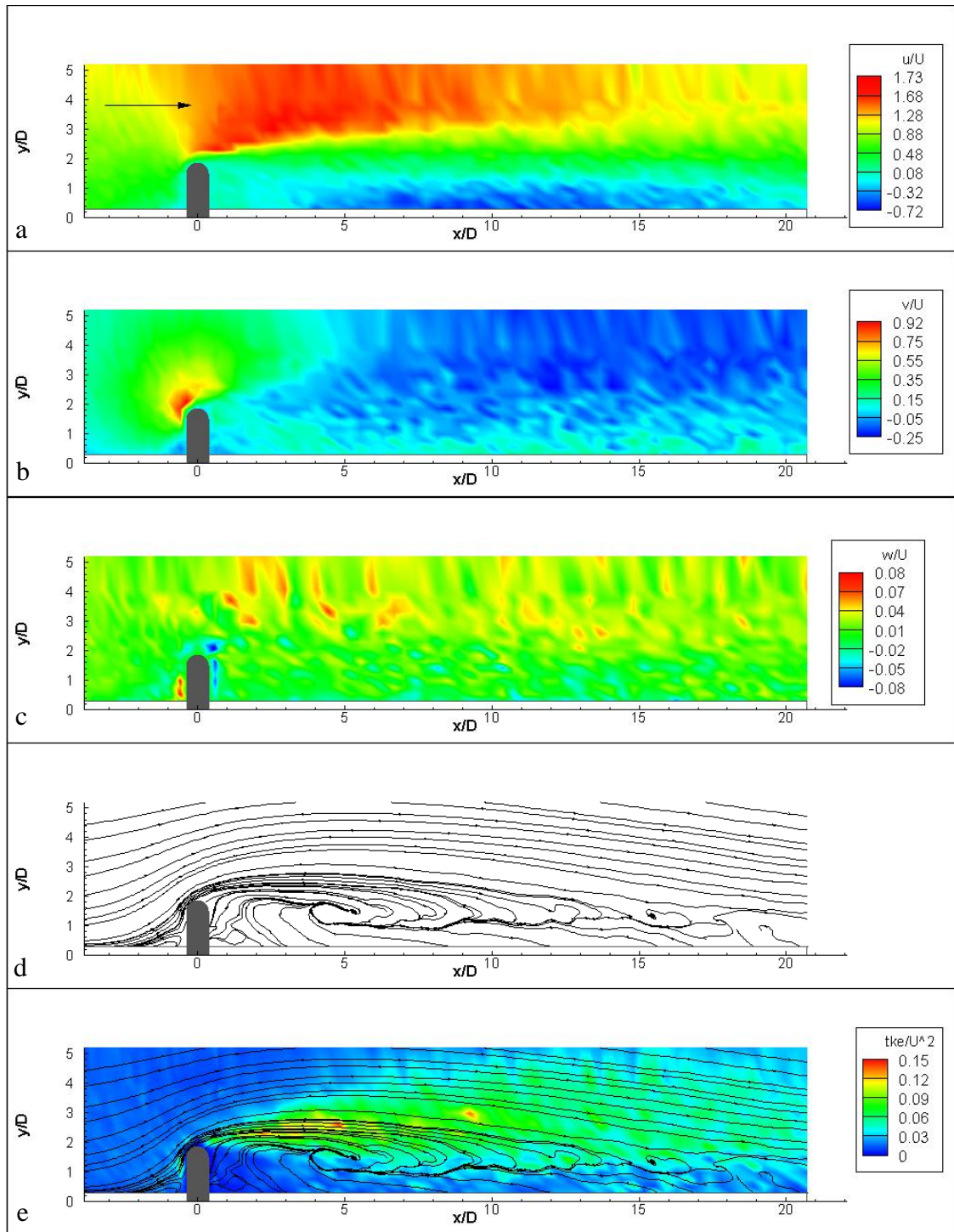


Figure 5.6 SCE abutment with abutment length,  $L=25$  cm, and at flow depth,  $D_1=0.1D$ :  
 (a) Streamwise velocity contours (b) Lateral velocity contours (c) Velocity contours in gravity direction (d) Streamlines of the flow (e)  $tke$  contours with streamlines

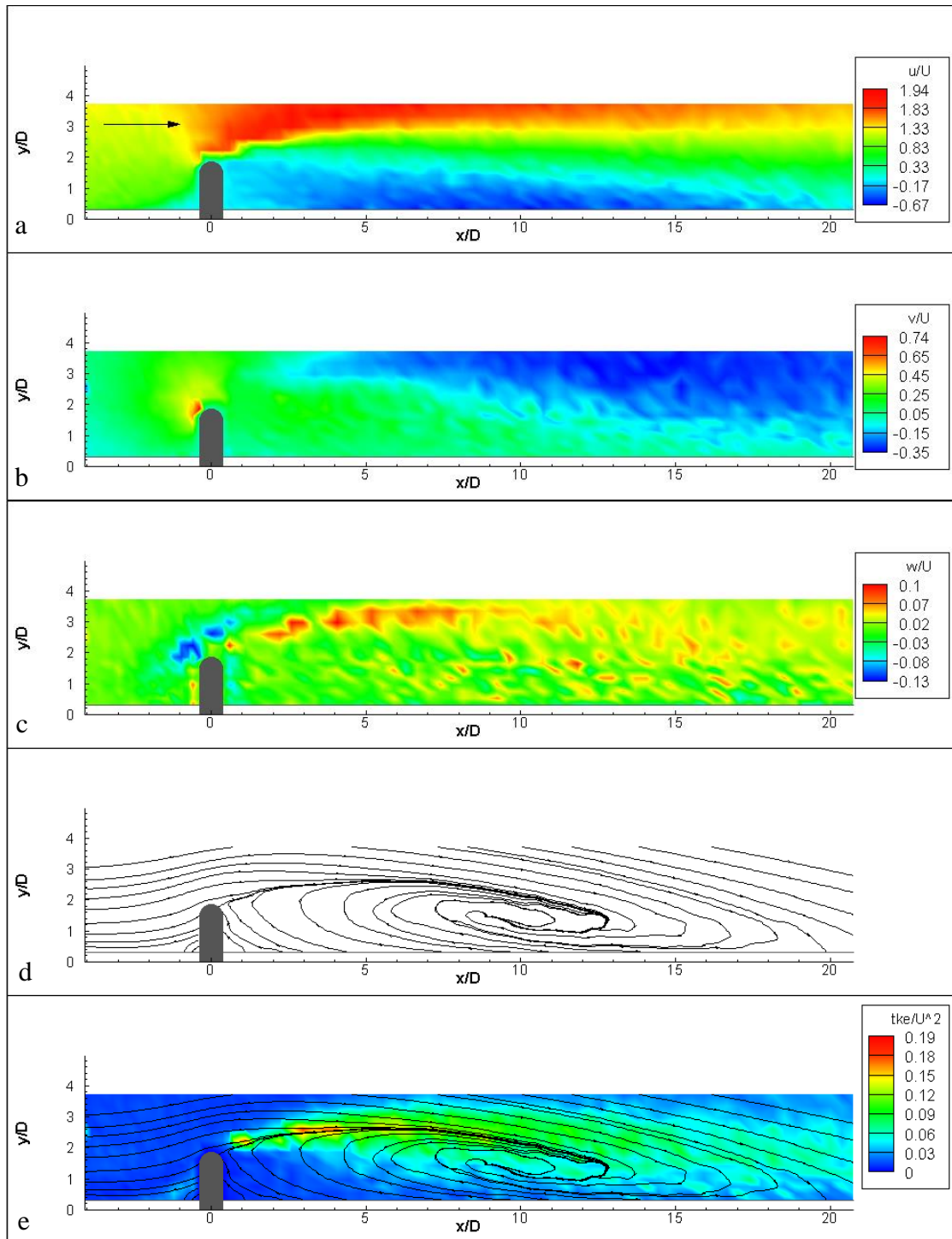


Figure 5.7 SCE abutment with abutment length,  $L=25$  cm, and at flow depth,  $D_2=0.5D$ :  
 (a) Streamwise velocity contours (b) Lateral velocity contours (c) Velocity contours in gravity direction (d) Streamlines of the flow (e)  $tke$  contours with streamlines

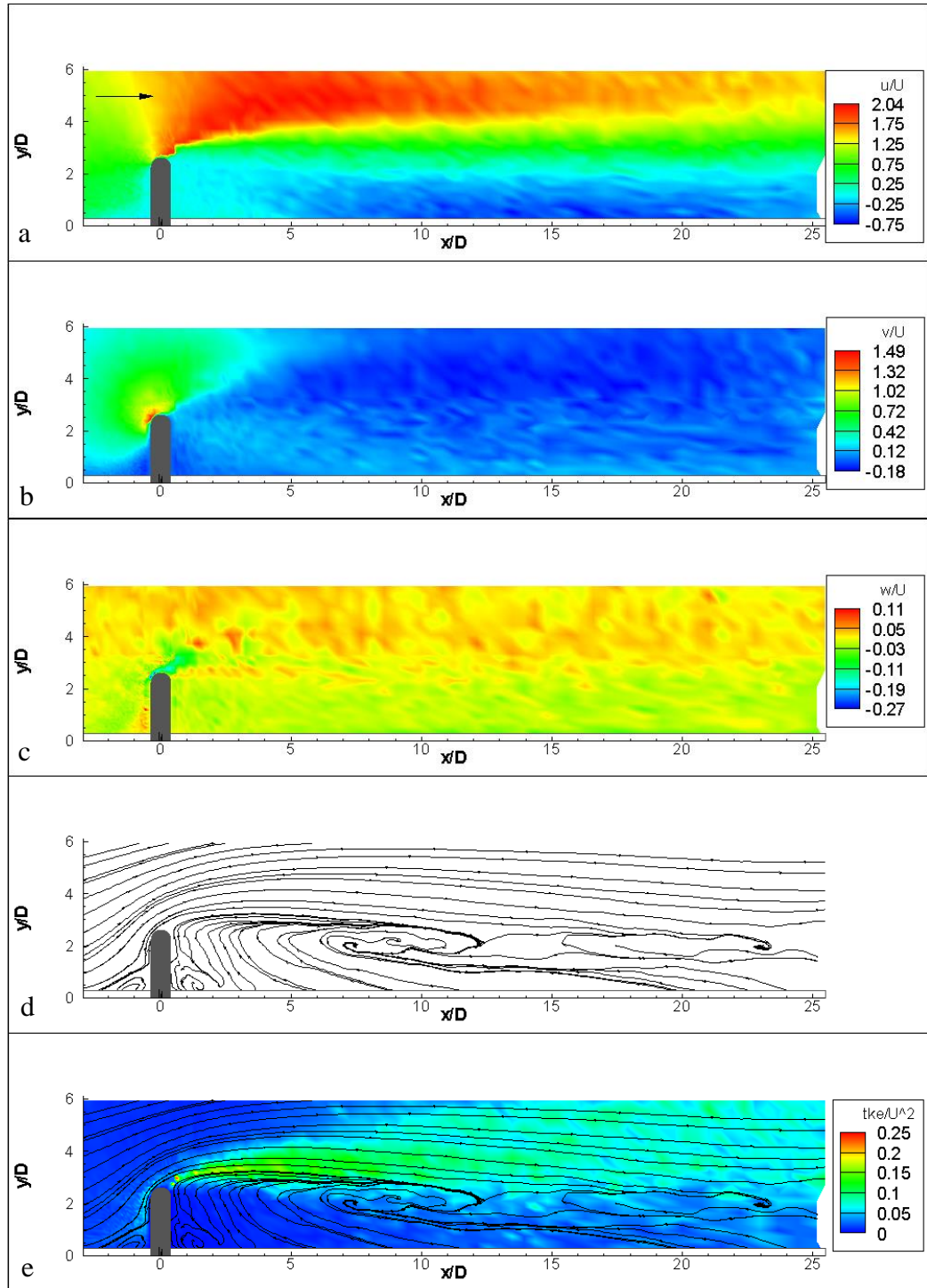


Figure 5.8 SCE abutment with abutment length,  $L=35$  cm, and at flow depth,  $D_1=0.1D$ :  
 (a) Streamwise velocity contours (b) Lateral velocity contours (c) Velocity contours in gravity direction (d) Streamlines of the flow (e)  $tke$  contours with streamlines

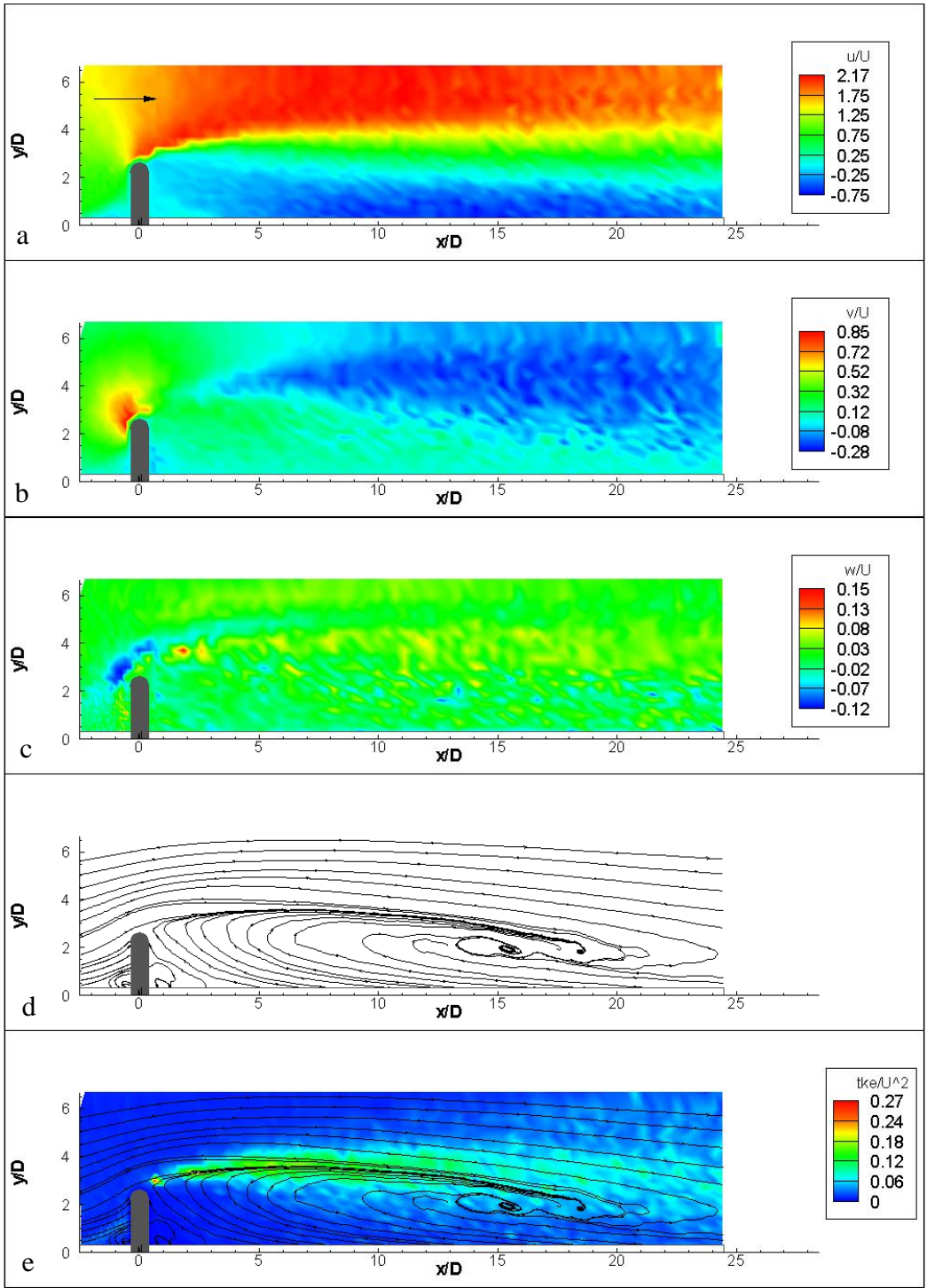


Figure 5.9 SCE abutment with abutment length,  $L=35$  cm, and at flow depth,  $D_2=0.5D$ :  
 (a) Streamwise velocity contours (b) Lateral velocity contours (c) Velocity contours in gravity direction (d) Streamlines of the flow (e)  $tke$  contours with streamlines

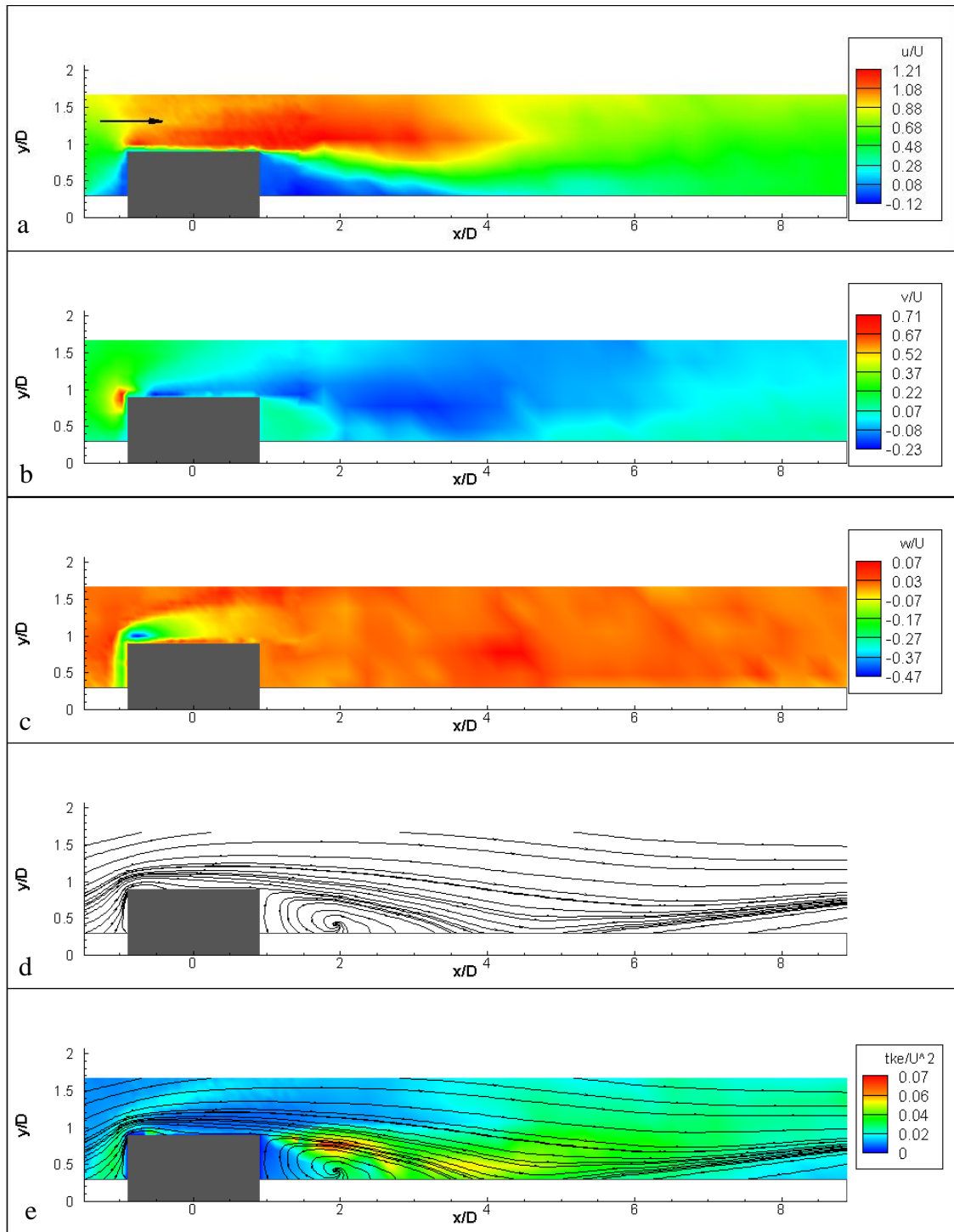


Figure 5.10 Spill-through abutment with abutment length,  $L=8.9$  cm, and at flow depth,  $D_1 = 0.1D$ : (a) Streamwise velocity contours (b) Lateral velocity contours (c) Velocity contours in gravity direction (d) Streamlines of the flow (e)  $tke$  contours with streamlines

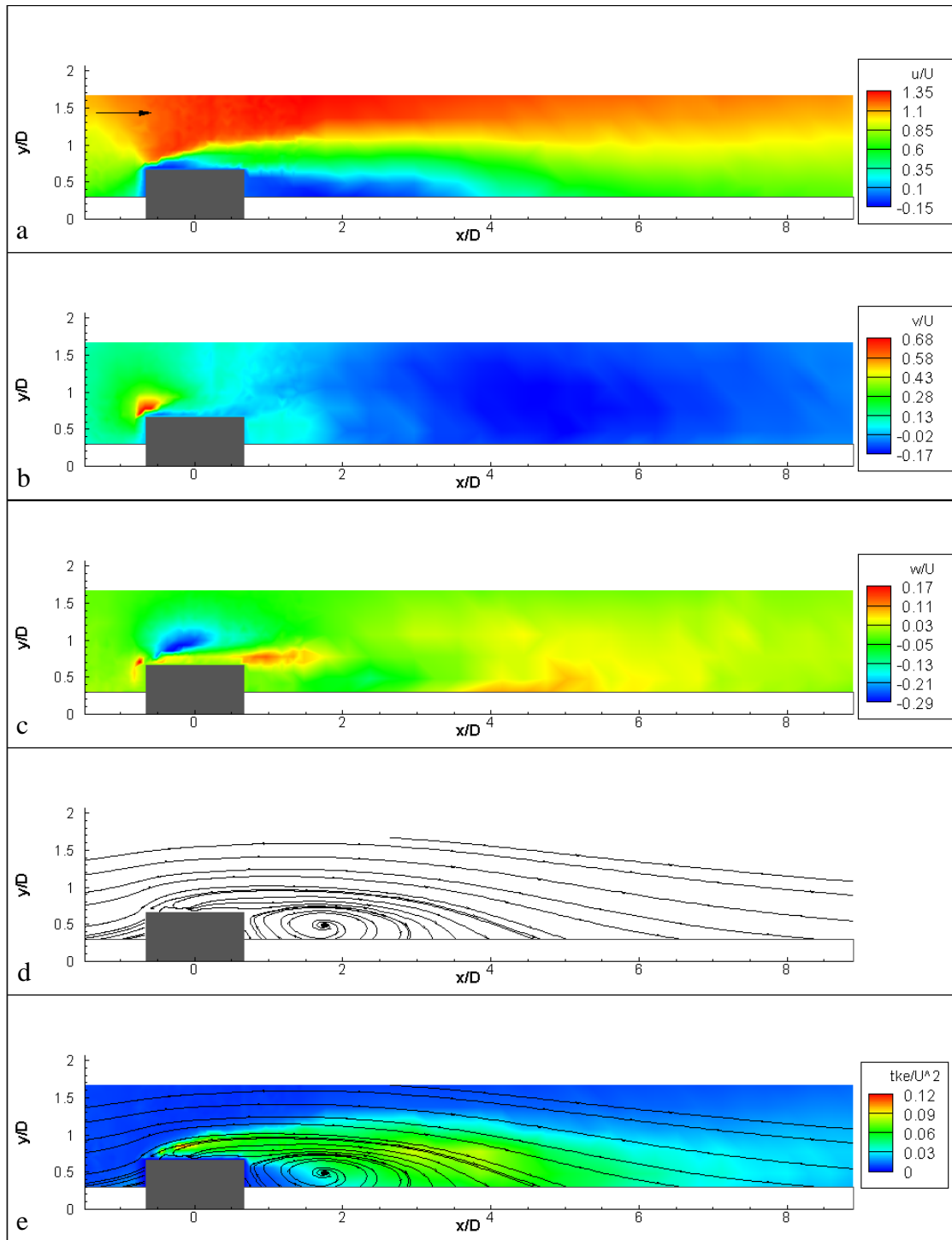


Figure 5.11 Spill-through abutment with abutment length,  $L=8.9$  cm, and at flow depth,  $D_2 = 0.5D$ : (a) Streamwise velocity contours (b) Lateral velocity contours (c) Velocity contours in gravity direction (d) Streamlines of the flow (e)  $tke$  contours with streamlines

### 5.2.1 Discussion of Results

In Figures 5.4 to 5.11, the (a), (b) and (c) frames demonstrates the velocity contours in x, y and z directions, respectively. The velocity values are non-dimensionalized with the mean approach channel velocity ( $U= 0.335$  m/s). As can be seen from (a) frames, the flow accelerates close to the abutment tip due to section contraction. It can be seen that, as expected, the x-component of the velocity is higher in mid-depth of the flow compared with the depth close to the bed. It increases to 1.7 times of the approach flow velocity for the shortest abutment length of the SCE abutment ( $\beta= 0.100$ ). As the abutment length increases, the contraction ratio of the section increases and the flow accelerates more. Then, the ratio of the accelerated velocity to the approach flow velocity increases to 1.94 and 2.17 for contraction ratios,  $\beta= 0.167$  and 0.233, respectively. It should be noted that, due to the previously stated constraint in the measurements, these values do not contain the regions corresponding to the 4 cm zone near the abutment vertical wall. It can be seen from Figure 5.11 that, the maximum increase of the velocity around the spill-through abutments equals to the 1.35 times the approach flow velocity. It should be noted that, unlike the scour experiments for spill-through abutments, the experiments discussed here were conducted by placing only one abutment model in the contracted section. Hence a quite small contraction ratio ( $\beta= 0.059$ ) was obtained for this case. The difference of the contraction ratios would be the reason of the difference in maximum velocity value at the contracted section, along with the abutment type. It should be noted that, the spill-through abutments cause less scour than the SCE abutments for the same contraction ratio.

As can be seen from (b) frames of Figures 5.4 to 5.11, the dimensionless lateral velocity component directs through flume axis and increases at the upstream face of the abutment as the flow faces with the obstruction. While the lateral velocity gives higher values at the depth closer to the flume bed for SCE abutments, the values at the deeper depth and the mid-depth are close around spill-through abutment. It should also be noted that, while the contraction ratio increases, the lateral velocity increases for the SCE abutment. It is around 1.5 times of the approach flow velocity for the largest contraction value and at the depth closer to the flume bed.

The (c) frames of Figures 5.4 to 5.11 shows the contours for the dimensionless velocity component in z-direction. These figures should have been related to the downflow at the upstream face of the abutment; however, due to the previously stated constraint in the measurements, the figures for SCE abutments do not include the downflow components. It can be seen from the maximum values of the  $w/U$  values in gravity direction, the figures correspond to the spill-through abutments give higher values than the figures of SCE abutments. Besides, the location of the primary vortex can be identified after observing the rapid increase and decreases in  $w/U$  starting from just upstream of the abutment and continuing towards downstream.

By examining the (d) frames of Figures 5.4 to 5.11, which show the streamlines of the flow, recirculation regions can clearly be identified at each plane. While, the downstream recirculation regions can be identified from all figures, the upstream recirculation regions could not be identified in some figures. The reason is the lack of data points close to the wall, as it is known that upstream recirculation region occurs near the flume wall and abutment wall in relatively small area compared with the downstream recirculation region. However, in Figures 5.6, 5.8 and 5.9 the upstream recirculation region was partially captured for the SCE abutments. Those figures correspond to the abutment lengths of  $L= 25$  cm and 35 cm. As the abutment length increases the area of the recirculation regions increase. Hence, the upstream recirculation region becomes observable for the longest two abutments while it grows up to a value bigger than the area covered by the 4-cm blind zone. The downstream recirculation region was totally captured for the abutment with  $L = 15$  cm only as for the longer abutment lengths, the downstream recirculation region is elongated and exceeded the test region.

In Table 5.1, the values of the parameters obtained from the experimental measurements are given. In the Table, the lateral length of the downstream recirculation region ( $L_1/D$ ), the longitudinal length of the downstream recirculation region ( $L_2/D$ ) and the distance of the core of the downstream recirculation region to the abutment axis ( $L_c/D$ ) are given in non-dimensional terms. These parameters are demonstrated schematically in Figure 5.12.

Table 5.1 Parameters related to the downstream recirculation region

Abutment Type	L/D	Plane	L <sub>1</sub> /D	L <sub>2</sub> /D	L <sub>c</sub> /D	L <sub>1</sub> /L	L <sub>2</sub> /L	L <sub>c</sub> /L
SCE	1.11	D <sub>1</sub>	1.81	8.65	1.81	1.63	7.79	1.63
SCE	1.11	D <sub>2</sub>	2.04	8.84	5.98	1.84	7.96	5.38
SCE	1.85	D <sub>1</sub>	3.09	NA*	5.43	1.67	NA*	2.93
SCE	1.85	D <sub>2</sub>	3.67	NA*	8.89	1.98	NA*	4.80
SCE	2.59	D <sub>1</sub>	4.16	NA*	7.43	1.60	NA*	2.87
SCE	2.59	D <sub>2</sub>	5.70	NA*	15.45	2.20	NA*	5.96
Sp-Th	0.66	D <sub>1</sub>	0.85	2.61	1.95	1.29	3.96	2.96
Sp-Th	0.66	D <sub>2</sub>	0.88	2.86	1.77	1.33	4.34	2.69

\*: The length could not be measured as the downstream recirculation region elongated and exceeded the area of measurement.

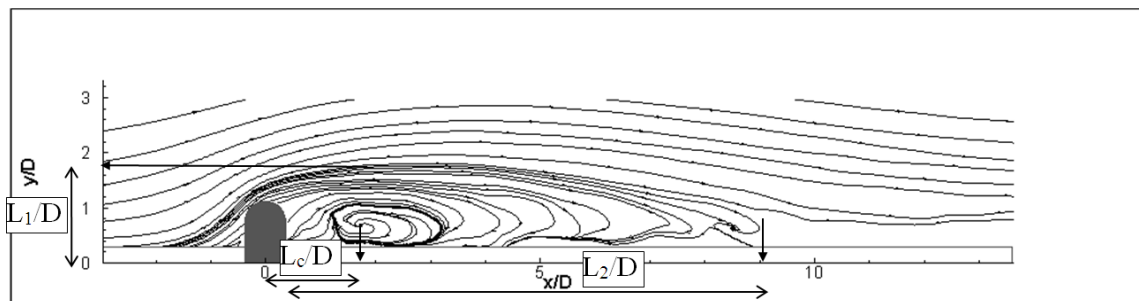


Figure 5.12 Demonstration of parameters regarding the downstream recirculation region

It can easily be seen from Figures 5.4 (d) to 5.9 (d) that; for all abutment lengths, from depth  $D_1$  to depth  $D_2$ , the core of the recirculation region shifts downstream significantly for the SCE abutment. On the contrary, for the spill-through abutments, the core of the downstream recirculation zone shifts slightly upstream from depth  $D_1$  to depth  $D_2$  (Figures 5.10 (d) and 5.11 (d)).

For SCE abutment, the length of the downstream recirculation region in the transverse direction ( $L_1$ ) increases slightly from depth  $D_1$  to depth  $D_2$ . It increases from  $1.81D$  to  $2.04D$  for abutment length  $L = 15$  cm, from  $3.09D$  to  $3.67D$  for abutment length  $L = 25$  cm and from  $4.16D$  to  $5.70D$  for abutment length  $L = 35$  cm. However, the

corresponding length does not change significantly with depth for the spill-through abutment.

The length of the downstream recirculation region in the longitudinal direction ( $L_2$ ) could only be measured for the shortest SCE and the spill-through abutments. For SCE abutment, this length increases from  $8.65D$  to  $8.84D$  from depth  $D_1$  to depth  $D_2$ ; whereas, for spill-through abutment, the length increases from  $2.61D$  to  $2.86D$  from depth  $D_1$  to depth  $D_2$ .

It can be seen from Figures 5.4 to 5.11 that,  $tke$  increases in the regions where coherent structures have influence. By considering frame (e) of all figures, the  $tke$  increase at the downstream of the abutment can be observed, which correspond to the detached shear layer zone. It can be certainly stated that; each horizontal measurement plane cuts through the detached shear layer zone as that zone consists of vortex tubes forming vertically. Besides, the maximum  $tke$  values at  $D_2$  depths are higher than the values at  $D_1$  depths. This might be related to the loss of coherence for the vortex tubes close to the channel bed.

On the upstream side of the abutment,  $tke$  values are larger at depths  $D_1$  which are close to the flume bed. These increases correspond to the region of primary vortex formation. It is known that the primary vortex forms around the abutments close to the flume bed; therefore, any  $tke$  amplifications due to primary vortex formation were not observed at  $D_2$  depths.  $tke$  amplifications were not observed at  $D_1$  depths of the shortest two abutment lengths of SCE abutments as well. This may be because  $D_1$  depth might not be cutting through the vortex core or the primary vortex formation fell inside the blind zone of recording. The primary vortex formation is observable for the SCE abutment with the longest abutment length and for the spill-through abutment.

### **5.2.2 Comparison of Results with the Results of Similar Studies in Literature**

In literature, there exist studies dealing with the amplifications in velocity field parameters and the limits of the recirculation areas at the existence of an abutment. The comparison of the results obtained from the present study and the past studies will be accomplished within this part.

Molinas et al. (1998) has conducted an experimental study on velocity field measurement around a vertical wall abutment. They have observed maximum velocities as  $1.18U$ ,  $1.24U$  and  $1.50U$  for contraction ratios,  $\beta= 0.1, 0.2$  and  $0.3$ , respectively, while  $U$  denotes the approach velocity. After comparing these findings with the findings of the present study, it can be stated that, in the present study, much higher velocity amplifications were observed for close contraction ratios. Also, it should be noted that, Molinas et al. (1998) measured the velocities on vertical sections at various longitudinal coordinates. Therefore, there is a great possibility that, they would have missed the location of the maximum velocity.

Kwan and Melville (1994) have measured the velocity field around a wing-wall abutment with a scour hole. They have stated the maximum downflow measured around the abutment equals to  $0.75U$  and maximum upflow measured around the abutment equals to  $0.3U$ . It should be stated that both these maximum values were recorded within the scour hole. While in the present study, flat bed experiments were conducted and maximum downflow was recorded as  $0.47U$  and maximum upflow was recorded as  $0.17U$  around spill-through abutment. It should be noted that, although the type of the abutment would lead some differences between the results of two experimental studies, existence of a scour hole makes the flow conditions very different.

Zhang and Nakagawa (2008) stated that the center of the recirculation zone locates at  $6L$  away from spur dykes, which are identical to the vertical wall abutments. In the present study, it was demonstrated that, while this distance varies with the abutment type; it is around  $6L$  for the SCE abutment and around  $3L$  for spill-through abutment.

Moreover, Koken (2005) presented that, Chen and Ikeda (1997) expressed the downstream recirculation area length as  $14L$  measured from the abutment ( $L_2$ ). In the present study, it was stated that, this length varies with abutment type. It was measured around  $8L$  for SCE abutment and  $4.5L$  for spill-through abutments for considerably small contraction ratios with  $\beta= 0.1$  and  $0.059$ , respectively. Moreover, it can be considered that, the length of the downstream recirculation zone for  $\beta= 0.167$  and  $0.233$  are greater than  $11.34L$  and  $9.6L$ , respectively, which exceeds the length of the measurement domain.



## CHAPTER 6

### NUMERICAL ANALYSES OF FLOW AND SCOURING AROUND BRIDGE ABUTMENTS

The numerical analysis of the problem of flow and scour around bridge abutments have been studied previously. Although the studies on numerical analyses of flow field around abutments have accomplished an advance, a reliable model has not been offered for the analysis of scour around abutments yet. In this study, the analysis of the flow and scouring around abutments has been accomplished by using commercially available CFD software, FLOW-3D ver. 10.1 by Flow Science Inc.

For this purpose, first the CFD simulations of the flow field around abutments on the non-erodible and flat bed were accomplished after searching for the optimum turbulence model and mesh size for the problem. Afterwards, the simulations were run for the erodible bed by taking the sediment scour around abutment into account. The details of these works will be discussed in this chapter and it will be covered by three parts as: “Overview”, “Flat Bed Simulations” and “Erodible Bed Simulations”.

#### 6.1 Overview

In this section, first, the applicable models used by FLOW-3D will be discussed. The theory behind the turbulence model solvers and scour model will be expressed in details. Afterwards, the preliminary runs accomplished within the present study before the main simulations will be presented.

##### 6.1.1 Turbulence Model Solvers

FLOW-3D has 5 turbulence models for solving turbulent flow. These are; Prandtl’s mixing length model, one-equation ( $k$ ) model, two-equation ( $k$ - $\varepsilon$ ) model, Renormalized group (RNG) model and Large Eddy Simulation (LES) model. In the present study, two

of these models were tested for turbulence modeling. RNG model was tested because it can accurately simulate turbulence flow with high shear regions (FLOW 3-D User Manual, 2013). Afterwards, LES model was tested as the flow around bridge abutments were recommended to be solved with eddy resolving methods (Koken and Constantinescu, 2008).

The RNG model is a developed model of a standard  $k-\varepsilon$  model (Yakhot and Orzsag, 1986). The model is based on Reynolds averaging. The equation constants which were derived empirically in  $k-\varepsilon$  model were derived explicitly in RNG model.

LES model bases on computing all the large scale turbulent structures within the computational grid, and modeling the smaller structures which are out of the grid resolution (Smagorinsky, 1963). In the model, the effect of turbulence on smaller structures was represented by a term called eddy viscosity, which is proportional to length scale times a measure of velocity fluctuations on that scale. It is stated in FLOW-3D User Manual (2013) that, LES model often provides more information than the models based on the Reynolds averaging.

### **6.1.2 Sediment Scour Model**

The scour solution in FLOW-3D is achieved by defining a packed sediment bed for the flume bed around the abutment and activating the scour model. In the present case, the packed sediment bed was defined as uniform sediment material with the sediment properties as defined within the thesis.

The solution methodology of the scour model offered in FLOW-3D is based on drift and lift of sediment species (Brethour and Burnham, 2010). The solution methodology is achieved by combining the equations related to the drift and lift, with the mass and the momentum conservation equations of the flow. The equations are applied to each computational cell. The drift velocity was defined physically with the given equation below;

$$u_{drift,i} = u_{s,i} - \bar{u} \quad (6.1)$$

where  $u_{drift,i}$  and  $u_{s,i}$  are the drift velocity and sediment velocity in each computational cell,  $i$  and  $\bar{u}$  is the mean bulk fluid velocity.

After subtracting the momentum equation for mean flow from the momentum equation for each sediment phase,  $i$ ; the following equation was introduced (Brethour and Burnham, 2010);

$$\frac{\partial u_{drift,i}}{\partial t} + \bar{u} \cdot \nabla u_{drift,i} = \left( \frac{1}{\bar{\rho}} - \frac{1}{\rho_{s,i}} \right) \nabla P - \frac{K_i}{f_{s,i} \rho_{s,i}} u_{r,i} \quad (6.2)$$

where  $\bar{\rho}$  and  $\rho_{s,i}$  are mean bulk density and the sediment density in the cell, respectively,  $P$  is the pressure,  $K_i$  is the drag function and  $f_{s,i}$  is the volume fraction of sediment species,  $i$ ,  $u_{r,i}$  is the relative velocity defined by;

$$u_{r,i} = u_{s,i} - u_{f,i} \quad (6.3)$$

where  $u_{f,i}$  is the velocity of the fluid in each computational cell,  $i$ . The drag function used in the methodology is defined as follows combining the form and Stokes drags;

$$K_i = \frac{3}{4} \frac{f_{s,i}}{d_{s,i}} \left( C_D \|u_{r,i}\| + 24 \frac{\mu_f}{\rho d} \right) \quad (6.4)$$

where  $C_D$  and  $d$  are drag coefficient and particle diameter of sediment, respectively; and  $\rho$  and  $\mu_f$  are the density and the dynamic viscosity of fluid, respectively.

After assuming steady flow within the computational time step and also neglecting advection term due to expecting very small drift velocity gradients in the computational cell, Equation (6.2) was simplified to the following equation;

$$u_{r,i} = \frac{\nabla P}{\bar{\rho} K_i} (\rho_{s,i} - \rho) f_{s,i} \quad (6.5)$$

After defining the mean bulk fluid velocity as follows;

$$\bar{u} = \left( 1 - \sum_{j=1}^N f_{s,j} \right) u_f + \sum_{j=1}^N f_{s,j} u_{s,j} \quad (6.6)$$

The drift velocity for each sediment species,  $i$ , is calculated with the formula below;

$$u_{drift,i} = (1 - f_{s,i}) u_{r,i} - \sum_{j=1}^N f_{s,j} u_{r,j} \quad (6.7)$$

The method solves Equations (6.4), (6.5) and (6.7) to obtain the drift velocity (Brethour and Burnham, 2010).

It is stated in Brethour and Burnham (2010) that, the drift velocity is developed by assuming the sediment particles do not interact with each other. Although, the use of this velocity in suspended flow conditions is more applicable, it is also used in the drifting of sediment particles in scour analysis within the methodology.

The other important velocity term of the scour problem is the lift velocity of sediment particles. It is computed at the interface of the packed sediment region. The following equation is used to calculate lift velocity in the methodology offered previously by Mastbergen and Von Den Berg (2003);

$$u_{lift,i} = \varphi n_s d_*^{0.3} (\theta_i - \theta_{cr,i})^{1.5} \sqrt{\frac{\|g\| d_{s,i} (\rho_{s,i} - \rho)}{\rho}} \quad (6.8)$$

where  $\varphi$  is the entrainment coefficient,  $n_s$  is the normal vector pointing outwards,  $\|g\|$  is the magnitude of the gravitational acceleration vector and  $d_*$  is the dimensionless mean particle diameter, given as follows;

$$d_* = d_{50} \left[ \frac{\rho(\rho_{s,i} - \rho) \|g\|}{\mu_f^2} \right]^{\frac{1}{3}} \quad (6.9)$$

$\theta_i$  and  $\theta_{cr,i}$  stands for the local Shields parameter at the interface and the dimensionless critical Shields parameter, respectively. The local Shields parameter is calculated as follows based on the local shear stress,  $\tau$ ;

$$\theta_i = \frac{\tau}{\|g\| d_{s,i} (\rho_{s,i} - \rho)} \quad (6.10)$$

and the dimensionless critical Shields parameter is calculated from Shields-Rouse equation and given below;

$$\theta_{cr,i} = \frac{0.1}{R_i^{*3}} + 0.054 \left[ 1 - \exp\left(\frac{-R_i^{*0.52}}{10}\right) \right] \quad (6.11)$$

the  $R_i^*$  term in the equation is defined as the Rouse Reynolds number and given by the following formula;

$$R_i^* = d_{s,i} \frac{\sqrt{0.1(\rho_{s,i}-\rho)\rho\|g\|d_{s,i}}}{\mu_f} \quad (6.12)$$

The effect of bed slope on the critical Shields parameter is inserted with the following formula;

$$\theta_{cr,i}' = \theta_{cr,i} \frac{\cos \varphi_1 \sin \varphi_2 + \sqrt{\cos^2 \varphi_2 \tan^2 \theta - \sin^2 \varphi_1 \sin^2 \varphi_2}}{\tan \theta} \quad (6.13)$$

where  $\varphi_1$  is the angle between flow and the upslope direction,  $\varphi_2$  is the angle between the computed normal vector of the packed sediment interface and the gravitational vector,  $g$ , and  $\theta$  is the angle of repose of the sediment material.

Along with the drift and lift velocities of the sediment particles, the model also uses the bed load transport equations. It uses Meyer-Peter and Muller formula for bed load transportation. According to this formula, the following equation was used to calculate volumetric bed load transport rate per unit width;

$$q_{i,b} = \omega_i (\theta_i - \theta_{cr,i}')^{1.5} \left[ \|g\| \left( \frac{\rho_{s,i}-\rho}{\rho} \right) d_{s,i}^3 \right]^{0.5} \quad (6.14)$$

where  $\omega_i$  is the bed load coefficient remained as input in the scour model.

### 6.1.3 Preliminary Runs

Before conducting the simulations on flat bed and erodible bed, a simulation on flat bed was run on a periodic channel (infinitely long channel) without placing an abutment model, to obtain the fully developed flow to be used as the inlet for the main simulations. In order to accomplish this simulation, a flume model was developed using two solid components for flume walls and one solid component for flume bed with the same roughness as the laboratory flume, where the experiments were conducted. The domain was selected as 6.2 m long in x-direction. The laboratory flume geometry was kept the same on the model having 1.5 m width and 0.2 m depth. The depth of the flume was selected slightly larger than the flow depth to allow undulations on the free surface.

Figure 6.1 shows the boundary conditions (BC) defined for the simulation. At the inlet and the outlet, periodic BC was selected. This BC works by transferring the output of the domain to the input. Selection of the periodic BC helps to converge to the fully developed flow. Figure 6.2 shows the mesh, developed for the periodic flow simulations. FLOW 3-D allows only usage of structured. The mesh was refined in y- and z-directions near the flume walls, while the first grid point was situated at approximately 67 non-dimensional wall units ( $y^+$ ) from the solid surface. The mesh includes 100000 real cells and a simulation with 300 seconds of simulation time took about 42 minutes to be completed in a 4-processor computer.

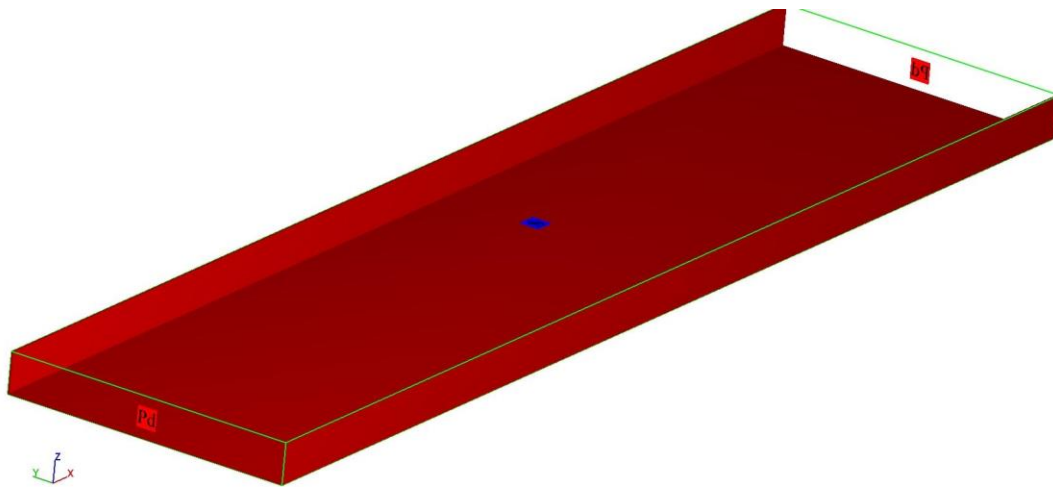


Figure 6.1 Boundary conditions defined for the preliminary simulation

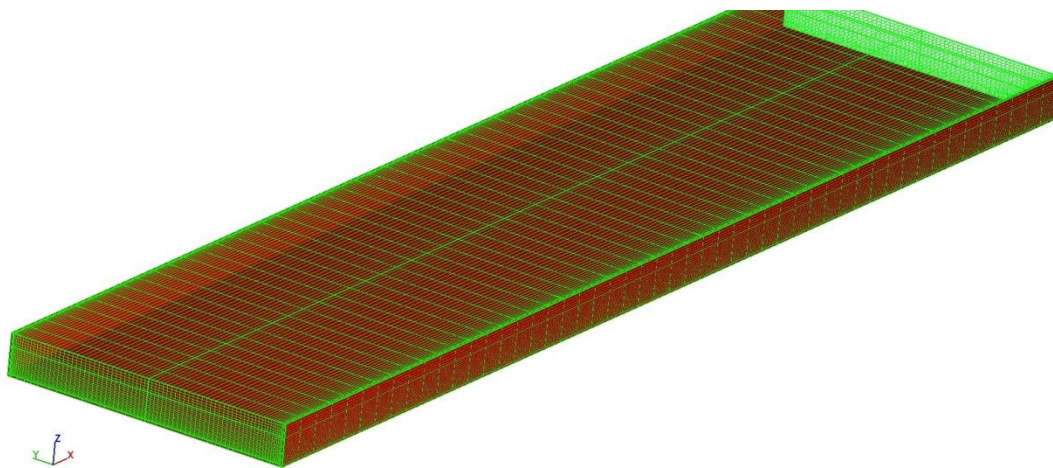


Figure 6.2 A view of the mesh constructed for the preliminary simulation

For this simulation only two models of the FLOW-3D were activated (Figure 6.3). The “Gravity and non-inertial reference frame” model was activated to define the gravity and the slope of the channel in terms of gravity components in x- and z-directions. The “Viscosity and turbulence” model was activated to select the solver among the laminar and one of the turbulence solvers. In this simulation, RNG model was selected. The velocity distribution in vertical direction obtained from the results of the simulation was compared with the logarithmic vertical wall velocity distribution assumption in Figure 6.4, which is formulated below (Schlichting, 1987; Keulegan, 1938);

$$\frac{u_2 - u_1}{u_*} = 5.75 \log \left( \frac{z_2}{z_1} \right) \quad (6.15)$$

where  $u_2$  and  $u_1$  are the velocity values at vertical positions  $z_2$  and  $z_1$ , respectively, and  $u_*$  is the bed shear velocity.

For the present problem, the bed shear velocity in the approach channel was calculated and given in Appendix B. The logarithmic distribution was obtained for the mean unit discharge value. The distributions from the simulation were obtained at the outlet section for the last time step which would be the inlet of the main simulations. The distributions were taken at two y-coordinates; one at the middle of the channel width ( $y = 0.75$  m) which results with the highest velocity values in a given y-z plane and one closer to the wall ( $y = 0.30$  m). It can be seen from the comparison figure that, the results show a reasonable agreement, and the simulation outputs can be used as inlet of the main simulations.

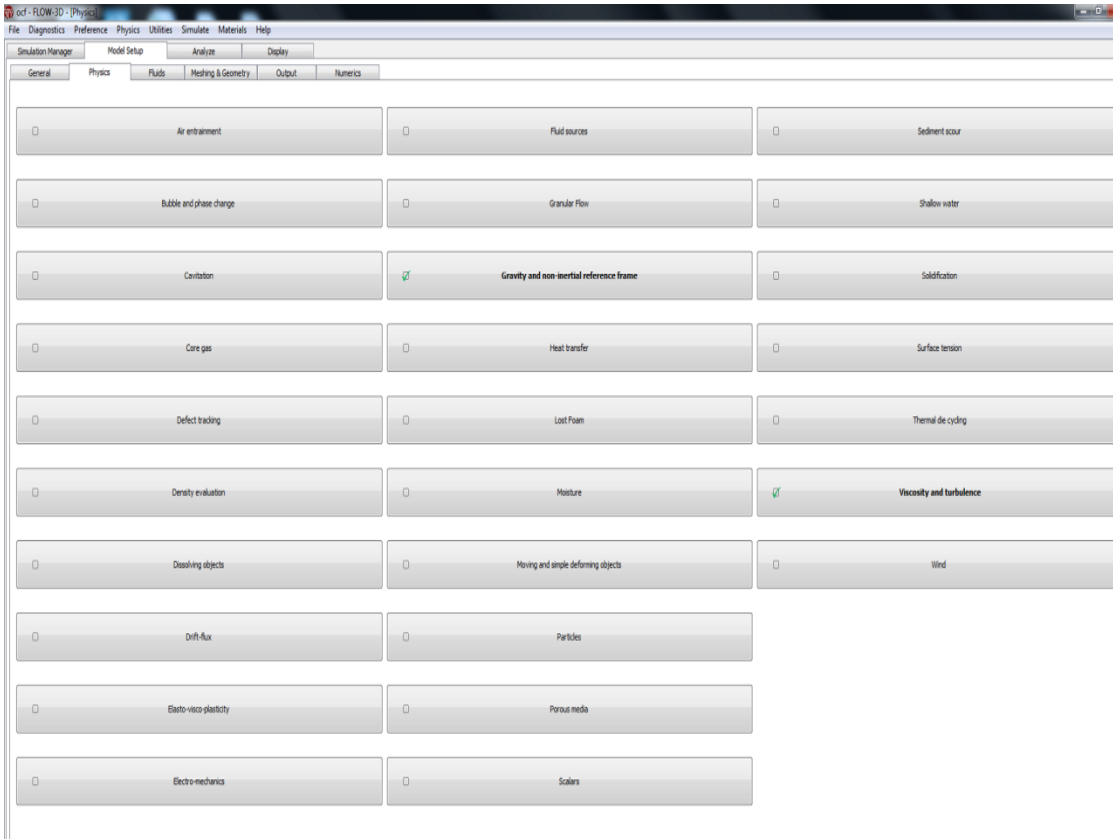


Figure 6.3 GUI of the software showing the Physics Tab of the model

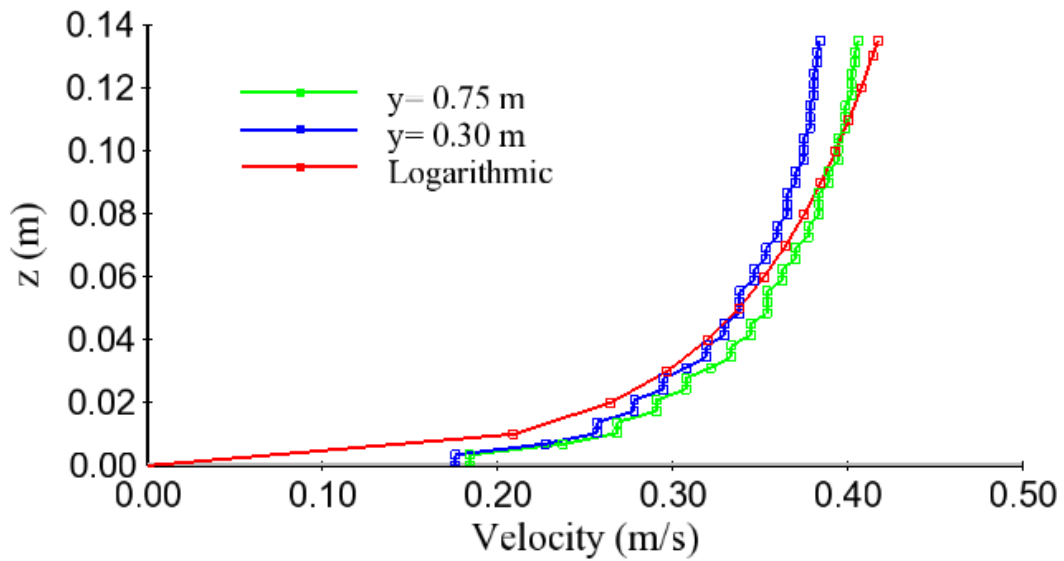


Figure 6.4 Comparison of the velocity distributions obtained from simulation output with the theoretical equation

## **6.2 Flat Bed Simulations**

Before conducting the scour simulations, the turbulence solver models of the software were tested for the competency in handling the hydrodynamics of this kind of flows. The simulations were conducted after placing a SCE abutment model with  $L= 15$  cm on one side of the channel wall. The domain of the simulations was extended 1.1 m upstream of the abutment and 5 m downstream of the abutment in the streamwise direction. By this manner the flow field for the smallest SCE abutment was obtained. The velocity fields obtained from the two turbulence model solvers were compared with the results of the velocity field measurement experiments conducted within this thesis study (Chapter 5). As defined in the Overview section of this chapter, the turbulence model solvers tested within the present study are RNG model and LES model. In this section the development of the model and the results will be given for the tested solvers separately.

### **6.2.1 Flat Bed Simulations using RNG Model**

As stated in FLOW-3D User Manual (2013), RNG Model can simulate the turbulent flows with high shear regions accurately. Additionally, this turbulence model is advised for the scour simulations in the user manual. To simulate the flow with the given model a structured mesh was developed. The developed mesh for the simulations is given in Figure 6.5. The mesh was constructed having approximately  $1.98 \times 10^5$  real cells and it was constructed by making mesh refinement around abutment, where the vortex structures form. The inlet BC was selected as ‘Grid Overlay’ BC, which transfers the outlet flow conditions of the preliminary simulation to the new simulation as inlet flow conditions. The outlet BC was selected as “Pressure” type BC by defining the flow depth at the outlet as 0.135 m. The upper BC was selected as “Symmetry” and the other BCs were coincided with the wall components. The simulation was solved for a simulation time of  $t= 300$  seconds and the flow conditions were reached a nearly steady condition after 300 seconds. Streamwise velocity magnitudes at different transversal sections were compared with the experimental results. In Figure 6.6, these comparison graphs are given. It can be seen from the figures that, the simulation gives close results to the experimental results.

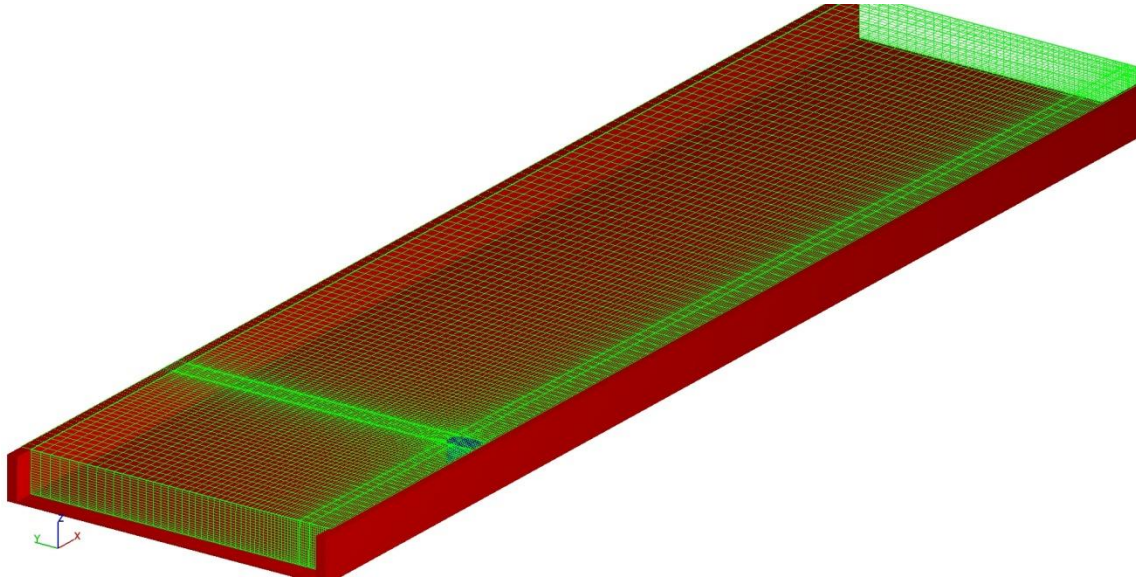


Figure 6.5 A view of the mesh constructed for the flat bed (RNG) simulation

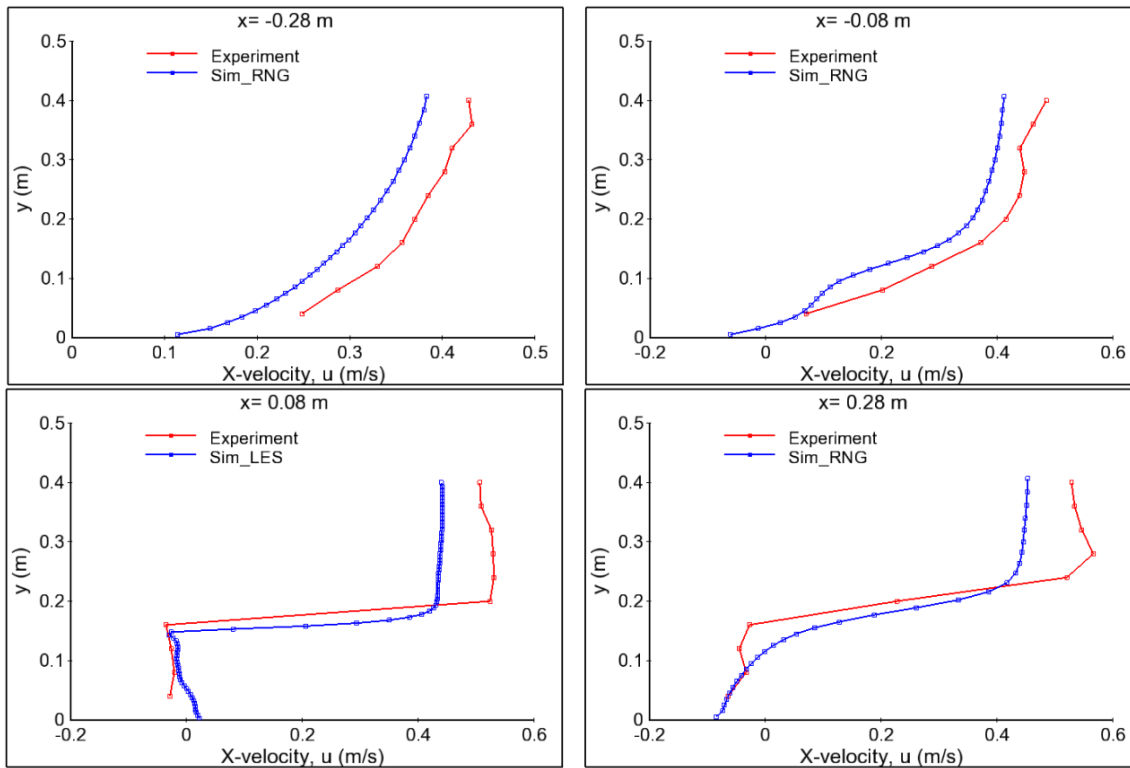


Figure 6.6 X-velocity comparisons of RNG Simulation at depth  $z=0.0675$  m

## 6.2.2 Flat Bed Simulations using LES Model

LES model was the second type of turbulence model used to simulate the flow. The case simulated by RNG model previously, which contains a SCE abutment model with  $L=15$  cm, was also tested with the LES model. The mesh size was selected by considering the applicability of the long duration scour simulations and it was developed with  $3.37 \times 10^5$  real cells. The mesh was constructed by making mesh refinement around abutment, where the vortex structures form. The first grid point away from the solid surface in  $z$ -direction was set to 67 non-dimensional wall units. A view of the mesh is given in Figure 6.7. The simulation was run for 300 seconds. The simulation was finalized in 50 minutes with a 16-processor cluster PC.

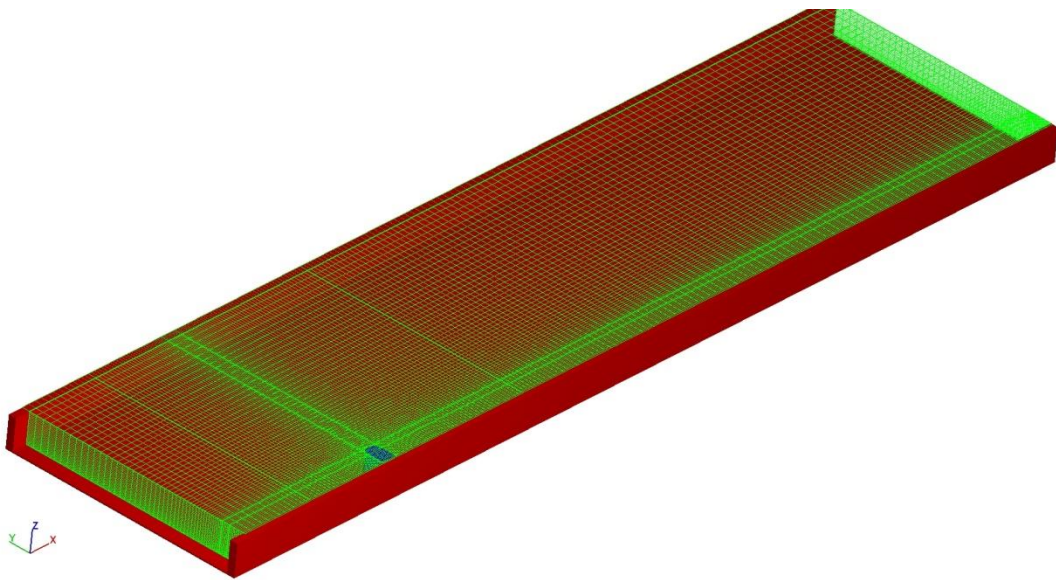


Figure 6.7 A view of the mesh constructed for the flat bed (LES) simulation

The boundary conditions were selected as the same as the RNG model simulation, which is described in the previous section. The streamwise velocity magnitudes, at the same sections given in the previous subsection, are compared with the experimental values and given in Figures 6.8. One can see from these graphs that, the LES model has solved

the flow accurately and it gives closer results to the experimental ones compared with the results of the RNG model.

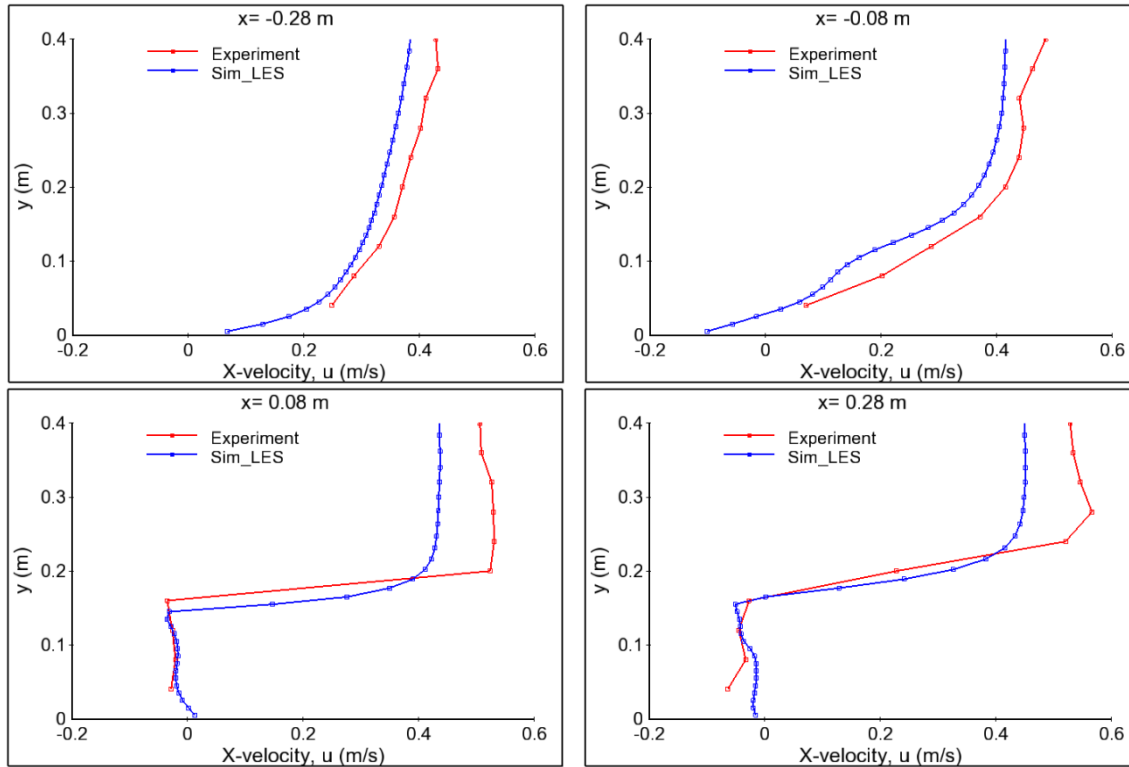


Figure 6.8 X-velocity comparisons of LES Simulation at depth  $z = 0.0675$  m

### 6.3 Erodible Bed Simulations

After the results of the velocity field simulations of RNG and LES turbulence solver models have given satisfactory correlation with the experimental data, the scour simulations were run with FLOW-3D by using these two turbulence solver models. To simulate this case, in addition to the previously stated options used in the flat bed simulations a sediment storage portion was defined around the abutment and the sediment scour model of the software was activated.

The Graphical User Interface (GUI) of the sediment scour model of the FLOW-3D is given in Figure 6.9.

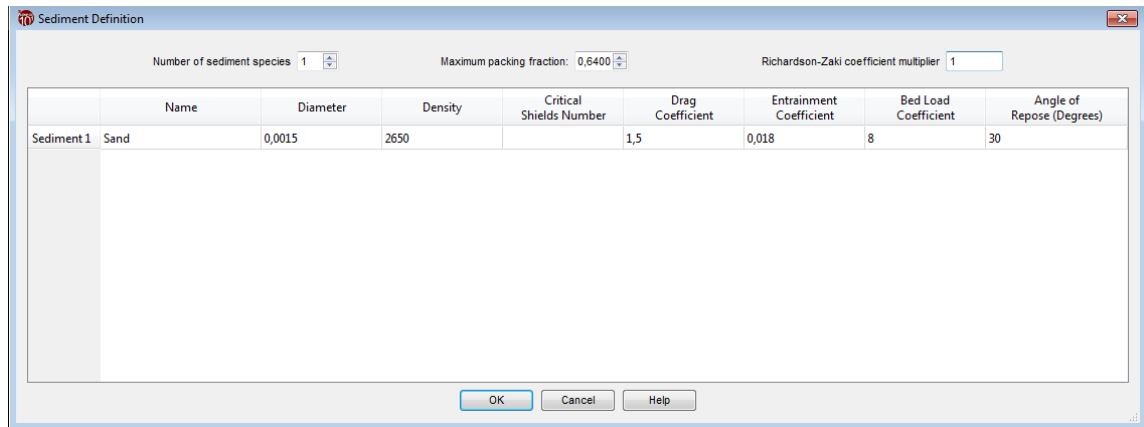


Figure 6.9 The GUI of the sediment scour model

In this window, the density, mean diameter and the angle of repose of the material used in the experiments were inserted as given in the figure. Drag coefficient was selected as 1.5 which is the drag coefficient value for the particles with spherical shape. Critical Shields Number is a property that depends on fluid and sediment properties as given by Equation (6.10). This parameter was used to calibrate the results of the model. Entrainment and the bed load coefficients are the other parameters which were used to calibrate the model with the experimental results. The values shown in Figure 6.9 are the default values that FLOW-3D uses for these coefficients. In Kayser and Gabr (2013), the ranges of entrainment and bed load coefficients were given in 0.009 to 0.036 and 4 to 8, respectively based on the studies of Rubey (1933) and Wu and Wang (2006).

Although the erodible bed simulations were handled by using two turbulence models as did for the flat bed simulations, the mesh used in the simulations was selected as the same for both models. The developed mesh is given in Figure 6.10 with the components defined for the scour simulations.

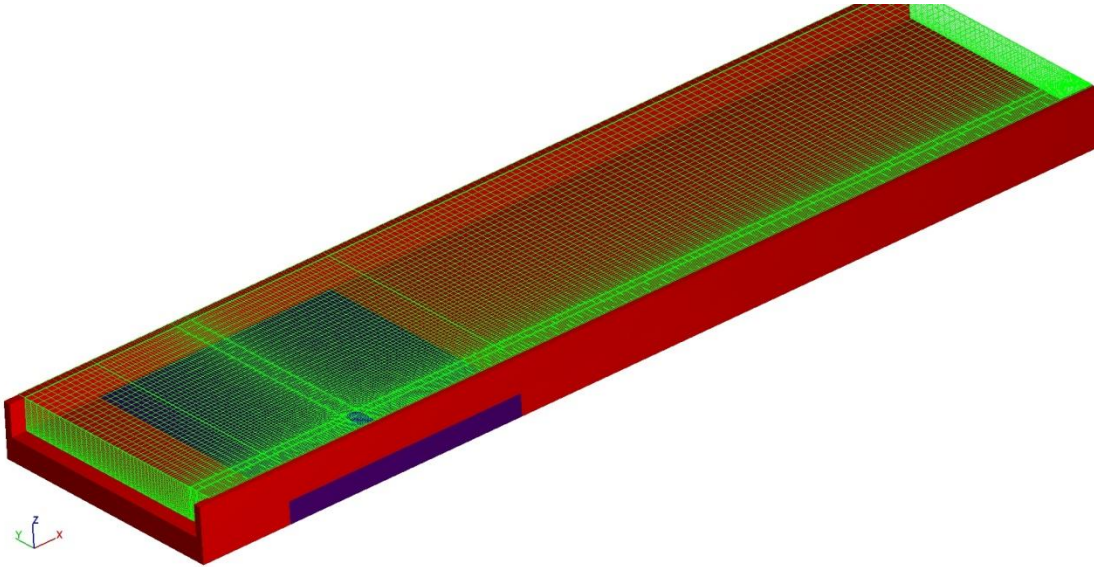


Figure 6.10 A view of the mesh constructed for the erodible bed simulation

As can be seen from Figure 6.10, a sediment layer (the purple component) with 15 cm thickness was defined around the abutment lying from  $x = -0.6$  m to  $x = 1.0$  m. The sediment material was defined with the same properties of the bed material of the experimental problem. The solid components defining the flume wall and flume bed (the red components) were elongated in negative  $z$  direction having the same  $z$ -coordinate with the sediment component.

The mesh size is very important for the applicability of the scour simulations as they should run for hours of simulation time to make a reliable calibration with the experimental results. Therefore, a structured mesh was constructed with great concern with  $5.83 \times 10^5$  real cells, having minimum  $y^+$  value equals to 67 in  $z$  direction and 134 in both  $x$  and  $y$  directions. The domain was elongated to  $z = -0.15$  m to cover the sediment layer.. Generally the erodible bed simulations conducted in this study were run for 2 hours to make a comparison with the experimental results and each one was lasted for around 26 hours with a 16-processor PC by using this mesh.

The boundary conditions were defined similar to the mesh used for the flat bed simulations.

The simulations were conducted by using two turbulence solver models like the flat bed simulations. The model calibration was done thereafter. The two parts of this section will cover the simulations done by using RNG and LES models.

### 6.3.1 Erodible Bed Simulations using RNG Model

First, the RNG model was tested for the erodible bed simulations as the model was advised to be used in scour simulations for its competency on high shear flows (FLOW-3D User Manual, 2013).

All the tuning parameters of the scour model were tested in various combinations for this case. However, for any combination of model parameters tested, the simulation with RNG model has not given any reasonable eroded bed profile. The eroded bathymetry of the bed around abutment model is given in Figure 6.11 after the default values of the parameters were used. It is clear that the eroded bed bathymetry given in the figure does not fit the physics of the problem as the initiation of the scour occurs at far downstream from the abutment.

As the other tested simulations with different scour model parameter combinations gave similar outputs, it can be seen that the RNG turbulence model is not a good choice for scour simulations and the analyses with RNG model were terminated for the rest of the study.

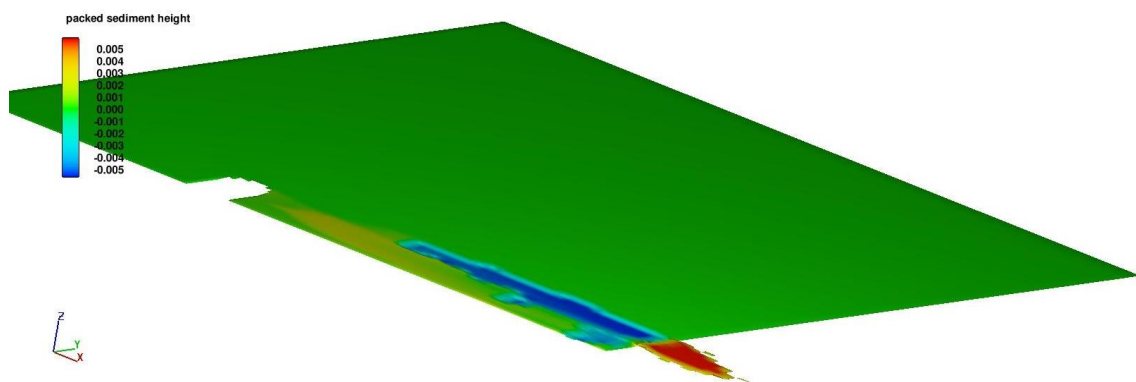


Figure 6.11 The eroded bed bathymetry obtained after RNG Model

### 6.3.2 Erodible Bed Simulations using LES Model

Secondly, the LES turbulence model was tested for the scour simulations. After the preliminary runs gave qualitatively acceptable bed bathymetry profiles, the calibration study of the model by using the experimental data was done.

#### 6.3.2.1 Calibration of the Model

First the Critical Shields Number ( $\theta_{cr}$ ) effect on the maximum scour depth was analyzed by keeping the other parameters in their default values.

The value of  $\theta_{cr}$  for the problem was calculated as 0.03852 and the scour pattern given in Figure 6.12 was obtained by using that value after 2 hours of simulation time.

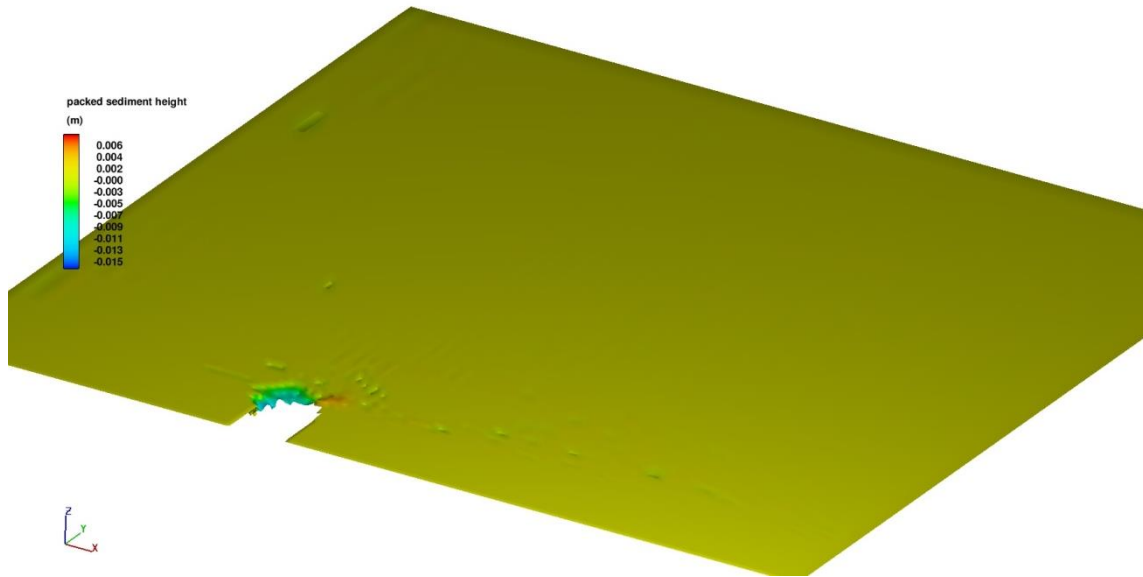


Figure 6.12 The eroded bed bathymetry obtained for  $\theta_{cr} = 0.03852$  after 2 hours

It can be seen from Figure 6.12 that, the position of the scouring region is true compared it with the experimental results, however; the value of the maximum scour depth ( $d_s = 1.55$  cm) is fairly low compared it with the experimental result of the same case presented in Chapter 3 ( $d_s = 8.78$  cm). It should be noted that when  $\theta_{cr}$  is low, more scour

is expected. Therefore, while testing the model in terms of  $\theta_{cr}$ , the values smaller than the calculated value were used. Figures 6.13 to 6.16 show the 3-D bathymetry views of the models having  $\theta_{cr}$  0.018 to 0.030.

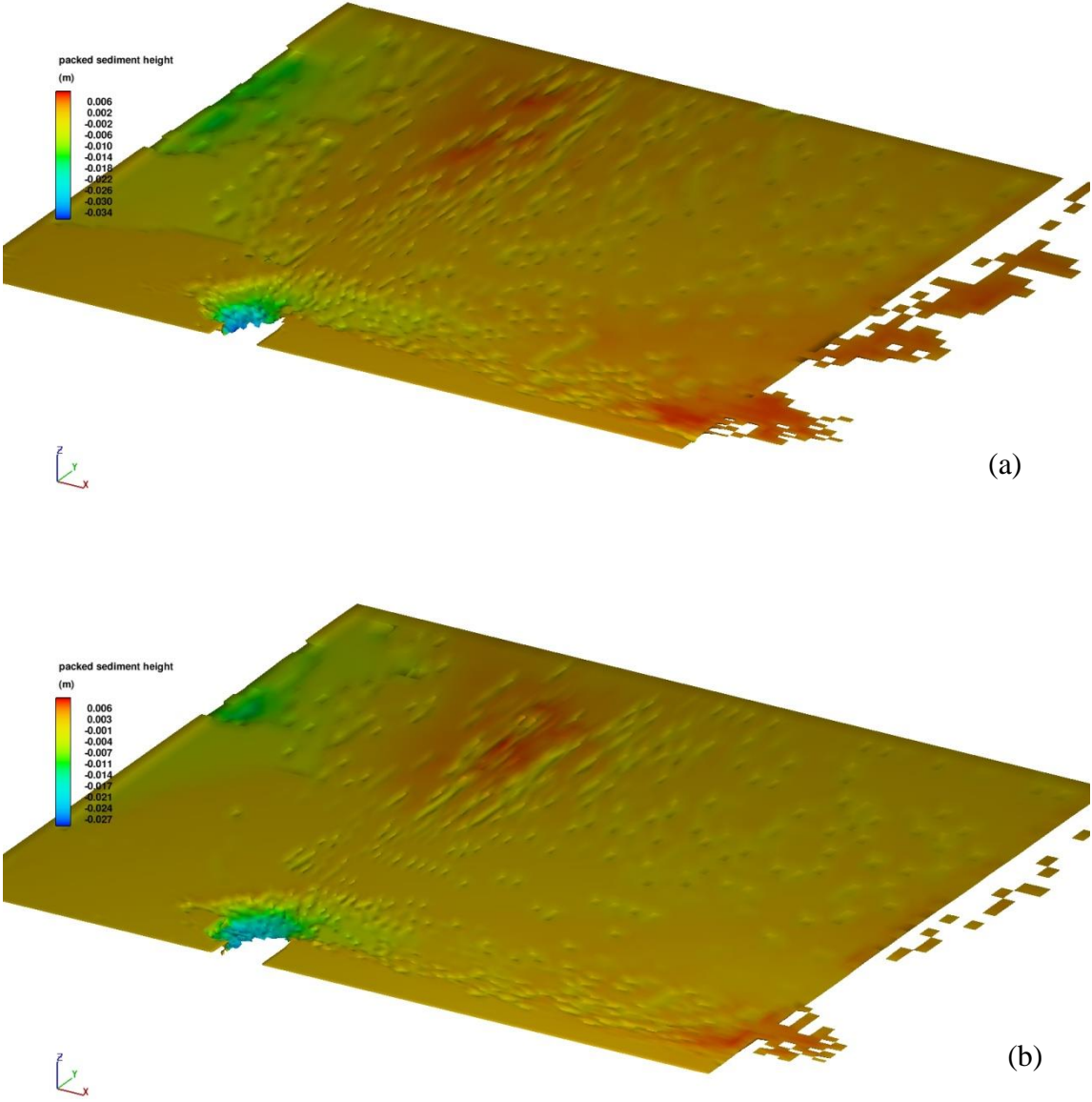


Figure 6.13 The eroded bed bathymetry obtained for (a)  $\theta_{cr} = 0.018$ , (b)  $\theta_{cr} = 0.020$

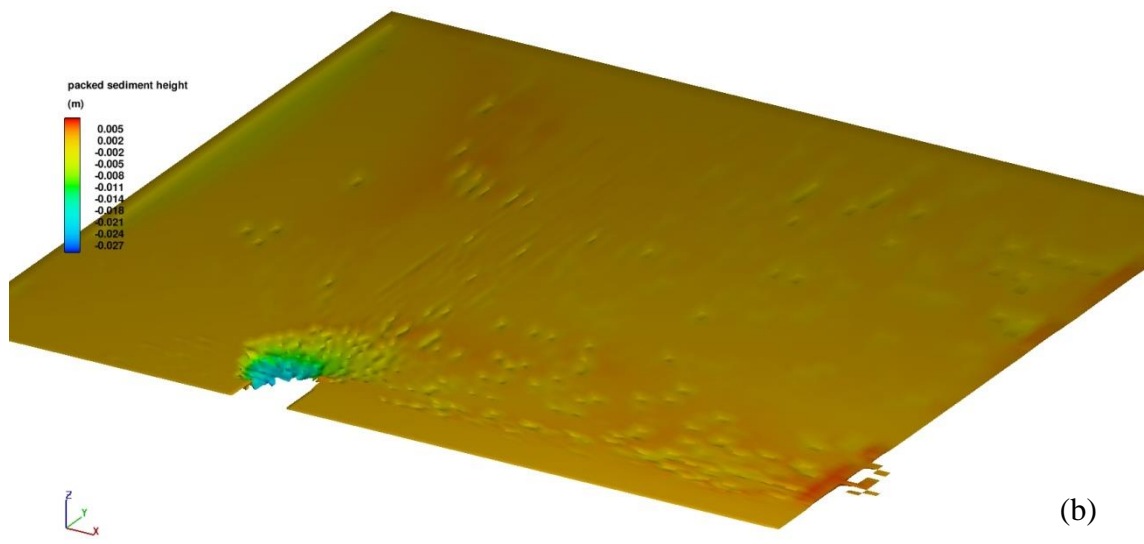
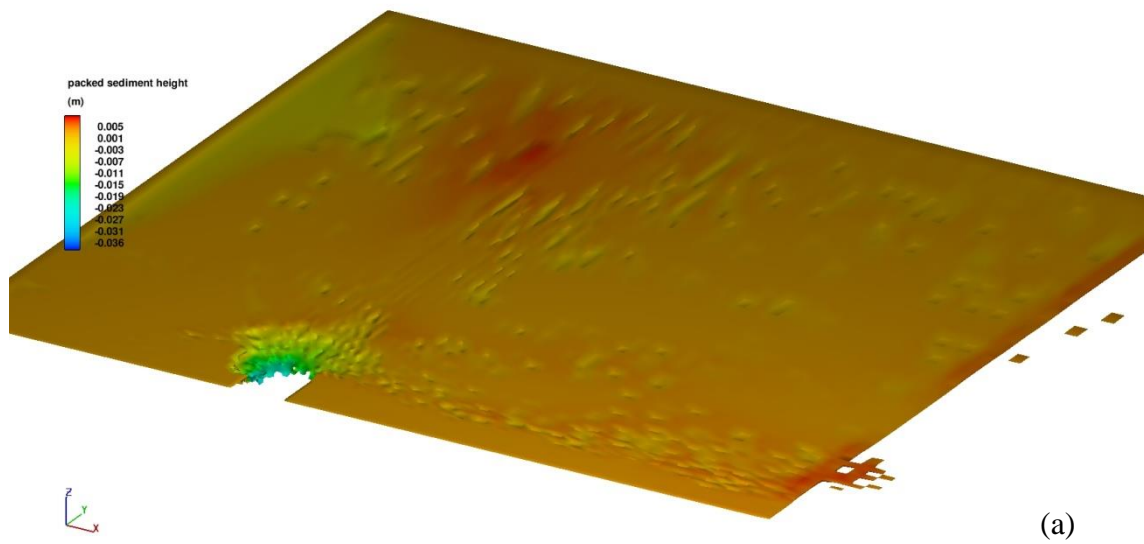


Figure 6.14 The eroded bed bathymetry obtained for (a)  $\theta_{cr} = 0.022$ , (b)  $\theta_{cr} = 0.024$

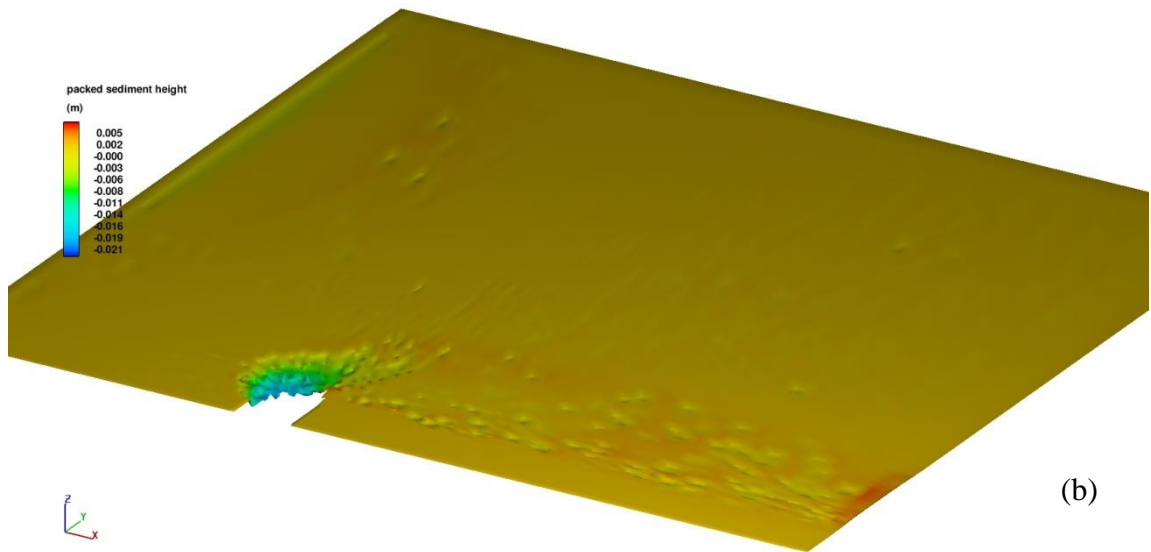
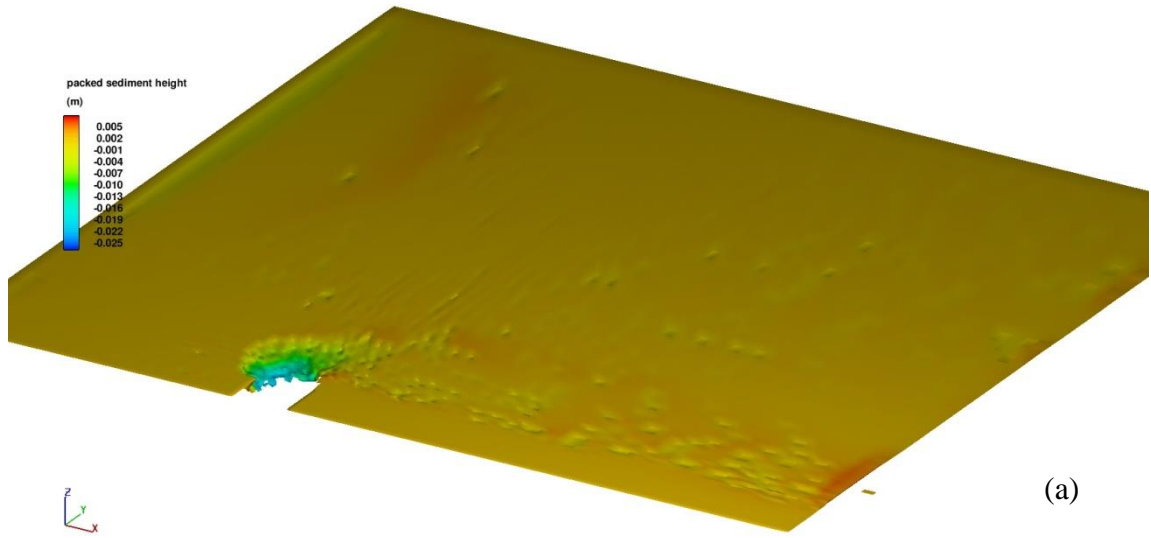


Figure 6.15 The eroded bed bathymetry obtained for (a)  $\theta_{cr} = 0.026$ , (b)  $\theta_{cr} = 0.028$

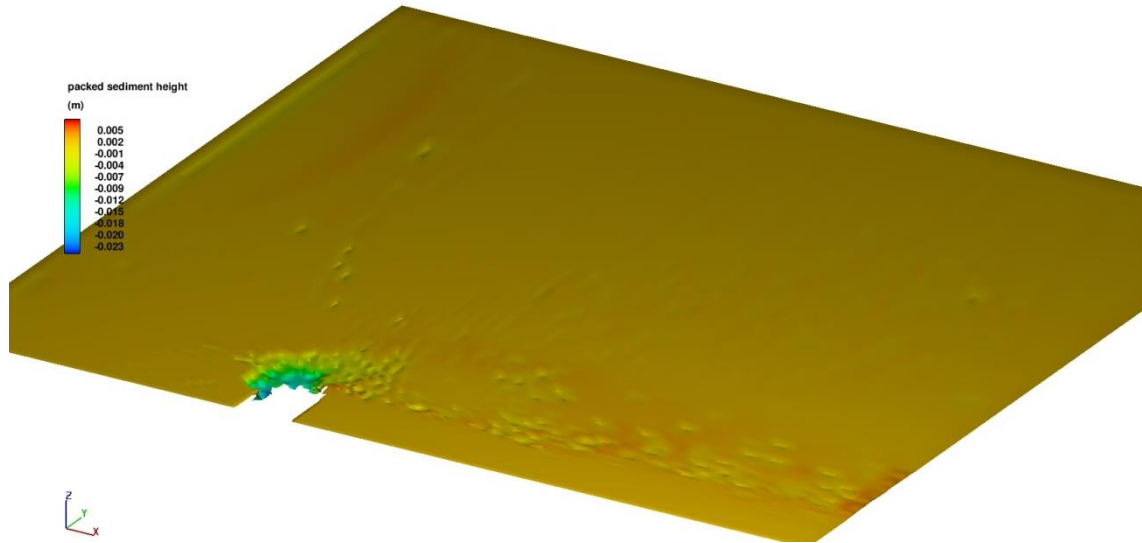


Figure 6.16 The eroded bed bathymetry obtained for  $\theta_{cr} = 0.030$

It can be seen from the figures that, lowering  $\theta_{cr}$  causes additional scour not only in regions around abutment but also the bed in the main channel regions. This result is not comparable with the real case as the case of concern has a clear water flow condition and no scour is expected in the main channel regions. Therefore,  $\theta_{cr} = 0.030$  was selected as the parameter value as it gives maximum scour depth value closer to the experimental result and no excess scour was resulted in the main channel region. The maximum scour depth values obtained in these tests are given in Table 6.1. It can be seen from Table 6.1 and Figure 6.17 that, there exists a trend of increase in maximum scour depth when  $\theta_{cr}$  decreases, which is an expected result.

Table 6.1 Maximum scour depths obtained in testing  $\theta_{cr}$  effect

$\theta_{cr}$	$d_s$ (cm)
0.018	3.657
0.02	2.763
0.022	3.660
0.024	2.722
0.026	3.145
0.028	2.152
0.03	2.436
0.038	1.551

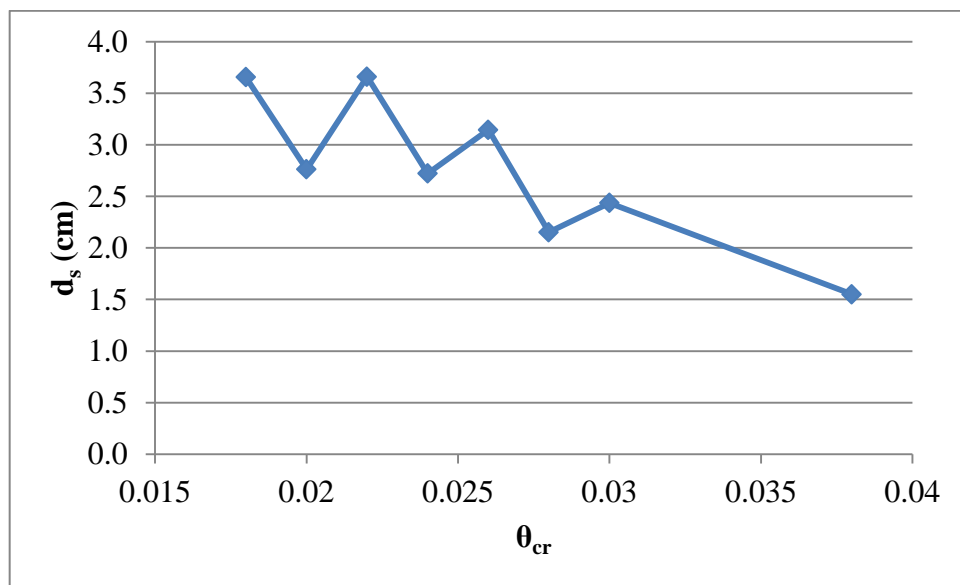


Figure 6.17 Effect of  $\theta_{cr}$  change on maximum scour depth

After decided the value of  $\theta_{cr}$ , the other three parameters were tuned to calibrate the model. For the remaining simulations  $\theta_{cr}$  was used equal to 0.03. Then, the effect of entrainment coefficient ( $\varphi$ ) on maximum scour depth was tested. In Brethour and Burnham (2010), the default value of the entrainment coefficient in FLOW-3D was stated to be decided for the entrainment coefficient of submarine sand which equals to 0.018. As stated in Section 6.1.2, this coefficient has an important effect on scour entrainment and it should be tuned to calibrate the model. For testing entrainment coefficient, the simulations were conducted by keeping remaining two coefficients on

their default values. Although in Kayser and Gabr (2013) the range of entrainment coefficient was defined between 0.009 and 0.036, in the present study some values out from this range were tested to obtain the variation trend. Figures 6.18 to 6.20 show the eroded bed bathymetry graphs for the tested cases.

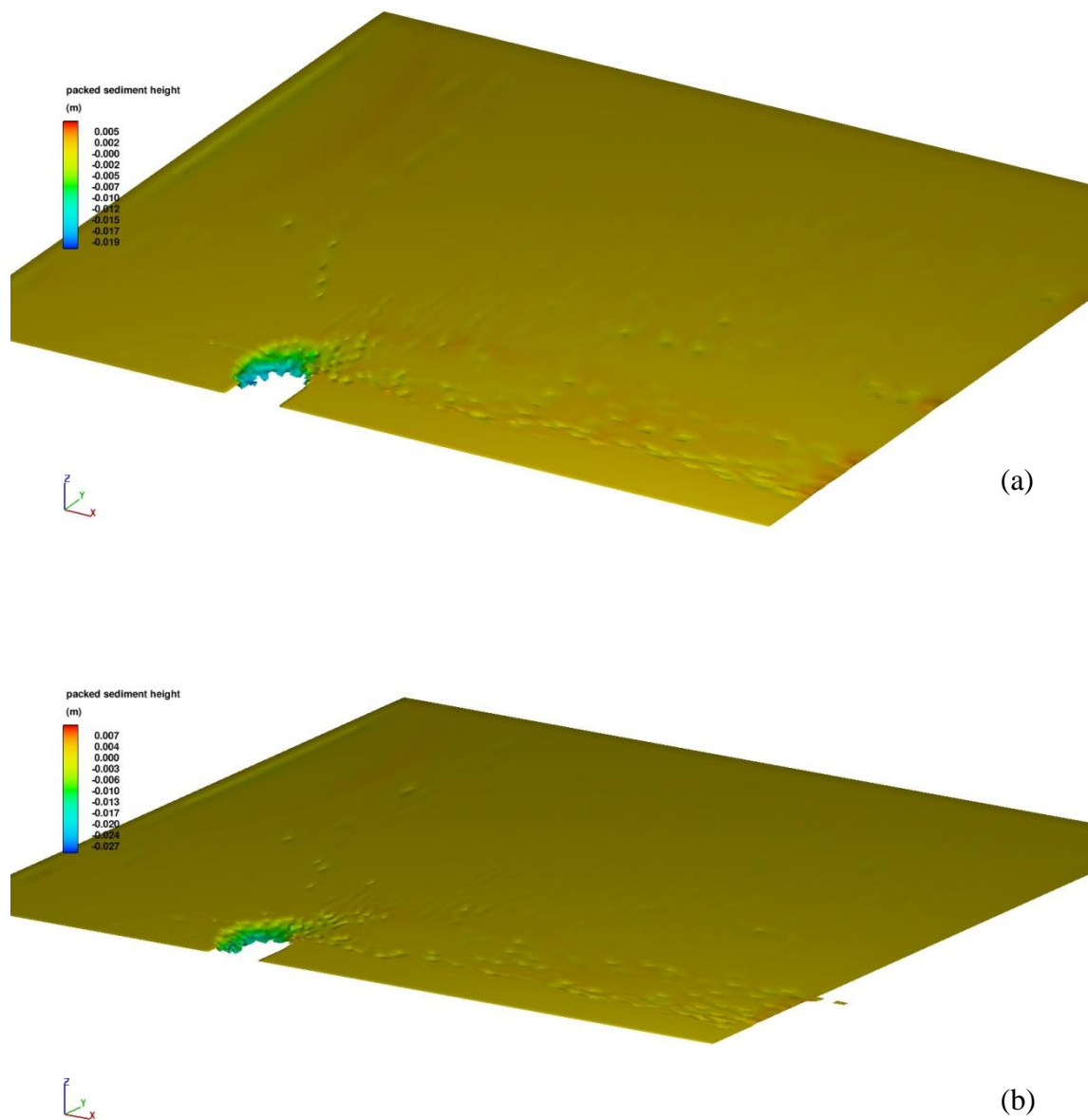


Figure 6.18 The eroded bed bathymetry obtained for (a)  $\varphi = 0.005$  (b)  $\varphi = 0.009$

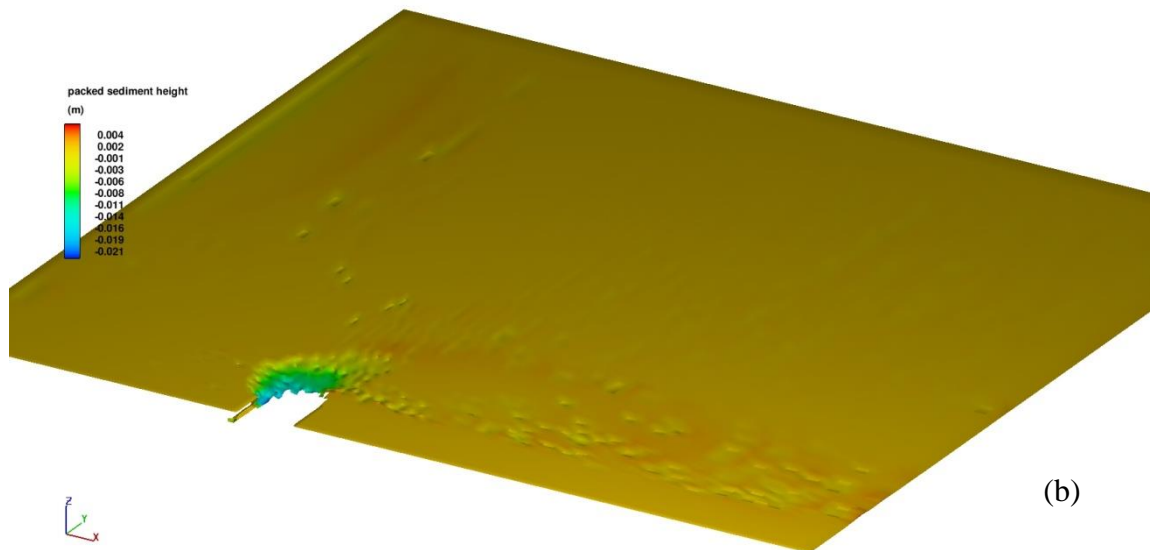
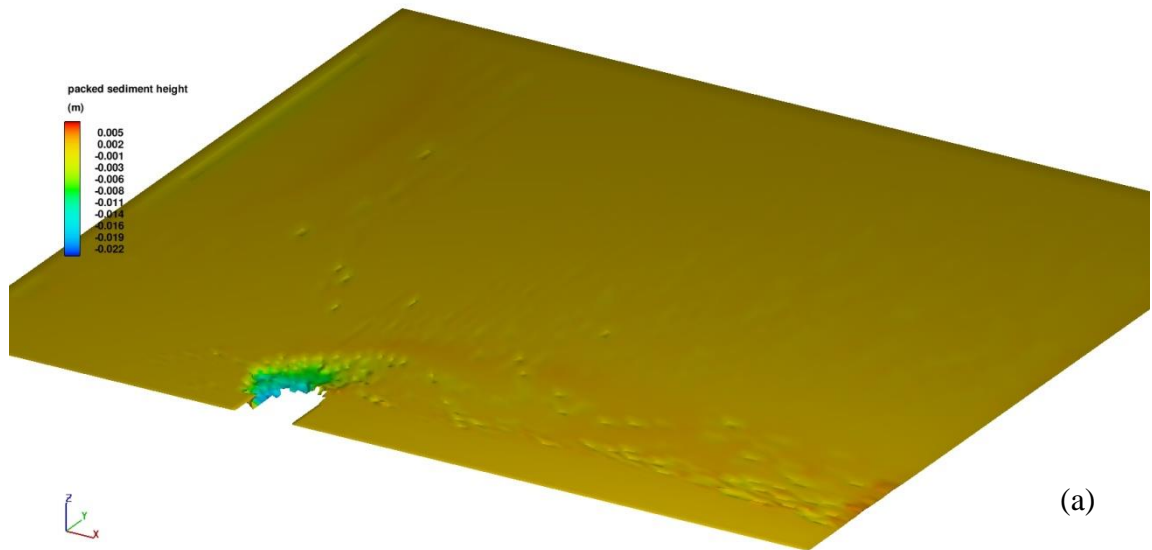
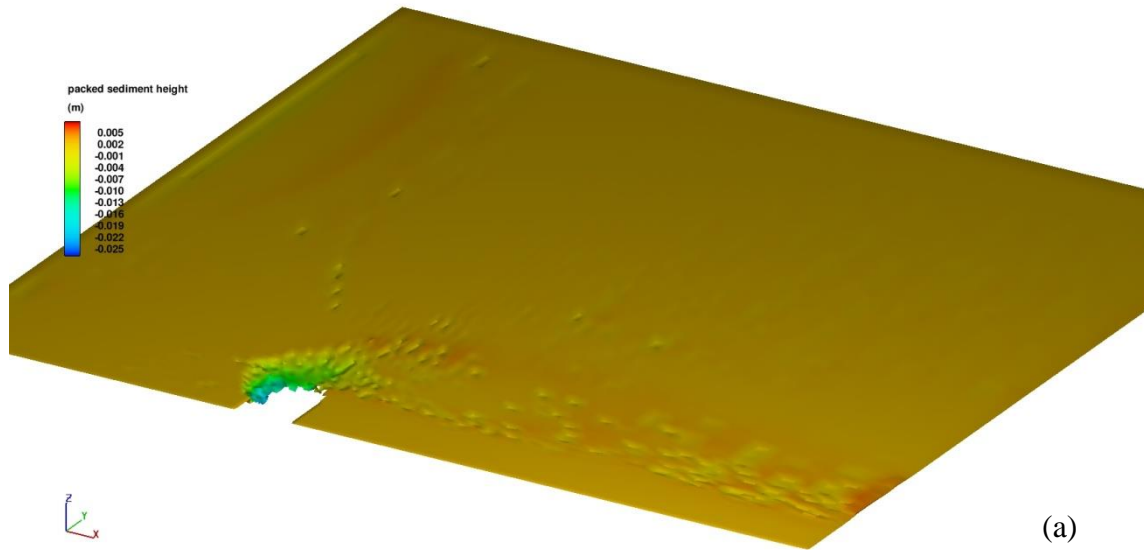
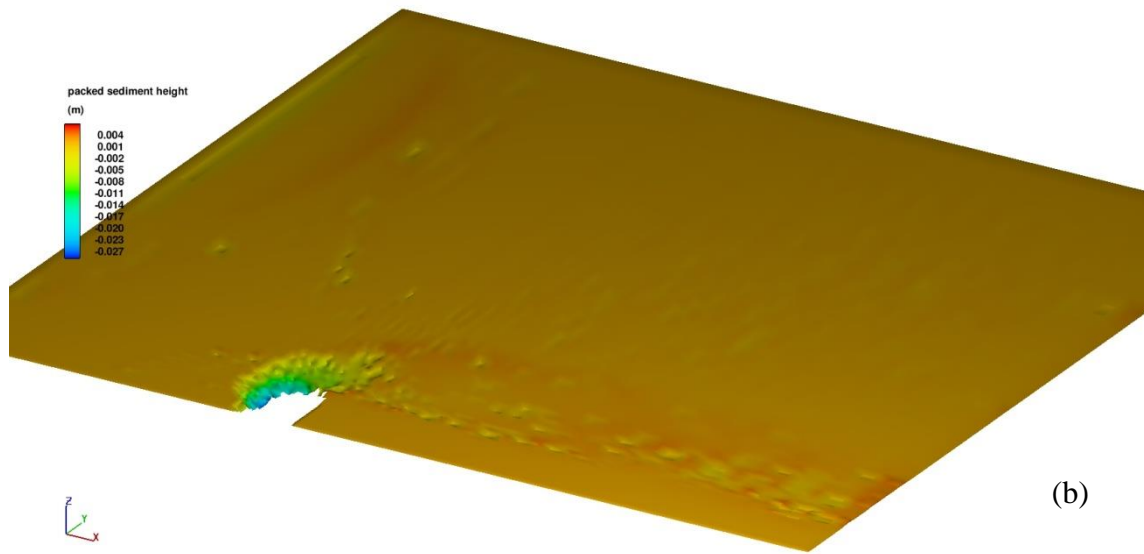


Figure 6.19 The eroded bed bathymetry obtained for (a)  $\varphi = 0.012$  (b)  $\varphi = 0.027$



(a)



(b)

Figure 6.20 The eroded bed bathymetry obtained for (a)  $\varphi = 0.036$  (b)  $\varphi = 0.060$

It can be seen from Figures 6.18 to 6.20 that, although the change in  $\varphi$  does not change the scour pattern dramatically, slight expansion of scour hole in horizontal directions can be observed. Figure 6.21 shows the variation of maximum scour depth with the change of  $\varphi$ . In Table 6.2, numerical values used in the figure are presented. It can be seen from the figure that, there does not exist an observable trend in the relation of maximum scour

depth and  $\varphi$ , however;  $\varphi = 0.009$  results with the biggest value which is closer to the experimental result, therefore, 0.009 was decided to be the value of the  $\varphi$  for this problem.

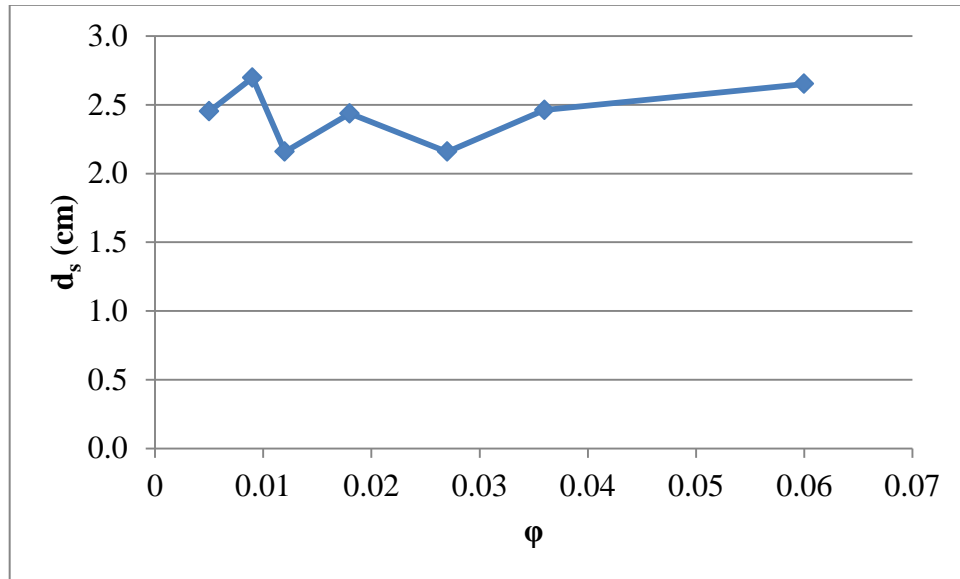


Figure 6.21 Effect of Entrainment Coefficient change on maximum scour depth

Table 6.2 Maximum scour depths obtained in testing Entrainment Coefficient effect

$\varphi$	$d_s$ (cm)
0.001	1.579
0.005	2.451
0.009	2.697
0.012	2.158
0.018	2.436
0.027	2.158
0.036	2.462
0.060	2.652

Finally, the effect of bed load coefficient ( $\omega$ ) change on scour pattern and maximum scour depth was investigated. Although the flow regime is defined as clear-water flow and no bed load would be expected and observed from the simulations until now, the tuning of this coefficient was achieved as it may have effect within the scour hole. The

default  $\omega$  value is 8 and in Brethour and Burnham (2010) the ranges of  $\omega$  were defined as 5 to 5.7 for low transport, 8 for intermediate transport and 13 for very high transport regimes. In this study, besides the default value of 8, two additional values were tested as 4 and 16 to see the effect of it on scour pattern and maximum scour depth variation. The eroded bed bathymetry graphs were not presented here to save space as significant changes were not obtained in bathymetries with the change of bed load coefficient. Besides, Figure 6.22 shows the effect of  $\omega$  change on maximum scour depth and Table 6.3 gives the numerical values used in the figure. As can be seen from the figure the value of 8 which is the default value of  $\omega$  gives the maximum of maximum scour depth, which is the closest value to the experimental result. Therefore, 8 is chosen for the bed load coefficient value for the analysis.

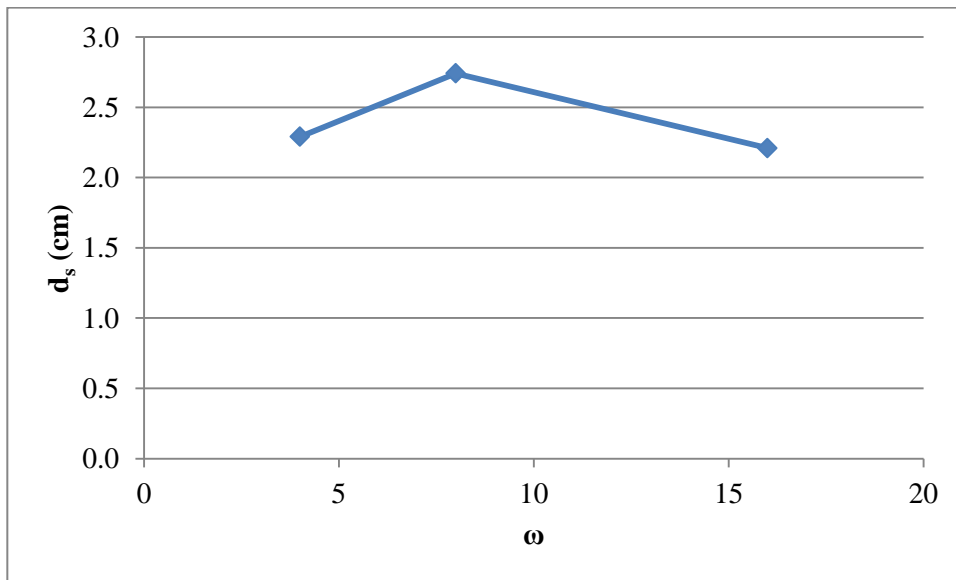


Figure 6.22 Effect of Bed Load Coefficient change on maximum scour depth

Table 6.3 Maximum scour depths obtained in testing Bed Load Coefficient effect

$\omega$	$d_s$ (cm)
4	2.29
8	2.74
16	2.21

### 6.3.2.2 Comparison of the Simulation Results with the Experimental Results

It can be seen from the presented outputs in the previous section; the model predicts the position and pattern of the scouring well but underestimates the value of the maximum scour depth by large amounts after two hours of scouring for abutment length of ,  $L= 15$  cm. In this section the comparison of the model with the experimental results will be achieved in terms of bed profiles and the comparisons will be extended for the different time periods and abutment lengths.

First, a bed profile was taken from the simulation output on the fourth section that was discussed in Chapter 3, which can be seen from Figure 3.35 (a). Figure 6.23 was developed by inserting the simulation result into the experimental results. The simulation output bed profile in Figure 6.23 was obtained after running a new simulation with finer mesh. The reason to do this is that, the bed profile output of the coarse mesh simulation has so many oscillations that the profile can not be identified properly. The comparison of the coarse and fine mesh solution at the same section is given in Figure 6.24. It can be seen that, the coarse mesh result is close to the fine mesh result in terms of the maximum scour depth and overall shape. The fine mesh was developed having a minimum of 0.001 m grid spacing ( $y^+=14$ ) in z direction with  $9.14 \times 10^5$  real cells in total. The simulations conducted with the latter mesh lasted in about eleven times of the computational time corresponding to the former mesh (Figure 6.10). Even by using the coarse mesh (Figure 6.10), the simulations with two, four and eight hours of simulation times were finalized in 26, 107 and 278 hours, respectively by using a 16-processor cluster PC. Therefore, considering the computational cost, the simulations were conducted with the former mesh.

It can be seen from Figure 6.23 that, although the simulation underestimates the scour depth value by large amounts, it predicts the shape of the profile reasonably well compared with the experimental results.

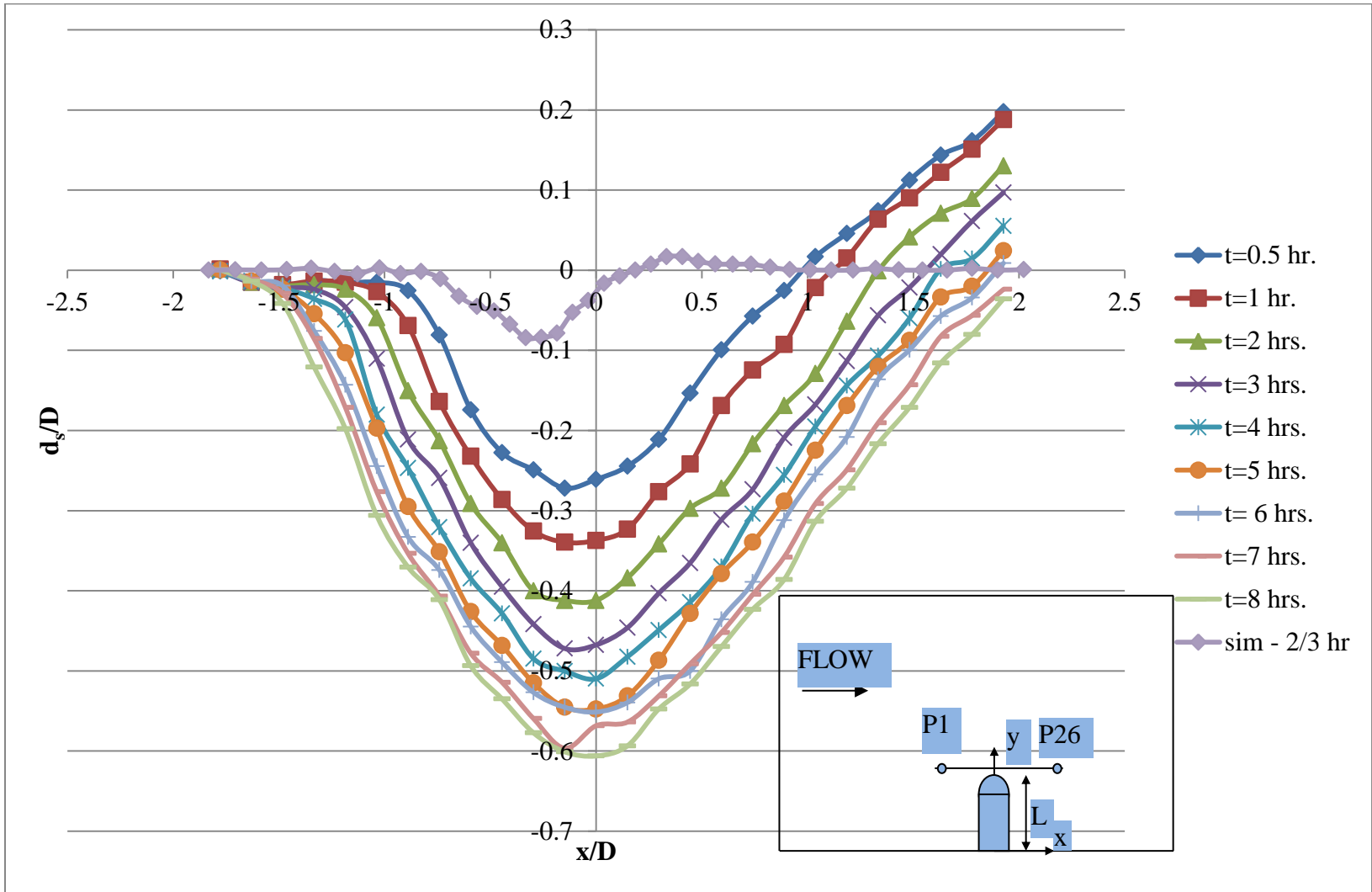


Figure 6.23 Comparison of bed profiles of simulation output and experimental results

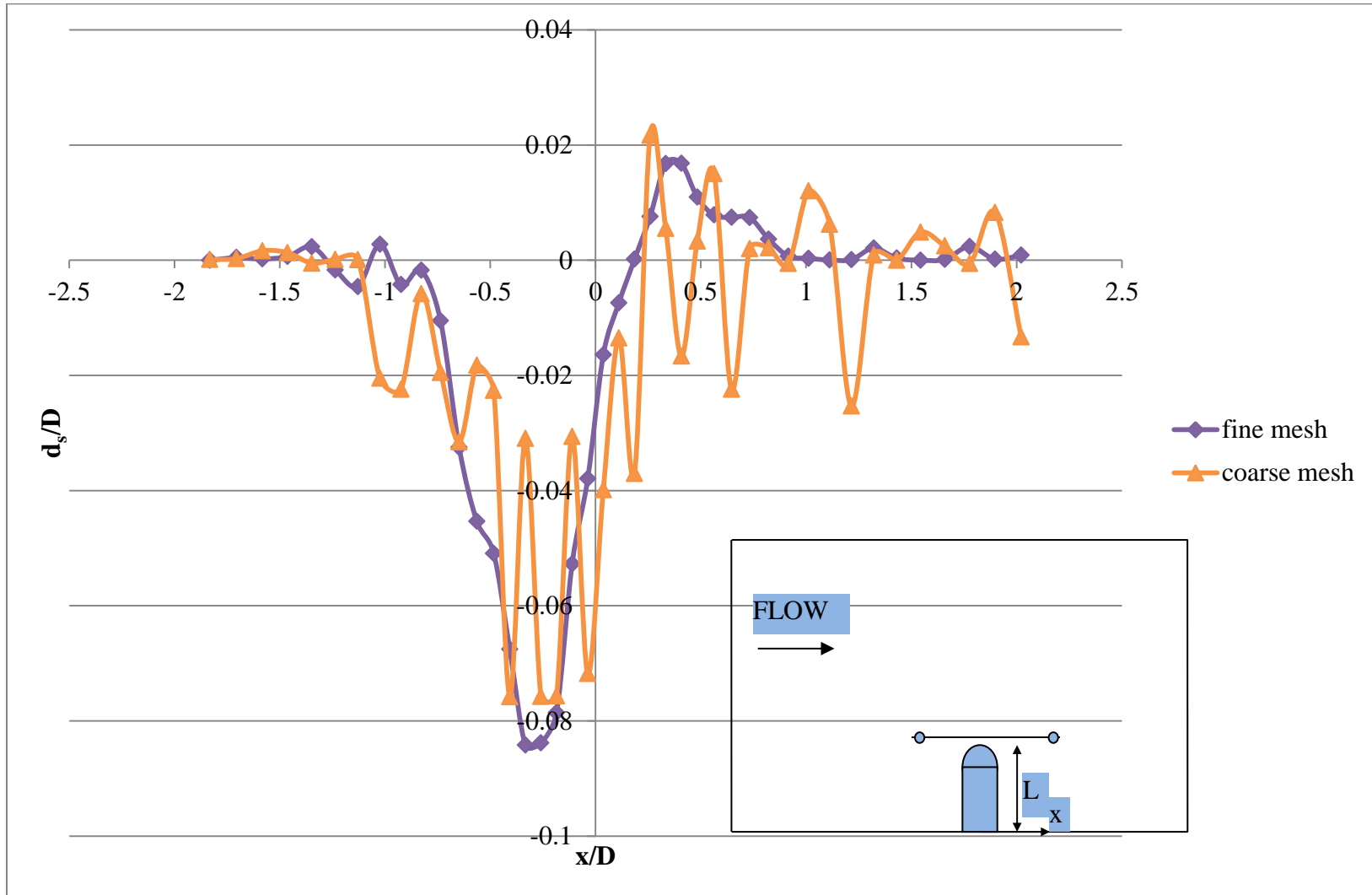


Figure 6.24 Comparison of bed profiles of simulation outputs with coarse mesh and fine mesh

The additional comparisons of the simulation results with experimental results were achieved by; first simulating the case with abutment length,  $L= 15$  cm till  $t= 8$  hours and second conducting a new simulation for the case with abutment length,  $L= 35$  cm for  $t= 2$  hours. By this manner the comparisons were achieved in terms of maximum scour depth and the length of the scour hole values. Table 6.4 shows the comparisons of these variables for the above mentioned cases. The eroded bed bathymetry figure of the case for abutment length,  $L= 35$  cm is given in Figures 6.25. As the scour hole extended by containing more computational cells compared to the one for the short abutment case ( $L= 35$  cm), the computational time of the latter simulation has increased 6.7 times of the one corresponding to the short abutment case with the same simulation times. It can be seen from the figures and the table that; the positions of the scouring and deposition regions were predicted well by the model, but the values of the quantities of the scour hole were underestimated by large amounts.

Table 6.4 Comparison of simulation results with the experimental results

$L$ (cm)	$t$ (hr)	Exp. $d_s$ (cm)	Sim. $d_s$ (cm)	% dev.	Exp. $X_s$ (cm)	Sim. $X_s$ (cm)	% dev.
15	2	8.71	2.74	68.5	43.61	13.00	70.2
15	4	11.06	3.10	72.0	51.03	19.20	62.4
15	8	13.18	3.60	72.7	62.91	25.07	60.1
35	2	16.49	6.86	58.4	76.28	45.15	40.8

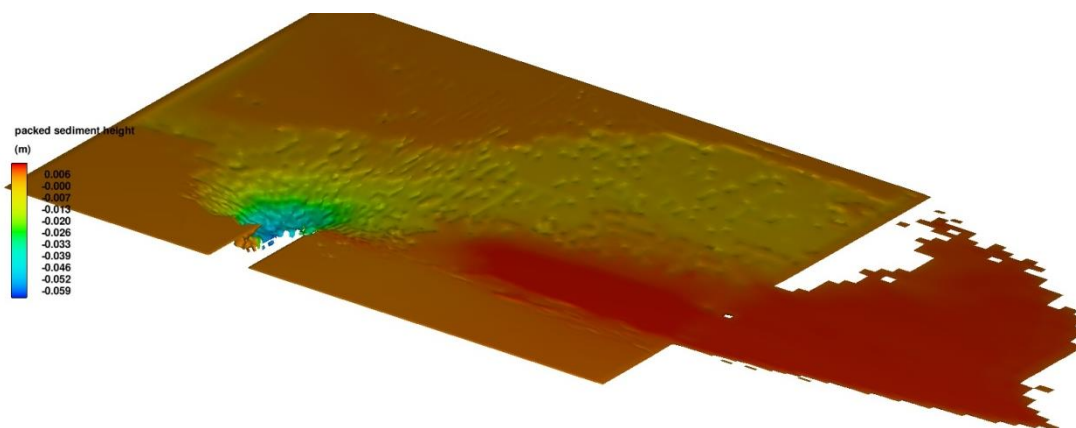


Figure 6.25 The eroded bed bathymetry obtained for  $L= 35$  cm and  $t= 2$  hours

## CHAPTER 7

### CONCLUSION

The present study has been conducted to contribute to the discussions of flow around bridge abutments and the scour phenomena around bridge abutments. The analyses have been extended by including various aspects including; the experimental work to obtain velocity field and scouring around abutments and the numerical analysis of scouring. The conclusions of the study will be summarized and the recommendations to the future researches will be done within this chapter.

#### 7.1 Summary of the Conclusions

The experimental study covered in Chapter 3 provides results of the bathymetry and the temporal scour measurements by using an isolated SCE abutment at bridge crossing. The variation of the dimensionless maximum scour depth ( $d_s/D$ ) with the dimensionless abutment length ( $L/D$ ) was found as very close to linear for various time periods. However, it was noticed that this relation had local scour and contraction scour components inside and the limit ratio of the contraction over which the contraction scour contributes to the total scour was found as 15% for the present experimental conditions. Besides, the time development of scour depth was obtained as very rapid in the early periods of scouring and the rate of increase lessened with time. 50% of the final scour depth was reached in the 1/16 and 1/8 of the total duration for the long abutment ( $L= 35$  cm) and short abutment ( $L= 15$  cm) cases, respectively. The variations of the dimensionless scour hole lengths ( $X_s/D$ ,  $X_l/D$ ,  $X_c/D$ ) with the dimensionless abutment length ( $L/D$ ) were also found to be very close to linear for various time periods. This

showed that the horizontal and vertical growth of the scour hole have similar trends over time. Correspondingly, the variation of the dimensionless scour hole volume ( $V_s/D^3$ ) with dimensionless maximum scour depth ( $d_s/D$ ) was defined with a power function regardless of time and abutment length with an R-squared value very close to one. This supports the idea that, the side slopes of the scour hole remains constant over time whereas the growths of it on horizontal and vertical directions have similar trends. Also, the time development of profiles taken within the scour hole shows that, the scour hole always grows in vertical direction with time and the side slopes of the scour hole is very close to the angle of repose of the sediment at every time step. A step like formation was observed within the scour hole close to the flume axis for the long abutment case, which was not observed clearly for the short abutment case. Besides, it was observed for the long abutment case that, the deposition hill has initiated far from the flume side wall and shifted towards the wall until the fifth hour of the experiment. It then kept its position for the rest of the experiment having side slopes on both sides equal to each other.

The analysis of the scour experiments conducted after obtaining contraction with two spill-through abutments was provided in Chapter 4. Like the results obtained for SCE abutment, the dimensionless maximum scour depth ( $d_s/D$ ) and dimensionless scour hole lengths ( $X_s/D$ ,  $X_l/D$ ,  $X_r/D$ ) varies linearly with the change in contraction ratio ( $\beta$ ). Similarly, the variation of the dimensionless scour hole volume ( $V_s/D^3$ ) with the dimensionless maximum scour depth ( $d_s/D$ ) was defined with a power function with an R-squared value very close to 1. By comparing the data sets regarding the two abutment types, it has observed that SCE abutments resulted with larger scour depth and larger scour hole length within a factor range of 1.3 to 2.0 compared to the spill-through abutments with the same contraction ratio and experimental duration. The variations of  $X_s/D$  with  $d_s/D$  and the variation of  $V_s/D^3$  with  $d_s/D$  were summarized with two relations separately regardless of the abutment type, abutment length and the experiment duration. It was observed that,  $V_s/D^3$  values for SCE abutment were slightly higher for the ones

corresponding to the spill-through abutments for the same  $d_s/D$  value. This might be related to the variation in abutment width. The position of the maximum scour depth was observed just at the upstream of the abutment tip, regardless of the experimental duration, abutment type or length. Temporal variations of scour pattern showed similar behaviors in two abutment types. However there was a step formation within the scour hole for the long abutment case ( $L=35$  cm) of the SCE abutment whereas, for spill-through abutments, this formation was only observed for small contraction ratio ( $\beta=0.119$ ). In the large contraction case ( $\beta=0.452$ ), the scour hole was elongated and combined with the scour hole of the opposite abutment, which prevented us to observe the formation of the step in the scour hole. The interaction of contraction scour with local scour was investigated for these cases, and unlike the ratio obtained from the experiments of SCE abutment, the limit ratio of contraction is found as 20% over which the contraction scour has contribution on total scour.

The analysis of the velocity field measurement data was presented in Chapter 5. It was observed that the streamwise velocity values obtained at the contracted sections of the measurement domain were amplified over two times of the approach flow velocity for the SCE abutment with a 23% contraction. The streamwise velocity and the turbulence kinetic energy (*tke*) values were observed bigger at the mid depth compared with the depth close to the bed at all cases. It was observed that, along the separated shear layers and the core of the primary vortex, the values were amplified.

Numerical analysis part of the study was conducted using the software FLOW-3D v.10.1 and the results were discussed in Chapter 6. It was observed that, RNG and LES turbulence models have given reasonably well velocity field outputs for flat bed simulations. However, RNG turbulence model has failed in erodible bed simulations. Although, the erodible bed simulations using LES turbulence model has predicted the position and the pattern of the scouring around abutments accurately, the values of the geometric parameters of the scour pattern has diverged from the experiments by large

amounts. Some runs with the beta release of the FLOW-3D v.11 have recently conducted and it seemed to give better results than v.10.1. However, as this was not the official version, which is still open to modifications, the results have not been presented here.

## **7.2 Recommendations for the Future Researches**

As the problem handled in this study is open to development in experimental and numerical ways, many recommendations may be listed for the future researches in order to extend the area of knowledge. However, the recommendations listed below are the ones directly related to this study;

- In order to extend the analysis on the interaction of local and contraction scours; experiments should be conducted with varying flow intensities.
- The experiments should be conducted with varying abutment widths, in order to obtain a more universal relation on the variation of  $V_s/D^3$  with  $d_s/D$ .
- Conducting experiments on a channel with flood plains and using unsteady stream inflow would make the test results closer to the real life analyses.
- In order to obtain accurate results from the erodible bed simulations, the governing equations of the sediment scour model might be modified before conducting additional simulations.

## REFERENCES

- Arneson, L.A., Zevenbergen L.W., Lagasse P.F., Clopper, P.E. (2012) “Evaluating Scour at Bridges”, 5<sup>th</sup> Edition, Rep. No.: FHWA-HIF-12-003 HEC-18, US FHWA
- Ahmed, F. and Rajaratnam, N. (2000) “Observations on flow around an abutment”, *Journal of Engineering Mechanics*, ASCE, Vol. 126, No. 1, pp 51-59
- Ballio, F. and Orsi, E. (2001) “Time Evolution of Scour around Bridge Abutments”, *Water Engineering Research*, 2, pp 243-259
- Ballio, F., Teruzzi, A. and Radice, A. (2009) “Constriction Effects in Clear-Water Scour at Abutments”, *Journal of Hydraulic Engineering*, ASCE, Vol. 135, No. 2, pp 140-145
- Barbhuiya, A. K. and Dey, S. (2003a) “Velocity and turbulence at a wing-wall abutment”, *Sadhana* Vol. 28, pp 35–56
- Barbhuiya, A. K. and Dey, S. (2003b) “Vortex flow field in a scour hole around abutments”, *International Journal of Sediment Res.* Vol. 18, pp 1–16
- Barbhuiya, A. K. and Dey, S. (2004) “Measurements of turbulent flow field at a vertical semicircular cylinder attached to the sidewall of a rectangular channel”, *Flow Measurement and Instrumentation* Vol. 15, pp 87–96
- Biglari, B. and Sturm, T. W. (1998) “Numerical modeling of flow around bridge abutments in compound channel”, *Journal of Hydraulic Engineering*, ASCE Vol. 124, pp 156–164
- Breusers, H.N.C. and Raudkivi, A.J. (1991) “Scouring”, *IAHR Hydraulic Structures Design Manual*, Balkema, Rotterdam
- Brethour, J. and Burnham, J. (2010) “Modeling Sediment Erosion and Deposition with the FLOW-3D Sedimentation & Scour Model”, *Flow Science Technical Note*, FSI-10-TN85, pp. 1-22
- Cardoso, A.H. and Bettess R. (1999) “Effects of Time and Channel Geometry on Scour at Bridge Abutments”, *Journal of Hydraulic Engineering*, ASCE Vol. 125 No. 4, pp 388–399
- Chabert, J. and Engeldinger, P. (1956) “Etude des affouillements autour des piles de ponts”, *Serie A, Laboratoire National d’Hydraulique*. Chatou, France

Chen, F. and Ikeda, S. (1997) "Horizontal separation flows in shallow open channels with spur dikes", *Journal of Hydrosience and Hydraulic Engineering*, Vol 15, No. 2, pp 15-29

Chrisohoides, A. and Sotiropoulos, F. (2003) "Experimental visualization of Lagrangian coherent structures in aperiodic flows", *Physics of Fluids*, Vol. 15, No. 3, pp 25-28

Chrisohoides, A., Sotiropoulos, F. and Strum, T. W. (2003) "Coherent structures in flat-bed abutment flow: computational fluid dynamics simulations and experiments", *Journal of Hydraulic Engineering*, Vol. 129, No. 3, pp 177-186

Coleman, S. E., Lauchlan, C. S. and Melville, B. W. (2003) "Clear water scour development at bridge abutments", *Journal of Hydraulic Research, International Association for Hydraulic Research (IAHR)*, Vol. 41, No. 5, pp 521-531

Cunha, L.V. (1973), "discussion", *Journal of Hydraulics Division*, 98(HY9), pp. 1637-1639

Dey, S. and Barbhuiya, A. K. (2005a) "Flow Field at a Vertical-Wall Abutment", *Journal of Hydraulic Engineering, ASCE*, Vol. 131, No. 12, pp 1126-1135

Dey, S. and Barbhuiya, A. K. (2005b) "Turbulent flow field in a scour hole at a semicircular abutment", *Canadian Journal of Civil Engineering*, 32, pp 213-232

Dey, S. and Barbhuiya, A. K. (2005c) "Time Variation of Scour at Abutments", *Journal of Hydraulic Engineering, ASCE*, Vol. 131, No. 1, pp 11-13

Dey, S. and Barbhuiya, A. K. (2006a) "Velocity and turbulence in a scour hole at a vertical-wall abutment", *Flow Measurement and Instrumentation*, 17, pp 13-21

Dey, S. and Barbhuiya, A. K. (2006b) "3D flow field in a scour hole at a wing-wall abutment", *Journal of Hydraulic Research, International Association for Hydraulic Research (IAHR)*, Vol. 44, No. 1, pp. 33-50

Dey, S. and Debnath, K. (2001) "Sediment pick-up on stream-wise sloping beds", *Journal of Irrigation and Drainage Engineering, ASCE*, Vol. 127, No. 1, pp 39-43

Dongol, D.M.S. (1994) "Local scour at bridge abutments", Rep. No. 544, School of Engineering, University of Auckland, Auckland, New Zealand

Duc, B. and Rodi, W. (2008) "Numerical Simulation of Contraction Scour in an Open Laboratory Channel", *Journal of Hydraulic Engineering, ASCE*, 134(4), 367-377

FLOW-3D (2011) "User Manual", Flow Science, Inc.

Franzetti S., Malavasi S., Piccinin C. (1994) "Sull'erosione alla base delle pile di ponte in acque chiare", *Atti del XXIV Convegno di Idraulica e Costruzioni Idrauliche, Napoli*, Vol. II, T4, pp 13-24.

- Garde, R., Subrmanaya, K., and Nambudripad, K. (1961) "Study of scour around spur dikes" *Journal of Hydraulic Engineering, ASCE*, Vol. 87, No. 4, pp 23-37
- Gill, M.A. (1981) "Bed Erosion in Rectangular Long Contraction", *ASCE Journal of Hydraulic Division*, Vol. 107, n. HY3, pp 273-284
- Kayatürk, Ş. Y. (2005) "Scour and Scour Protection at Bridge Abutments" PhD Thesis submitted to METU Graduate School of Natural and Applied Sciences, Ankara, Turkey
- Kayser, M. and Gabr, M.A. (2013) "Scour Assessment of Bridge Foundations Using an In Situ Erosion Evaluation Probe (ISEEP)" *Proc. of 92<sup>nd</sup> Transportation Research Board Annual Meeting*, January 13-17, Washington, D.C.
- Keulegan, G. H. (1938) "Laws of turbulent flow in open channels" *J. Res. of the Nat. Bureau of Standards*, 21(Dec.), pp 707-741.
- Kohli, A. and Hager, W. H. (2001) "Building scour in floodplains." *Water and Maritime Engineering, Institution of Civil Engineers, London*, 148, pp 61–80
- Koken, M. (2005) "A Numerical Study of the Role of Coherent Structures in the Flow around a Vertical Spur Dike", PhD Thesis submitted to the University of Iowa, USA
- Koken, M. (2011) "Coherent Structures around Isolated Spur Dikes at Various Approach Flow Angles", *Journal of Hydraulic Research, International Association for Hydraulic Research (IAHR)*, Vol. 49, No. 6, pp 736-743
- Koken, M. and Constantinescu, G. (2008a) "An investigation of the flow and scour mechanisms around isolated spur dikes in a shallow open channel: 1. Conditions corresponding to the initiation of the erosion and deposition process", *Water Resour. Res.*, 44, W08406
- Koken, M., and G. Constantinescu (2008b) "An investigation of the flow and scour mechanisms around isolated spur dikes in a shallow open channel: 2. Conditions corresponding to the final stages of the erosion and deposition process", *Water Resour. Res.*, 44, W08407
- Koken, M., and G. Constantinescu (2009) "An investigation of the dynamics of coherent structures in a turbulent channel flow with a vertical sidewall obstruction", *Physics of Fluids*, 21, 085104
- Koken, M., and G. Constantinescu (2011) "Flow and turbulence structure around a spur dike in a channel with a large scour hole", *Water Resources Research*, Vol. 47, W12511
- Kothyari, U.C. and Ranga Raju, K.G. (2001) "Scour Around Spur Dikes and Bridge Abutments", *Journal of Hydraulic Research, IAHR*, Vol. 39, No.4, pp367-374
- Krishnappan, B.G. and Lau L.Y. (1986) "Turbulence Modeling of Flood Plain Flows", *Journal of Hydraulic Engineering*, Vol.112, No. 4, pp 251-266

Kumcu Ş. Y., Göğüş M. and Kökpınar M. A. (2007) "Temporal scour development at bridge abutments with a collar" Canadian Journal of Civil Engineering, 34, pp 549-556

Kwan, T. F. (1988) "A study of abutment scour", Rep. No. 451, School of Engineering, University of Auckland, Auckland, New Zealand

Kwan, T.F. and Melville, B. W. (1994) "Local scour and flow measurements at bridge abutments", Journal of Hydraulic Research, IAHR, Vol. 32, No.5, pp 661-673

Laursen, E. M. (1960) "Scour at bridge crossings", Journal of Hydraulic Divisions, ASCE, Vol. 89, No. HY2, pp 1-54

Laursen, E. M. (1962) "Scour at bridge crossings", Transactions, ASCE, Vol. 127, Part 1, pp 116-179

Laursen, E. M. (1963) "An analysis of relief bridge scour", Journal of Hydraulic Divisions, ASCE, Vol. 86, No. 2, pp 93-118

Lim, S. (1997) "Equilibrium clear-water scour around an abutment", Journal of Hydraulic Engineering, Vol.123, No. 3, pp 237-243

Liu, H. K., Chang, F.M., and Skinner, M.M. (1961) "Effect of bridge construction on scour and backwater", Colorado State Univ., Civil Engineering Section, Ft. Collins, CER 60 HKL 22

Liu, J., Tominaga, A. and Nagao, M. (1994) "Numerical simulation of the flow around the spur dikes with certain configuration and angles with bank", Journal of Hydroscience and Engineering, Vol. 12, No. 2, 85-100

Mastbergen, D.R. and Von den Berg, J.H. (2003) "Breaching in fine sands and the generation of sustained turbidity currents in submarine canyons", Sedimentology (50) pp 625-637

Mayerle, R., Toro, F. and Wang, S. (1995) "Verification of a three-dimensional numerical model simulation of the flow in the vicinity of spur dikes" Journal of Hydraulic Research, Vol. 33, No. 2, pp 243-256

Melville, B. W. (1992) "Local scour at bridge abutments" Journal of Hydraulic Engineering, Vol. 118, No. 4, pp 615-631

Melville, B. W. (1995) "Bridge Abutment Scour in Compound Channels", Journal of Hydraulic Engineering, Vol. 121, No. 12, pp 863-868

Melville, B. W. (1997) "Pier and abutment scour: integrated approach" Journal of Hydraulic Engineering, Vol. 123, No. 2, pp 125-136

Melville, B. W. and Coleman, S. E. (2000) "Bridge Scour" Water Resources Publications, LLC, Colorado, U.S.A.

- Michiue, M., and Hinokidani, O. (1992) "Calculation of 2-dimensional bed evolution around spur-dike" *Annual Journal of Hydraulic Engineering*, Vol. 36, pp 61–66
- Molinas, A., Kheireldin, K. and Wu, B. (1998) "Shear Stress around Vertical Wall Abutments", *Journal of Hydraulic Engineering*, Vol. 124, No. 8, pp 822-830
- Morales, R. and Ettema, R. (2013) "Insights from Depth-Averaged Numerical Simulation of Flow at Bridge Abutments in Compound Channels", *Journal of Hydraulic Engineering*, Vol. 139, No. 5, pp 470–481
- Nagata, N., Hosoda, T., Nakato, T., and Muramoto, Y. (2005) "Three-dimensional numerical model for flow and bed deformation around river hydraulic structures", *Journal of Hydraulic Engineering*, Vol. 131, No. 12, pp 1074-1087
- Nakagawa, H., Tsujimoto, T., and Murakami, S. (1986) "Nonequilibriumbed load transport along side slope of an alluvial stream" *Proc., 3rd Int. Symp. on River Sedimentation*, Univ. of Mississippi, pp 885–893
- Naot, D., Nezu, I., and Nakagawa, H. (1993) "Hydrodynamic behavior of compound rectangular open channels" *Journal of Hydraulic Engineering*, ASCE, Vol. 119, No. 3, pp 390–408
- Oliveto, G., and Hager, W. H. (2002) "Temporal evolution of clear-water pier and abutment scour" *Journal of Hydraulic Engineering*, Vol. 128, No. 9, pp 811–820
- Oliveto, G., and Hager, W. H. (2005) "Further Results to Time-Dependent Local Scour at Bridge Elements" *Journal of Hydraulic Engineering*, Vol. 131, No. 2, pp 97–105
- Olsen, N.R.B. and Kjellesvig, H.M. (1998) "Three dimensional numerical flow modeling for estimation of maximum local scour depth", *Journal of Hydraulic Research*, Vol. 36, No. 4, pp 579-590
- Olsen, N.R.B. and Melaaen, M.C. (1993) "Three dimensional calculation of scour around cylinders", *Journal of Hydraulic Engineering*, ASCE, Vol. 119, No. 9, pp 1048–1054
- Ouillon, S. and Dartus, D. (1997) "Three-dimensional computation of flow around groyne", *Journal of Hydraulic Engineering*, ASCE, Vol. 123, No. 11, pp 962-970
- Pezzinga, G. (1994) "Velocity distribution in compound channel flows by numerical modeling", *Journal of Hydraulic Engineering*, ASCE, Vol. 120, No. 10, pp 1176-1197
- Prinos, P. (1990) "Turbulence modeling of main channel-floodplain flows with an algebraic stress model" *Int. Conf. on River Flood Hydr.*, W. R. White ed., John Wiley & Sons, Inc., New York, N.Y.
- Rajaratnam, N. and Nwachukwu, B.A. (1983) "Flow Near Groyne-Like Structures", *Journal of Hydraulic Engineering*, Vol. 109, No.3

- Richardson, J.R. and Richardson, E.V. (1993) "Discussion of Melville (1992)", *Journal of Hydraulic Engineering*, Vol. 119, pp 1069-1071
- Rubey, W. (1933) "Settling Velocities of Gravel, Sand and Silt Particles" *American Journal of Science*, Vol. 25, No. 148, pp. 325–338
- Schlichting, H. (1987) "Boundary Layer Theory", 7<sup>th</sup> Edition, McGraw Hill Book Co. Inc., New York, U.S.A.
- Smagorinsky, J. (1963) "General Circulation Experiments with the Primitive Equations", *Mon. Wea. Rev.*, Vol. 91, pp 99–164
- Teruzzi, A., Ballio, F. and Armenio, V. (2009) "Turbulent Stresses at the Bottom Surface near an Abutment: Laboratory-Scale Numerical Experiment", *Journal of Hydraulic Engineering*, Vol. 135, No. 2, pp 106-117
- Tey, C. B. (1984) "Local scour at bridge abutments" Report No. 329, School of Engineering, University of Auckland, Auckland, New Zealand
- Vanoni, V.A. (1975) "Sedimentation Engineering" ASCE, Manuals and Reports on Engineering Practice, No. 54
- Webby, M. G. (1984) "General scour at contraction" RRU Bulletin 73, National Roads Board, Bridge Design and Research Seminar, New Zealand, pp 109-118
- Wong, W. H. (1982) "Scour at bridge abutments" Report No. 275, School of Engineering, University of Auckland, Auckland, New Zealand
- Wu, W., and Wang, S. S. Y. (2006) "Formulas for Sediment Porosity and Settling Velocity" *Journal of Hydraulic Engineering*, Vol. 132, No. 8, pp. 858-862.
- Yakhot, V., and Orszag, S. A. (1986) "Renormalization group analysis of turbulence: I. basic theory", *J. Sci. Comp.*, Vol. 1, pp 1-51
- Yanmaz, A. M., and Altinbilek, H. D. (1991) "Study of time-dependent local scour around bridge piers" *J. Hydraul. Eng.*, Vol. 117, No. 10, pp 1247–1268
- Yanmaz, A. M. (2002) "Köprü Hidroliği" METU Press, Ankara Turkey (in Turkish)
- Yanmaz, A. M. and Kose, O. (2007) "Time-wise variation of scouring at bridge abutments" *Sadhana*, 32(3), pp 199-213
- Yanmaz, A. M. and Kose, O. (2009) "A Semi-empirical model for scour evolution at bridge abutments", *Journal of Hydraulic Research*, Vol. 47, No. 1, pp 110-118
- Zaghloul, N. and McCorquodale, J. (1973) "A numerical model for flow past a spur-dike" *Proceedings of the First Canadian Hydraulic Conference*, Edmonton, Canada

Zhang, H. and Nakagawa, H. (2008) "Scour around Spur Dyke: Recent advances and Future Researches", Annuals of Disas. Prev. Res. Inst., Kyoto University, No. 51B

Zhang, H., Nakagawa, H., Ishigaki, T. and Muto, Y. (2005) "Prediction of 3D Flow Field and Local Scouring around Spur Dykes" Annual Journal of Hydraulic Engineering, JSCE, Vol. 49, pp 1003-1008



## APPENDIX A

### SIEVE ANALYSIS GRAPH

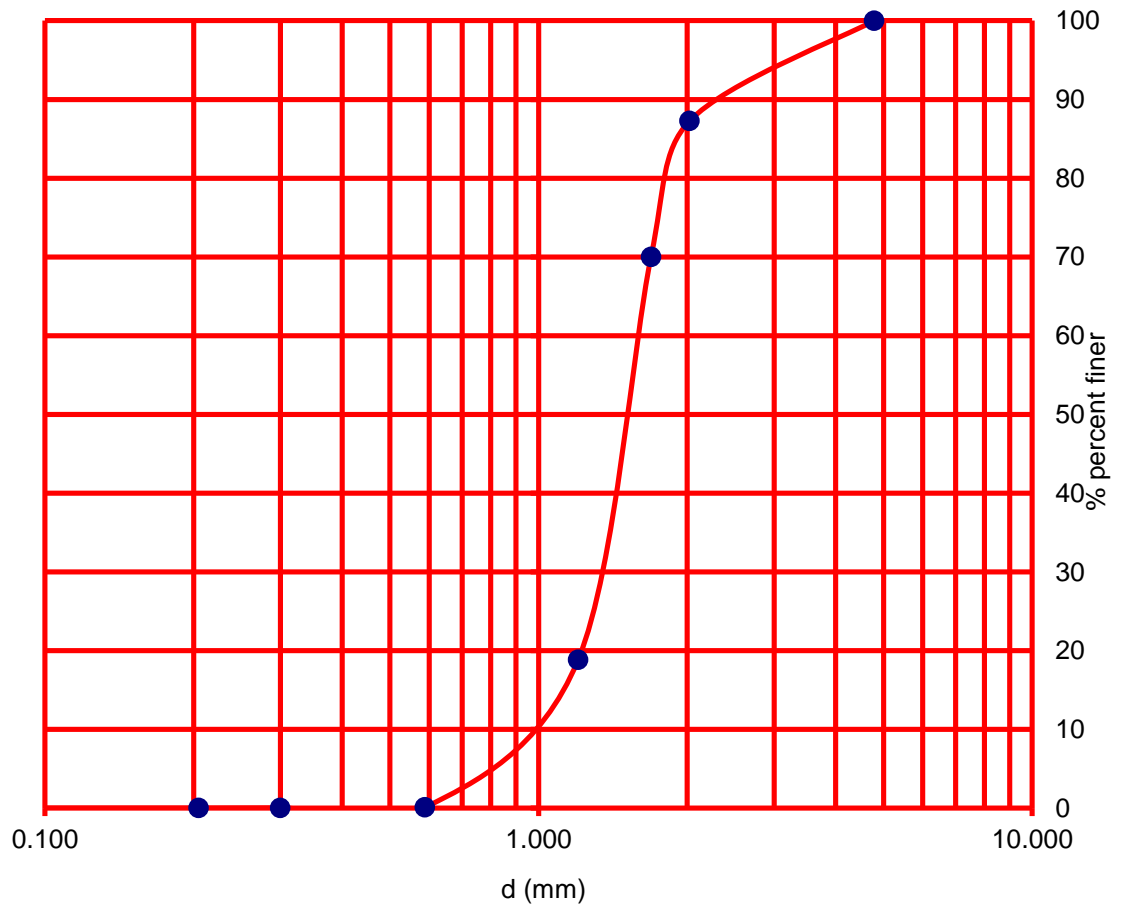


Figure A.1 Sieve Analysis graph of the sediment used in the experiments

## APPENDIX B

### CALCULATION OF CRITICAL SHEAR VELOCITY FROM EXPERIMENTS AND FROM SHIELDS DIAGRAM

First of all, critical shear velocity of the existing condition is calculated with the observed critical depth of the flow. The critical depth at the test condition is as below;

$$y_c = 0.90 * y = 0.90 * 0.135 = 0.1215 \text{ m}$$

Then, critical hydraulic radius and critical bed shear stress can be calculated as shown below;

$$R_c = \frac{A}{P} = \frac{0.1215 * 1.5}{2 * 0.1215 + 1.5} = 0.10456 \text{ m}$$

$$\tau_{0c} = \gamma * R_c * S = 9810 * 0.10456 * 0.001 = 1.02574 \text{ N/m}^2$$

And the critical shear velocity is;

$$(u_{*c})_{exp} = \sqrt{\tau_{0c}/\rho} = \sqrt{1.02574/1000} = 0.032 \text{ m/s}$$

Then, the theoretical value is calculated from Shield's diagram. The following formula is given by Melville and Coleman (2000) equivalent for Shield's diagram for median grain size diameters between 1 mm and 100 mm which is the case for the present study;

$$u_{*c} = 0.0305\sqrt{D_{50}} - \frac{0.0065}{D_{50}}$$

Then the critical shear velocity of the present study can be calculated as follows by theoretical methods;

$$(u_{*c})_{shields} = 0.0305\sqrt{1.5} - \frac{0.0065}{1.5} = 0.033 \text{ m/s}$$

## VITA

### PERSONEL INFORMATION

Surname, Name: Yıldız, Burhan  
Nationality: Turkish  
Date and Place of Birth: 31 December 1983, Ankara  
E-mail: [burhanyildiz23@gmail.com](mailto:burhanyildiz23@gmail.com)

### EDUCATION

Degree	Institution	Year of Graduation
M.Sc.	METU Civil Engineering Dept.	2009
B.Sc.	METU Civil Engineering Dept.	2006
High School	Fethiye Kemal Mumcu Anadolu Lisesi, Ankara	2001

### EXPERIENCE

Year	Place	Enrollment
2006-2013	METU Civil Engineering Dept.	Research Assistant
2006 (6 Mo.)	EN-SU Engineering Co., Ankara	Design Engineer
2005 July	Kemal Türkaslan Engineering Co., Ankara	Intern Engineer
2004 July	Baysan Yapı Denetim, Ankara	Intern Engineer

### FOREIGN LANGUAGES

English (Fluent), German (Beginner), French (Beginner), Russian (Beginner)

### PUBLICATIONS

1. Yıldız B., Altan-Sakarya B.A., Ger, M., 2014 Optimum Design of Slurry Pipelines by Genetic Algorithms, submitted to *Civil Engineering and Environmental Systems* (in press)
2. Yıldız B., Koken M., Gogus M. Temporal Development of Scour Hole Around Spill Through Bridge Abutments, *35<sup>th</sup> IAHR World Congress, 8-13 September 2013, Chengdu, China*

3. Gogus M., Koken M., Yildiz B. Effect of Abutment Length on Scour Pattern for Abutments with Curved Toe, *10<sup>th</sup> International Congress on Advances in Civil Engineering, 17-19 September 2012, Ankara, Turkey*
4. Yildiz B., Koken M., Gogus M. Değişken Daralma Oranlarında Dökme Duvar Tipi Kenar Ayaklarda Oyulmanın Zamanla Değişimi, *İMO 3. Su Yapıları Sempozyumu, 7-8 December 2013, Ankara, Turkey*
5. Yildiz B., Koken M., Gogus M. Abutment Scour Simulations by Using FLOW-3D, *FLOW-3D World Users Conference, 19-20 September 2013, Chicago, USA*
6. Altan-Sakarya B.A., Yildiz B., Ger, M., Ozturk, H. Comparison of Slurry Pipelines with Traditional Transportation Options: A Case Study for Turkey's Mines, *26th European Conference on Operational Research, 1-4 July 2013, Rome, Italy*
7. Yildiz B., Altan-Sakarya B.A., Ger M. Optimum Design of Slurry Pipelines, *24th European Conference on Operational Research, 11-14 July 2010, Lisbon, Portugal*